
Correlation Analysis of JNES Seismic Wall Pressure Data for ABWR Model Structures

Manuscript Completed: December 2007
Date Published: January 2008

Prepared by:
Jim Xu, Jinsuo Nie, Carl Costantino and Charles Hofmayer

Brookhaven National Laboratory
Upton, New York 11973-5000

Herman Graves, NRC Program Manager

Prepared for:
Office of Nuclear Regulatory Research
U.S. Nuclear Regulatory Commission
Washington, DC 20555
NRC Job Code Y-6718

ABSTRACT

To investigate the applicability of existing seismic soil-structure interaction (SSI) computer codes to deeply embedded and/or buried (DEB) structures, Brookhaven National Laboratory (BNL) performed a correlation analysis. The correlation analysis was performed using recorded earthquake response data from tests conducted by the Nuclear Power Engineering Corporation (NUPEC) of Japan. The NUPEC tests used 1/10th scale models, based on outer structural dimensions similar to the advanced boiling water reactor (ABWR) building structures. The ABWR models were embedded below grade to approximately 50% of the overall height of the model. The NUPEC earthquake response data were provided by the Japan Nuclear Energy Safety Organization (JNES, successor of NUPEC seismic test data) as part of the US-Japan collaborative effort in the area of seismic engineering research. The computer programs used in the correlation analysis are the System for Analysis of Soil-Structure Interaction (SASSI) and LS-DYNA programs, which represent the sub-structuring sub-traction and direct finite element methods. An assessment of the SASSI and LS-DYNA programs was made based on the insights gleaned from the correlation results.

The following results are discussed: 1) the correlation analysis using SASSI and LS-DYNA with the recorded earthquake response data in terms of the in-structure response spectra (ISRS) and seismic induced soil pressures, 2) an assessment of the adequacy and performance of the analysis methods, and 3) quantification of the effect of the soil uncertainty on the seismic response computations by SASSI and LS-DYNA. This study concludes that for moderate earthquakes, the computer codes SASSI and LS-DYNA have reasonably captured the seismic response parameters in terms of ISRS and the seismic induced side and base pressures for the DEB structures. Furthermore, the level of uncertainty in the soil properties for the site was estimated by SASSI and LS-DYNA programs using the best fit with the ISRS from the recorded response data, which is within the range currently considered in the geotechnical engineering practice.

Paperwork Reduction Act Statement

This NUREG does not contain information collection requirements and, therefore, is not subject to the requirements of the Paperwork Reduction Act of 1995 (44 U.S.C. 3501 et seq.).

Public Protection Notification

The NRC may not conduct or sponsor, and a person is not required to respond to, a request for information or an information collection requirement unless the requesting document displays a current OMB control number.

FOREWORD

Over the past three decades, the scientific community has performed extensive research to study the phenomenon of soil-structure interaction (SSI) and its impact on seismic response, especially for nuclear power plant (NPP) structures. To date, this research has considerably advanced the understanding of the interacting mechanisms associated with SSI, led to the development of analytical methods and computer programs for seismic response, and been the source of much-needed field data from actual earthquake events.

The established computer codes used for SSI analysis in the nuclear industry have primarily been developed for current light-water reactors, and applied to coupled SSI models in which the structures are founded at or near the ground surface with shallow embedment. Several NPP designs have proposed utilizing deeply embedded and/or buried (DEB) structural configurations. For example, in two new designs that have been submitted for preliminary review by the U.S. Nuclear Regulatory Commission (NRC), the entire reactor building and a significant portion of the steam generator building are either partially or completely embedded below the ground surface.

The current seismic analysis methods have been developed for shallowly embedded structures and the existing regulatory guidance, codes, and standards suggest that simple formulations may be used to model the embedment effect when the depth of embedment is less than 30% of the structure's foundation equivalent-radius. [Consider, for example, the American Society of Civil Engineers Standard No. 4 (ASCE-4), "Seismic Analysis of Safety-Related Nuclear Structures."] Therefore, to support the review of preliminary applications for new reactor designs, the NRC sponsored a research program, under which Brookhaven National Laboratory (BNL) investigated the extent to which the existing regulatory guidance, seismic design practices, and SSI codes (acceptable for shallow embedments) also apply to deeper embedments. In so doing, the overall objective of this research is to recommend any modifications that may be necessary to adapt the existing guidance, design practices, and computer codes to DEB structures.

This report, produced in connection with the BNL investigation, discusses the SSI models used in the System for Analysis of Soil-Structure Interaction (SASSI) and the Livermore Software Dynamic Finite Element Analysis (LS-DYNA) computer code for the one-tenth scale model of an advanced boiling-water reactor (ABWR) containment with 50% embedment. In addition, this report assesses the adequacy of the SASSI and LS-DYNA SSI models to predict the seismic responses of embedded structures, and it correlates the analytical results with recorded field data from actual earthquake events.

On the basis of the results of this study, the NRC staff concluded that existing linear SSI methods can be extended, to varying degrees, to produce acceptable SSI response calculations for DEB structures. However, extending the existing methods requires that (1) the SSI response induced by the ground motion must be very much within the linear regime, or (2) the non-linear effect (such as those experienced in strong ground motion) must not be expected to control the SSI response parameters. Strong ground motion response data from additional tests or earthquake recordings would be necessary to determine if the existing methods could be utilized for strong ground motion non-linear conditions.

Jennifer L. Uhle, Director
Division of Engineering
U.S. Nuclear Regulatory Commission

TABLE OF CONTENTS

	<u>Page No.</u>
Abstract.....	iii
Foreword.....	v
Table of Contents.....	vii
List of Figures.....	ix
List of Tables.....	xv
Executive Summary	xvii
Acknowledgements.....	xxi
 1. INTRODUCTION	 1
1.1 Background.....	1
1.2 Scope and Objectives.....	2
1.3 Report Organization.....	2
 2. DESCRIPTION OF FIELD TESTS AND COMPUTER PROGRAMS USED FOR PREDICTIVE ANALYSES.....	 5
2.1 Description of Field Tests	5
2.2 Computer Programs Used for Predictive Analyses	7
2.2.1 SASSI Sub-structuring Method for SSI Responses.....	7
2.2.2 LS-DYNA Method for SSI Responses	9
 3. SASSI ANALYSIS.....	 33
3.1 Twin-Reactor Configuration.....	33
3.1.1 Test Modeling Description	33
3.1.2 Results and Comparisons with JNES data.....	34
3.2 Reactor-Turbine Configuration	57
3.2.1 Test Modeling Description	57
3.2.2 Analysis Results and Comparisons with Recorded Data	58
3.3 Methodology Assessment	83
 4. LS-DYNA Analysis.....	 85
4.1 Twin Reactors Test Model.....	85
4.1.1 LS-DYNA Modeling Description	85
4.1.2 LS-DYNA Analysis Results and Comparisons with JNES Recorded Data	86

4.2	R-T Test Model.....	105
4.2.1	LS-DYNA Modeling Description	105
4.2.2	LS-DYNA Analysis Results and comparisons with JNES Recorded Data	105
4.3	Methodology Assessment	126
5.	CONCLUSIONS AND RECOMMENDATIONS	135
6.	REFERENCES	137

LIST OF FIGURES

<u>Figure No.</u>		<u>Page No.</u>
Figure 2-1	Location of NUPEC Field Test Site in Japan	12
Figure 2-2	Overall Plan for NUPEC Field Tests	13
Figure 2-3	Layout of Models at NUPEC Field Test Site	14
Figure 2-4	Cross Section of Reactor and Turbine Building Model	15
Figure 2-5	Embedment Conditions for the Building Models	16
Figure 2-6	NUPEC Field Test Model of Reactor Building without Embedment	17
Figure 2-7	NUPEC Field Test Model of Adjacent Twin Reactor Buildings without Embedment	18
Figure 2-8	NUPEC Field Test Model of Adjacent Reactor -Turbine Buildings without Embedment	19
Figure 2-9	NUPEC Field Test Model of Reactor Building with Embedment	20
Figure 2-10	NUPEC Field Test Model of Adjacent Twin Reactor Buildings with Embedment.....	21
Figure 2-11	NUPEC Field Test Model of Adjacent Reactor-Turbine Buildings with Embedment.....	22
Figure 2-12	Location of Boring Points under Building Models and Cross Sections for Soil Profiles.....	23
Figure 2-13	Soil Profile for Section A-A (Refer to Figure 2-12 for Section Location)	24
Figure 2-14	Soil Profile for Section B-B (Refer to Figure 2-12 for Section Location)	25
Figure 2-15	Soil Profile for Reactor-Turbine Buildings.....	26
Figure 2-16	Test Configurations for Seismic Induced Earth Pressures	27
Figure 2-17	Locations of Pressure Sensors for the Test Structures under the Basemat.....	28
Figure 2-18	Locations of Pressure Sensors for the BAs Structure on Side Wall	29
Figure 2-19	Locations of Pressure Sensors for the BAn Structure on Side Wall	30
Figure 2-20	Locations of Pressure Sensors for the DA Structure on Side Wall	31
Figure 2-21	Locations of Pressure Sensors for the DF Structure on Side Wall	32
Figure 3.1-1	Twin Reactor Configuration Soil Profile and JNES Properties	39
Figure 3.1-2	Twin Configuration Seismometer Locations and Designations	40
Figure 3.1-3	Input Ground Motions for Twin Configuration Analysis.....	41
Figure 3.1-4	SASSI Model for Structures and Surrounding Soil	41
Figure 3.1-5	SASSI Model for Excavated Soil	42
Figure 3.1-6	Comparison of Horizontal Response Spectra at Basemat Center.....	42
Figure 3.1-7	Comparison of Horizontal Response Spectra at Roof Center of Twin Model	43
Figure 3.1-8	Comparison of Seismic Induced Soil Pressure at Sensor BAS-SE-S1 ..	44
Figure 3.1-9	Comparison of Seismic Induced Soil Pressure at Sensor BAS-SE-S2 ..	45
Figure 3.1-10	Comparison of Seismic Induced Soil Pressure at Sensor BAS-SE-S4 ..	46
Figure 3.1-11	Comparison of Seismic Induced Soil Pressure at Sensor BAN-SE-N3.....	47
Figure 3.1-12	Comparison of Seismic Induced Soil Pressure at Sensor BAN-SE-N6.....	48
Figure 3.1-13	Comparison of Seismic Induced Soil Pressure at Sensor BAN-SE-N13	49

Figure 3.1-14	Comparison of Fourier Spectra of Soil Pressure at Sensor BAS-SE-S1	50
Figure 3.1-15	Comparison of Fourier Spectra of Soil Pressure at Sensor BAS-SE-S2	50
Figure 3.1-16	Comparison of Fourier Spectra of Soil Pressure at Sensor BAS-SE-S4	51
Figure 3.1-17	Comparison of Fourier Spectra of Soil Pressure at Sensor BAN-SE-N3	51
Figure 3.1-18	Comparison of Fourier Spectra of Soil Pressure at Sensor BAN-SE-N6	52
Figure 3.1-19	Comparison of Fourier Spectra of Soil Pressure at Sensor BAN-SE-N13	52
Figure 3.1-20	Comparison of Vertical Spectra at Basemat Center of Twin Model.....	53
Figure 3.1-21	Comparison of Vertical Spectra at Roof Center of Twin Model	53
Figure 3.1-22	Comparison of Averaged Vertical Seismic Induced Soil Pressure for BAN.....	54
Figure 3.1-23	Comparison of Averaged Vertical Seismic Induced Soil Pressure for BAS.....	55
Figure 3.1-24	Comparison of Fourier Spectra of Soil Pressure for BAS Basemat.....	56
Figure 3.1-25	Comparison of Fourier Spectra of Soil Pressure for BAN Basemat	56
Figure 3.2-1	JNES R-T Configuration Soil Profile	62
Figure 3.2-2	JNES R-T Configuration Soil Properties.....	63
Figure 3.2-3	Locations and Designations of Seismometers on R-T Model.....	64
Figure 3.2-4	R-T Model Input Motions	65
Figure 3.2-5	SASSI R-T Structural Model	65
Figure 3.2-6	SASSI R-T Excavated Soil Model.....	66
Figure 3.2-7	Comparison of Horizontal Response Spectra at Basemat Center.....	66
Figure 3.2-8	Comparison of Horizontal Response Spectra at Roof Center of Reactor for R-T Model.....	67
Figure 3.2-9	Comparison of Horizontal Response Spectra at Basemat Center of Turbine for R-T Model	67
Figure 3.2-10	Comparison of Horizontal Response Spectra at Roof Center of Turbine for R-T Model	68
Figure 3.2-11	Comparison of Seismic Induced Soil Pressure at Sensor DA-SE-N1	69
Figure 3.2-12	Comparison of Seismic Induced Soil Pressure at Sensor DA-SE-N2	70
Figure 3.2-13	Comparison of Seismic Induced Soil Pressure at Sensor DA-SE-N4	71
Figure 3.2-14	Comparison of Seismic Induced Soil Pressure at Sensor DF-SE-S1	72
Figure 3.2-15	Comparison of Seismic Induced Soil Pressure at Sensor DF-SE-S3.....	73
Figure 3.2-16	Comparison of Seismic Induced Soil Pressure at Sensor DF-SE-S4.....	74
Figure 3.2-17	Comparison of Fourier Spectra of Soil Pressure at Sensor DA-SE-N1	75
Figure 3.2-18	Comparison of Fourier Spectra of Soil Pressure at Sensor DA-SE-N2	75
Figure 3.2-19	Comparison of Fourier Spectra of Soil Pressure at Sensor DA-SE-N4	76

Figure 3.2-20	Comparison of Fourier Spectra of Soil Pressure at Sensor DF-SE-S1	76
Figure 3.2-21	Comparison of Fourier Spectra of Soil Pressure at Sensor DF-SE-S3.....	77
Figure 3.2-22	Comparison of Fourier Spectra of Soil Pressure at Sensor DF-SE-S4.....	77
Figure 3.2-23	Comparison of Vertical Response Spectra at Basemat Center of Reactor for R-T Model.....	78
Figure 3.2-24	Comparison of Vertical Response Spectra at Roof Center of Reactor for R-T Model.....	78
Figure 3.2-25	Comparison of Vertical Response Spectra at Basemat Center of Turbine for R-T Model	79
Figure 3.2-26	Comparison of Vertical Response Spectra at Roof Center of Turbine for R-T Model.....	79
Figure 3.2-27	Comparison of Averaged Vertical Seismic Induced Soil Pressure for DA.....	80
Figure 3.2-28	Comparison of Averaged Vertical Seismic Induced Soil Pressure for DF	81
Figure 3.2-29	Comparison of Fourier Spectra of Vertical Soil Pressure at DA Basemat	82
Figure 3.2-30	Comparison of Fourier Spectra of Vertical Soil Pressure at DF Basemat	82
Figure 4.1-1	LS-DYNA Model for Twin Reactors Test Configuration.....	90
Figure 4.1-2	Zoom-in View of LS-DYNA Model of R-T Test Configuration	90
Figure 4.1-3	Comparison of Horizontal Response Spectra at Basemat Center of Twin Reactors Model	91
Figure 4.1-4	Comparison of Horizontal Response Spectra at Roof Center of Twin Reactors Model	91
Figure 4.1-5	Comparison of Seismic Induced Soil Pressure at Sensor BAS-SE-S1 ..	92
Figure 4.1-6	Comparison of Seismic Induced Soil Pressure at Sensor BAS-SE-S2 ..	93
Figure 4.1-7	Comparison of Seismic Induced Soil Pressure at Sensor BAS-SE-S4 ..	94
Figure 4.1-8	Comparison of Seismic Induced Soil Pressure at Sensor BAN-SE-N3	95
Figure 4.1-9	Comparison of Seismic Induced Soil Pressure at Sensor BAN-SE-N6	96
Figure 4.1-10	Comparison of Seismic Induced Soil Pressure at Sensor BAN-SE-13.....	97
Figure 4.1-11	Comparison of Fourier Spectra of Soil Pressure at Sensor BAS-SE-S1	98
Figure 4.1-12	Comparison of Fourier Spectra of Soil Pressure at Sensor BAS-SE-S2	98
Figure 4.1-13	Comparison of Fourier Spectra of Soil Pressure at Sensor BAS-SE-S4	99
Figure 4.1-14	Comparison of Fourier Spectra of Soil Pressure at Sensor BAN-SE-N3	99
Figure 4.1-15	Comparison of Fourier Spectra of Soil Pressure at Sensor BAN-SE-N6	100
Figure 4.1-16	Comparison of Fourier Spectra of Soil Pressure at Sensor BAN-SE-N13	100
Figure 4.1-17	Comparison of Vertical Response spectra at Basemat Center of Twin Reactors Model	101

Figure 4.1-18	Comparison of Vertical Response spectra at Roof Center of Twin Reactors Model	101
Figure 4.1-19	Comparison of Vertical Soil Pressure on BAN Basemat of Twin Reactors Model	102
Figure 4.1-20	Comparison of Vertical Soil Pressure on BAS Basemat of Twin Reactors Model	103
Figure 4.1-21	Comparison of Fourier Spectra of Vertical Soil Pressure on BAN Basemat of Twin Reactors Model	104
Figure 4.1-22	Comparison of Fourier Spectra of Vertical Soil Pressure on BAS Basemat of Twin Reactors Model	104
Figure 4.2-1	LS-DYNA Model of R-T Test Configuration	109
Figure 4.2-2	Zoom-in View of LS-DYNA Model of R-T Test Configuration	109
Figure 4.2-3	Comparison of Horizontal Response at Basemat Center of R-T Reactor.....	110
Figure 4.2-4	Comparison of Horizontal Response at Roof Center of R-T Reactor.....	110
Figure 4.2-5	Comparison of Horizontal Response at Basemat Center of R-T Turbine	111
Figure 4.2-6	Comparison of Horizontal Response at Roof Center of R-T Turbine	111
Figure 4.2-7	Comparison of Seismic Induced Soil Pressure at Sensor DA-SE-N1 ..	112
Figure 4.2-8	Comparison of Seismic Induced Soil Pressure at Sensor DA-SE-N2 ..	113
Figure 4.2-9	Comparison of Seismic Induced Soil Pressure at Sensor DA-SE-N4 ..	114
Figure 4.2-10	Comparison of Seismic Induced Soil Pressure at Sensor DF-SE-S1 ...	115
Figure 4.2-11	Comparison of Seismic Induced Soil Pressure at Sensor DF-SE-S3...	116
Figure 4.2-12	Comparison of Seismic Induced Soil Pressure at Sensor DF-SE-S4...	117
Figure 4.2-13	Comparison of Fourier Spectra of Soil Pressure at Sensor DA-SE-N1	118
Figure 4.2-14	Comparison of Fourier Spectra of Soil Pressure at Sensor DA-SE-N2	118
Figure 4.2-15	Comparison of Fourier Spectra of Soil Pressure at Sensor DA-SE-N4	119
Figure 4.2-16	Comparison of Fourier Spectra of Soil Pressure at Sensor DF-SE-S1	119
Figure 4.2-17	Comparison of Fourier Spectra of Soil Pressure at Sensor DF-SE-S3.....	120
Figure 4.2-18	Comparison of Fourier Spectra of Soil Pressure at Sensor DF-SE-S4.....	120
Figure 4.2-19	Comparison of Vertical Response Spectra at Basemat Center of R-T Reactor.....	121
Figure 4.2-20	Comparison of Vertical Response Spectra at Roof Center of R-T Reactor.....	121
Figure 4.2-21	Comparison of Vertical Response Spectra at Basemat Center of R-T Turbine	122
Figure 4.2-22	Comparison of Vertical Response Spectra at Roof Center of R-T Turbine	122
Figure 4.2-23	Comparison of Seismic Induced Vertical Soil Pressure on Basemat of R-T Reactor.....	123
Figure 4.2-24	Comparison of Seismic Induced Vertical Soil Pressure on Basemat of R-T Turbine	124

Figure 4.2-25	Comparison of Fourier Spectra for Vertical Soil Pressure on Basemat of	125
Figure 4.2-26	Comparison of Fourier Spectra for Vertical Soil Pressure on Basemat of	125
Figure 4.3-1	Comparison of Response Spectra at Basemat of Twin Reactors Model between LS-DYNA and SASSI.....	128
Figure 4.3-2	Comparison of Response Spectra at Roof of Twin Reactors Model between LS-DYNA and SASSI.....	128
Figure 4.3-3	Comparison of Fourier Spectra of Soil Pressure at Sensor BAS-SE-S1 of Twin Reactors Model between LS-DYNA and SASSI...	129
Figure 4.3-4	Comparison of Fourier Spectra of Soil Pressure at Sensor BAS-SE-S2 of Twin Reactors Model between LS-DYNA and SASSI...	129
Figure 4.3-5	Comparison of Fourier Spectra of Soil Pressure at Sensor BAS-SE-S4 of Twin Reactors Model between LS-DYNA and SASSI....	130
Figure 4.3-6	Comparison of Fourier Spectra of Soil Pressure at Sensor BAN-SE-N3 of Twin Reactors Model between LS-DYNA and SASSI ...	130
Figure 4.3-7	Comparison of Fourier Spectra of Soil Pressure at Sensor BAN-SE-N6 of Twin Reactors Model between LS-DYNA and SASSI ...	131
Figure 4.3-8	Comparison of Fourier Spectra of Soil Pressure at Sensor BAN-SE-N13 of Twin Reactors Model between LS-DYNA and SASSI .	131
Figure 4.3-9	Comparison of Vertical Response Spectra at Basemat of Twin Reactors Model between LS-DYNA and SASSI.....	132
Figure 4.3-10	Comparison of Vertical Response Spectra at Roof of Twin Reactors Model between LS-DYNA and SASSI.....	132
Figure 4.3-11	Comparison of Fourier Spectra of Vertical Soil Pressure on BAN Basemat of Twin Reactors Model.....	133
Figure 4.3-12	Comparison of Fourier Spectra of Vertical Soil Pressure on BAS Basemat of Twin Reactors Model.....	133
Figure 4.3-13	Summary of Analytical Cases and Associated Soil Uncertainties Performed for this Report.....	134

LIST OF TABLES

Table 2-1 Major Earthquake Events Recorded at the NUPEC Field Test Site	11
---	----

EXECUTIVE SUMMARY

As seismic analysis methods that incorporate the effect of soil-structure interaction (SSI) have improved over the years, the development of numerical simulation programs which implement various SSI methods has also improved, especially for nuclear power plant (NPP) structures. However, it is understood that established SSI analysis computer codes which are used in the nuclear industry have been primarily developed for the current generation of Light Water Reactors (LWRs) and applied to coupled soil-structure models where the structures are founded at or near the ground surface with shallow embedment. Therefore, from a regulatory standpoint the applicability of SSI methods and associated computer programs used to predict the seismic response of deeply embedded and/or buried (DEB) structures should be assessed. The adequacy of various SSI programs should also be validated against known recorded earthquake ground motion data with DEB structural features.

In an effort to collect earthquake response data of embedded NPP structures, the Nuclear Power Engineering Corporation (NUPEC) of Japan conducted a multi-year field test for the 1/10th scale models, based on overall structural dimensions similar to the advanced boiling water reactor (ABWR) building structures; these structures were embedded below grade to about 50% of the structural height. Recently, as part of the US-Japan collaborative effort in the area of seismic engineering research, the Japan Nuclear Energy Safety Organization (JNES, successor of NUPEC) has provided Brookhaven National Laboratory (BNL) with the field recorded earthquake data from the NUPEC tests. As part of a U. S. Nuclear Regulatory Commission (NRC) research program, BNL has performed a correlation analysis of the JNES earthquake response data, using the SASSI and LS-DYNA computer programs. An assessment of the analysis programs was made based on the insights gleaned from the correlation analysis. This report presents and discusses the BNL correlation analysis and assessment of the SASSI and LS-DYNA computer programs.

The objectives of this study are to 1) develop SSI models using SASSI and LS-DYNA, and generate SSI analysis solutions in terms of the in-structure response spectra (ISRS) and seismic induced soil pressures for the JNES model structures and compare the BNL analysis results with the recorded data provided by JNES, 2) assess the adequacy and performance of the analysis methods which are employed for the correlation study, and 3) determine the effect of the soil uncertainty on the seismic response computations.

The earthquake data provided by JNES consist of a low level ground motion with the maximum free field acceleration less than 0.1g. It is believed that such small ground motions are insufficient to induce any non-linearity in the response of the SSI test models. However, these data are valuable for validating the adequacy of the SSI analysis methods in computations of the linear response. Therefore, the scope of the correlation analysis is limited to SSI response calculations within the linear regime. The response parameters considered in the correlation analysis include the ISRS and the seismic induced soil pressure on the structural wall below grade.

In the process of performing the SSI analyses, the JNES geotechnical soil data were treated as the best estimate or mean soil properties, and the uncertainty of the soil

properties was estimated by the SASSI and LS-DYNA computer codes using the best fit to the recorded ISRS. By incorporating the soil uncertainty in the SSI analyses, an assessment can be made of the analytical capability of the two codes, which employed vastly different approaches to treating the SSI effect. The insights into the modeling performance by both computer codes are also obtained from the comparisons between the analysis results and the JNES recorded response data.

Based on the study performed, the following observations and conclusions are reached.

1. For the low level ground motion analyzed, both SASSI and LS-DYNA performed extremely well in predicting ISRS for the test models, as exhibited by the comparisons.
2. The level of uncertainty in the soil properties for the site was estimated by the SASSI and LS-DYNA programs through best fit to the ISRS computed from the JNES recorded response data. Although the soil uncertainty level is computed differently for the two computer codes, the uncertainty estimates are well within the range of acceptable practice in geotechnical engineering applications.
3. The computation models by both codes appear to have difficulties in capturing the ISRS peaks induced by the structure-structure interactions. This may be due to the lack of information on the soil property of the backfill between the structures (The analysis assumes the free field property for the backfill).
4. For seismic induced side soil pressures, both codes can generally capture the frequency content of the test data and the analyses using modified soil columns correlate well with the recorded pressures. In addition, the LS-DYNA computed pressures appear closer to the recorded pressures than the SASSI results, although not to the extent that one would reach a different conclusion about the performance of the two computer codes.
5. As discussed in Section 4.3, a number of pressure gauges were identified having been contaminated with noises, thus resulting in differences in the comparison of the recorded data with the computed response.
6. With respect to the vertical response analyses, both codes computed very similar ISRS that are close to the recorded data. Similar to the horizontal analyses, the uncertainty estimates of the soil columns for the site by the two computer codes are slightly different with LS-DYNA having a smaller range.
7. For the vertical soil pressures, SASSI estimates the vertical soil pressures much closer to the recorded pressures than LS-DYNA. However, for some frequencies, the SASSI estimate of the soil pressures fall below the recorded pressures. On the other hand, LS-DYNA over-predicts the pressures with respect to the recordings. It should be mentioned that the upward drift in the low frequencies of the recordings should be ignored due to the noise contained in the recorded data.
8. With respect to the effort required to develop the SSI models and to compute the SSI responses, the level of effort required for running the SASSI program amounts to only a small fraction of what is required for executing the corresponding LS-DYNA analysis. Although LS-DYNA has an advantage of

many built-in non-linear features, it would not be a practical and effective choice when linear SSI responses are sought. For such cases, SASSI is the better choice.

In summary, the SASSI and LS-DYNA computer codes have reasonably captured the seismic response parameters in terms of ISRS and the seismic induced side and base pressures when the response parameter is in the linear regime. The level of soil uncertainty for the site estimated by both computer codes through best fitting the recorded ISRS is well within the range currently employed in the geotechnical engineering practice.

However, this study only validated the methods for linear SSI response analyses, which can not be extended to addressing SSI effects due to strong ground motions. In the later cases, many non-linear phenomena are expected to occur in the response of the soil-structure systems, such as the soil-structure interface separation and large degradation in the soil properties, which affect the SSI response calculations by various codes. The adequacy and accuracy of the SSI analyses performed using the SASSI and LS-DYNA computer codes remain to be validated for documented strong ground motion data. Therefore, one goal of future research is to collect strong ground motion data to extend the correlation analysis as described in this report to the non-linear SSI regime and to develop insights into the performance of these analysis programs (LS-DYNA and SASSI) for computing structural wall pressure induced by large earthquake events.

ACKNOWLEDGEMENTS

This report was prepared as part of a research program sponsored by the Office of Nuclear Regulatory Research of the U.S. Nuclear Regulatory Commission. The authors would like to express their gratitude to Mr. Herman Graves, NRC Project Manager, for his encouragement, and the technical and administrative support he has provided throughout the course of this study.

The earthquake data utilized in this correlation study were provided by the Japan Nuclear Energy Safety Organization (JNES), for which the authors would like to express their appreciation and acknowledgement to JNES. The authors also thank Mr. Y. Uchiyama (JNES), Dr. Y. Kitada and Mr. K. Kusama, for their support and assistance in providing the field test configurations and associated data which are essential to the performance of this study.

A special appreciation is acknowledged to Dr. Charles A. Miller, who passed away before completion of this report. Dr. Miller has played a pivotal role in directing and performing the research crucial to the success of this program. During the last few months of his life, even with grave illness and intolerable pain, Dr. Miller would still be personally involved in the program; he frequently asked about the progress of the project and provided many invaluable advises to other BNL staffers. His caring, work ethics and professionalism set an exceptional example and provide an inspiration for all of us. He will be surely missed by his colleagues from BNL and NRC.

The authors also express special thanks to Ms. Susan Monteleone for her secretarial help in the preparation of this report.

1 INTRODUCTION

1.1 Background

Motivated by many design and access considerations, several conceptual designs for advanced reactors have proposed that certain safety related nuclear power plant (NPP) structures will be partially or completely embedded below grade. For the seismic design and analysis of these types of deeply embedded structures, the soil-structure interaction (SSI) effect needs to be considered. Sponsored by the US Nuclear Regulatory Commission (NRC), Brookhaven National Laboratory (BNL) has undertaken a multi-year research program to provide information and research necessary for developing a technical basis to support the safety evaluation of deeply embedded and/or buried (DEB) structures as proposed for advanced reactor designs.

As seismic analysis methods that incorporate the effect of soil-structure interaction (SSI) have improved over the years, the development of numerical simulation programs which implement various SSI methods has also improved, especially for nuclear power plant (NPP) structures. However, it is understood that established SSI analysis computer codes which are used in the nuclear industry have been primarily developed for the current generation of Light Water Reactors (LWRs) and applied to coupled soil-structure models where the structures are founded at or near the ground surface with shallow embedment [Xu, et al., 2003]. Therefore, from a regulatory standpoint the applicability of SSI methods and associated computer programs used to predict the seismic response of deeply embedded and/or buried (DEB) structures should be assessed. The adequacy of various SSI programs should also be validated against known recorded earthquake ground motion data with DEB structural features.

In a recent study, BNL has performed a methodology assessment [Xu, 2005] to determine the applicability and the performance of representative analysis methods and the associated computer programs commonly utilized for computation of the seismic responses including the soil-structure interaction (SSI) effects for DEB structures.

In the BNL study, several SSI programs representative of methodologies typically employed by the nuclear industry were assessed to determine the extent to which computer programs that implemented these analysis methodologies can capture the major seismic design and analysis parameters pertaining to DEB structures. The BNL study has found that the SSI responses computed with these programs are sensitive to the pertinent assumptions made in different methodologies and modeling details of the SSI system, especially involving structures with deep embedment. This assessment further substantiates the need for making available more experimental data to validate the important aspects of analysis programs and the SSI modeling details.

Over the last two decades or so, systematic experimental programs to provide seismic response data on large scale NPP model structures have been seriously attempted, with the most prominent one being the Lotung and Hualien SSI model experiments [EPRI, 1989] for the PWR containment, jointly sponsored by EPRI and NRC, in association with other international partners. For deeply embedded NPP structures, the Nuclear Power Engineering Corporations (NUPEC) has conducted a multi-year field test for the 1/10th scale models, based on outer structural dimensions similar to the advanced boiling water reactor (ABWR) building structures; these structures are embedded below grade to about 50% of the structural height. Recently, as part of the US-Japan collaborative effort

in the area of seismic engineering research, the Japan Nuclear Energy Safety Organization (JNES, successor of NUPEC seismic test data) has provided BNL with the field recorded data from the NUPEC test. It is the subject of this report to present and discuss the BNL correlation analysis with the JNES recorded data.

1.2 Scope and Objectives

The study reported hereinafter is part of a research program, sponsored by The Office of Nuclear Regulatory Research (RES) of the US NRC under JCN Y-6718. The overall objective of this research program is to provide information and research necessary to develop a technical basis to support the safety evaluation of DEB structures proposed for advanced reactor designs. For two of the new reactor designs submitted to the NRC for preliminary review [NRC RES, 2002, General Atomics, 1996], the entire reactor building and a significant portion of the steam generator building are to be partially or completely embedded below grade. Therefore, it is imperative that from a regulatory standpoint, all practical aspects of existing methods and computer programs need to be evaluated to determine their applicability and adequacy in capturing the seismic behavior of DEB NPP structures.

The objectives of this study are to 1) develop SSI models using SASSI and LS-DYNA, and generate SSI analysis solution in terms of the in-structure response spectra (ISRS) and seismic induced soil pressures for the JNES model structures and compare the BNL analysis results with the recorded data provided by JNES, 2) assess the adequacy and performance of the analysis methods which are employed for the correlation study, and 3) determine the effect of the soil uncertainty on the seismic response computations.

The earthquake data provided by JNES consist of a low level ground motion with the maximum free field acceleration less than 0.1g. It is believed that such small ground motions are insufficient to induce any non-linearity in the response of the SSI test models. However, these data are valuable for validating the adequacy of the SSI analysis methodologies in computations of the linear response. Therefore, the scope of the correlation analysis is limited to SSI response calculations within the linear regime. The response parameters considered in the correlation analysis include the ISRS and the seismic induced soil pressure on the structural wall below grade.

It is expected that the findings from the correlation analysis will provide insights into the performance of the SSI analysis methods, and confirm and validate computer programs for computing linear response of DEB NPP structures.

1.3 Report Organization

This report is organized in five sections. Section 1 is the introduction. Following this section, a description of the NUPEC field test programs and the recorded data provided by JNES are described in Section 2.

Two computer programs are used for the correlation analysis, which are SASSI and LS-DYNA, respectively, and are described in Section 2. SASSI is a linear SSI program using the sub-structuring method, while LS-DYNA is a general purpose finite element program with an explicit solution algorithm and interface modeling capability. Both programs were used in a previous BNL study [Xu, 2005] for assessing pertinent SSI effects associated with DEB structures and the capability of the programs to capture them. The SASSI models for the NUPEC test structures and the analysis results are

discussed in Section 3, including both ISRS and seismic induced soil pressures and their comparisons with field recorded data at various channels. Section 4 describes the LS-DYNA models and the corresponding analysis results, as well as the response comparisons with the recorded channel data.

Based on the results of the correlation analysis and discussions, conclusions and recommendations are provided in Section 5.

2 DESCRIPTION OF FIELD TESTS AND COMPUTER PROGRAMS USED FOR PREDICTIVE ANALYSES

This section provides a general description of the field tests and the test data which were provided to BNL by JNES. Also described in this section are the methods and associated computer programs employed for the correlation analysis to be performed in this report.

2.1 Description of Field Tests

Prior to the establishment of the Japan Nuclear Energy Safety Organization (JNES), the Nuclear Power Engineering Corporation (NUPEC) of Japan conducted a series of large-scale field tests for the Ministry of Economy, Trade and Industry (METI) of Japan to address various aspects of the soil-structure interaction (SSI) effect on the seismic response of nuclear power plant (NPP) structures. The experimental studies used several scaled models of nuclear power plant buildings, which were constructed at field sites typical of an actual NPP site. The following programs have been conducted by NUPEC since 1980:

1. Model Tests on Dynamic Interaction between Reactor Building and Soil (1980-1986) [Iguchi, 1987]
2. Model Test on Embedment Effect of Reactor Building (1986-1994) [Nasuda, 1991]
3. Model Test on Dynamic Cross-Interaction Effects of Adjacent Structures (1994-2002) [Kitada, 2001]

The field tests for the second and third programs listed above were performed at the same site which is located at the Higashi-dori site in Aomori Prefecture in the northern part of Honshu Island in Japan as shown in Figure 2-1, a region which experiences frequent seismic activities. Large-scale models with dynamic characteristics similar to typical NPP structures were constructed on the soils at this site which are representative of actual NPP sites. The third program, which is the subject of an earlier NUPEC-NRC collaborative study [Xu, 2003], made use of some of the model structures from the second program. Some of the recorded earthquake motions from the second program were also made available for use in this collaborative study to investigate the embedment effect on the in-structure response spectra (ISRS).

The Dynamic Cross-Interaction (DCI) tests were carried out by NUPEC as an 8-year project from Japanese fiscal year 1994 to 2002 (each fiscal year in Japan starts on April 1 of that year). The tests considered three building construction conditions: a) single reactor as reference for comparison purposes, b) closely spaced twin reactors, and c) a reactor and a turbine building in close proximity to each other. The field tests also considered both excavated and embedded foundations and two types of loading conditions: 1) forced vibrations and 2) observations of the structural response to real earthquake ground motions. The latter was accomplished by pre-installed seismometers in the structures and free field. Figure 2-2 shows the overall plan for the field tests.

To supplement the field tests, laboratory tests were also performed by NUPEC using a shaking table and smaller scaled DCI soil-structure models. The distance between

adjacent buildings and the adjacent effect of three closely constructed buildings were the main test parameters for these tests. These tests were carried out using 1/230-scale building models made of aluminum and an artificial ground model made of silicone rubber. The evaluation of these tests was not included in this collaborative study. Further information on these tests can be obtained in papers by Kitada [Kitada, 2001] and Hirotsu [Hirotsu, 2001].

Figure 2-3 depicts a plan layout of the NUPEC DCI field test models. The single reactor building is designated as Model AA, the closely constructed twin reactor buildings are designated as Models BAN and BAS, and the reactor and turbine building models are designated as Models DA and DF, respectively.

Although three different model-building configurations were utilized in the NUPEC tests, there are only two structurally distinct model buildings, namely, the reactor building and the turbine building. The reactor building is a three-story reinforced concrete structure (1/10th scale of outer structural dimensions similar to the typical reactor building in a commercial NPP in Japan). The building has dimensions of 8m by 8m in plan and 10.5m in height and weighs about 660 metric tons. The turbine building is a two-story reinforced concrete structure and is 6.4m by 10m in plan and 6.75m high and weighs about 395 metric tons. A cross section of the reactor and turbine building models is shown in Figure 2-4. The single reactor building is situated in the base of a pre-excavated pit of trapezoidal shape as shown in Figure 2-3 and Figure 2-5. For the single reactor building, the excavated pit is 10m by 10m in plan at the base and 20m by 20m in plan at the ground surface. The base of the pit is 5m below the ground surface with the sidewalls inclined at a 45-degree angle with the ground surface. The excavated pit for the twin-reactor building is located to the east of the single reactor building and has a rectangular opening of 10m by 18.6m at the base and 20m by 28.6 at the ground surface, and is 5m deep. The longer side of the pit is in the north-south direction (x-axis). As shown in Figure 2-3, the twin-reactor buildings are situated in the north-south direction at the base center of the pit with a gap of 0.6m between the two reactor buildings. The reactor-turbine buildings are situated in an excavated pit, which is located to the north of the twin reactor buildings and has an opening of 11m by 17.2m at the base and 19m by 25.2m at the surface. The pit is 4m deep and the basement of the reactor building is embedded into the base foundation by 1m as indicated by Figure 2-4. As shown in this figure, the gap between the reactor and the turbine buildings is 0.1m.

Photographs of the NUPEC field test models, both with and without embedment, are shown in Figure 2-6 through Figure 2-11.

The site geological features consist of primarily weathered-pyroclastic and pyroclastic rocks overlain by a 5-8m layer of overburden comprised of weathered sandstones and diluvial loams. The site water table is located between 7-10m from the ground surface. Ultrasonic wave tests were performed at the locations where the test models were built. In addition, the site geological features were examined. The locations of the boring points under the building models are shown in Figure 2-12. The soil profiles under the buildings, as shown in Figure 2-13 through Figure 2-15, indicate fairly horizontal uniformly layered soils across the site.

During the period of 1989-1999, the test site experienced 27 earthquake events with maximum free-field accelerations exceeding 10 gal (Note: 980 gal = 1g). Two of these events had recorded maximum free-field accelerations of over 100 gal. As part of the

US-Japan collaboration effort to investigate the DCI phenomenon, NUPEC provided the seismometer measurements of responses in both structures and free fields from eight earthquake events, including two major events with maximum free-field accelerations of 109 and 174 gal. Table 2-1 summarizes these events with respect to their occurrence time, source location, magnitude, epicenter and focal distances from the site, as well as maximum acceleration induced in the free field. A study [Xu, 2003] was performed by BNL to assess the current regulatory approach to accounting for local soil uncertainty in the computation of seismic induced ISRS. This study was carried out using the SASSI program and the procedure outlined in the NRC standard review plan [NUREG-0800, 1989] for soil uncertainty consideration to predict the earthquake data (the recorded ISRS) afforded by NUPEC. For the earthquake events provided, BNL analyses had shown that the regulatory procedure of accounting for soil uncertainty in SSI ISRS calculations are conservative.

As part of the NRC program under JCN Y-6718, BNL performed studies to investigate the seismic characteristics of deeply embedded and/or buried (DEB) structures and analysis methods for quantifying their effects. The primary aim of the BNL methodology assessment [Xu, 2005] is the capability of the SSI methodologies to capture seismic induced passive soil pressure response, in addition to the seismic induced ISRS. At the request of NRC, JNES (part of NUPEC was integrated with some other organizations to establish a new organization called JNES) furnished the recorded response data due to the earthquake event No. 172, including both ISRS and the seismic induced earth pressures on the test structures which are the source of the subject study summarized in this report.

Of the earthquakes listed in Table 2-1, the seismic induced soil pressures were recorded for only one event (No. 172). As indicated by the note for Figure 2-16, even though the backfill of the excavations was completed for the test structures, the event No. 164 occurred before the installation for the recording instruments for pressures was completed for the test structures. As provided in Table 2-1, the maximum acceleration of the free field induced by the event No. 172 is less than 14 gal, which is a small ground motion and unlikely to induce any non-linear response in the test structures. However, this small level ground motion is suitable for checking linear analysis methods, especially for the computation of seismic induced passive pressures.

Figure 2-17 through Figure 2-21 provide the locations and designations of the pressure sensors which were installed on the test structures. Since the recorded event was small, very few sensors actually recorded the seismic pressures. While the symbols of circles represent the locations of the installed pressure sensors, only the solid circles represent the sensors which have recorded the earthquake induced soil pressure data. Of the three test configurations, the data recorded for the single reactor structure (designated as AA) do not resemble earthquake response and appear to be completely masked by the noise of the instrument. Therefore, the AA structure was removed from the BNL study.

2.2 Computer Programs Used for Predictive Analyses

2.2.1 SASSI Sub-structuring Method for SSI Responses

One of the numerical models developed for the predictive SSI analysis of the JNES test data uses the sub-structuring method as implemented in SASSI2000, which was developed by Lysmer and his team at U.C. Berkeley [Lysmer, 1981 and 1999]. The

SASSI program has gone through extensive improvement in recent years, especially SASSI 2000. In addition to the sub-structuring methods such as the flexible volume, flexible boundary and rigid boundary methods as in the previous versions, SASSI 2000 implemented a subtraction method, which the BNL study used to carry out the SSI response calculations for the JNES test structures. Given the overwhelming amount of SSI calculations required for the BNL study, it would have been an insurmountable task without using the subtraction method. The subtraction method has proven to be quite an efficient algorithm with no compromise for quality for the SSI response calculations. This sub-section describes briefly the basic approach in the sub-structuring methods, with special emphasis on the subtraction method. The material used in the following discussion was drawn primarily from the SASSI 2000 theoretical manual [Lysmer, 1999].

The sub-structuring approach divides the SSI problem into several sub-problems including: 1) the site response problem (the free field with the absence of structure), 2) the scattering problem, 3) the impedance problem, and 4) the structural response problem. For the rigid and flexible boundary methods, since the embedment is explicitly modeled in the free field, all four sub-problems are required to be solved. While for the flexible volume and subtraction methods, the scattering problem is not required due to the use of superposition to avoid explicit modeling of the embedment in the free field; although the other three sub-problems are still needed to be solved. However, the treatment of impedance analysis for the flexible volume and subtraction methods is quite different from the rigid and flexible boundary methods. The impedance is computed for the rigid and flexible boundary methods in the free field with the indentation of the structural embedment. For the flexible volume and subtraction methods, the impedance is calculated in the free field without the indentation of the structural embedment, therefore significantly simplifying the SSI problem.

In contrast to the impedance treatment for the flexible volume method which computes the impedance at every nodal point within the embedment, the newly implemented subtraction method recognizes that the soil-structure interaction takes place only at the common boundary of the soil and the structure, and formulates the dynamic equations of motion in such a way that the interior nodes of the embedment are eliminated. Therefore, for the subtraction method, the impedance is computed only for the interfacing nodes of the soil and the structure, resulting in significant savings in computing time. In addition, the site response calculation for the subtraction method is performed only for the interaction nodes as opposed to all nodes within the embedment for the flexible volume method. This results in additional savings for the subtraction method. For a more detailed description, the reader is referred to the SASSI 2000 theoretical manual.

The treatment of damping in SASSI is to use the material damping in the formulation. The advantage of the material damping is that the damping is frequency independent and is easily implemented in a frequency domain analysis which modifies the stiffness term by $(1+i2\xi)$, where ξ represents the material damping and i is equal to $(-1)^{1/2}$. The material damping also affects the stress calculations since the same damping term is used to modify the Young's and shear moduli, which is different from other representations of damping which only affects the motion parameters but not the stress computations.

Because of the frequency domain solution algorithm employed by SASSI, which implies application of the principle of superposition, the SASSI code is limited mainly to linear problems. As discussed previously, the earthquake No.172 is a small ground motion

event which is not expected to induce any non-linear effect on the site. Therefore, SASSI is an appropriate code to be used in this context. However, to assess the aspect of the SASSI capability in addressing strong earthquake induced non-linear SSI phenomena, strong ground test data are required, which are scarcely limited to date.

2.2.2 LS-DYNA Method for SSI Responses

The second numerical model used for the predictive SSI analysis is LS-DYNA [LSTC, 2001], which is a code that operates in time domain as opposed to the frequency domain programs such as SASSI, but is specialized for non-linear problems, including both the material non-linearity and the geometric non-linearity effects. LS-DYNA is a general-purpose transient dynamic finite element (FE) program capable of simulating complex real world problems. Its versatility and reliability for modeling a wide spectrum of different physical problems makes it popular in applications such as: crashworthiness, occupant safety, metal forming and cutting, biomedical, blast loading, fluid-structure interaction, and earthquake engineering. LS-DYNA has extensive element and material libraries as well as well-defined interfaces, which are suitable for the non-linear effects such as separation of the foundation walls from the surrounding soil and large strains in soils that are expected in a strong ground event.

A key aspect associated with DEB structures is the interaction effect at the interface between the part of the structure below grade and the surrounding soils. The conventional linear analyses, such as SASSI, typically assume perfect bonding between the structure and the surrounding soils. Therefore, such analyses are incapable of addressing the non-homogeneous behavior of soils, as well as the possible separation effect occurring at the soil-structure interface. However, unlike SASSI which uses a closed form solution to address the wave propagations in the half-space, LS-DYNA must resort to an approximate approach to this issue. Since LS-DYNA can only model the physical world with explicit finite elements, the half-space wave propagation problem has to be modeled with a finite domain with a transmitting boundary to ensure that the outgoing waves are not reflected.

The LS-DYNA models developed in the BNL study fall into the category of continuum models. While following the philosophy of the direct method, the LS-DYNA models are developed in the 3-dimensional domain. The soil and structure are modeled with explicit FEs, and the boundaries of the FE soil model are connected with a series of viscous dampers which are to ensure non-reflection of outgoing waves. In LS-DYNA, the approach used by Cohen and Jennings [Cohen, 1983] who in turn credited the method to Lysmer and Kuhlemeyer [Lysmer, 1969] was implemented, in which viscous normal and shear stresses are applied to the boundaries in a manner as defined in the following equations:

$$\sigma_{\text{normal}} = -\rho c_d V_{\text{normal}}$$

$$\sigma_{\text{shear}} = -\rho c_s V_{\text{tangential}}$$

where ρ , c_d , and c_s are the material density, material longitudinal and shear wave velocities of the transmitting media. These equations reveal that the magnitude of these stresses at the boundaries is proportional to the particle velocities in the normal, (V_{normal}) and tangential, ($V_{\text{tangential}}$) directions.

The Lysmer's dampers placed on the artificial boundary are effective in reducing unwanted wave reflections if the boundary of the finite element mesh is sufficiently far outward. However, in doing so, the size of the near field finite element mesh is increased significantly and so is the cost of running the dynamic analysis. The exact stress field on the soil boundary of the given problem is a function of frequency dependent dampers and springs. As shown by Wolf [Wolf, 1999], the springs dominate the boundary stress field in low frequencies and near field, and as the frequency and the mesh boundary approaches infinity, the boundary stress field becomes a function of dampers only. Therefore, for a finite mesh of the unbounded soil medium, an improved transmitting boundary can be developed by applying a combination of springs and dampers to the boundary.

Wolf [Wolf, 2000] and Luco [Luco, 2004] have proposed such advanced transmitting boundaries, which can be incorporated in codes that are amenable to source changes. In the BNL predictive analysis, the soil mesh for the LS-DYNA models is extended sufficiently far outward from the structure to negate the impact of not including the springs in the transmitting boundary. In addition to the transmitting boundary, a circular boundary is placed on the lateral end of the soil mesh to ensure proper wave propagation near the boundary and to avoid the so called "corner effect" which would occur if a rectangular boundary is imposed on the mesh.

The treatment of damping in the LS-DYNA analysis by BNL is to apply the Rayleigh damping to different material parts. This approach requires specification of two end frequencies for each material group encompassing the frequency range of interest to the analysis. The LS-DYNA User's Manual [LSTC, 2001] provides a guidance for the choice of these end frequencies. Since the damping is of viscous type, it should affect the computation of the motion parameters only, but not the stress calculations.

In computing the seismic induced soil pressure, an important consideration and a real challenge is how to represent the structure-soil interface as close as possible to the real situation. For the linear response, the bonding between the soil and the wall is not expected to break. Therefore, perfect bonding is reasonable assumption for the SSI model. This type of the interface condition is modeled in LS-DYNA using the LS-DYNA keyword `*CONTACT_TIED_SURFACE_TO_SURFACE`. The effect of the tied interface is to ensure that soil and the structure move together at the interface, so that nonlinearity due to the soil/structure interface opening does not occur. This modeling approach is employed in this report for the LS-DYNA models.

Although not utilized in the analysis summarized in this report, it is informative to state that LS-DYNA has other interface models which can be used to represent many soil/structure interface conditions that are expected to occur during strong ground motion events, notably the separation and slipping between the soil and the structure. One approach to modeling these non-linear effects is to use the LS-DYNA keyword `CONTACT_AUTOMATIC_SURFACE_TO_SURFACE`. The contact interface permits opening/closing and slipping at the soil/structure interface, which induces the effect of geometrical nonlinearity in the SSI model. The contact interface model is considered more realistic from a theoretical viewpoint. Practically speaking, however, the nonlinearity which is associated with the use of the contact interface requires more delicate treatment in developing the SSI model. Any mishandling could potentially trigger other numerical issues that may compromise the analysis result.

Table 2-1 Earthquake Events Recorded at the Field Test Site

Earthquake No.	Earthquake Occurrence Time	Source Location		Earthquake Magnitude (M)	Epicenter/Focal Distance (km)	Max old free field point acceleration GL-1.5m (gal)		Max new free field point acceleration GL-3.0m (gal)	
		East Longitude	North Latitude			NS	EW	NS	EW
34	03-05-1991	141'41.0	41'16.0	4	28/46	15.8	9.6		
89	12-28-1994	143'43.3	40'27.1	7.5	213/213	123.0	174.0		
131	02-17-1996	141'23.0	40'47.0	4.6	43/45	15.9	17.3	15.1	13.3
139	02-20-1997	142'52.0	41'45.0	5.6	140/146	9.3	8.9	11.4	11.6
157	01-03-1998	142'04.0	41'28.0	5.1	66/89	28.5	26.7	20.8	30.2
63	01-15-1993	144'23.0	42'51.0	7.8	294/310	109.0	98.0		
164	11-07-1998	142'03.0	41'34.0	4.6	71/95	8.9	8.5	6.3	10.8
172	05-11-1999	143'55.0	42'57.0	6.4	288/305	13.5	13.6	13.3	10.8

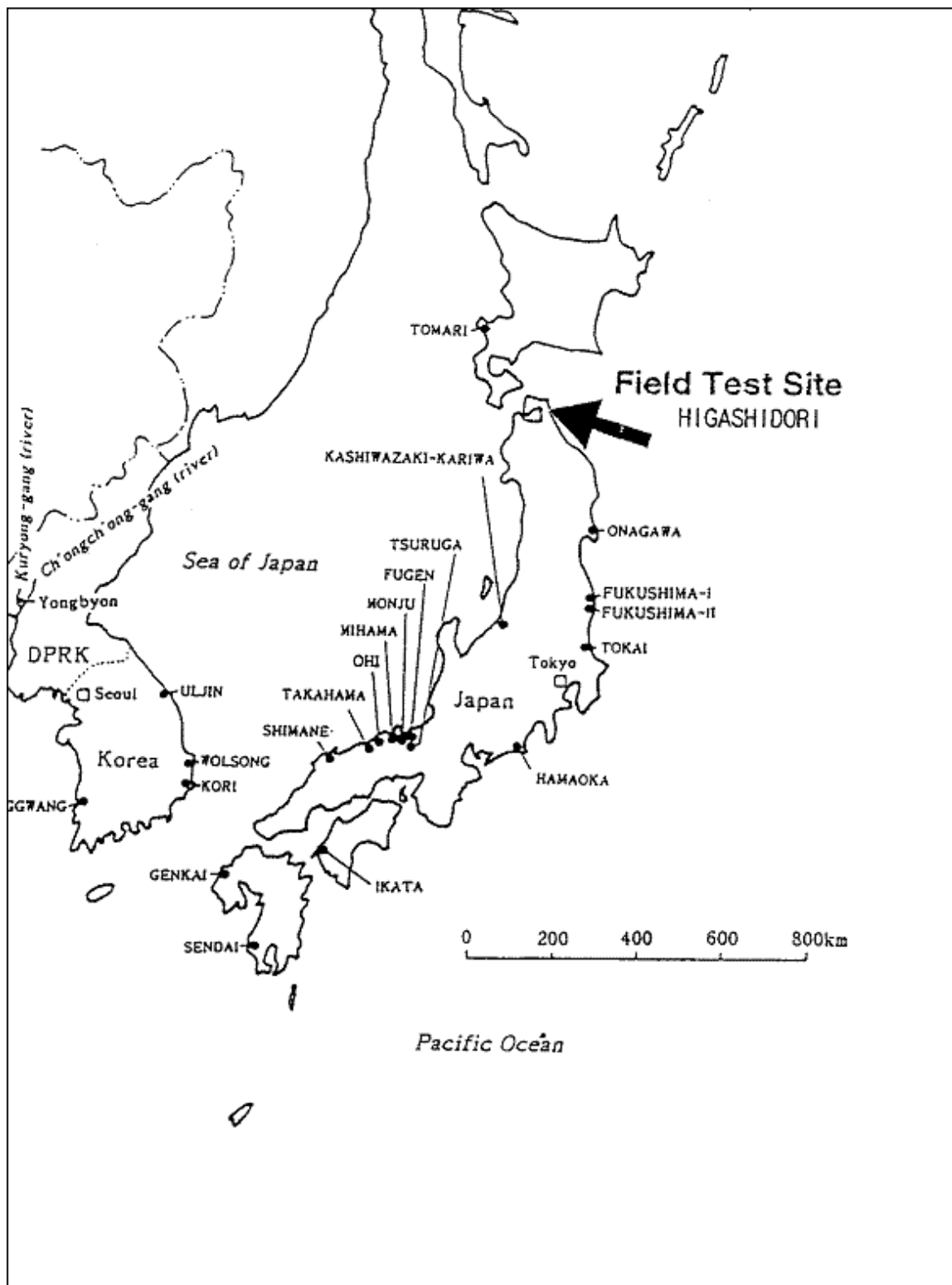


Figure 2-1 Location of Field Test Site in Japan

Source: J. Xu, C. Costantino and C. Hofmayer, *Collaborative Study of NUPEC Seismic Field Test Data for NPP Structures*, NUREG/CR-6822, U.S. Nuclear Regulatory Commission, Washington, DC, June 2003.


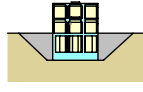
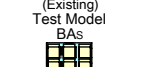
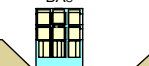


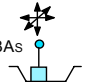
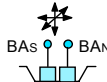
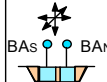
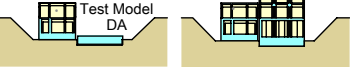
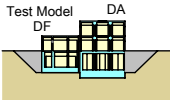
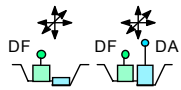
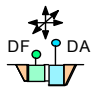
		PHASE-1				PHASE-2			
		FY 1994	FY 1995	FY 1996	FY 1997	FY 1998	FY 1999	FY 2000	FY 2001
Location A		(Existing) Test Model AA 				Test Model AA 		Overall evaluation	
single building	construct								
	Eavthquake observation		Single building, Without embedment			Single building, With embedment			
Location B		(Existing) Test Model BA _s 	Test Model BA _s 	Test Model BA _s Test Model BA _N 		Test Model BA _s Test Model BA _N 			
2 identical buildings	construct								
	Excitation Tests								
	Eavthquake observation	single building, Without embedment	single building, Without embedment	2 buildings, Without embedment		2 buildings, With embedment			
Location D				Test Model DF Test Model DA 		Test Model DF Test Model DA 			
2 different buildings	construct								
	Excitation Tests								
	Eavthquake observation			single building, Without embedment 2 buildings, Without embedment					

Figure 2-2 Overall Plan for Field Tests

Source: J. Xu, C. Costantino and C. Hofmayer, *Collaborative Study of NUPEC Seismic Field Test Data for NPP Structures*, NUREG/CR-6822, U.S. Nuclear Regulatory Commission, Washington, DC, June 2003.

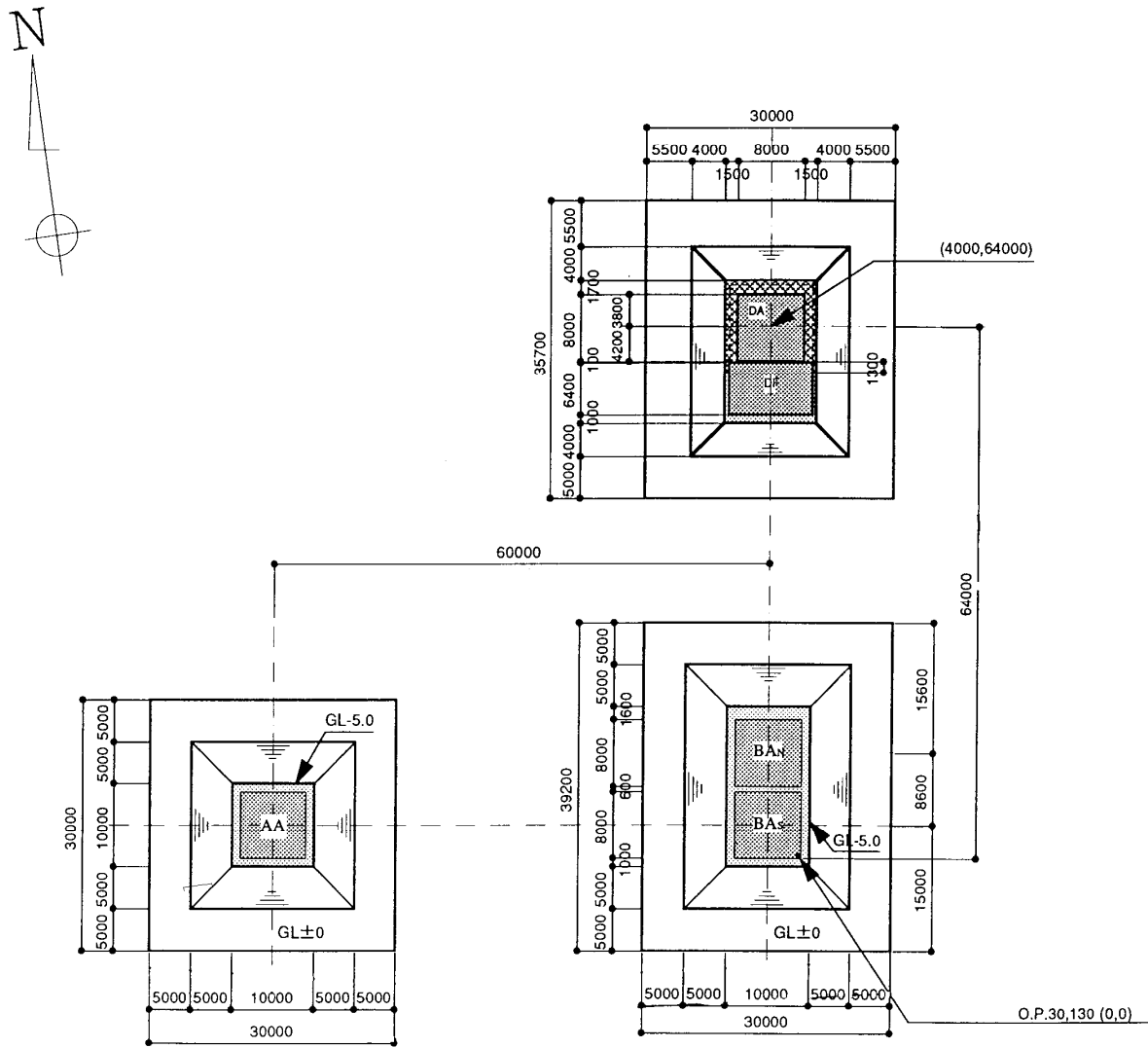


Figure 2-3 Layout of Models at Field Test Site [unit: mm; GL : m]

Source: J. Xu, C. Costantino and C. Hofmayer, *Collaborative Study of NUPEC Seismic Field Test Data for NPP Structures*, NUREG/CR-6822, U.S. Nuclear Regulatory Commission, Washington, DC, June 2003.

Figure 2-4 Cross Section of Reactor and Turbine Building Model [unit: mm]

Source: J. Xu, C. Costantino and C. Hofmayer, *Collaborative Study of NUPEC Seismic Field Test Data for NPP Structures*, NUREG/CR-6822, U.S. Nuclear Regulatory Commission, Washington, DC, June 2003.

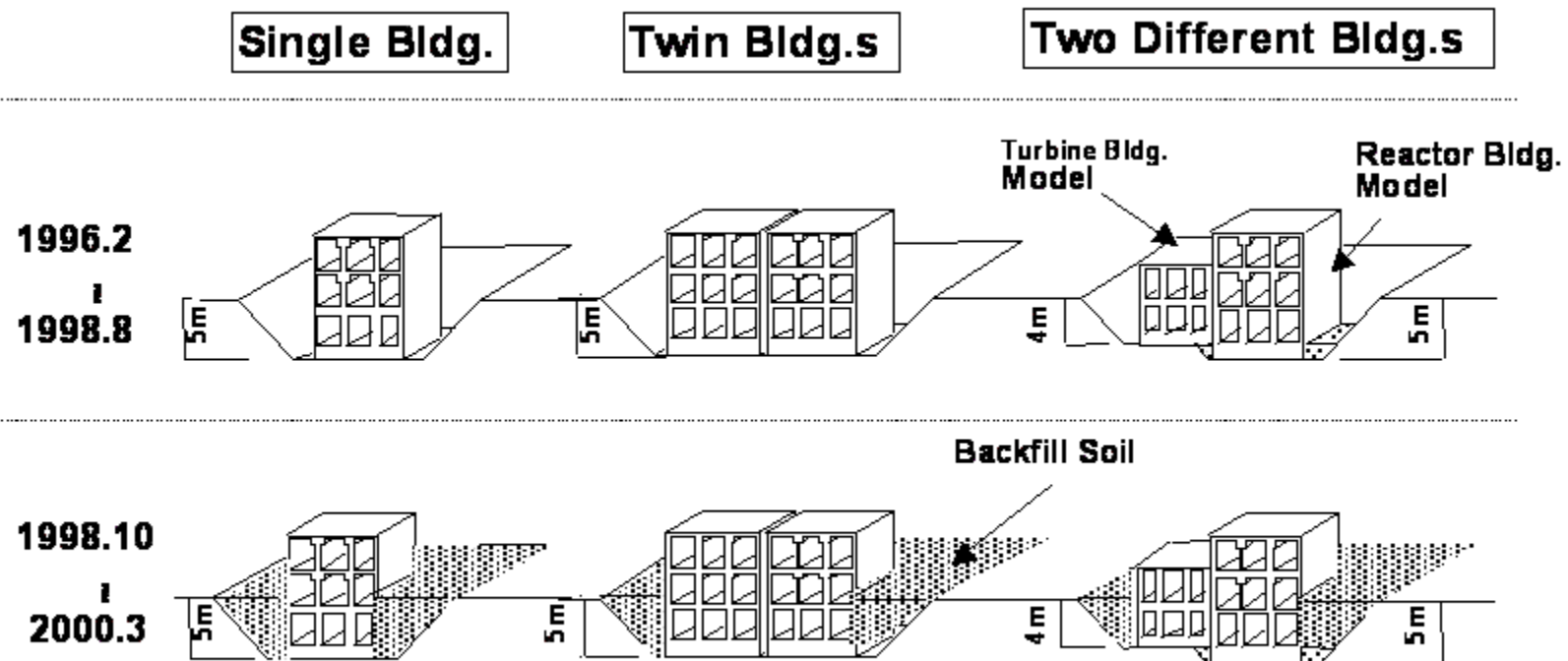


Figure 2-5 Embedment Conditions for the Building Models

Source: J. Xu, C. Costantino and C. Hofmayer, *Collaborative Study of NUPEC Seismic Field Test Data for NPP Structures*, NUREG/CR-6822, U.S. Nuclear Regulatory Commission, Washington, DC, June 2003.



Figure 2-6 NUPEC Field Test Model of Reactor Building without Embedment

Source: J. Xu, C. Costantino and C. Hofmayer, *Collaborative Study of NUPEC Seismic Field Test Data for NPP Structures*, NUREG/CR-6822, U.S. Nuclear Regulatory Commission, Washington, DC, June 2003.



Figure 2-7 NUPEC Field Test Model of Adjacent Twin Reactor Buildings without Embedment

Source: J. Xu, C. Costantino and C. Hofmayer, *Collaborative Study of NUPEC Seismic Field Test Data for NPP Structures*, NUREG/CR-6822, U.S. Nuclear Regulatory Commission, Washington, DC, June 2003.

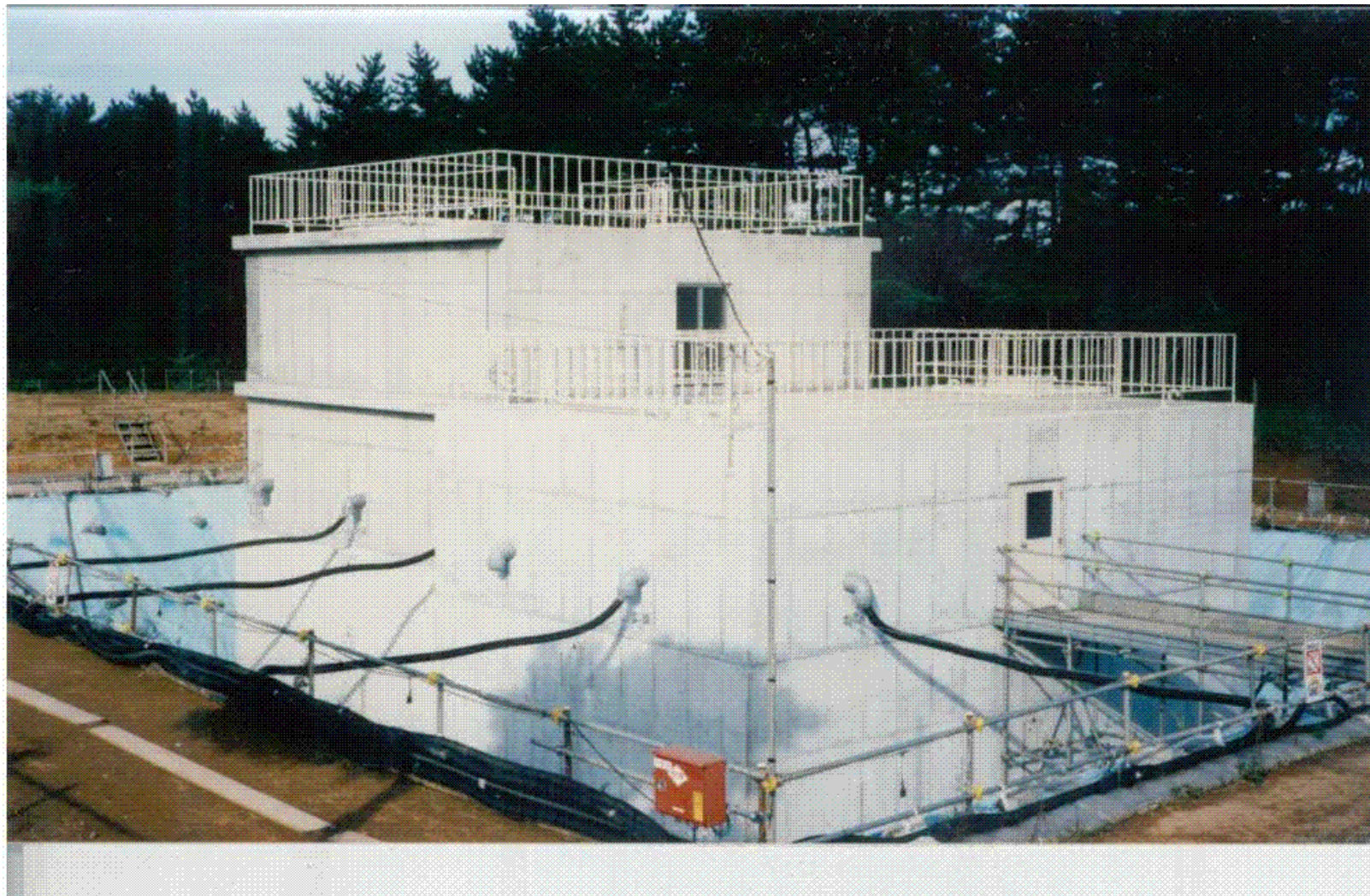


Figure 2-8 NUPEC Field Test Model of Adjacent Reactor -Turbine Buildings without Embedment

Source: J. Xu, C. Costantino and C.Hofmayer, *Collaborative Study of NUPEC Seismic Field Test Data for NPP Structures*, NUREG/CR-6822, U.S. Nuclear Regulatory Commission, Washington, DC, June 2003.



Figure 2-9 NUPEC Field Test Model of Reactor Building with Embedment

Source: J. Xu, C. Costantino and C. Hofmayer, *Collaborative Study of NUPEC Seismic Field Test Data for NPP Structures*, NUREG/CR-6822, U.S. Nuclear Regulatory Commission, Washington, DC, June 2003.



Figure 2-10 NUPEC Field Test Model of Adjacent Twin Reactor Buildings with Embedment

Source: J. Xu, C. Costantino and C. Hofmayer, *Collaborative Study of NUPEC Seismic Field Test Data for NPP Structures*, NUREG/CR-6822, U.S. Nuclear Regulatory Commission, Washington, DC, June 2003.



Figure 2-11 NUPEC Field Test Model of Adjacent Reactor-Turbine Buildings with Embedment

Source: J. Xu, C. Costantino and C. Hofmayer, *Collaborative Study of NUPEC Seismic Field Test Data for NPP Structures*, NUREG/CR-6822, U.S. Nuclear Regulatory Commission, Washington, DC, June 2003.

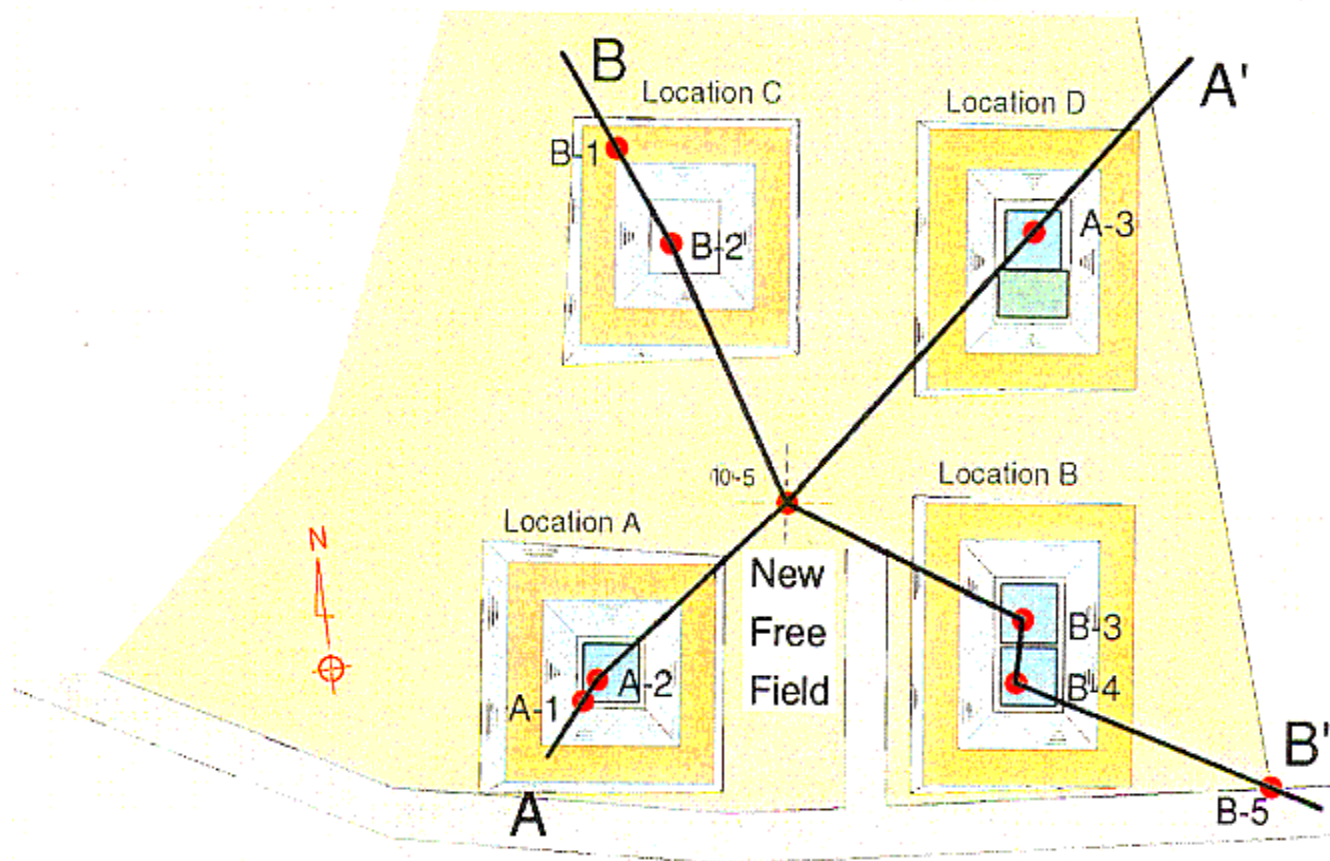


Figure 2-12 Location of Boring Points under Building Models and Cross Sections for Soil Profiles

Source: J. Xu, C. Costantino and C. Hofmayer, *Collaborative Study of NUPEC Seismic Field Test Data for NPP Structures*, NUREG/CR-6822, U.S. Nuclear Regulatory Commission, Washington, DC, June 2003.

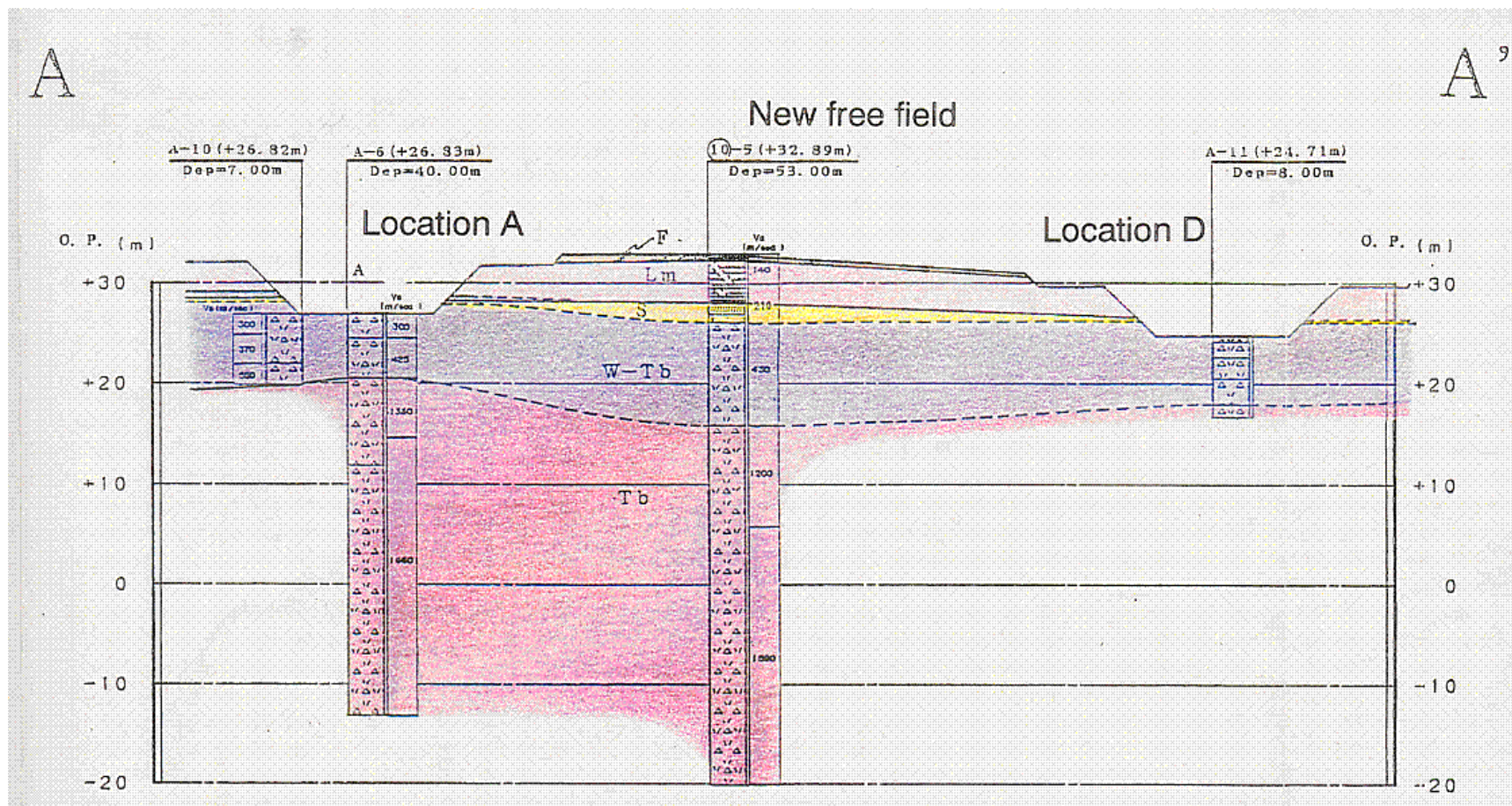


Figure 2-13 Soil Profile for Section A-A (Refer to Figure 2-12 for Section Location)

Source: J. Xu, C. Costantino and C. Hofmayer, *Collaborative Study of NUPEC Seismic Field Test Data for NPP Structures*, NUREG/CR-6822, U.S. Nuclear Regulatory Commission, Washington, DC, June 2003.

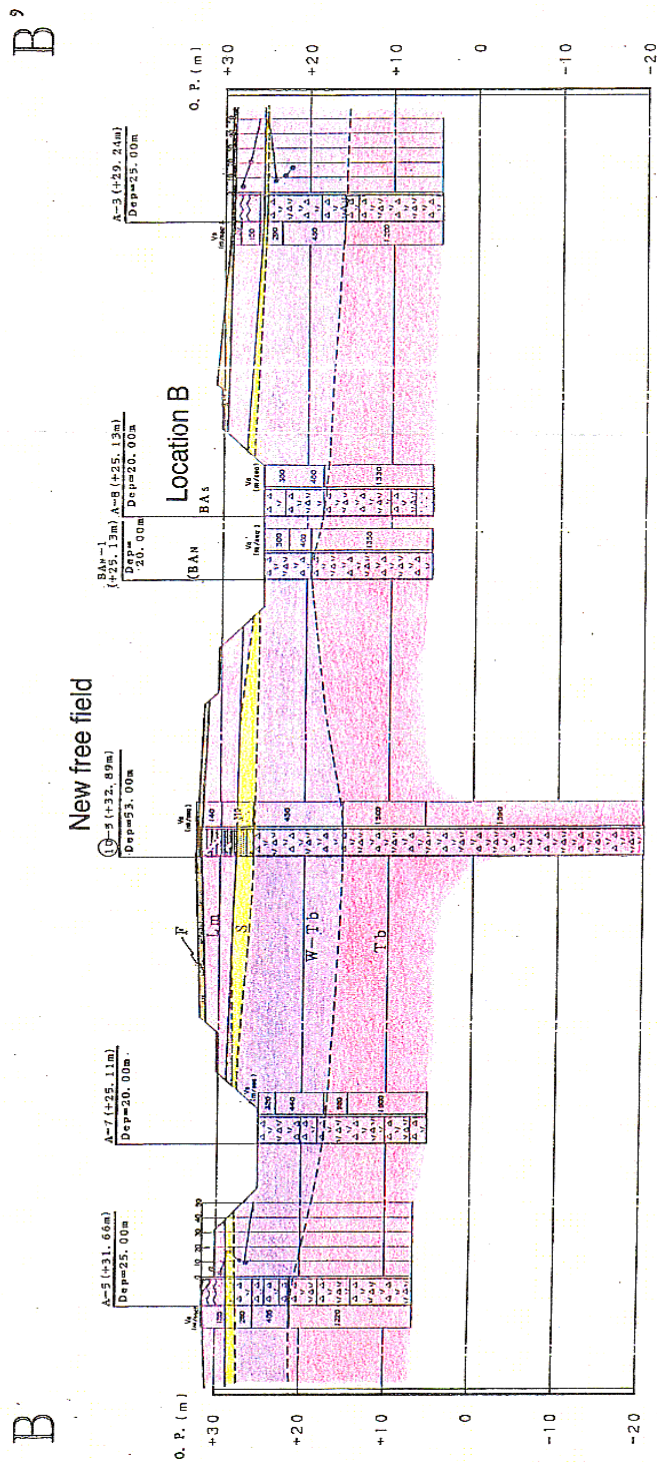


Figure 2-14 Soil Profile for Section B-B (Refer to Figure 2-12 for Section Location)

Source: J. Xu, C. Costantino and C. Hofmayer, *Collaborative Study of NUPEC Seismic Field Test Data for NPP Structures*, NUREG/CR-6822, U.S. Nuclear Regulatory Commission, Washington, DC, June 2003.

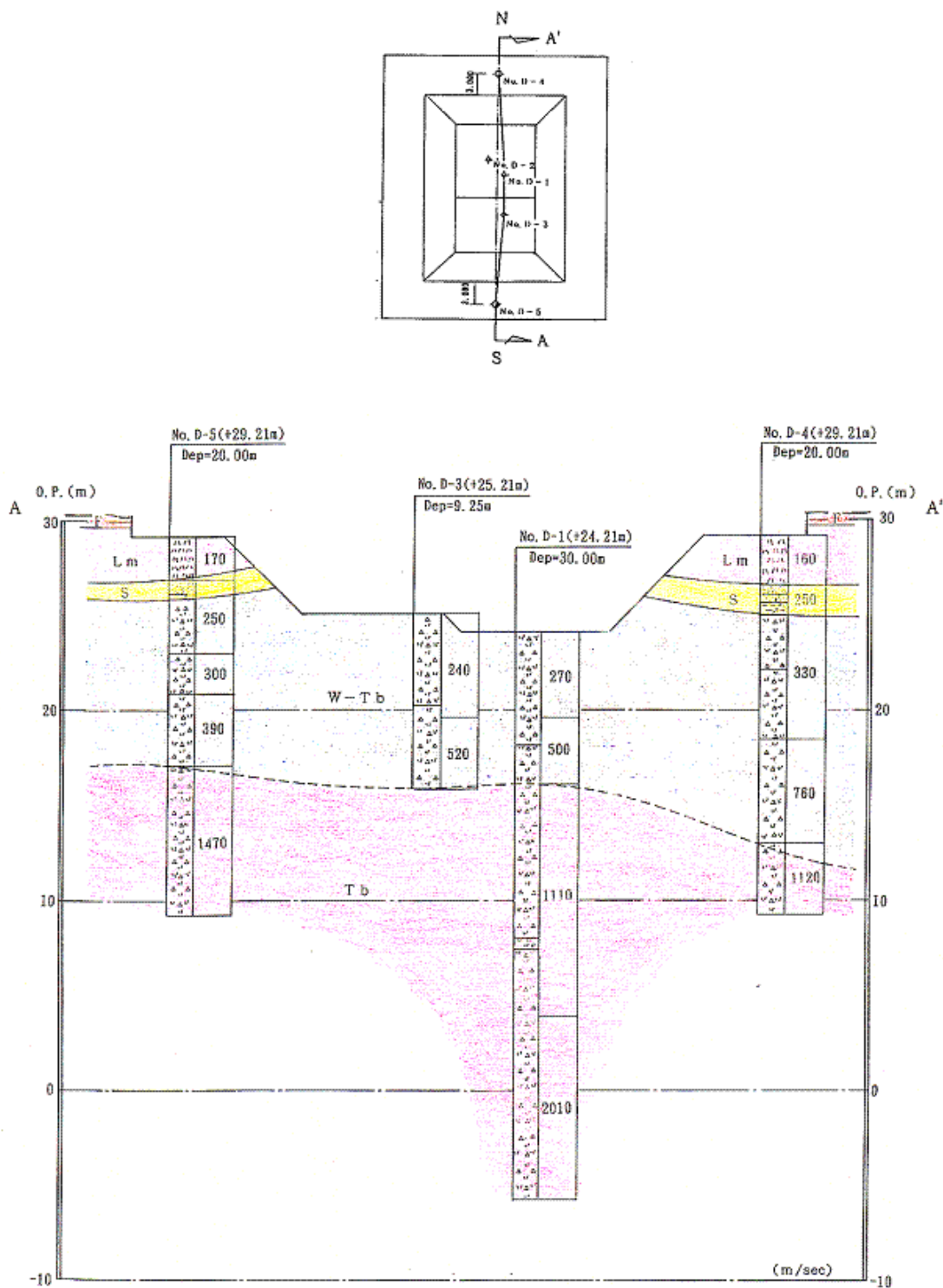
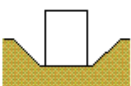

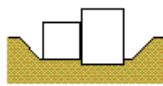
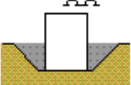




Figure 2-15 Soil Profile for Reactor-Turbine Buildings

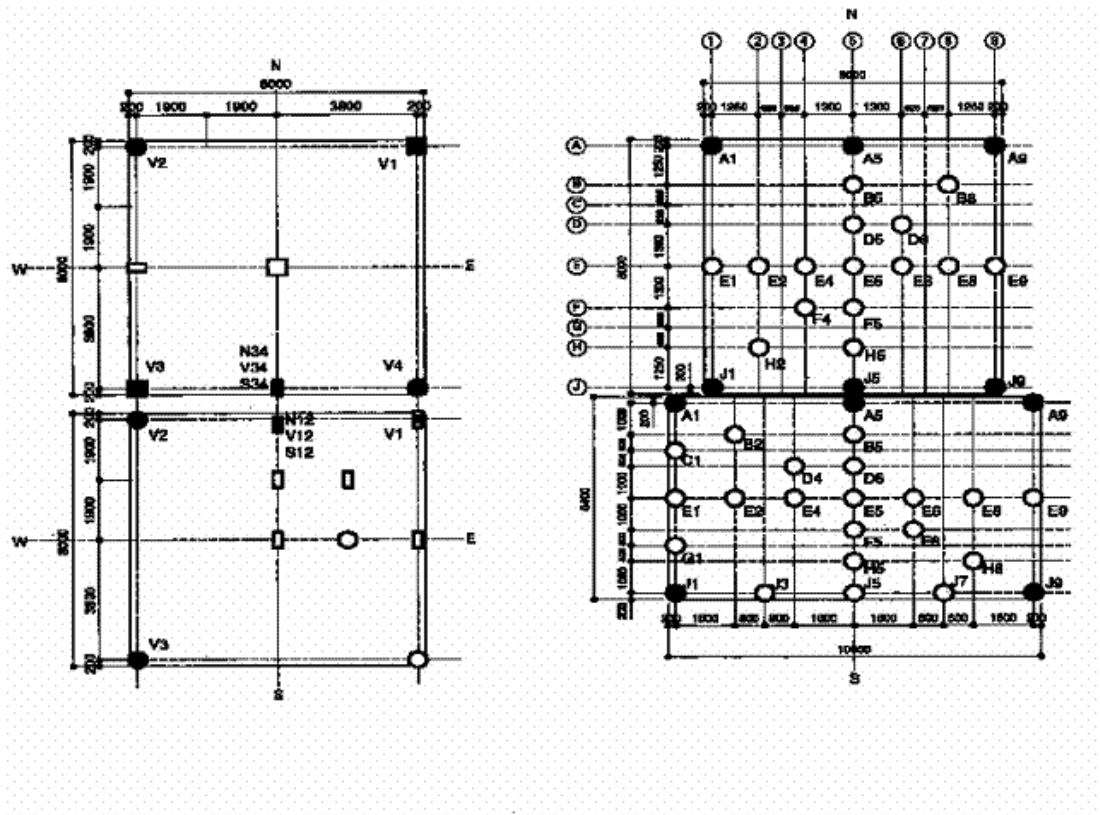
Source: J. Xu, C. Costantino and C. Hofmayer, *Collaborative Study of NUPEC Seismic Field Test Data for NPP Structures*, NUREG/CR-6822, U.S. Nuclear Regulatory Commission, Washington, DC, June 2003.

Test Case	Earthquake No., Date, Name	Location A	Location B	Location D
DCI Test	1 No. 157 1998/01/03 Aomori-ken Toho Oki	AA  Without embedment	BA _s BA _n  Without embedment	DF DA  Without embedment
	2 No. 164 1998/11/07 Urakawa Oki	AA  With embedment	BA _s BA _n  With embedment	DF DA  With embedment
	3 No. 172 1999/05/13 Kushiroshicho Chunanbu	ditto	ditto	ditto

Note: No.164 earthquake occurred before measuring systems of side earth pressure were ready.

Figure 2-16 Test Configurations for Seismic Induced Earth Pressures

Source: *Earth Pressure Data of Dynamic Cross Interaction Test*, Technical Report, Japan Nuclear Energy Safety Organization (JNES), Tokyo, Japan, April 2004. Permission to use this copyrighted material is granted by JNES.



BAn, BAs

DA, DF

Designated Sensor Name: BAN-BE-xxx,
BAS-BE-xxx

Designated Sensor Name: DA-BE-xxx,
DF-BE-xxx

Figure 2-17 Locations of Pressure Sensors for the Test Structures under the Basemat [unit: mm]

Source: *Earth Pressure Data of Dynamic Cross Interaction Test*, Technical Report, Japan Nuclear Energy Safety Organization (JNES), Tokyo, Japan, April 2004. Permission to use this copyrighted material is granted by JNES.

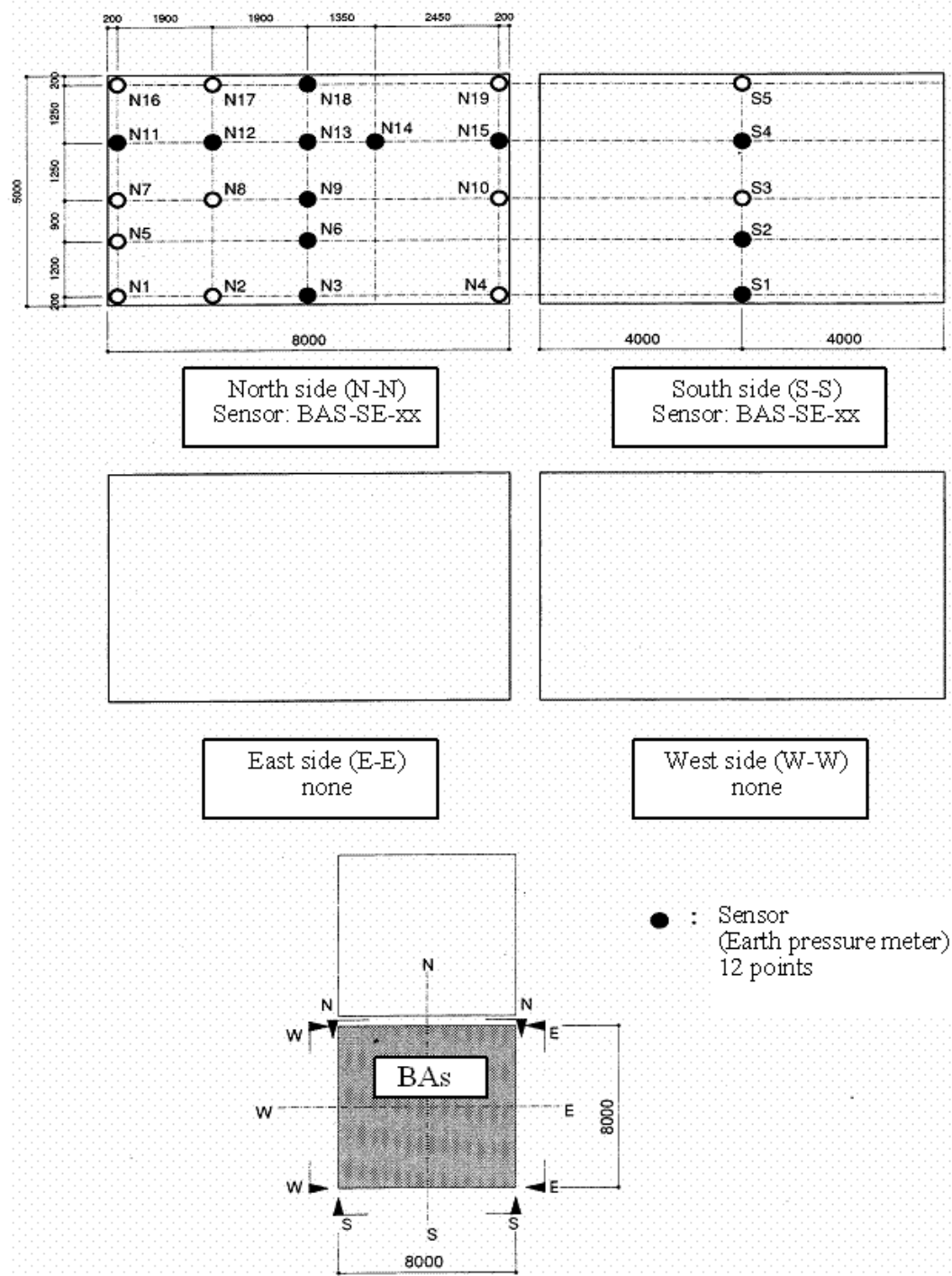


Figure 2-18 Locations of Pressure Sensors for the BAs Structure on Side Wall
[unit: mm]

Source: *Earth Pressure Data of Dynamic Cross Interaction Test*, Technical Report, Japan Nuclear Energy Safety Organization (JNES), Tokyo, Japan, April 2004. Permission to use this copyrighted material is granted by JNES.

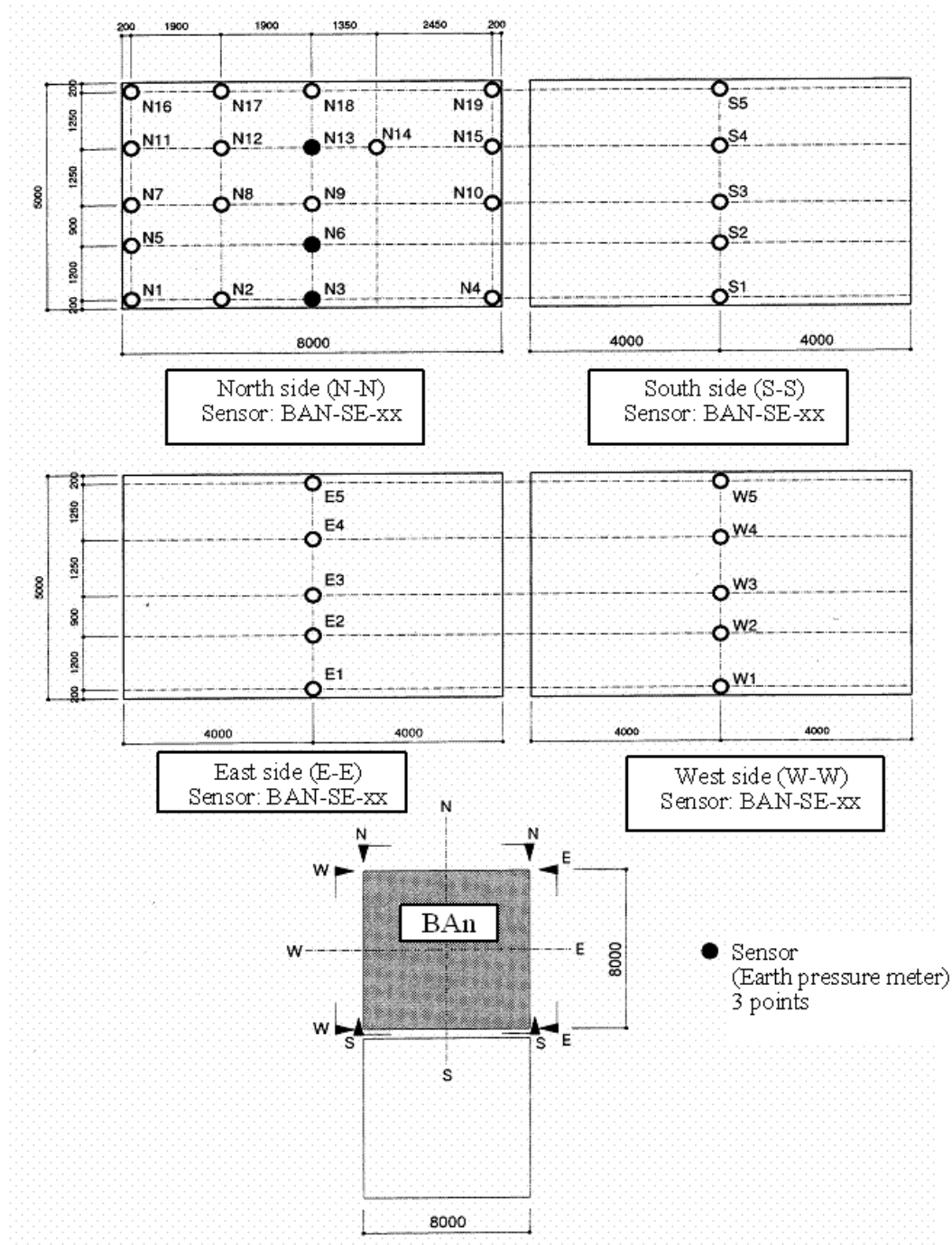


Figure 2-19 Locations of Pressure Sensors for the BAn Structure on Side Wall
[unit: mm]

Source: *Earth Pressure Data of Dynamic Cross Interaction Test*, Technical Report, Japan Nuclear Energy Safety Organization (JNES), Tokyo, Japan, April 2004. Permission to use this copyrighted material is granted by JNES.

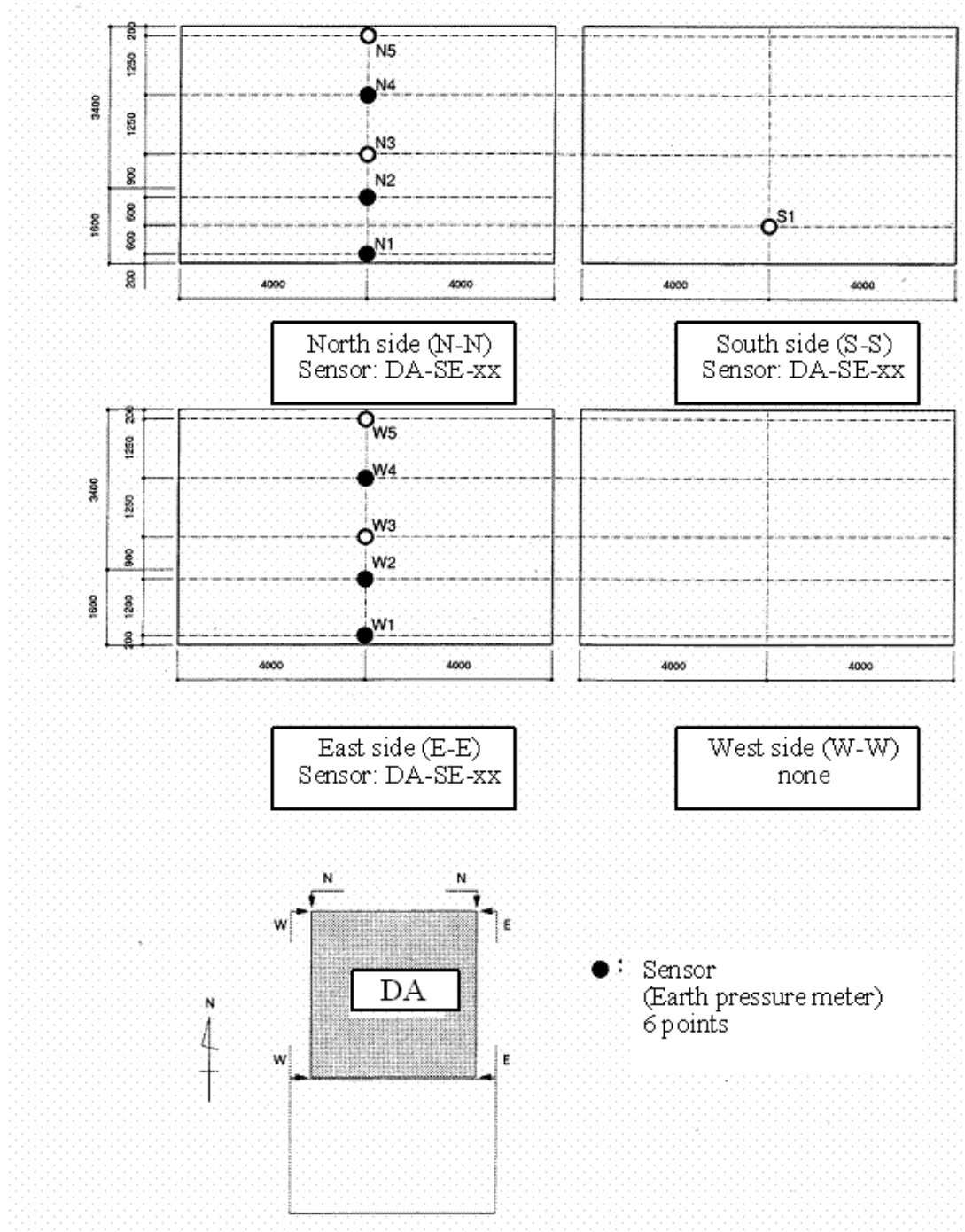


Figure 2-20 Locations of Pressure Sensors for the DA Structure on Side Wall
[unit: mm]

Source: *Earth Pressure Data of Dynamic Cross Interaction Test*, Technical Report, Japan Nuclear Energy Safety Organization (JNES), Tokyo, Japan, April 2004. Permission to use this copyrighted material is granted by JNES.

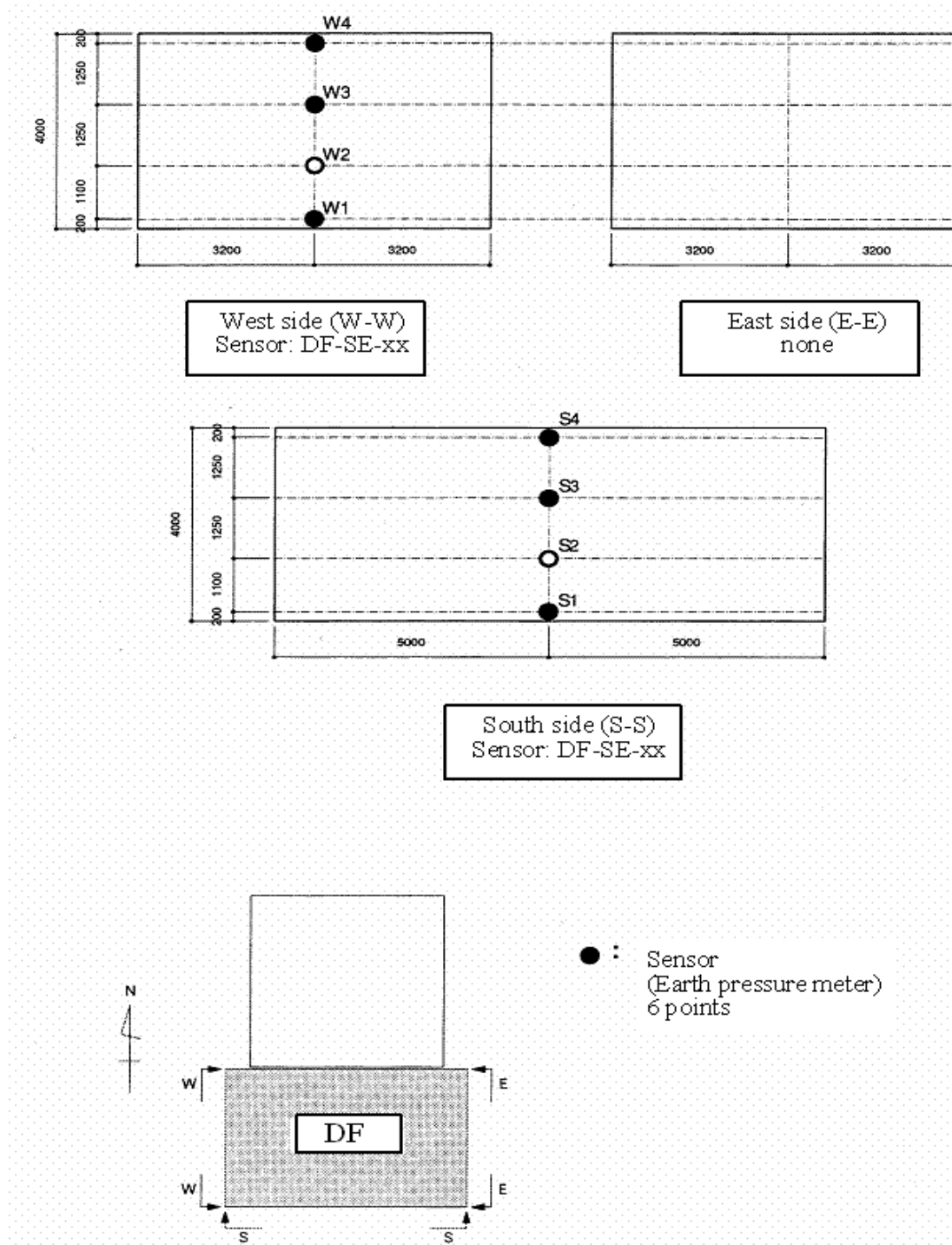


Figure 2-21 Locations of Pressure Sensors for the DF Structure on Side Wall
[unit: mm]

Source: *Earth Pressure Data of Dynamic Cross Interaction Test*, Technical Report, Japan Nuclear Energy Safety Organization (JNES), Tokyo, Japan, April 2004. Permission to use this copyrighted material is granted by JNES.

3 SASSI ANALYSIS

This section describes the correlation analysis of the JNES test structures using SASSI. The analysis is performed for two configurations. One configuration has two identical reactor buildings (Twin reactor model) located in close proximity to each other, and the second configuration consists of a reactor building and a turbine building in close proximity (R-T model). The SASSI analysis models are described first, followed by the discussion of the results of comparisons with the JNES recorded data, and a performance assessment of the SASSI analysis.

3.1 Twin-Reactor Configuration

3.1.1 Test Modeling Description

The twin reactor configuration consists of two identical three-story reinforced concrete structures ($1/10^{\text{th}}$ scale of outer structural dimensions similar to the typical ABWR reactor buildings in Japan). The building has dimensions of 8m by 8m in plane and 10.5m in height, and weighs about 660 metric ton. The space between the buildings is 0.6m.

The soil profile including backfills which are used by the BNL analysis is shown in Figure 3.1-1. The soil properties shown in this figure were provided by JNES, and are considered as the low strain best-estimate (to be referred to as the mean property in the BNL analysis). Since the earthquake event to be analyzed is not expected to excite large strain responses, the soil properties in Figure 3.1-1 are directly applied in the SASSI analysis.

The location and designation of seismometers installed on the twin reactor structures are shown in Figure 3.1-2. Dimensions applied in this figure are units in terms of millimeters. As shown in this figure, the seismometers within soil away from the structures are designated as SA-NS1 for the horizontal direction and SA-V1 for the vertical direction. They are located directly underneath the twin structural basemat about 13.2m below the ground surface. The 5% damped response spectra for the accelerations recorded by these two channels are plotted in Figure 3.1-3 and are used as the input motions to the BNL SASSI analyses.

Figure 3.1-4 and Figure 3.1-5 show the analysis model generated using the SASSI 2000 program. As depicted in Figure 3.1-4, the twin reactors and the surrounding soils are modeled in detailed finite elements. For the reactors, the portion located below the ground surface is modeled with explicit finite elements (e.g., 3-D bricks, shells and beams), while the superstructure above the ground surface is represented with simple lumped masses and 3-D beams. Three layers of brick elements were used to represent the soils that surround the structures. The purpose of using the soil brick elements is to compute the seismic induced soil pressure on the structures. It is done by calculating the stress component directly from the soil brick elements, which is perpendicular to the structural wall. Since the sub-structuring subtraction method is used by SASSI, the excavated soils need to be explicitly modeled. Figure 3.1-5 shows the excavated soil model with brick elements.

The SASSI model consists of a total of 4846 nodes with 922 nodes on the soil-structure interface as interaction nodes. The soil space replaced by the structure-soil system is defined as excavated soils which are modeled using 2322 brick elements. For the

structural portion, which includes the surrounding soils, the SASSI model contains 1890 brick elements, 504 shell elements and 156 beam elements. The masses of the superstructure, which are lumped at the floor locations assuming rigid diaphragm for floor slabs, are represented by three concentrated mass elements for each of the two reactors. The input motions are defined in the soil located at 13.2m below grade, which are provided by JNES as shown in Figure 3.1-3.

3.1.2 Results and Comparisons with JNES data

The following sub-sections discuss the key results from the SASSI analysis and their comparisons with the JNES measured response data. The horizontal responses are discussed first, followed by the comparisons of the vertical responses. The key results include comparisons of ISRS and the soil pressures between the SASSI analysis and the JNES recorded data.

Horizontal Response Analysis

The horizontal response analysis is performed by applying the input motion in the north-south (NS) direction. The ISRS results are computed at the centers of the basemat and the roof. At these locations of the test structures, accelerometer recordings are designated in Figure 3.1-2 as B1A-NS0 and RFA-NS0, respectively. The comparisons between the SASSI predicted ISRS and the accelerometer recordings are shown in Figure 3.1-6 and Figure 3.1-7, for the basemat and the roof, respectively.

Also in these figures, two sets of the SASSI analysis results are presented. The first analysis is performed using the JNES soil geotechnical data, which is interpreted as the best estimate soil property shown in the figures for this study as the mean soil V_s (V_s represents the material shear wave velocity of the soil). The second analysis is performed by adjusting the mean soil V_s to achieve the best fit of the computed ISRS to the recorded ISRS. The purpose is to assess the soil uncertainty effect on the response calculation.

Due to the nature of the narrow frequency band inherent in the seismic input, the ISRS computation is sensitive to the property of the soil column. As exhibited in Figure 3.1-6 and Figure 3.1-7 for the basemat and roof ISRS comparisons, the predicted spectral peak using the mean soil profile is shifted to the right in the frequency band from the recorded spectral peak. This suggests that the mean soil column appears stiffer and the soil column employed in the analysis should be softened with respect to the mean soil properties. The best fit of ISRS to the recordings is obtained in this analysis by reducing the shear wave velocity V_s of the soil column by 10%, which are shown as the solid lines in these figures. The analysis using the modified soil column results in an excellent match for the basemat spectral response. For the roof response, the recording shows two salient peaks, and the second peak appears to be associated with the adjacent structure-structure effect. However, the two peaks in the computed spectrum for the roof do not separate as much as that shown in the recorded spectrum.

In addition, the 10 percent reduction in V_s of the mean soil profile is equivalent to about 20 percent in the stiffness reduction of the corresponding soil column. In an uncertainty analysis, if the lognormal distribution is assumed for the soil stiffness, it translates to a value of about 0.2 for the COV of the soil stiffness reduction (coefficient of variation which is defined as [standard deviation]/mean). The value of COV equal to 0.2 for the soil stiffness is within the range of uncertainty typically used in geotechnical engineering

applications, and the BNL ISRS comparisons further substantiate the engineering practice to account for the soil uncertainty.

Figure 3.1-8 through Figure 3.1-13 present the JNES recorded seismic induced pressure time histories and the corresponding SASSI results for the pressure sensors at the various side wall locations of the twin reactors. The pressure sensors were installed on the test structure with their locations shown in Figure 2-18 and Figure 2-19. As indicated in the figures, the locations where the pressure sensors were installed are designated as circles. However, only the solid circles represent the sensors which have actually recorded the earthquake event. The sensors selected for the pressure comparisons are S1, S2 and S4 on the south side, and N3, N6 and N13 on the north side.

The seismic induced pressures from the SASSI model are computed in the soil elements closest to the locations of the pressure sensors, using the stress component perpendicular to the wall. Similar to the ISRS comparisons, two soil columns were applied for the pressure computation, which are the mean soil profile and the mean minus COV profile, respectively.

The comparison between the recorded time pressure and SASSI calculations for the sensor S1 near the base on the south side is shown in Figure 3.1-8. The SASSI result appears to be much larger than the recorded pressure (about a factor of 2). The occurrences of the pressure peaks are about consistent between the sensor and the computed results. They also indicate that there is a phase correlation between the SASSI model and the test data.

Figure 3.1-9 shows the comparison for the sensor S2 which is located near the mid height of the wall below grade. As indicated in the figure, the recorded sensor appears to have much smaller pressure amplitude (the pressure peak is around 70kN/m² compared to S1 which is about 500kN/m²). Further, it is observed that the time history of the sensor appears to have much higher noise to signal ratio, because its shape is inconsistent with typical earthquake response, and as indicated later in this section, the Fourier spectrum of the pressure sensor reveals a trend of upward drift of the Fourier amplitude in the low frequency range. The computed pressure in this case is smaller than the sensor.

The pressure comparison between the analysis and the recorded data for the sensor on the upper portion of the wall, as shown in Figure 3.1-10, is much better than the lower portion of the wall. This is due to a relatively larger pressure magnitude and lower noise/signal ratio for the sensor near the ground surface than other locations. Therefore, better comparison is achieved by the analysis. However, the pressure estimate does not seem to be much affected by changing the soil column stiffness by 20 percent as opposed to the ISRS calculation in which the soil stiffness plays a critical role in matching the spectral peaks.

Figure 3.1-11 through Figure 3.1-13 present the pressure time histories on the north side of the twin structures for both the sensors and the SASSI analyses. As shown by these figures, the observations made for the characteristics of the pressure comparisons for the south side of the structures can be extended to the north side. Since such a small earthquake event virtually ensures the linear elastic response for the structures, and also the fact that the same pressure transducers were installed leads to the high probability of similar recording quality (in terms of noise/signal ratios) for these sensors, the striking

similarity in the pressure comparisons for both sides of the structures reveals neither a surprise nor a coincidence.

Furthermore, because of the oscillatory nature of the earthquake responses, it is often more advantageous to determine the characteristics of SSI responses in the frequency domain. To this end, the Fourier spectra of the pressure time histories from both the recorded data and the SASSI analysis are computed and presented in Figure 3.1-14 through Figure 3.1-19. The Fourier spectra shown in these figures are smoothed with a triangular smoothing window to reduce unwanted spikes. The triangular window employed in this analysis is defined as:

$$A_s(f_m) = \frac{1}{\text{SUM}(i)} \sum_{\substack{\text{All } i \\ |f_i - f_m| \leq \Delta f_m / 2}} \alpha_i A_r(f_i) \quad , m=1, M$$

and,

$$\alpha_i = \frac{4}{\Delta f_m} [f_i - (f_m - \Delta f_m / 2)], \quad f_m - \Delta f_m / 2 \leq f_i \leq f_m$$

$$\frac{4}{\Delta f_m} [(f_m + \Delta f_m / 2) - f_i], \quad f_m < f_i \leq f_m + \Delta f_m / 2$$

where,

- Δf_m Width of the applied frequency window (0.5 Hz used for this study)
- $A_s(f_m)$ Smoothed Fourier ratios
- $A_r(f_i)$ Fourier ratios of recorded motions.

For the pressure sensors near the basemat (S1, N3) as indicated in Figure 3.1-14 and Figure 3.1-17, the comparison of the Fourier spectra show that the frequency content is closely matched between the computed and recorded pressure responses, and further, the pressure amplitudes from the SASSI analysis appear less agreeable to but generally higher than the recordings. The less accurate comparison in the pressure amplitudes may be due to the fact that in the computation algorithm, the soil pressure is treated as the secondary response in the SH wave field.

Previously, the examination of the pressure time histories for the sensors located near mid height of the wall (S2, N6) leads to the observation that there appear to have very high noise/signal ratio present in the recorded pressures at these locations. The Fourier spectra of these recorded pressures, as depicted in Figure 3.1-15 and Figure 3.1-18, also indicate that a persistent pattern of an upward drift of the Fourier amplitudes in the low frequency range is evident. Since these pressure time histories represent only the dynamic response to the seismic event, the Fourier amplitude should trend to null as the frequency approaches to zero. Therefore, the fact that the low frequency Fourier amplitudes of the recorder pressures drift higher in low frequencies further substantiates the observation made earlier in the time domain comparisons.

Finally, the frequency domain comparison for the sensors near the ground surface (S4, N13) as shown in Figure 3.1-16 and Figure 3.1-19 indicates very good match between

the recordings and the SASSI results in the dominant frequencies of interest. Also shown in these figures, the recorded responses still indicate the upward drift in low frequencies, which are apparently induced by the noise inherent in the pressure transducers. For frequencies between about 2-10 Hz, the estimated pressures mostly envelop the recordings and also achieve a good match in the frequency content. Further, the pressure result computed with the mean minus COV=0.2 soil column appears to be better than the pressure estimate with the mean soil column. This observation is also consistent with the ISRS results as discussed above.

Vertical Response Analysis

As opposed to the horizontal response analysis, the vertical seismic analysis is a rather complicated process in which the response quantities are influenced by both two orthogonal horizontal motions and one vertical motion. Apparently, there are many ways to compute the vertical seismic response, which all involve the three orthogonal seismic inputs. In this study, however, a simplified approach is taken in that the recorded sensors on the basemat of the structure are averaged to remove the influence due to the horizontal seismic input motions. Therefore, the averaged sensor pressure response is compared with the SASSI analysis using the vertical seismic input only. This approach greatly simplifies the SASSI analysis required for the comparison purpose.

Following the simplified analysis approach described above, the vertical response analysis is performed by applying the recorded free field motion in the vertical direction at the control point located 13.2m below grade. The vertical ISRS results are computed at the center of the basemat and the roof, which have accelerometer recordings designated in Figure 3.1-2 as B1A-V0 and RFA-V0, respectively. The comparisons between the predicted vertical ISRS and the vertical accelerometer recordings are shown in Figure 3.1-20 and Figure 3.1-21 for the basemat and the roof, respectively.

Similar to the SASSI analysis performed for the horizontal responses, the effect of the soil uncertainty is considered. The first analysis is performed using the JNES soil geotechnical data, which is interpreted as the best estimate soil property which is designated in the figures for this study as the mean soil V_p (V_p represents the material compressional wave velocity of the soil). Since the vertical response is controlled by the compressional wave, the second analysis is therefore performed by adjusting the mean soil p-wave velocity V_p to achieve the best fit of the computed vertical ISRS to the recorded ISRS.

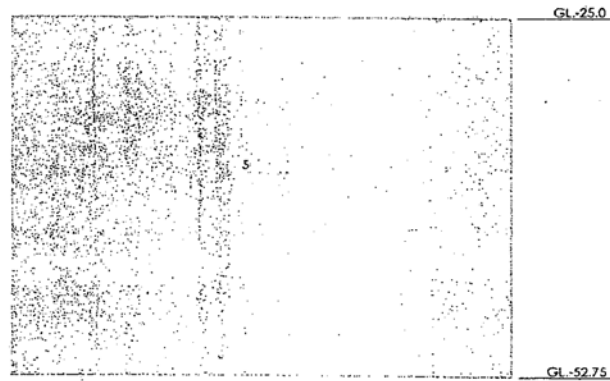
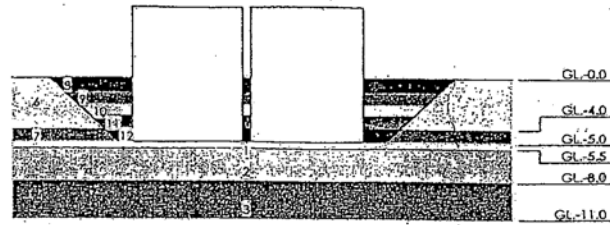
As shown in these figures for the vertical ISRS comparison, the SASSI prediction captures very well both the frequency content and the spectral peaks of the recorded ISRS. The uncertainty in the soil property is believed to be within 10% of the mean soil p-wave velocity (equivalent to 0.2 for the COV of the soil stiffness reduction). It is also observed that the vertical SASSI analysis achieves much better comparison between the computed vertical ISRS and the accelerometer recordings than the horizontal response analysis.

The seismic induced pressures on the basemat are then computed from the SASSI analysis for the soil columns with both the mean and the mean minus COV properties. As mentioned above, in order to remove the influence of the horizontal inputs from the recorded vertical pressure measurements on the basemat, the sensor pressures at the corner locations as shown in Figure 2-17 are averaged. The averaged vertical sensor

pressures are then compared with the predicted pressures computed at the center of the basemat. Figure 3.1-22 and Figure 3.1-23 show the averaged vertical pressure time histories from the JNES recorded vertical pressures and the computed basemat pressures for both the north and south structures. As indicated in Figure 2-17, the north structure has pressure sensors at all four corners of the basemat, while the south structure only has functional pressure sensors at the two corners. Because of the fewer sensors participating in the averaging scheme for the south structure, the averaged vertical pressure does not have as a good quality as the north structure which have all four corners participating in the averaging scheme. Figure 3.1-22 and Figure 3.1-23 reveal that the pressure comparison for the north structure is much better than the south structure.

These pressure comparisons can be further examined by their respective Fourier spectrum plots, which are shown in Figure 3.1-24 and Figure 3.1-25. These Fourier spectra are also smoothed using the triangular window as described earlier. The Fourier spectra for the averaged recorded pressures indicate the upward drift in the low frequency range, which implies that the recorded pressures have high noise/signal ratio. For the south structure, the recorded pressure is mostly higher than the predicted response, while for the north structure, the predicted pressure mostly envelops the recording. As far as the frequency content is examined, the analysis captures most of frequencies, except for a few isolated frequencies for the north structure where the computed peaks appear to be inverted as opposed to the peaks from the averaged recorded responses.

Finally, the soil uncertainty has little effect on the vertical pressure calculations. This may be due to the fact that the computed vertical ISRS are also less affected by the soil columns with different soil stiffness. Although in this case, the ISRS comparisons display an excellent match between the computed and recorded ISRS, the pressure comparisons are of much less quality.



Soil Properties of Twin Model BAs,BAn

NO.	Depth (m)	Layer thickness (m)	Vs (m/sec)	Vp (m/séc)	Poisson's ratio	Unit weight (tf/m3)	Damping h (%)
1	-5.0~-5.5	0.5	150	228	0.120	1.94	5
2	-5.5~-8.0	2.5	340	750	0.371	1.94	5
3	-8.0~-11.0	3.0	430	1130	0.415	1.94	2
4	-11.0~-25.0	14.0	1290	2990	0.386	2.21	2
5	-25.0~-52.75	27.75	1590	3250	0.343	2.21	2
6	Assumed 8-12 soil spread out beside the building in semi-infinite space. (For the case of embedment, the soil layers are modeled by thin-layer method)						
7							
8	0.0~-1.0	1.0	155	360	0.386	1.77	5
9	-1.0~-2.0	1.0	205	370	0.279	1.77	5
10	-2.0~-3.0	1.0	215	380	0.265	1.77	5
11	-3.0~-4.0	1.0	225	390	0.251	1.77	5
12	-4.0~-5.0	1.0	235	420	0.272	1.77	5

Figure 3.1-1 Twin Reactor Configuration Soil Profile and JNES Properties

Source: *Model Test on Dynamic Cross Interaction Effect on Nuclear Power Plant Buildings*, Technical Report, Japan Nuclear Energy Safety Organization (JNES), Tokyo, Japan, March, 2002. Permission to use this copyrighted material is granted by JNES.

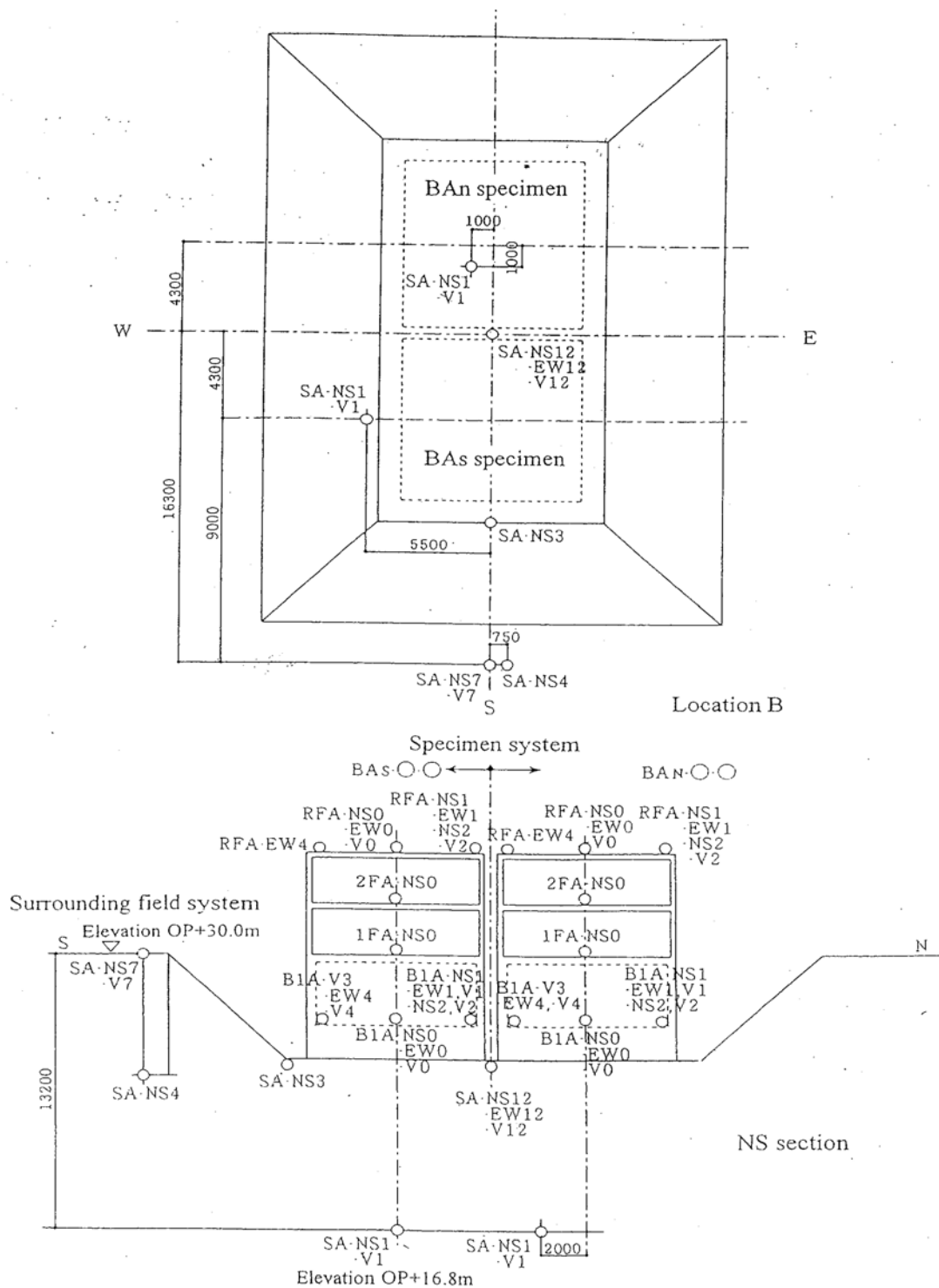


Figure 3.1-2 Twin Configuration Seismometer Locations and Designations, [unit: mm]

Source: *Model Test on Dynamic Cross Interaction Effect on Nuclear Power Plant Buildings*, Technical Report, Japan Nuclear Energy Safety Organization (JNES), Tokyo, Japan, March, 2002. Permission to use this copyrighted material is granted by JNES.

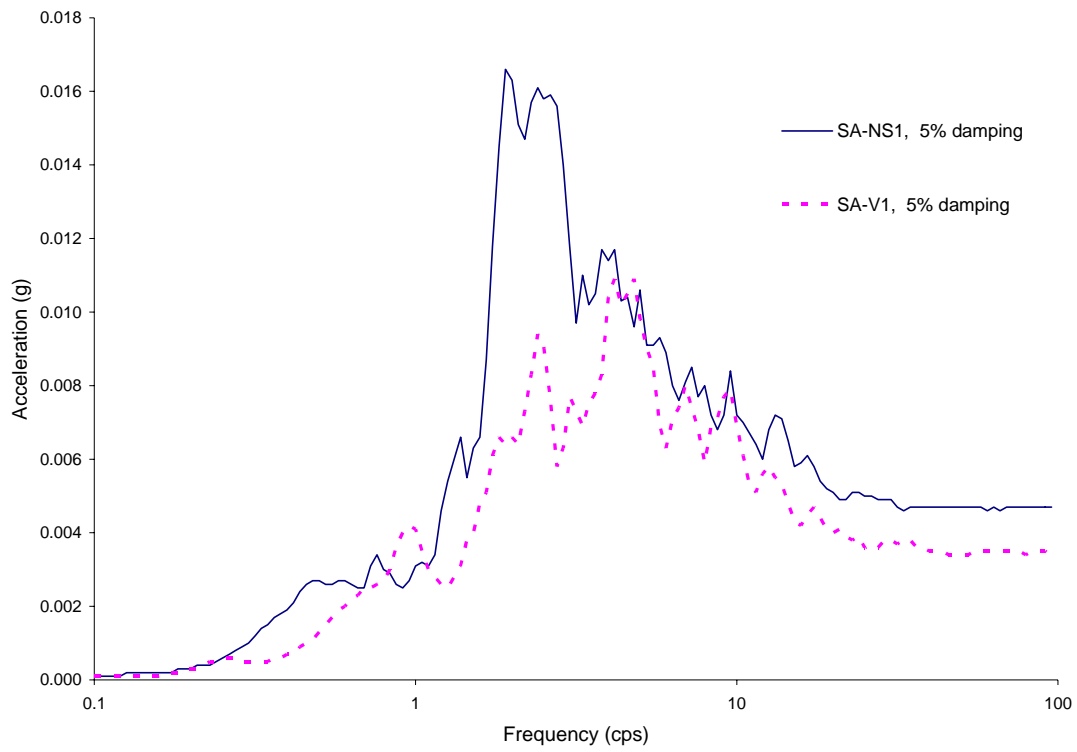


Figure 3.1-3 Input Ground Motions for Twin Configuration Analysis

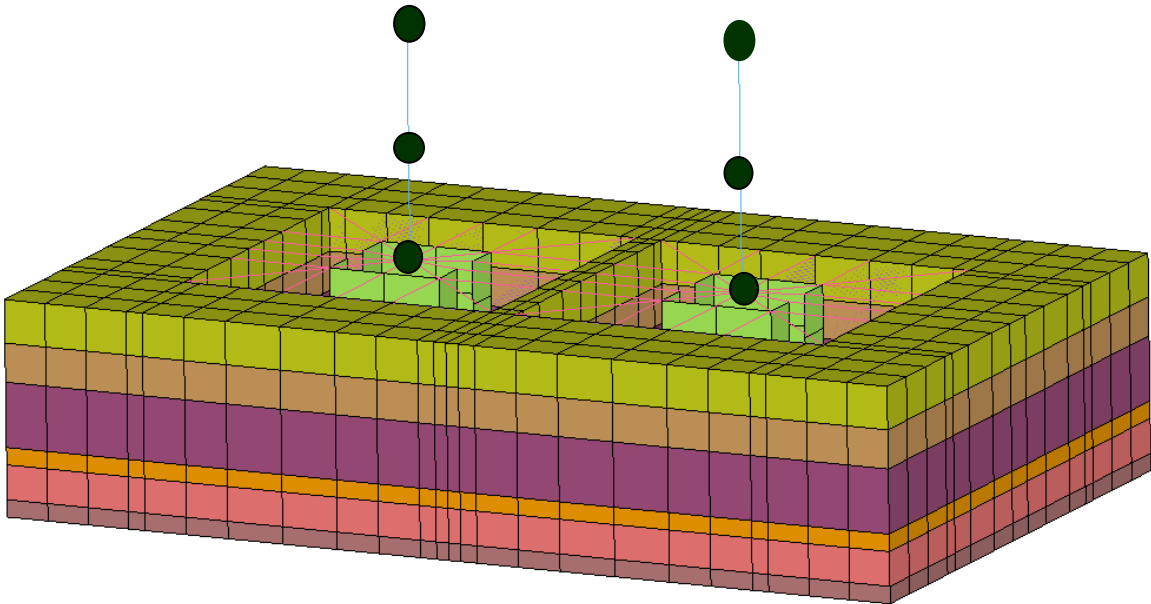


Figure 3.1-4 SASSI Model for Structures and Surrounding Soil

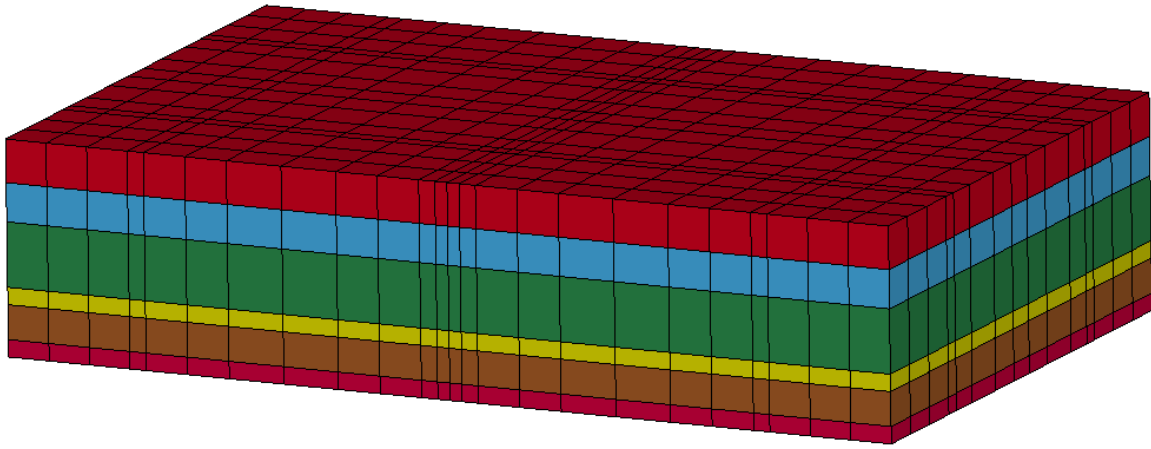


Figure 3.1-5 SASSI Model for Excavated Soil

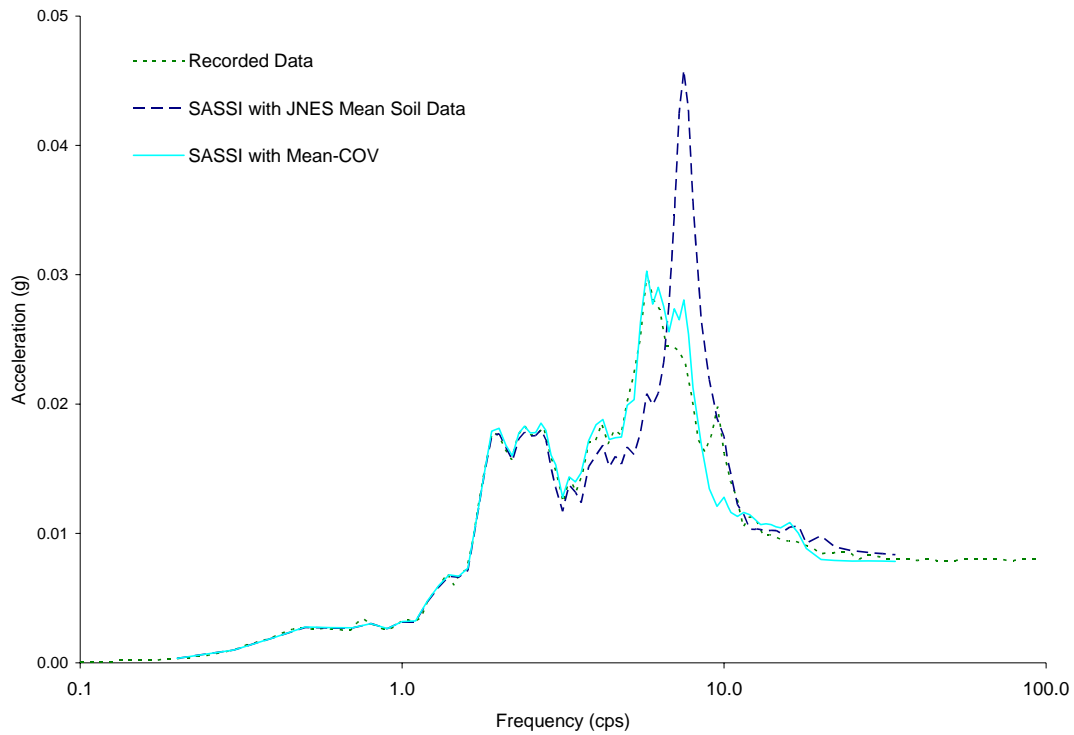


Figure 3.1-6 Comparison of Horizontal Response Spectra at Basemat Center of Twin Model

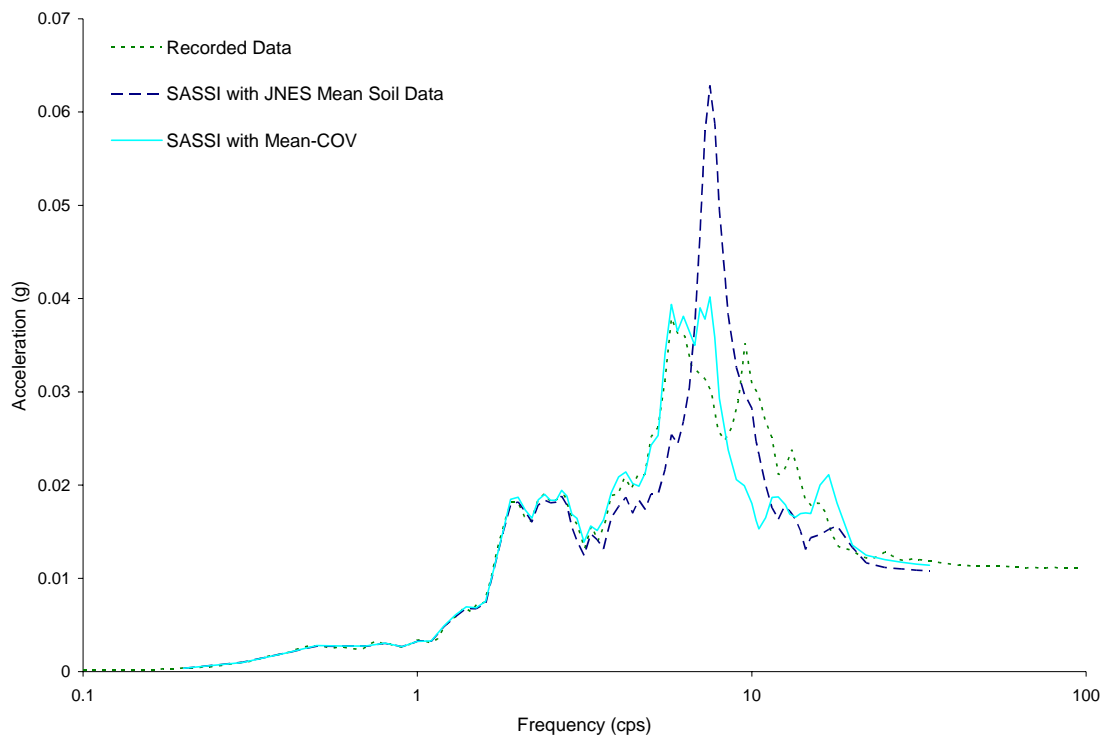


Figure 3.1-7 Comparison of Horizontal Response Spectra at Roof Center of Twin Model

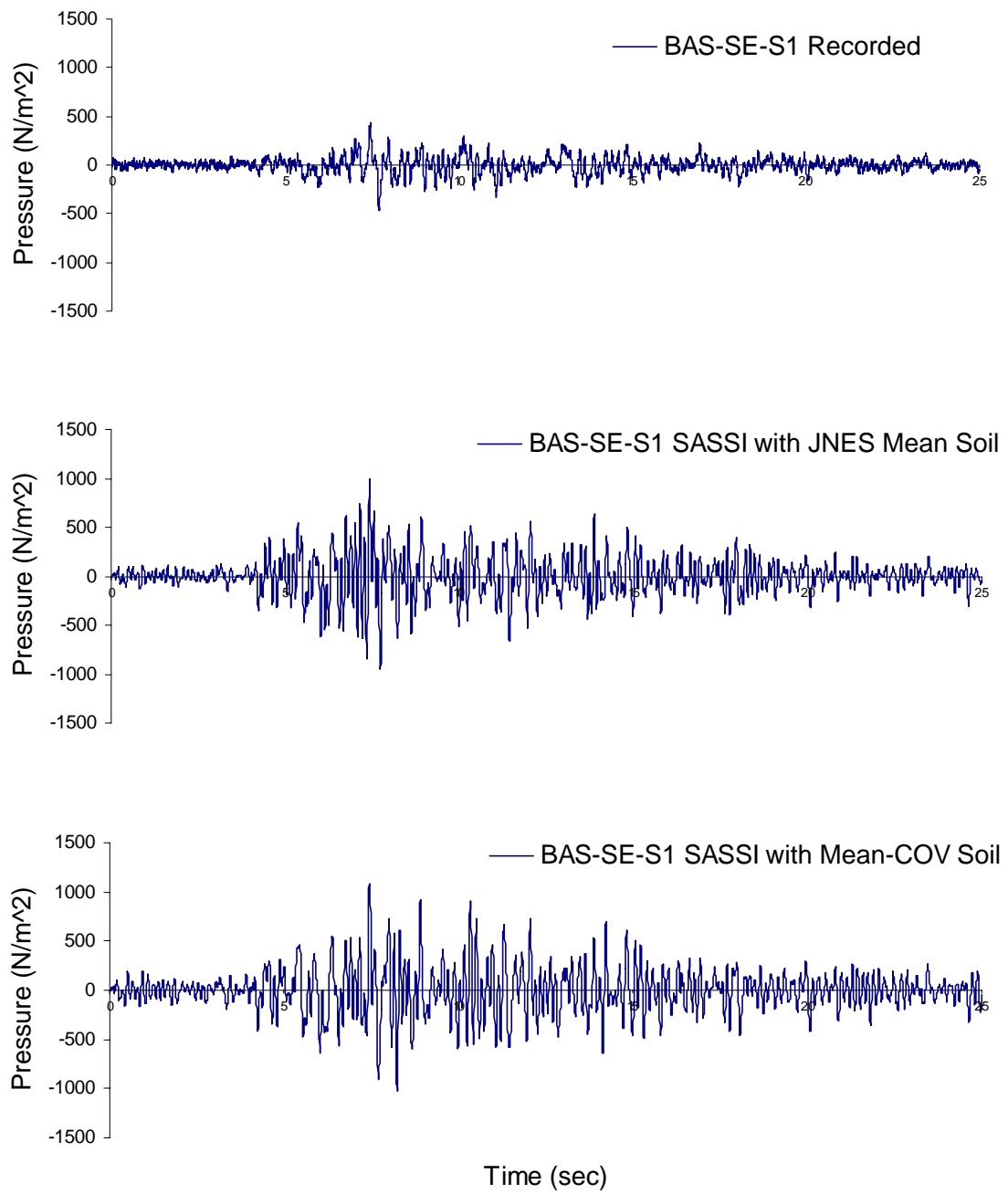


Figure 3.1-8 Comparison of Seismic Induced Soil Pressure at Sensor BAS-SE-S1

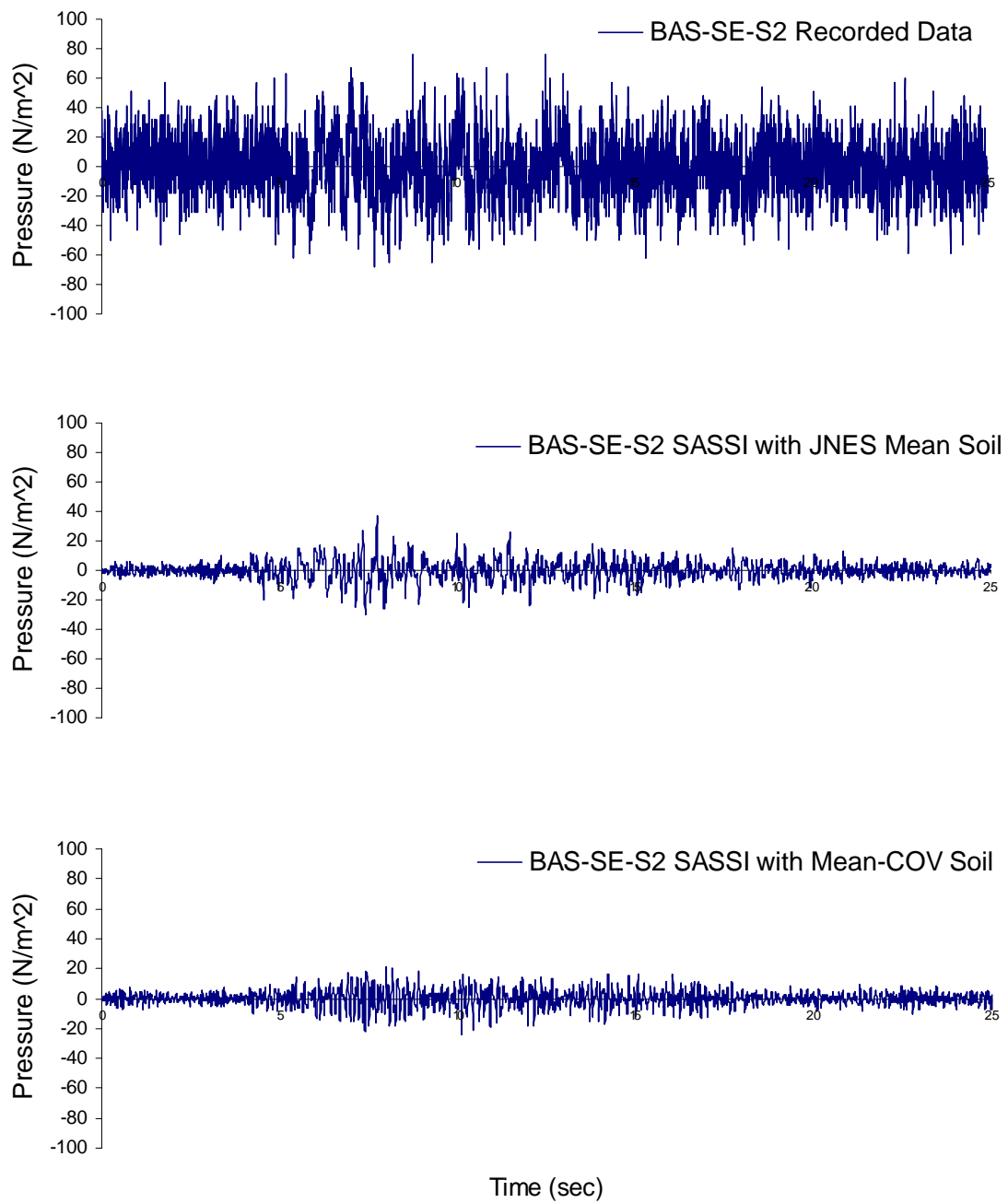


Figure 3.1-9 Comparison of Seismic Induced Soil Pressure at Sensor BAS-SE-S2

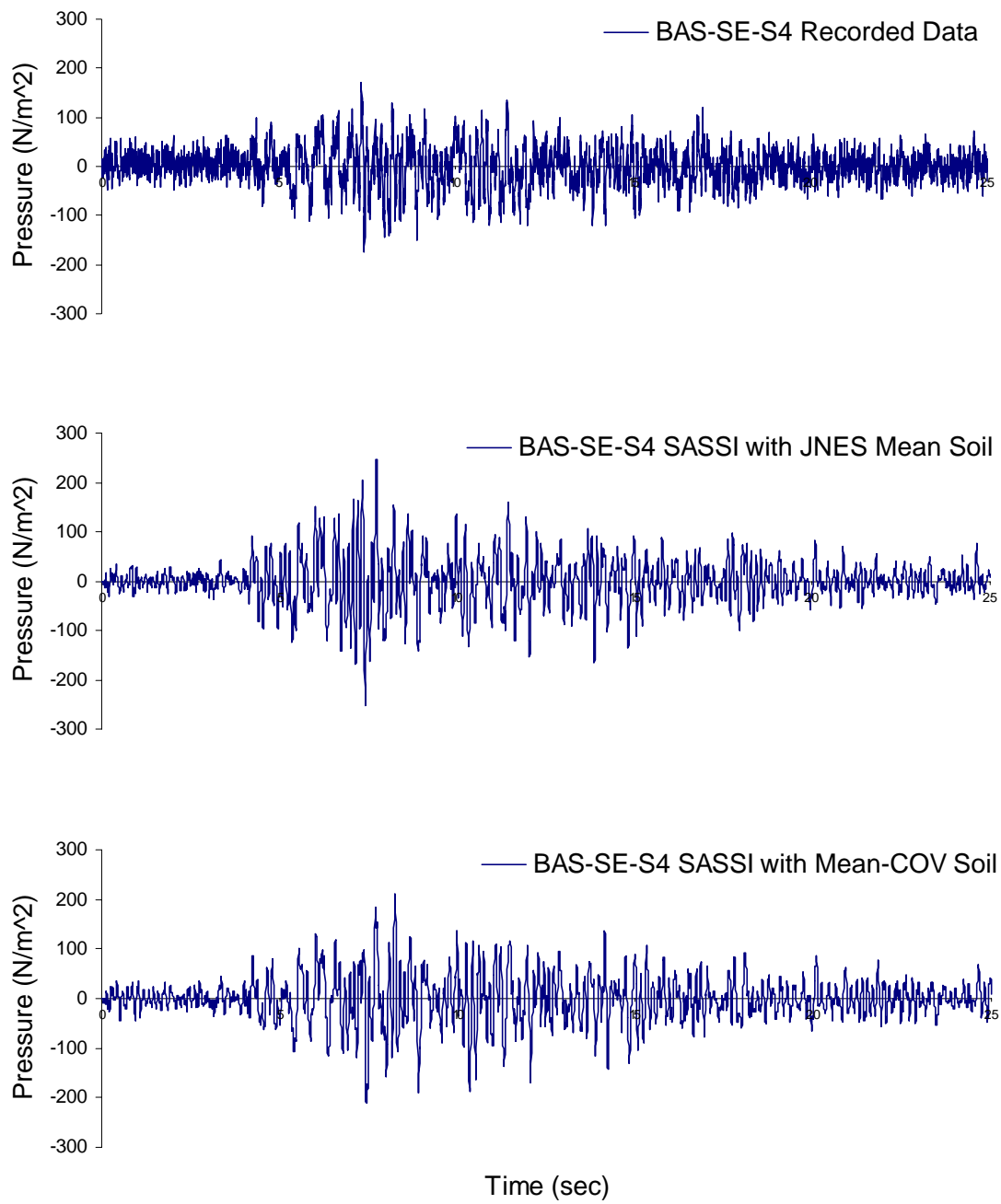


Figure 3.1-10 Comparison of Seismic Induced Soil Pressure at Sensor BAS-SE-S4

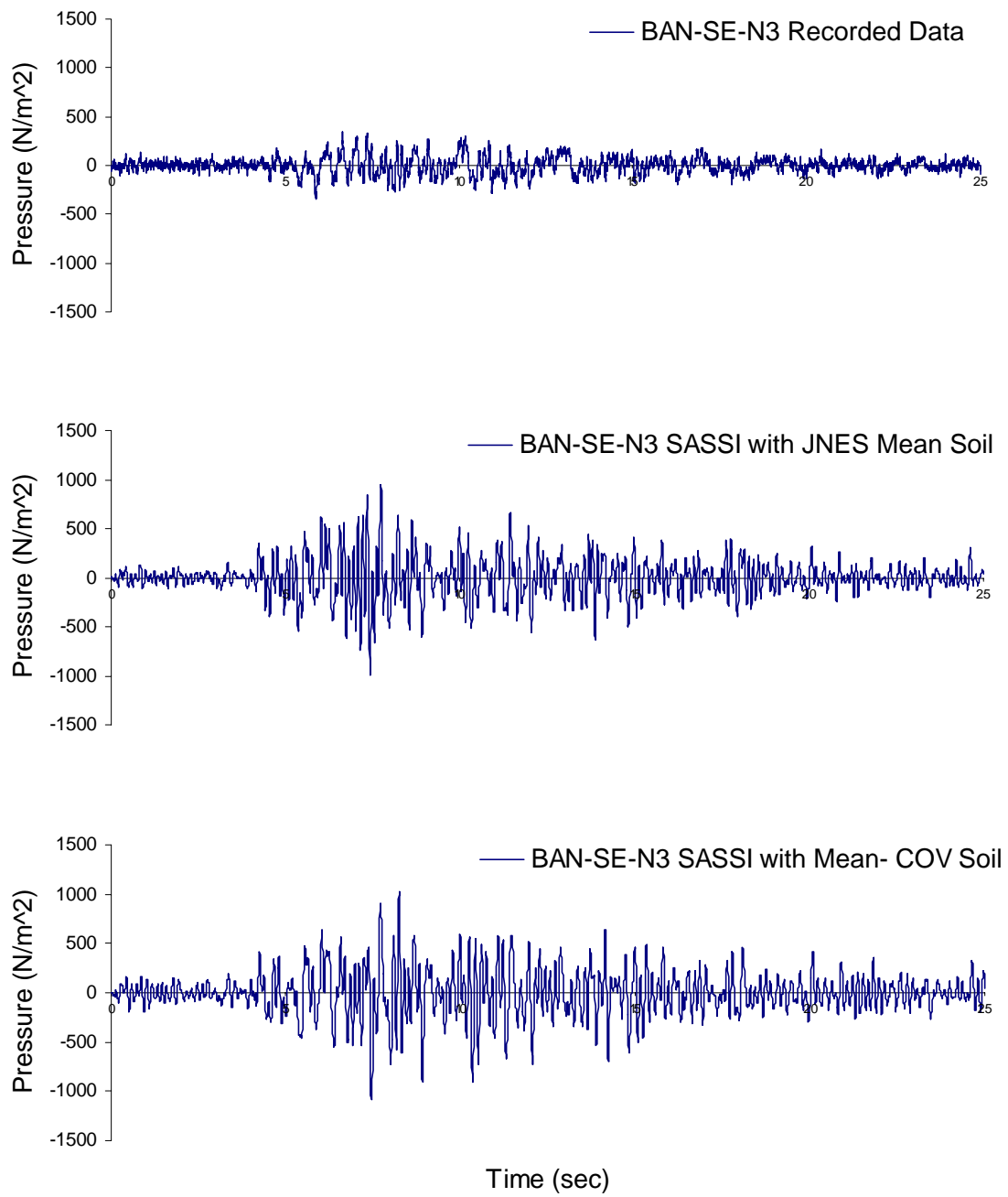


Figure 3.1-11 Comparison of Seismic Induced Soil Pressure at Sensor BAN-SE-N3

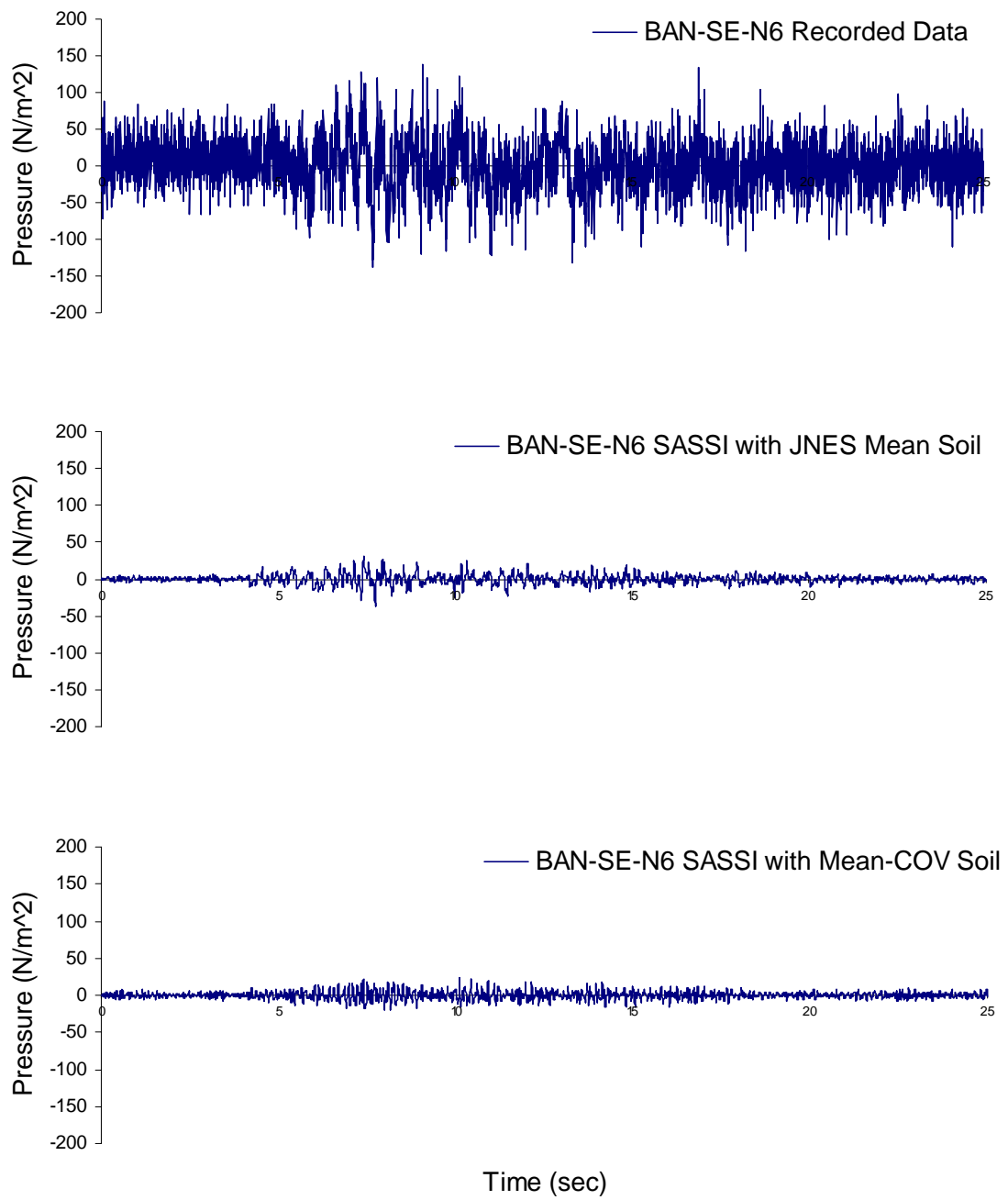


Figure 3.1-12 Comparison of Seismic Induced Soil Pressure at Sensor BAN-SE-N6

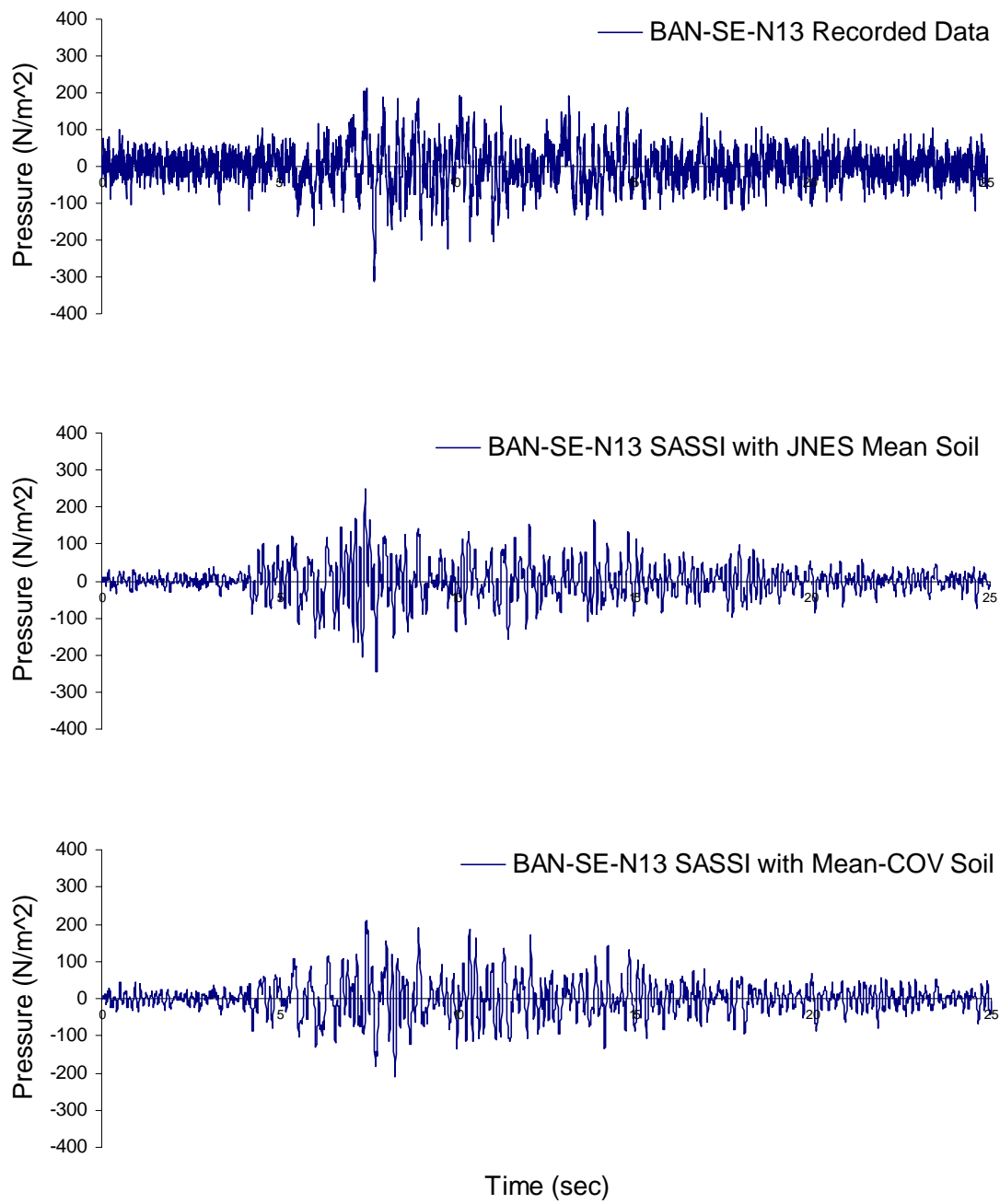


Figure 3.1-13 Comparison of Seismic Induced Soil Pressure at Sensor BAN-SE-N13

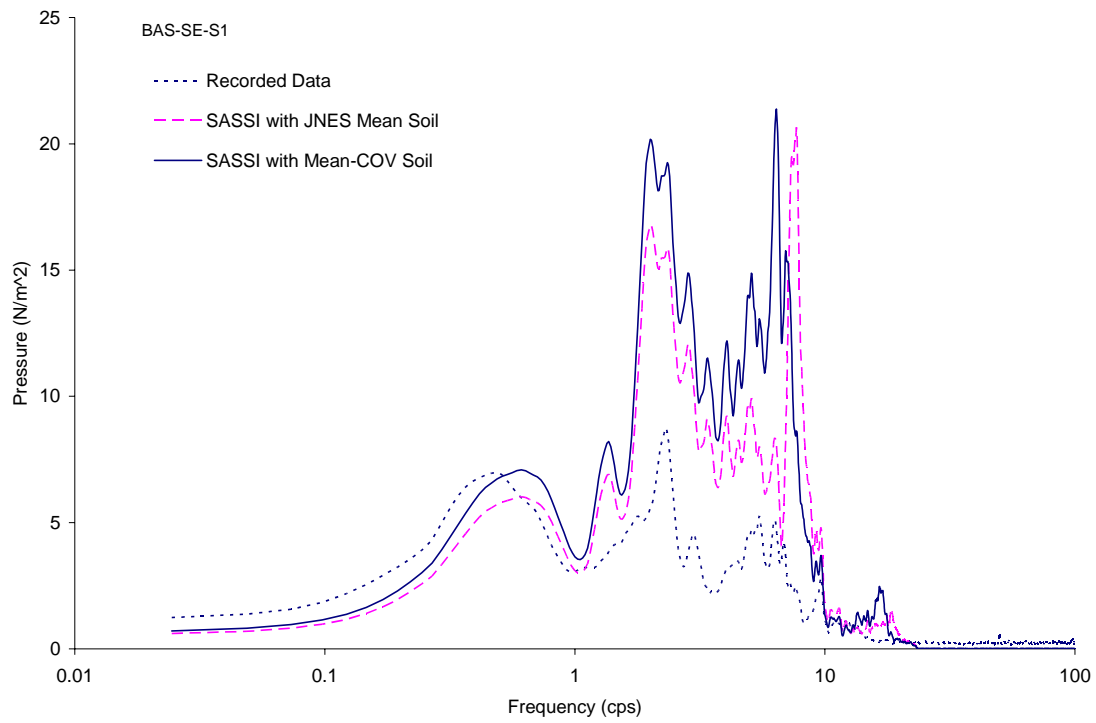


Figure 3.1-14 Comparison of Fourier Spectra of Soil Pressure at Sensor BAS-SE-S1

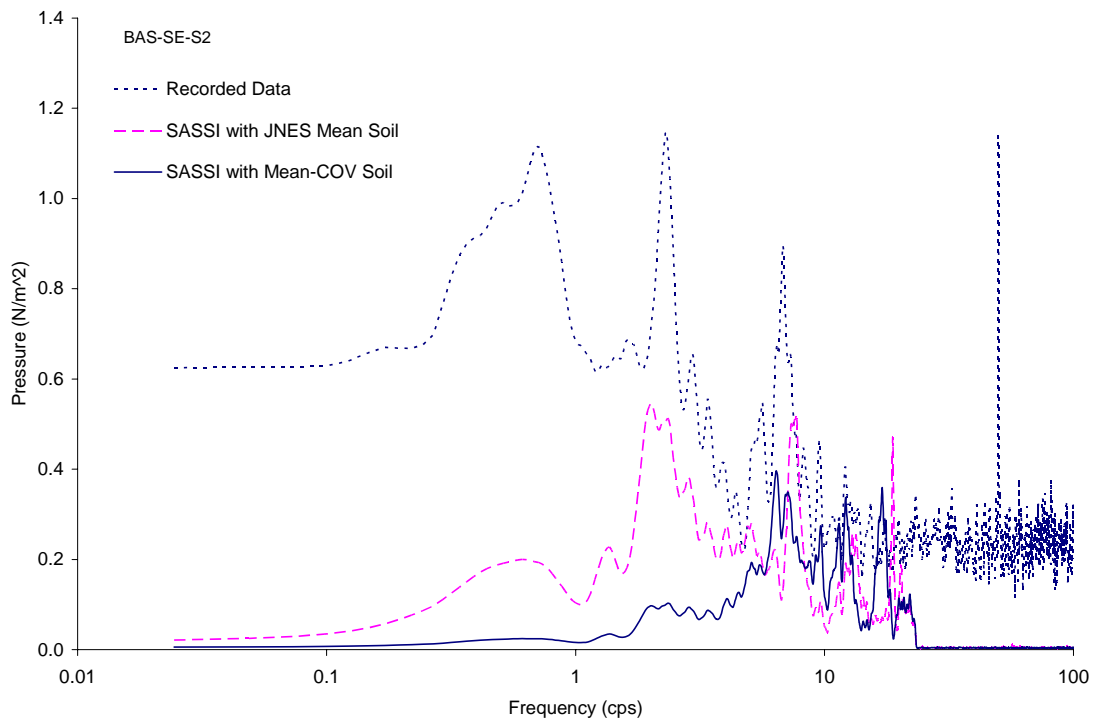


Figure 3.1-15 Comparison of Fourier Spectra of Soil Pressure at Sensor BAS-SE-S2

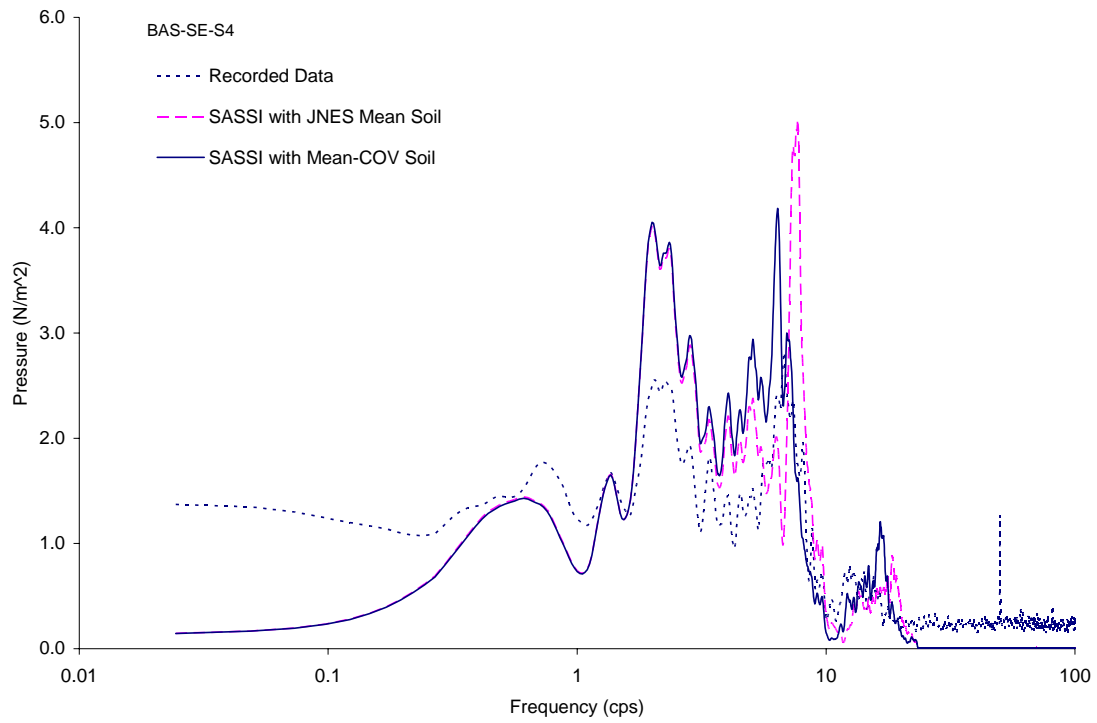


Figure 3.1-16 Comparison of Fourier Spectra of Soil Pressure at Sensor BAS-SE-S4

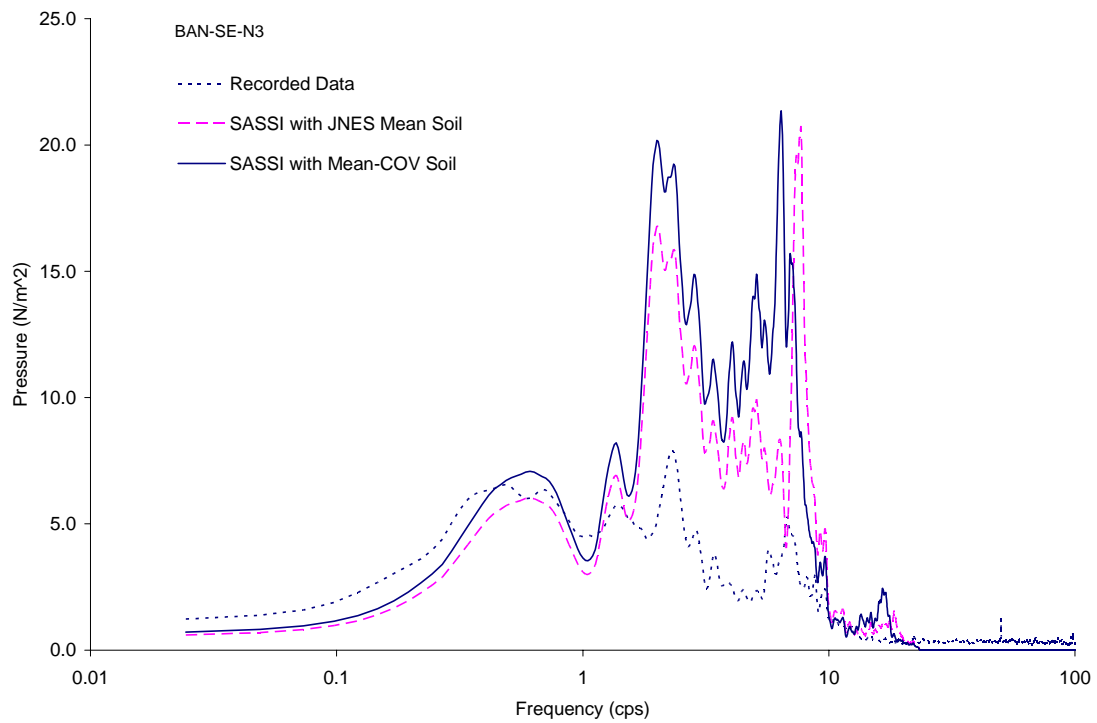


Figure 3.1-17 Comparison of Fourier Spectra of Soil Pressure at Sensor BAN-SE-N3

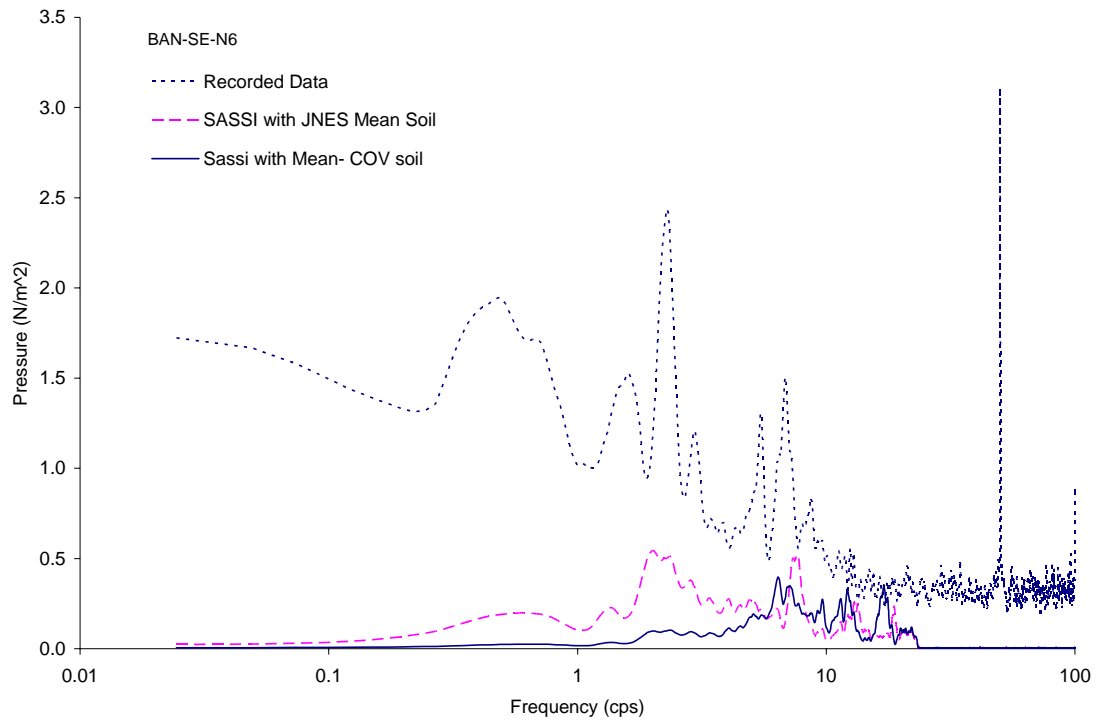


Figure 3.1-18 Comparison of Fourier Spectra of Soil Pressure at Sensor BAN-SE-N6

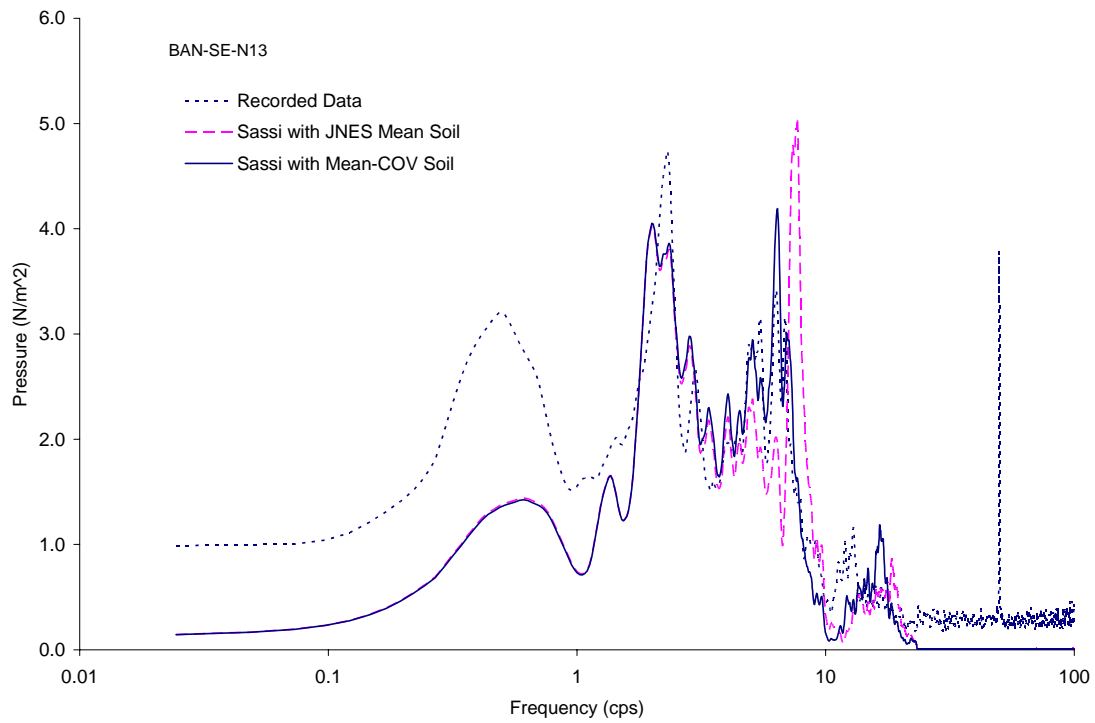


Figure 3.1-19 Comparison of Fourier Spectra of Soil Pressure at Sensor BAN-SE-N13

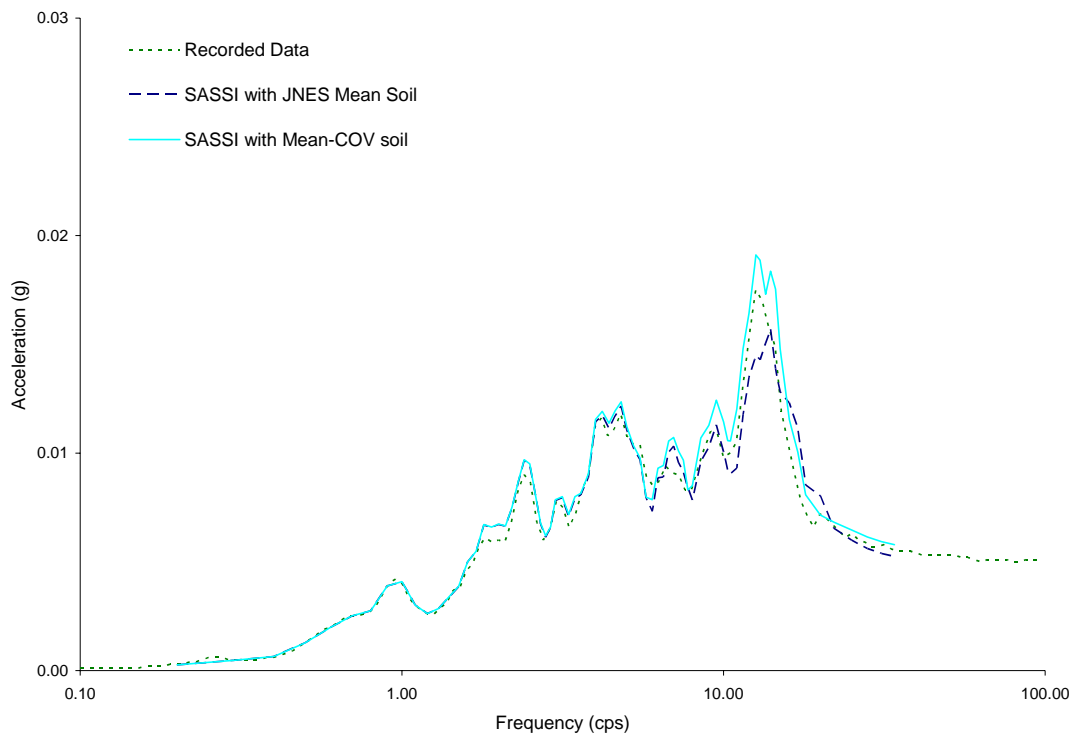


Figure 3.1-20 Comparison of Vertical Spectra at Basemat Center of Twin Model

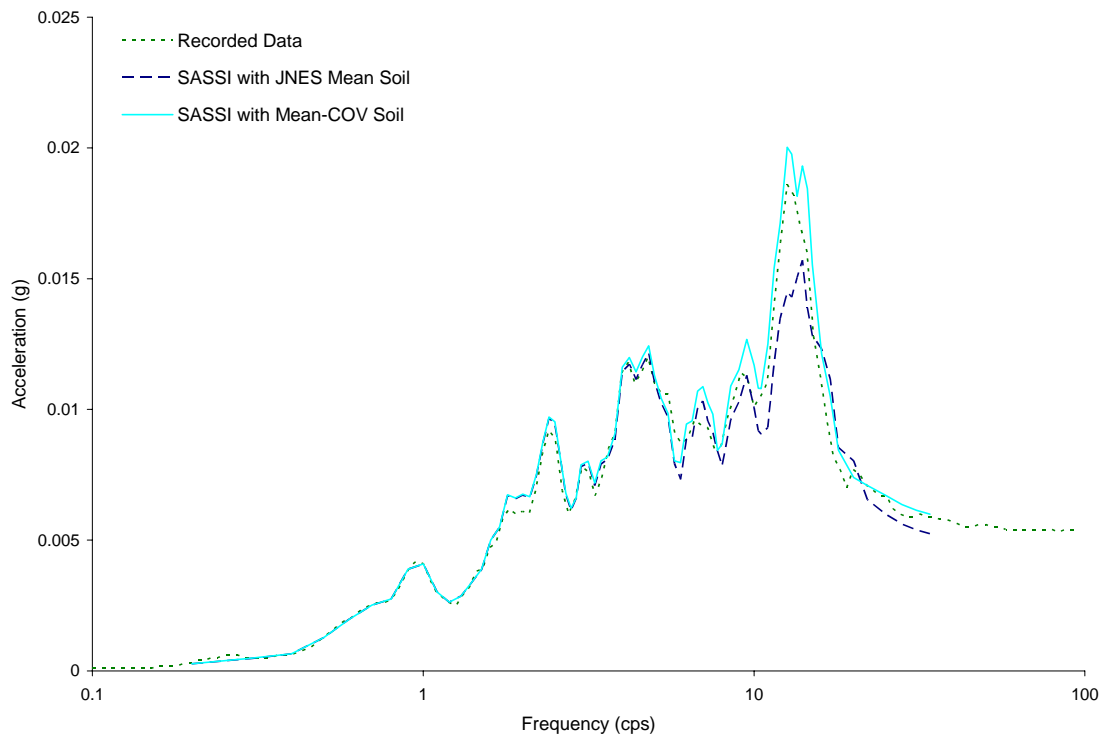


Figure 3.1-21 Comparison of Vertical Spectra at Roof Center of Twin Model

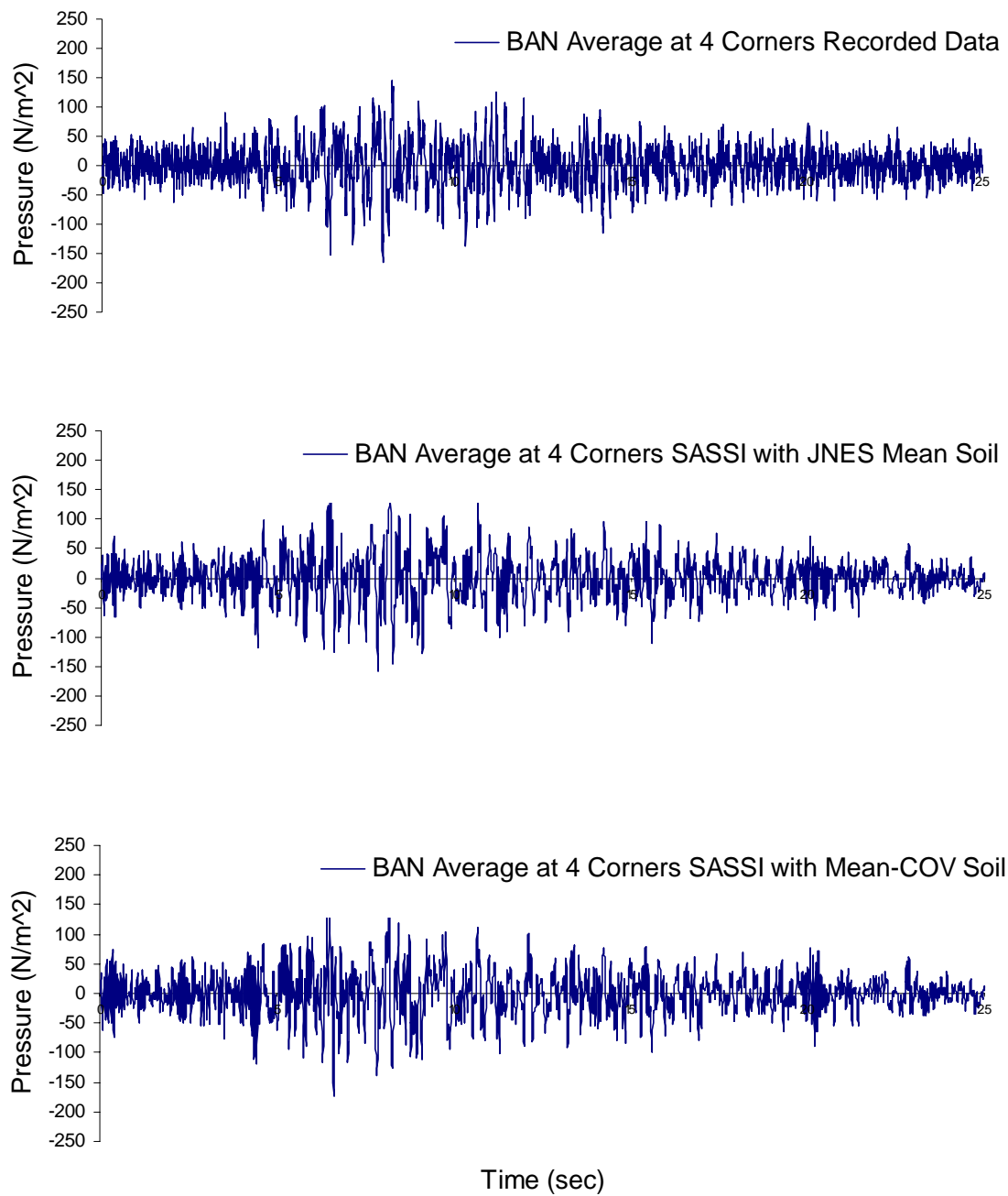


Figure 3.1-22 Comparison of Averaged Vertical Seismic Induced Soil Pressure for BAN

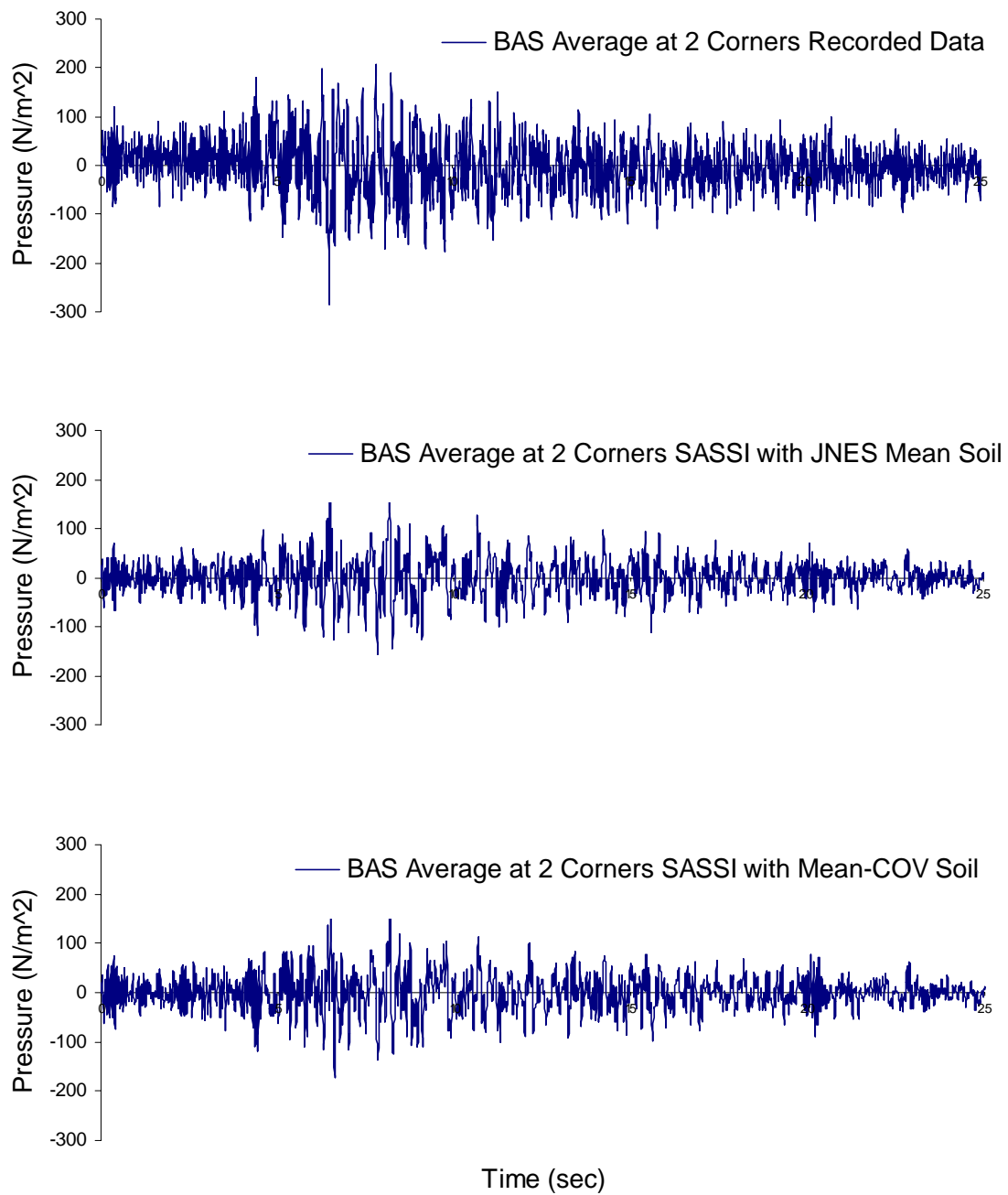


Figure 3.1-23 Comparison of Averaged Vertical Seismic Induced Soil Pressure for BAS

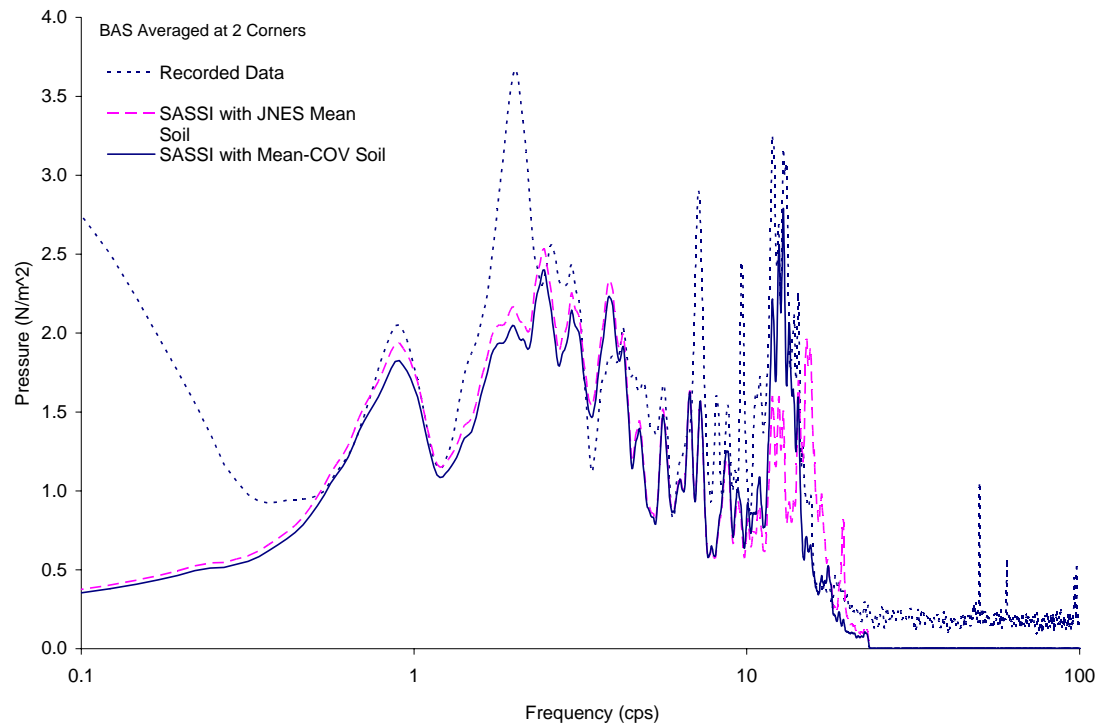


Figure 3.1-24 Comparison of Fourier Spectra of Soil Pressure for BAS Basemat

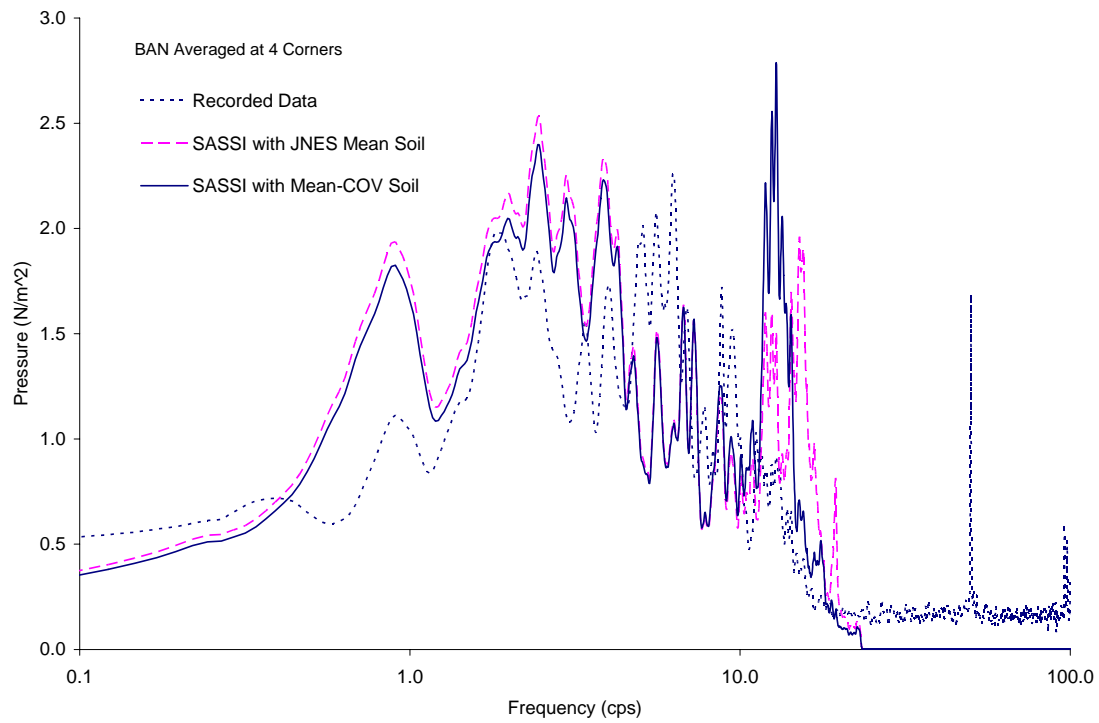


Figure 3.1-25 Comparison of Fourier Spectra of Soil Pressure for BAN Basemat

3.2 Reactor-Turbine Configuration

3.2.1 Test Modeling Description

The configuration for the reactor-turbine (R-T) model consists of a scaled reactor structure (the same structure as the twin reactor configuration) and a turbine structure, which is located about 0.1m from the reactor structure as shown in Figure 2-4. The turbine building has dimensions of 6.4m by 10m in plane and 6.75m in height, and weighs about 395 metric ton, and is embedded about 4m in the soil.

The soil profile including backfills for the R-T configuration used for the BNL analysis is shown in Figure 3.2-1. The soil properties for the profile shown in Figure 3.2-2 are provided by JNES, and are considered as the low strain best-estimate (to be referred to as the mean property in the BNL analysis). Since the earthquake event to be analyzed is not expected to excite large strain responses, the soil properties in Figure 3.2-2 are not expected to degrade with strains and are therefore directly applied in the BNL SASSI model.

The locations and designations of seismometers installed on the R-T test model are provided in Figure 3.2-3. Dimensions shown in this figure are units in terms of millimeters. As shown in this figure, the seismometers within the soil are located directly below but distant from the test model as designated by D-SA-NS1 for the horizontal direction and D-SA-V1 for the vertical direction. They are located directly underneath the R-T basemat and measured about 35m below the ground surface. The 5% damped response spectra for the recorded accelerations of both the horizontal and the vertical accelerometers are shown in Figure 3.2-4, which are to be used as the input motions to the BNL SASSI analyses for the R-T configuration.

The SASSI model developed for the R-T configuration is shown in Figure 3.2-5 and Figure 3.2-6 for the structural model with the surrounding soils and the soil excavation model. As displayed in Figure 3.2-5, the R-T structures and the surrounding soils are modeled in detailed finite elements. The portion of the R-T model located below the ground surface is modeled with explicit finite elements (e.g., 3-D bricks, shells and beams), while the superstructure above the ground surface is represented with simple lumped masses and 3-D beams. Three layers of brick elements were used to represent the soils that surround the structures. The purpose of using the soil brick elements is to compute the seismic induced soil pressure on the structures, which is done by calculating the stress component in the soil brick elements that is perpendicular to the respective structural wall. Since the sub-structuring subtraction method is used by SASSI, the excavated soils need to be explicitly modeled. Figure 3.2-6 shows the excavated soil model with brick elements.

The SASSI model for the R-T response analysis consists of a total of 6076 nodes with 1088 interaction nodes defined at the soil-structure interface. The excavated soil which is replaced by the structure-soil system is modeled using 2975 brick elements. For the structural portion, which includes the surrounding soils, the SASSI model contains 2303 brick elements, 750 shell elements and 123 beam elements. The masses of the superstructure, which are lumped at the floor locations assuming the rigid diaphragms for floor slabs, are represented by three concentrated mass elements for the reactor structure and two concentrated mass elements for the turbine structure. The input

motions are defined in the soil located at 35m below grade, which are provided by JNES as shown in Figure 3.2-4.

3.2.2 Analysis Results and Comparisons with Recorded Data

The key results from the SASSI analysis and their comparisons with the JNES measured response data for the R-T configuration are discussed in this section. The horizontal responses are presented first, followed by the comparisons of the vertical responses. Similar to the twin configuration, the results of both the ISRS and the soil pressures are included for the comparison between the SASSI analysis and the JNES recorded data.

Horizontal Response Analysis

The horizontal response analysis is performed for the input motion applied in the north-south (NS) direction. The ISRS results are computed at the centers of the basemat and the roof of the reactor and the turbine buildings, and the respective accelerometer recordings are depicted in Figure 3.2-3 as B1A-NS0 and RFA-NS0 for the reactor, and B1A-NS23 and RFA-NS0 for the turbine building. The comparisons between the SASSI computed ISRS and the JNES accelerometer recordings are plotted in Figure 3.2-7 and Figure 3.2-8, for the basemat and the roof of the reactor building, and Figure 3.2-9 and Figure 3.2-10 for the basemat and the roof of the turbine building.

The comparisons shown in these figures present two sets of computed responses from the BNL SASSI analysis. These two computed SASSI responses are obtained using the JNES best estimate soil data (referred to as the mean soil column) and the soil column which considers the soil uncertainty by best fitting to the recorded ISRS response, respectively. The uncertainty in terms of the soil stiffness is determined by fitting to the ISRS between the SASSI analysis and the recorded data, and is estimated to be about $COV = 0.1$. As displayed by these comparisons, The SASSI computed ISRS using both soil columns produce a close match with the recorded data, except that SASSI analysis does not match the frequency for the recorded spectral peak near about 10Hz for the roof of the reactor building. The spectral peak near 10Hz is believed to be excited by the cross interaction between the two structures. Since the soil property of the backfill between the two buildings is not well characterized in the JNES data, the free field property is applied in the SASSI analysis. That may be the reason why the computed peak is shifted toward higher frequency than the recording.

The seismic induced soil pressure time histories on the R-T structural walls are then computed from the SASSI results, which are calculated using both soil columns. These computed pressure time histories are then compared with the recorded pressure time histories from the respective pressure sensors. Figure 3.2-11 through Figure 3.2-16 present both computed and the JNES recorded seismic induced pressure time histories for the pressure sensors located on the test structures as indicated in Figure 2-20 and Figure 2-21, which designate the locations with circles where the pressure sensors were installed. However, only the solid circles represent the sensors which have actually recorded the earthquake event. The sensors selected for the pressure comparisons are N1, N2 and N4 on the north side wall of the reactor building, and S1, S2 and S4 on the south side wall of the turbine structure.

The seismic induced pressures from the SASSI model are computed from the stresses in the soil elements closest to the locations of the pressure sensors, using the stress component perpendicular to the wall.

The comparison between the recorded time pressure and SASSI calculation shows that the computed pressure peak appear to be much larger than the recorded pressure (about a factor of 2) for the sensor located on the reactor near the base (N1). For the sensor near the mid height of the embedded reactor wall (N2), the computed pressure is significantly less than the recorded pressure. However, the peak pressure for N2 (250N/m^2) is only a fraction of the peak pressure for N1 (1000N/m^2), and the large gap in the pressure comparison may be due to the large noise/signal ratio present in the recording, as will be discussed in the Fourier spectra analysis later in this section.

For the pressure sensor near the ground surface (N4), Figure 3.2-13 shows the lower prediction of the peak pressure by SASSI than the recorded pressure. However, as will be shown later, if the low frequency content of the recorded pressure is appropriately adjusted, the comparison between the computed and recorded pressures in the frequency range of interest would be much closer to each other. It is noted that the low frequency amplitudes in the Fourier spectrum are primarily attributed to the noise inherent in the pressure recording instrument.

For the turbine building, the trend of higher computed pressures than the recordings is evident for all the pressure sensors being compared, as indicated in Figure 3.2-14 through Figure 3.2-16. Also observed in these figures is that the pressure comparison made for the sensor near the ground appears better than the other sensors. This is due to the relatively larger pressure magnitude and lower noise/signal ratio for the sensor near the ground surface.

To compare the SASSI results with the sensor data in terms of the frequency content, the time history responses of both computed and recorded data are transformed in the frequency domain in terms of Fourier spectra of the respective quantity. Figure 3.2-17 through Figure 3.2-19 present the Fourier spectra of the pressure responses on the north side wall of the reactor building. The Fourier spectra shown in these figures are smoothed using the algorithm described in Section 3.1.2 of this report. These comparisons show that relatively good match of the frequency content is achieved by the SASSI analysis for all three locations. However, the Fourier amplitudes of the SASSI estimate are off compared with the sensors. For the sensor near the base (DA-SE-N1), the computed Fourier amplitude mostly envelope the sensor, except for low frequencies where it is believed that the sensor data were affected by the noise present in the recorded data. For the pressure sensors near the mid height wall (DA-SE-N2) and the ground surface (DA-SE-N4), the SASSI estimates fall below the recorded pressure response for both sensors.

For the turbine building, the comparisons of the Fourier spectra of the pressure responses between the SASSI estimate and the sensor recorded pressures are plotted in Figure 3.2-20 through Figure 3.2-22. These comparisons show that the SASSI result captures the overall frequency behavior of the recorded pressure response for the sensors compared. Furthermore, an excellent match for Fourier amplitude in the frequency band of interest is also achieved between the SASSI result and the recording for the sensor near the ground surface, as shown in Figure 3.2-22. Similar to what is observed in the quality of the sensor data for the twin reactor configuration, there is a persistent upward drift of the Fourier amplitude in low frequencies for the sensor pressure data. It is believed that this low frequency behavior is due to the presence of high noise/signal ratio in the recorded data.

Vertical Response Analysis

Similar to the twin reactor configuration, the correlation for the vertical seismic response is not as a straightforward process as for the horizontal response comparisons. The vertical seismic response is induced not only by the vertical seismic input, but also due to the two orthogonal horizontal seismic inputs through the rocking modes. Given the layout of the pressure sensors on the footprint of the R-T model shown in Figure 2-17, only the transducers located on the edges of the building basemat have actually recorded the pressure response; those sensors inside the basemat did not record any data. Therefore, in order to compare the vertical response analysis results with the recorded vertical pressure data, the horizontal effect on the vertical recorded pressure data need to be removed. This is done by taking an average over all vertical pressure data on the basemat. Therefore, the SASSI vertical response result is compared with the averaged sensor pressure response.

Following the approach described above, the vertical response analysis is performed by applying the recorded free field motion in the vertical direction at the control point located 35m below grade. The vertical ISRS results are computed at the center of the basemat and the roof, and are compared with the respective accelerometer recordings at these locations as designated in Figure 3.2-3 as B1A-V0 and RFA-V0, respectively. Note that the roof center of the reactor building was not instrumented for the vertical direction; therefore, the accelerometer installed on a corner of the roof is used for the comparison. The comparisons between the predicted vertical ISRS and the vertical accelerometer recordings are shown in Figure 3.2-23 through Figure 3.2-26, for the basemat and the roof, respectively.

Similar to the soil uncertainty considered for the horizontal response analysis, the effect of the soil uncertainty is also considered for the vertical response analysis by varying the P-wave velocity of the soil (V_p). One set of results is computed using the JNES soil geotechnical data, which is interpreted as the best estimate soil property, designated in the figures for this study as the mean soil V_p . Since the vertical response is controlled by the compressional wave, the second analysis is therefore performed by adjusting the mean soil p-wave velocity V_p to achieve the best fit of the computed vertical ISRS to the recording.

As shown in these figures for the vertical ISRS comparison, the SASSI prediction captures both the frequency content and the spectral peaks across the most of the frequency band, except for the high frequency peak at which the SASSI result with the JNES soil shifts to a lower frequency. However, when the uncertainty of about 10% the mean soil p-wave velocity (equivalent to a value of 0.2 for the COV of the soil stiffness reduction) is incorporated, excellent comparisons are achieved between the SASSI and recorded ISRS, with the exception of the reactor roof. As described in the previous paragraph, the accelerometer used for the roof comparison is located on a corner rather than in the center of the roof, therefore, the recorded ISRS at this location has both vertical and horizontal inputs, which is the reason why the SASSI result did not agree with the recorded ISRS response for the reactor roof. It is also observed that the vertical SASSI analysis achieves much better comparison between the computed vertical ISRS and the accelerometer recordings than the horizontal response analysis.

The seismic induced pressures on the basemat are then computed from the SASSI analysis for both the mean and the mean minus COV soil columns. As mentioned above, in order to remove the influence of the horizontal inputs from the recorded vertical pressure measurements on the basemat, the sensor pressures at the corner locations as shown in Figure 2-17 are averaged. The averaged vertical sensor pressures are then compared with the predicted pressures computed at the center of the basemat. Figure 3.2-27 and Figure 3.2-28 plot the averaged vertical pressure time histories from the JNES recorded vertical pressures and the SASSI computed basemat pressures for both the reactor and the turbine structures. As indicated by these figures, comparable pressures are obtained by the SASSI analysis.

The computed and recorded pressure data are then transformed in the frequency domain where their respective Fourier spectra are computed and smoothed using the algorithm described in Section 3.1.2 of this report. These Fourier spectra are then plotted and compared, as shown in Figure 3.2-29 and Figure 3.2-30. The Fourier spectra for the averaged recorded pressures still have a finite amplitude approaching to the zero frequency similar to the observation made in other cases as discussed earlier, suggesting high noise/signal ratio in the recorded data. As far as the frequency content is concerned, the analysis result predicted most of the frequencies. Although less accurate than the ISRS comparison, the computed pressure amplitudes for the vertical direction achieve much better comparisons with the recorded data than for the horizontal direction.

Soil Properties of Two different Model DA,DF

No.		Thickness (m)	Vs (m/sec)	Vp (m/sec)	Poisson's ratio	Unit weight (tf/m3)	Damping h(%)
1	0.0~-2.0	2.0	165	280	0.234	1.64	5
2	-2.0~-4.0	2.0	250	445	0.269	1.83	5
3	-4.0~-9.5	5.5	255	825	0.447	1.70	5
4	-9.5~-13.0	3.5	510	1665	0.448	2.05	2
5	-13.0~-25.2	12.2	1110	2770	0.404	2.15	2
6	-25.2~-52.75	27.55	2010	4350	0.364	2.25	2
7	0.0~-1.0	1.0	140	315	0.377	1.80	5
8	-1.0~-2.0	1.0	200	360	0.277	1.80	5
9	-2.0~-3.0	1.0	220	415	0.305	1.80	5
10	-3.0~-4.0	1.0	235	450	0.313	1.80	5
11	Soft Soil Layer	0.5	150	245	0.20	1.70	5

- 1) Below GL.-52.75m, soil is assumed as semi-infinite soil, which property is the same as layer 6.
- 2) Damping is calculated using Q. ($Q=V_s/15, h=1/(2Q)$)

$$\nu = \frac{(V_p/V_s)^2 - 2}{2[(V_p/V_s)^2 - 1]}$$

Figure 3.2-2 JNES R-T Configuration Soil Properties

Source: *Model Test on Dynamic Cross Interaction Effect for Nuclear Power Plant Buildings*, Technical Report, Japan Nuclear Energy Safety Organization (JNES), Tokyo, Japan, March 2002. Permission to use this copyrighted material is granted by JNES.

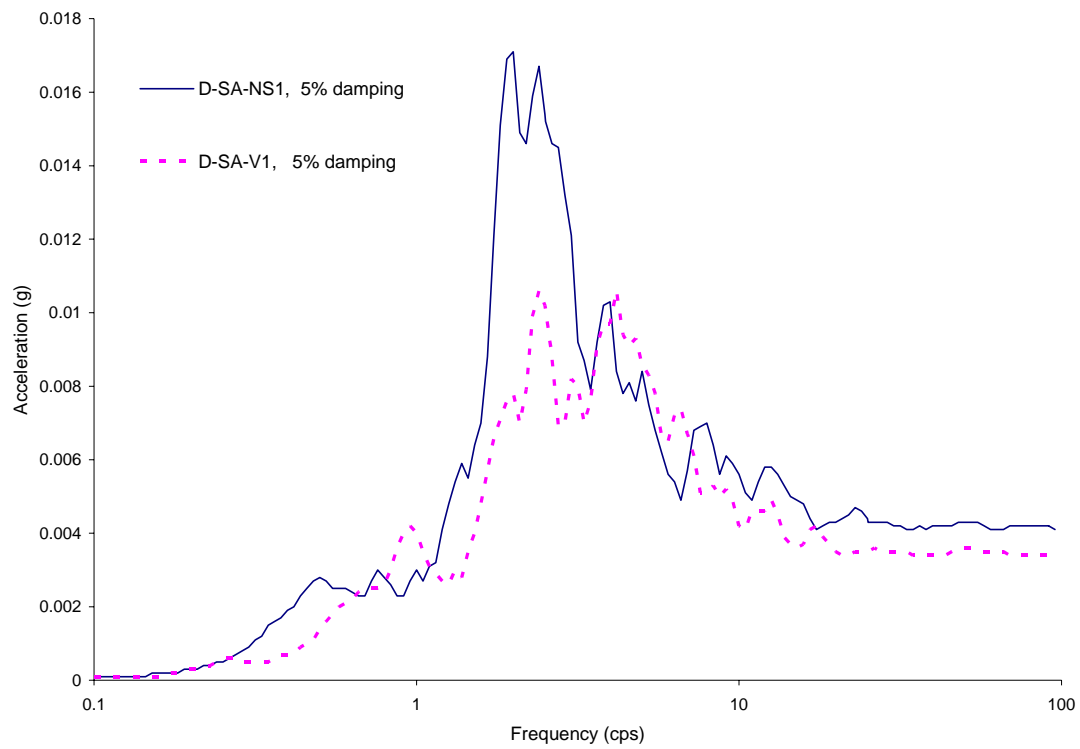


Figure 3.2-4 R-T Model Input Motions

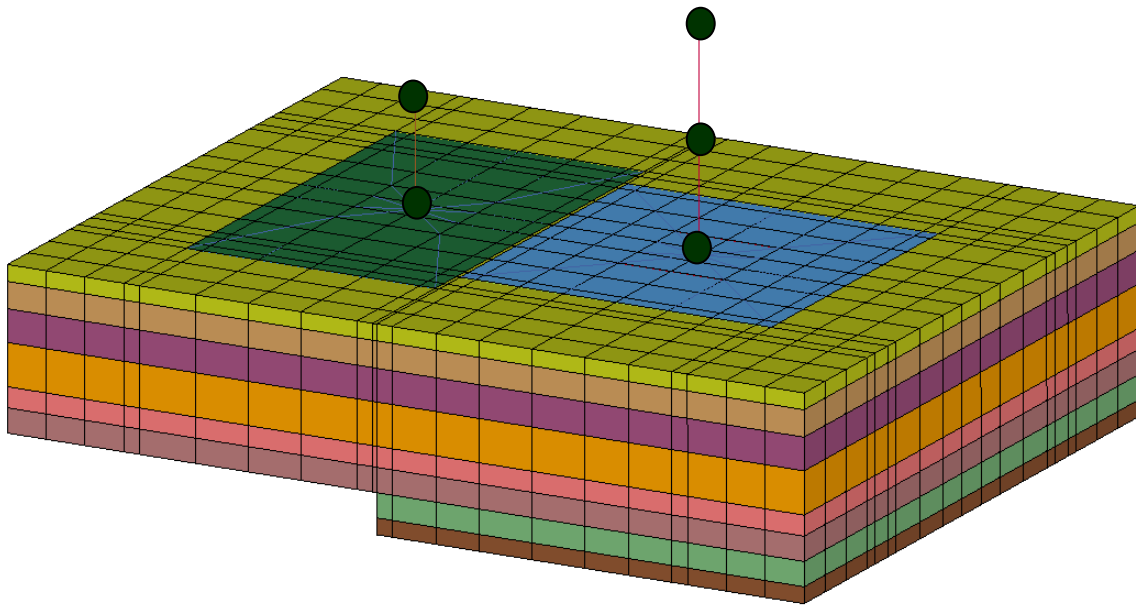


Figure 3.2-5 SASSI R-T Structural Model

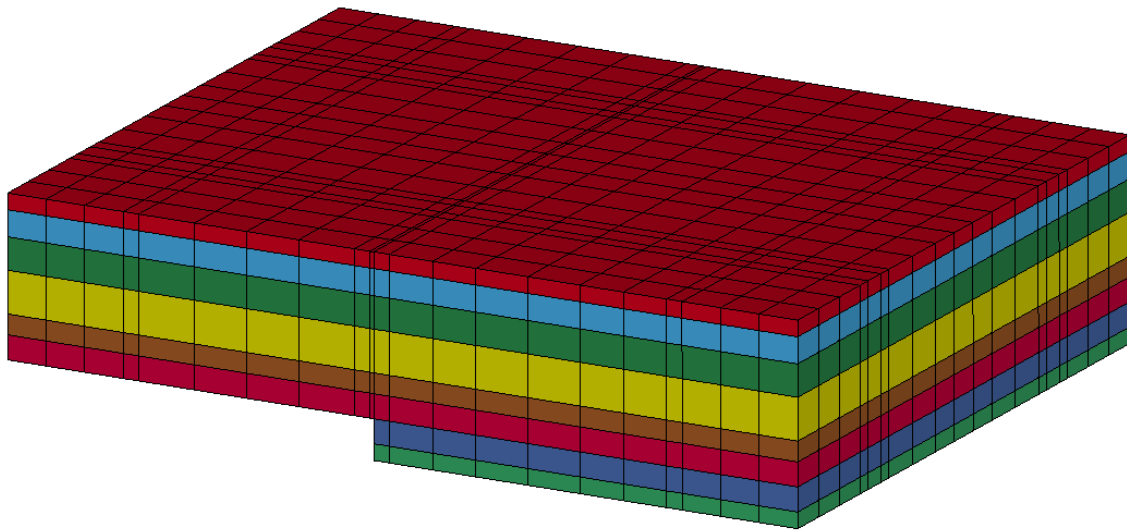


Figure 3.2-6 SASSI R-T Excavated Soil Model

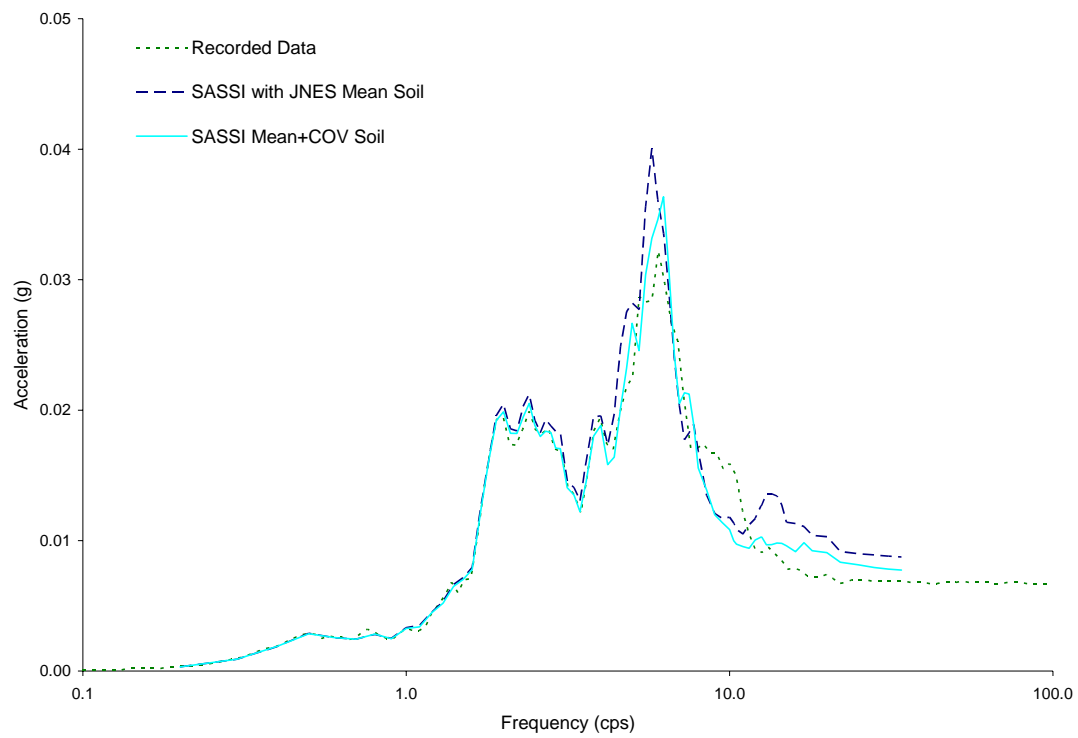


Figure 3.2-7 Comparison of Horizontal Response Spectra at Basemat Center of Reactor for R-T Model

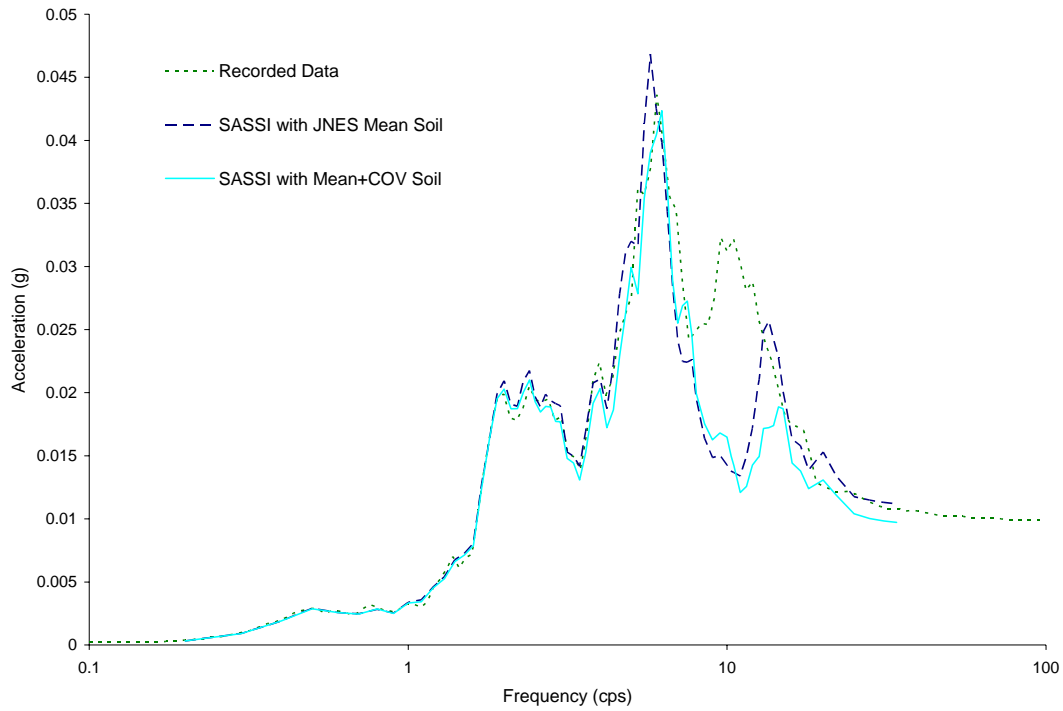


Figure 3.2-8 Comparison of Horizontal Response Spectra at Roof Center of Reactor for R-T Model

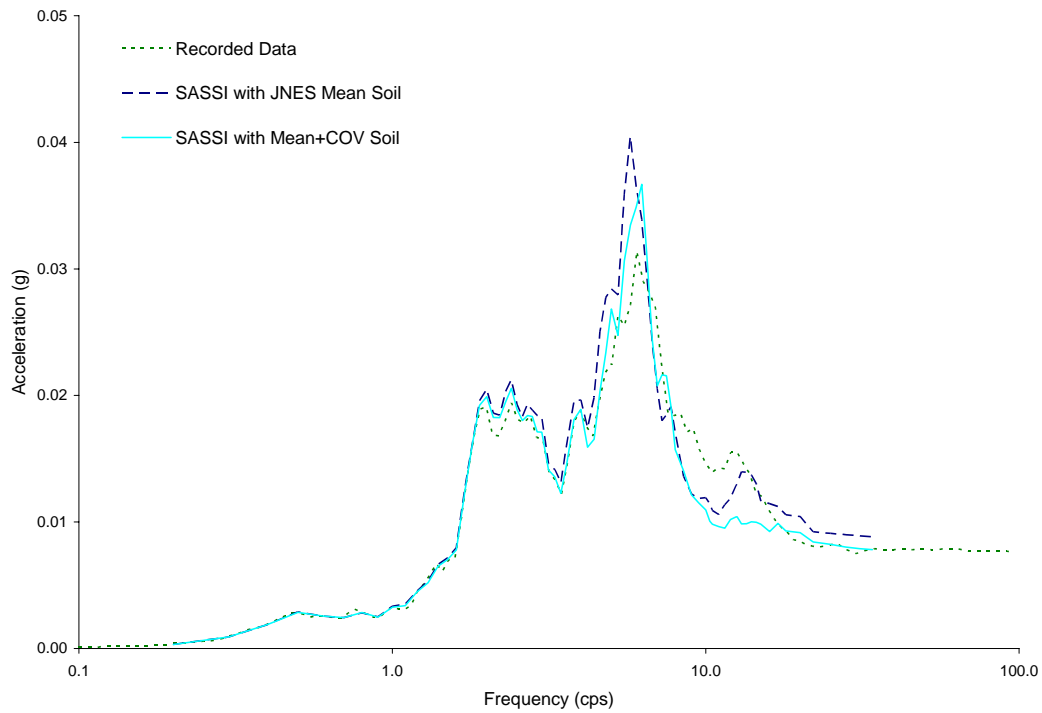


Figure 3.2-9 Comparison of Horizontal Response Spectra at Basemat Center of Turbine for R-T Model

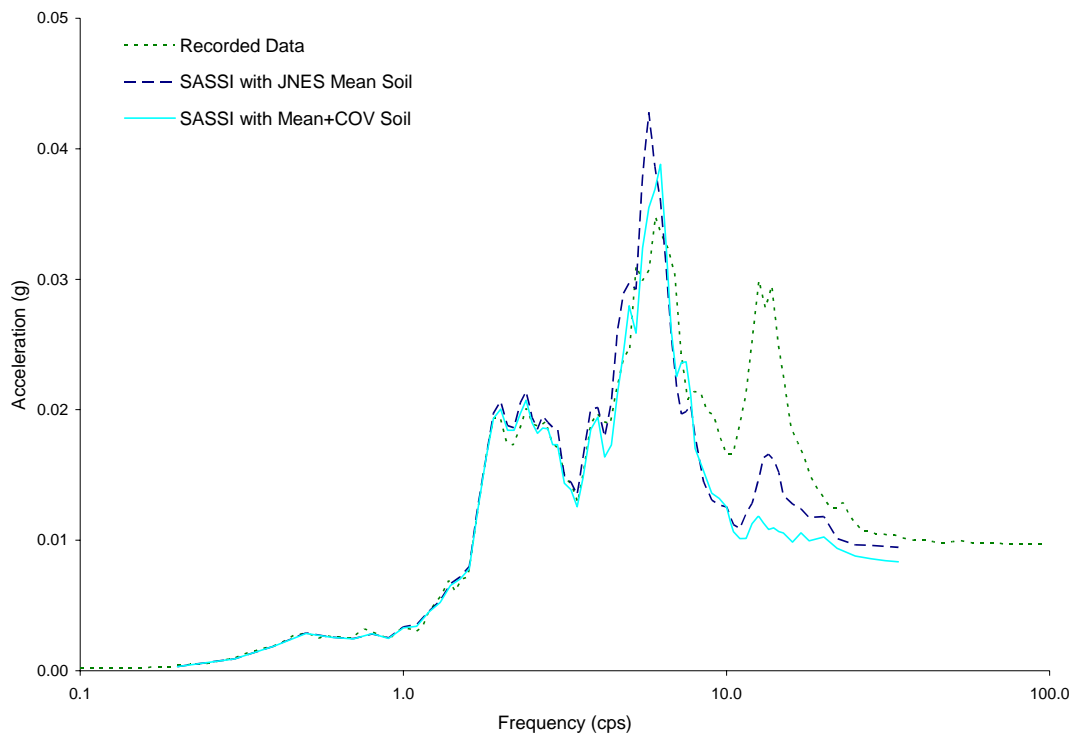


Figure 3.2-10 Comparison of Horizontal Response Spectra at Roof Center of Turbine for R-T Model

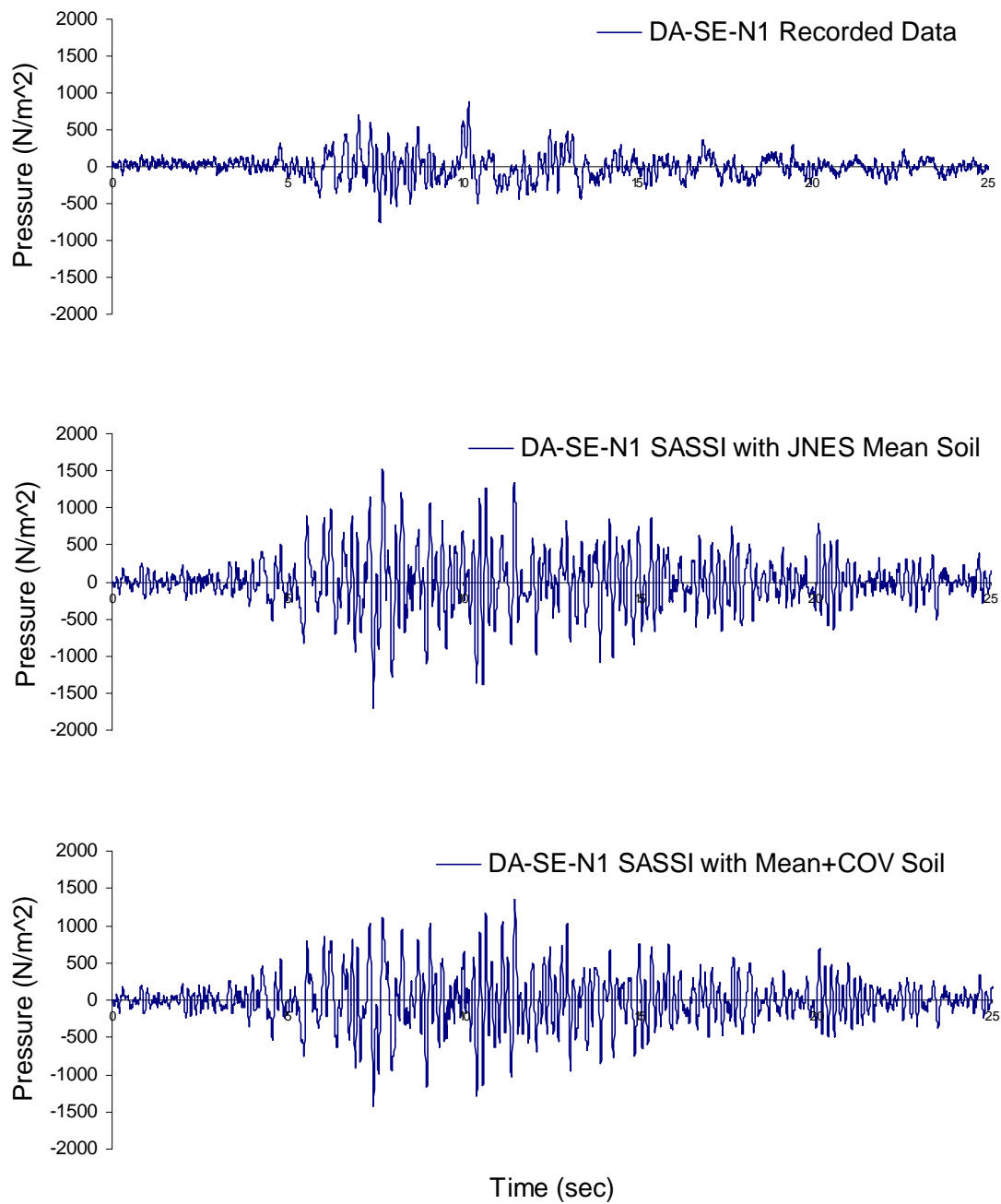


Figure 3.2-11 Comparison of Seismic Induced Soil Pressure at Sensor DA-SE-N1

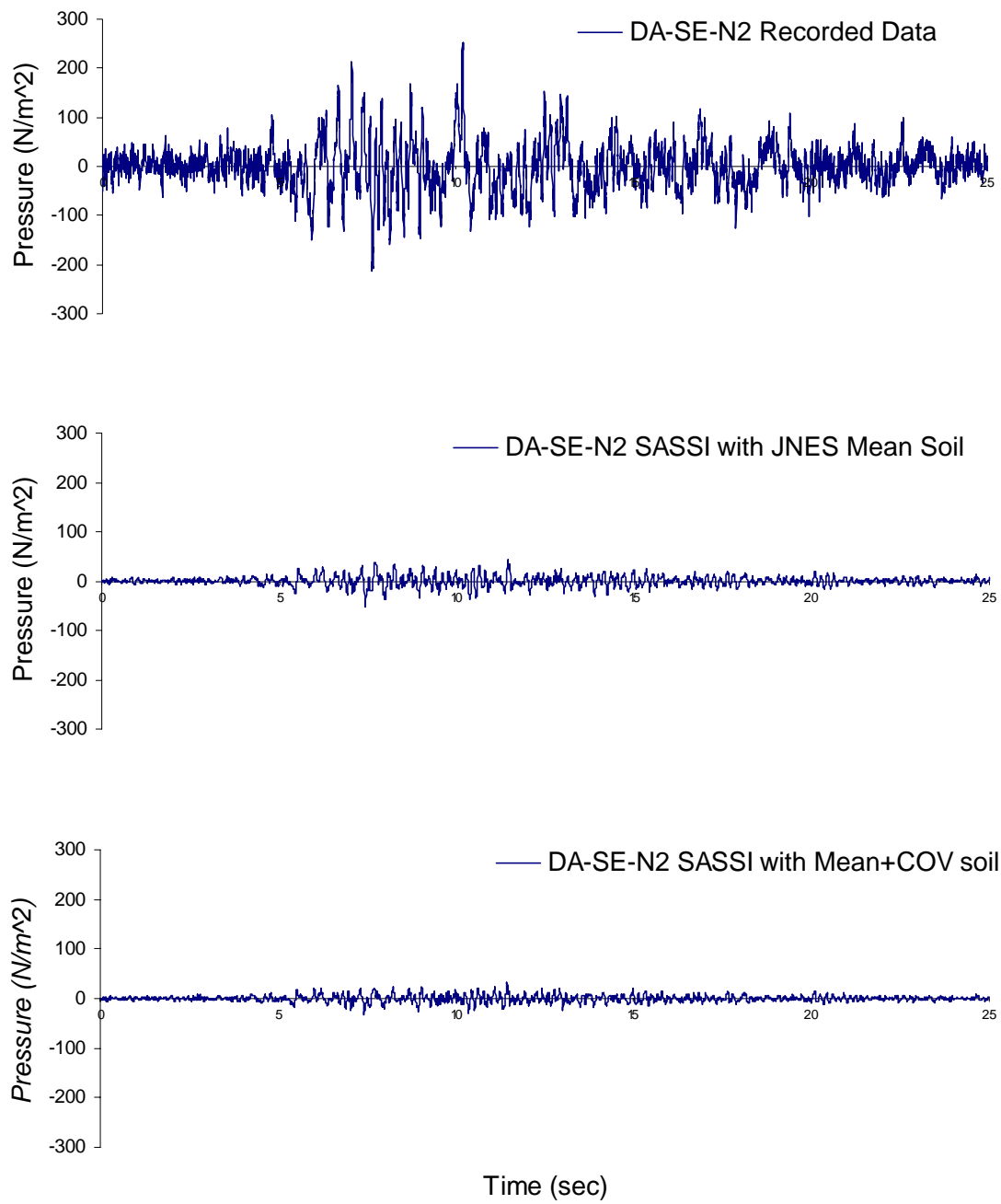


Figure 3.2-12 Comparison of Seismic Induced Soil Pressure at Sensor DA-SE-N2

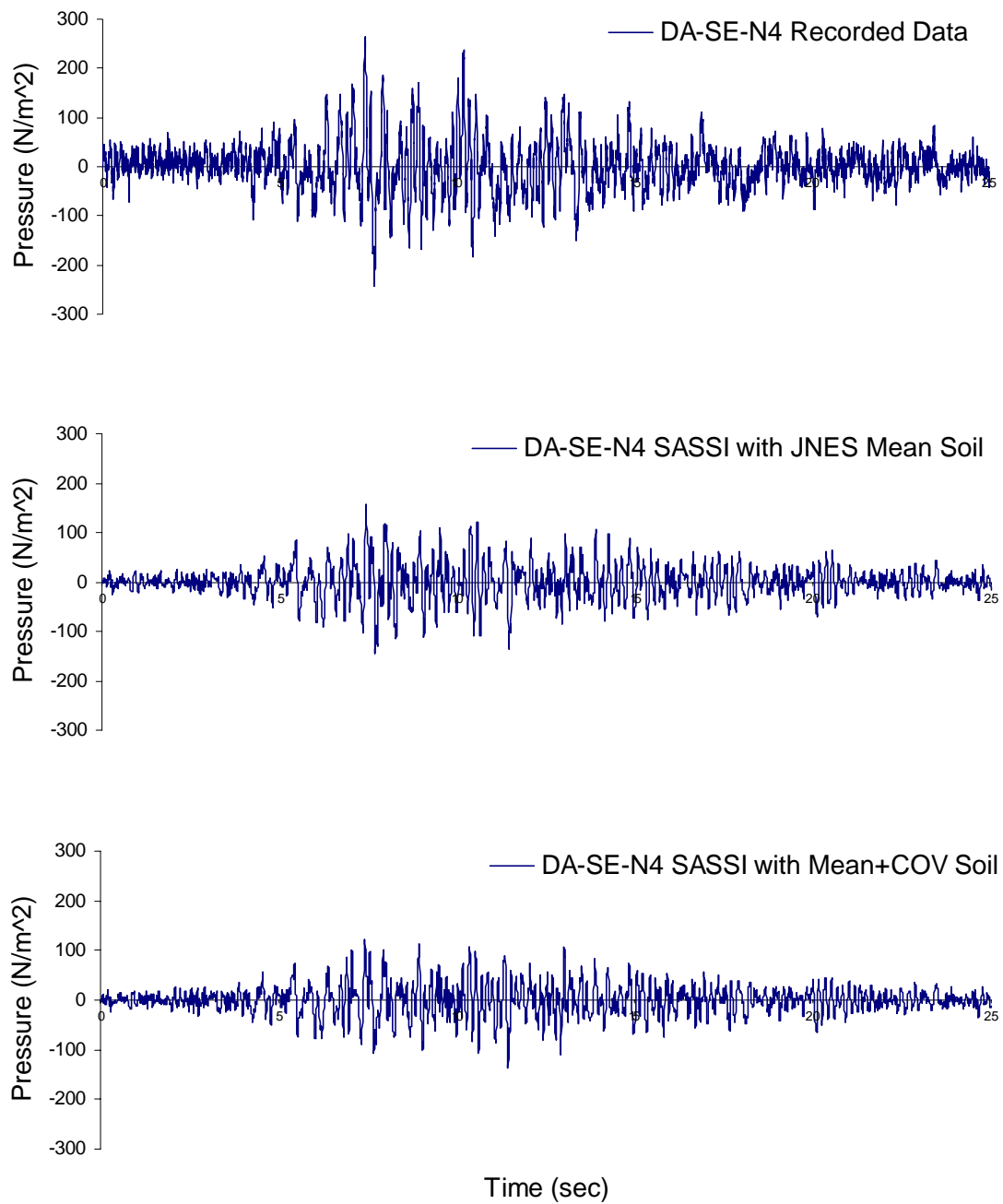


Figure 3.2-13 Comparison of Seismic Induced Soil Pressure at Sensor DA-SE-N4

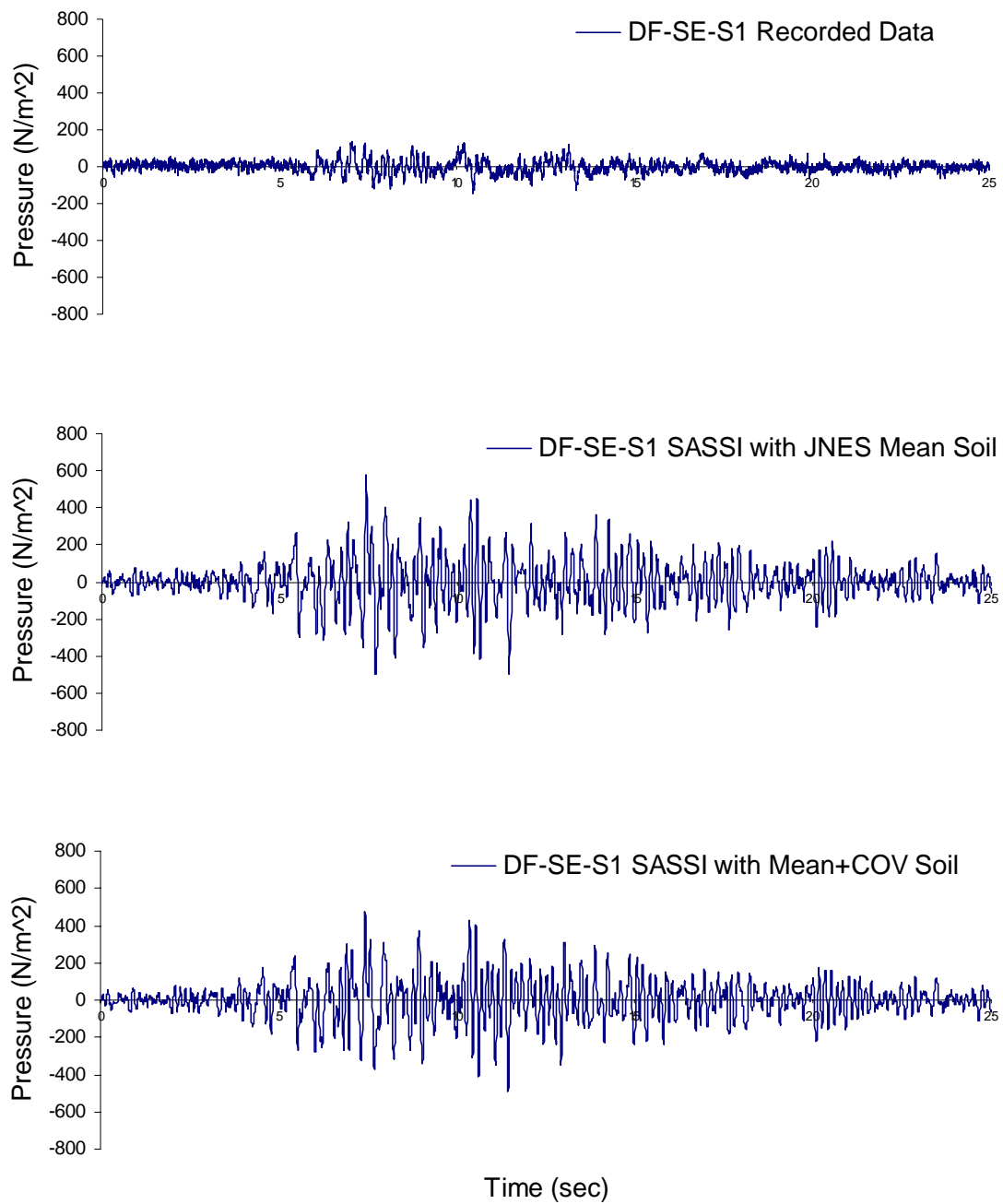


Figure 3.2-14 Comparison of Seismic Induced Soil Pressure at Sensor DF-SE-S1

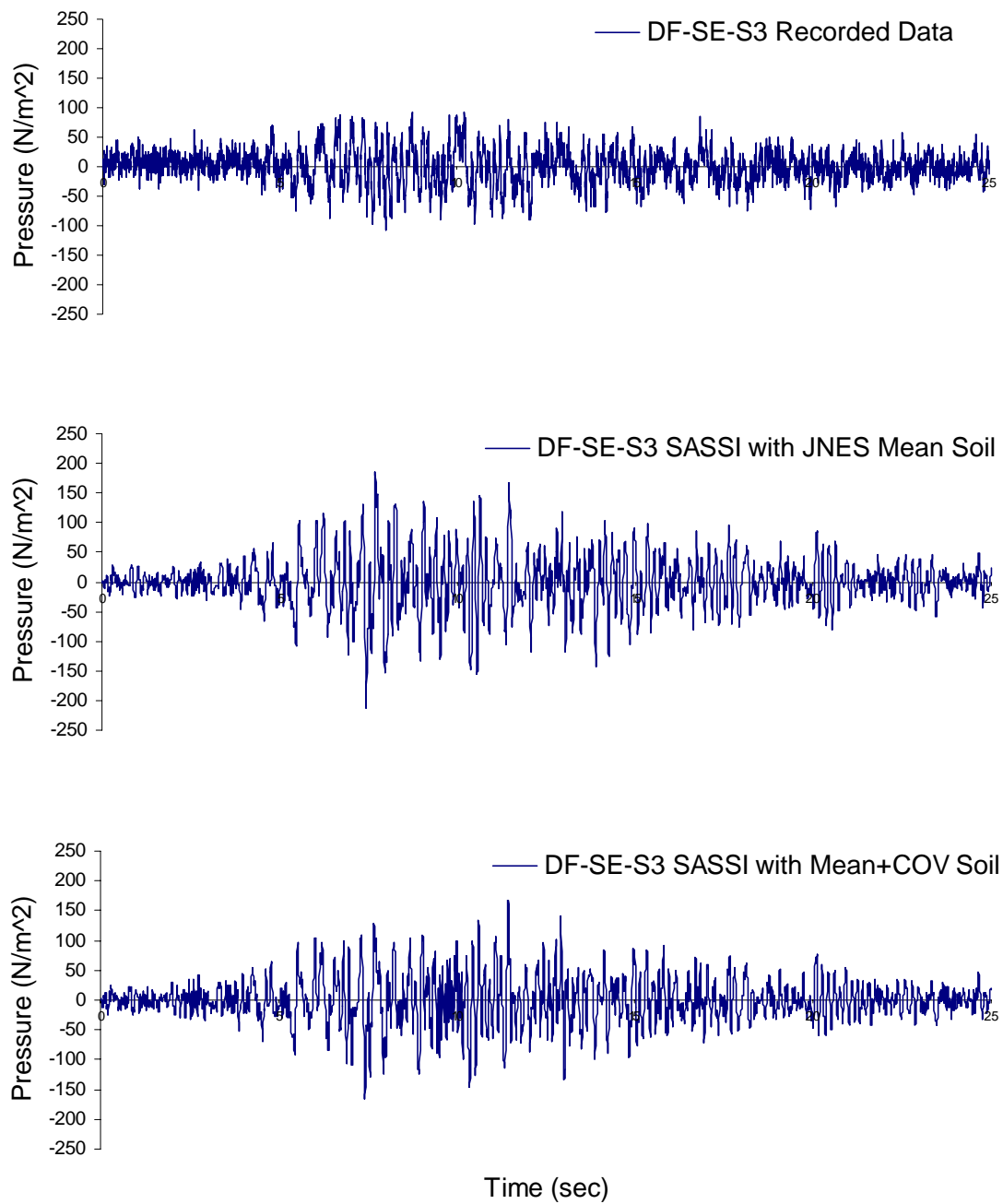


Figure 3.2-15 Comparison of Seismic Induced Soil Pressure at Sensor DF-SE-S3

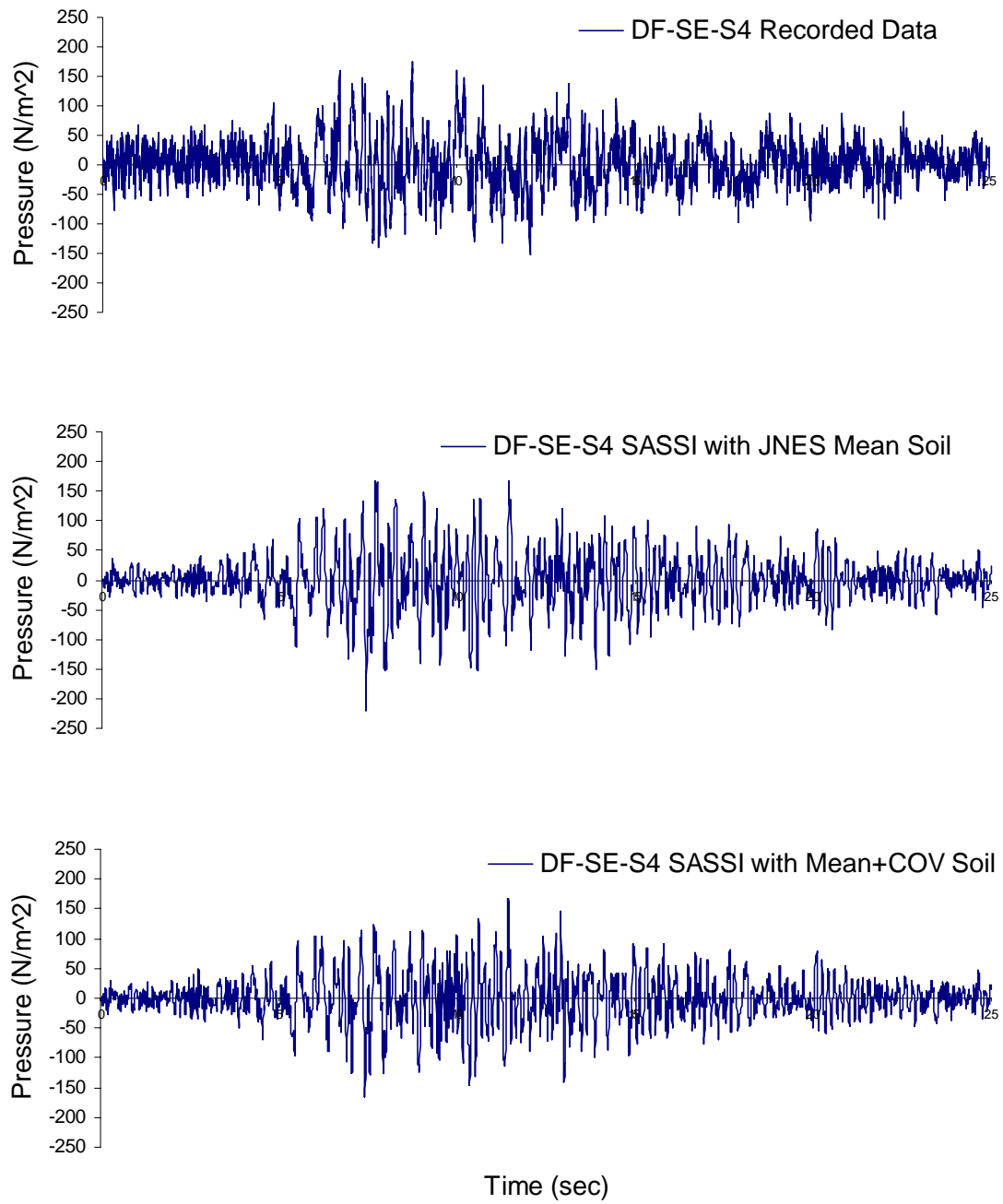


Figure 3.2-16 Comparison of Seismic Induced Soil Pressure at Sensor DF-SE-S4

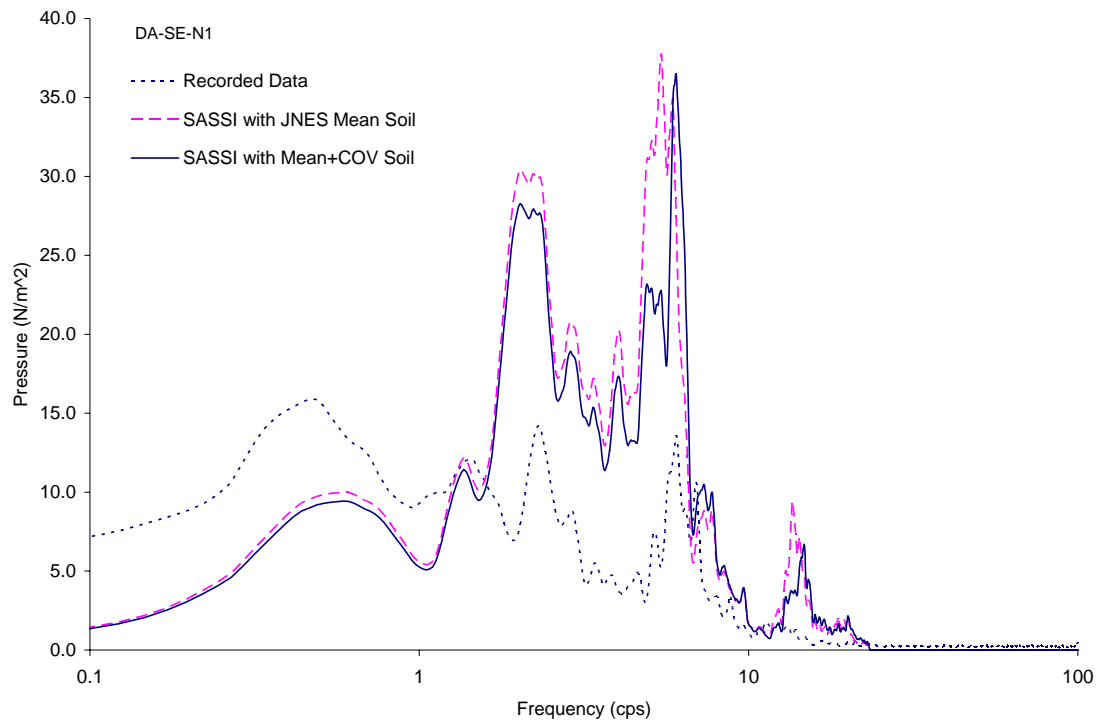


Figure 3.2-17 Comparison of Fourier Spectra of Soil Pressure at Sensor DA-SE-N1

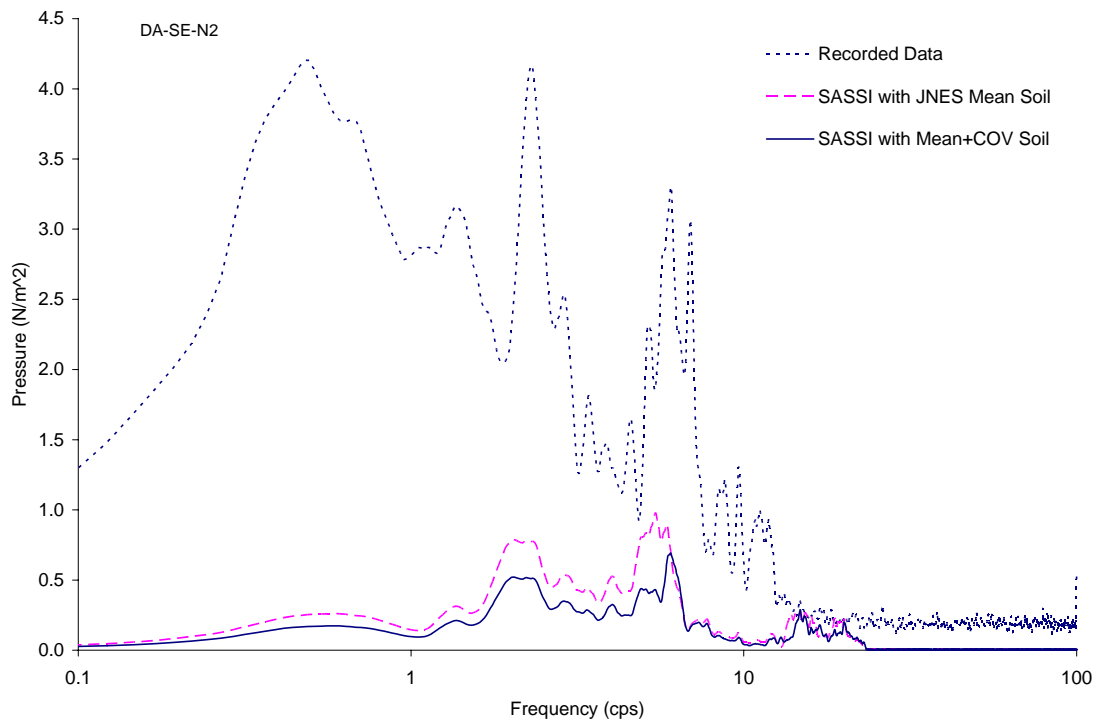


Figure 3.2-18 Comparison of Fourier Spectra of Soil Pressure at Sensor DA-SE-N2

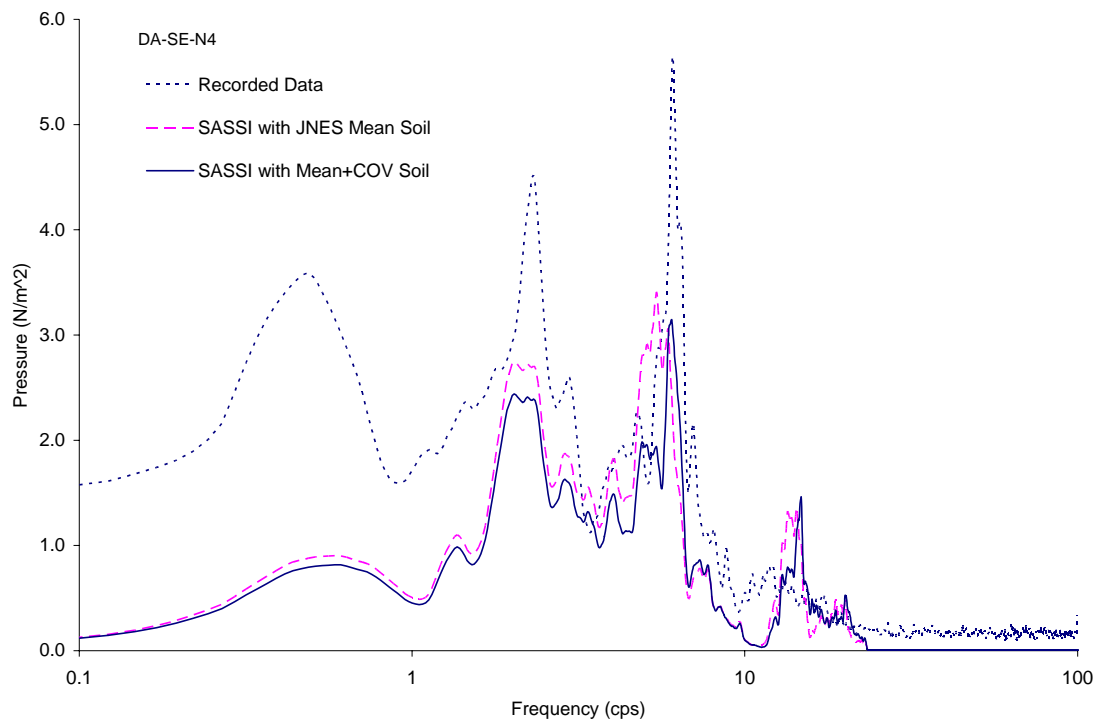


Figure 3.2-19 Comparison of Fourier Spectra of Soil Pressure at Sensor DA-SE-N4

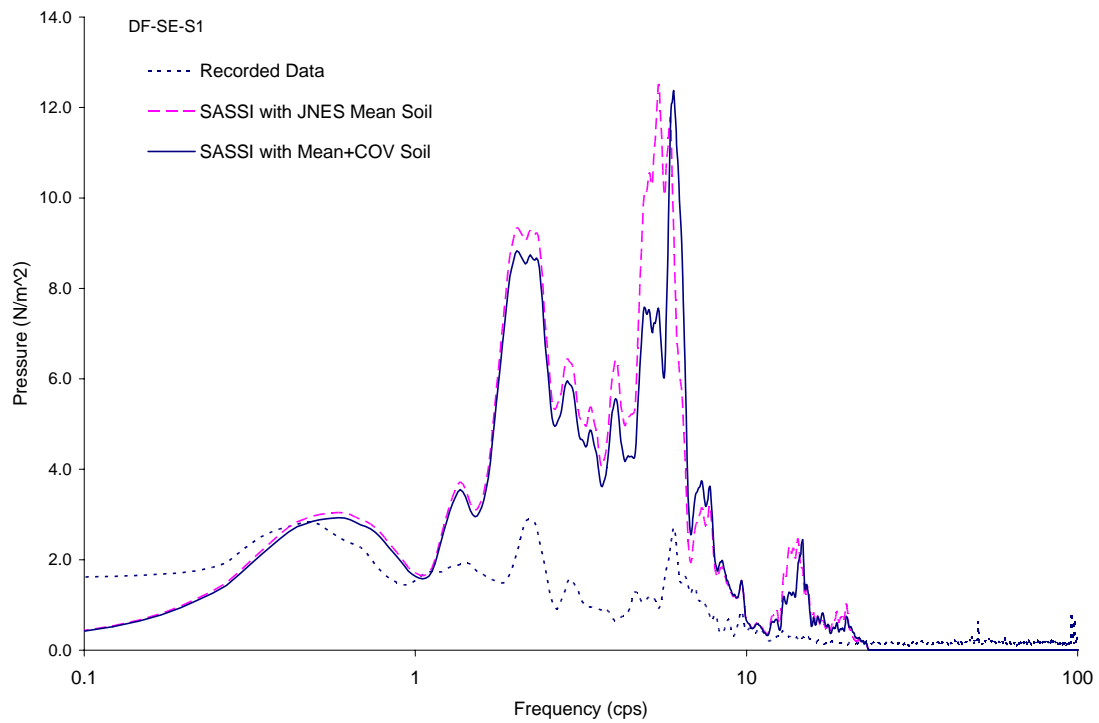


Figure 3.2-20 Comparison of Fourier Spectra of Soil Pressure at Sensor DF-SE-S1

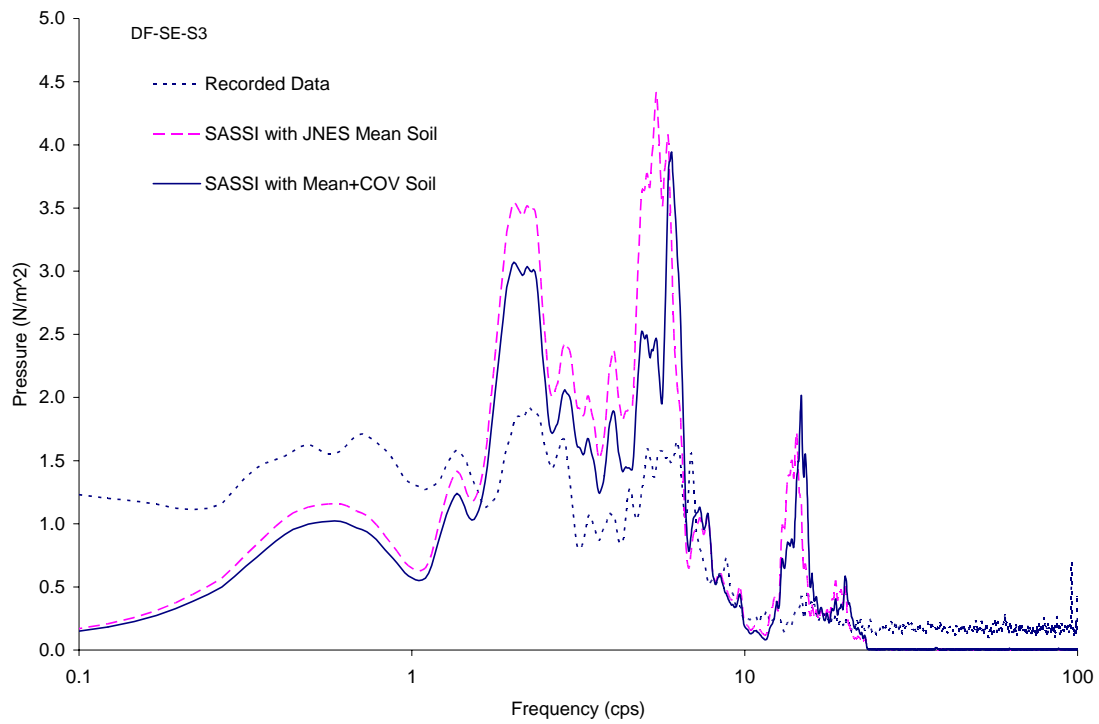


Figure 3.2-21 Comparison of Fourier Spectra of Soil Pressure at Sensor DF-SE-S3

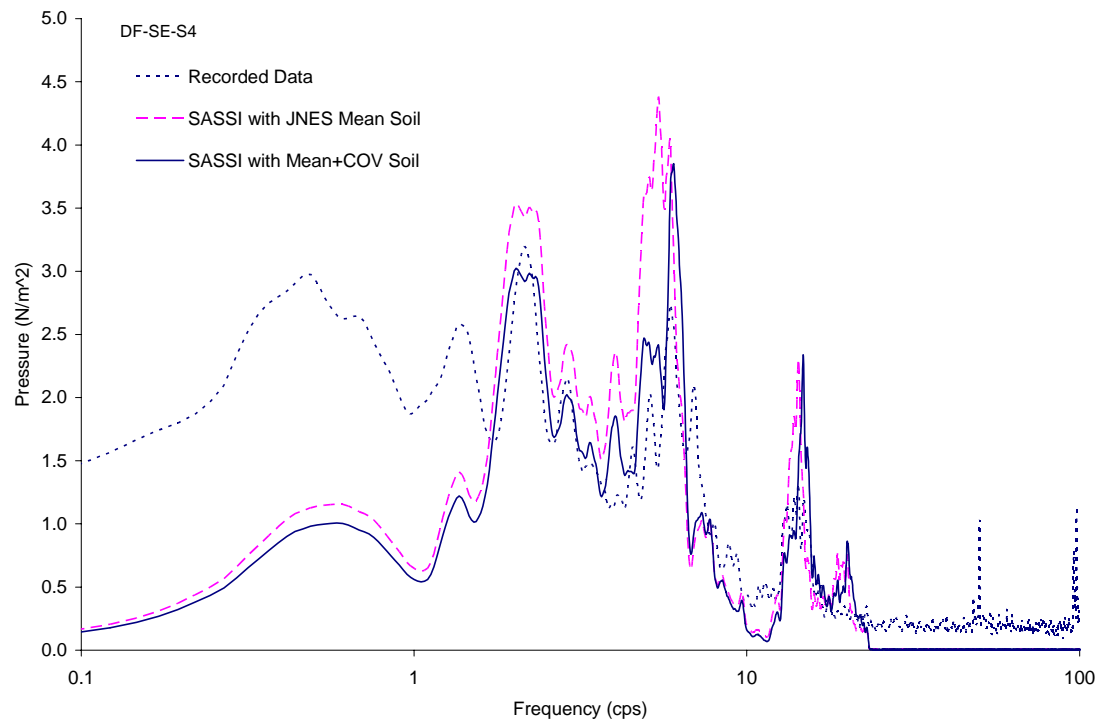


Figure 3.2-22 Comparison of Fourier Spectra of Soil Pressure at Sensor DF-SE-S4

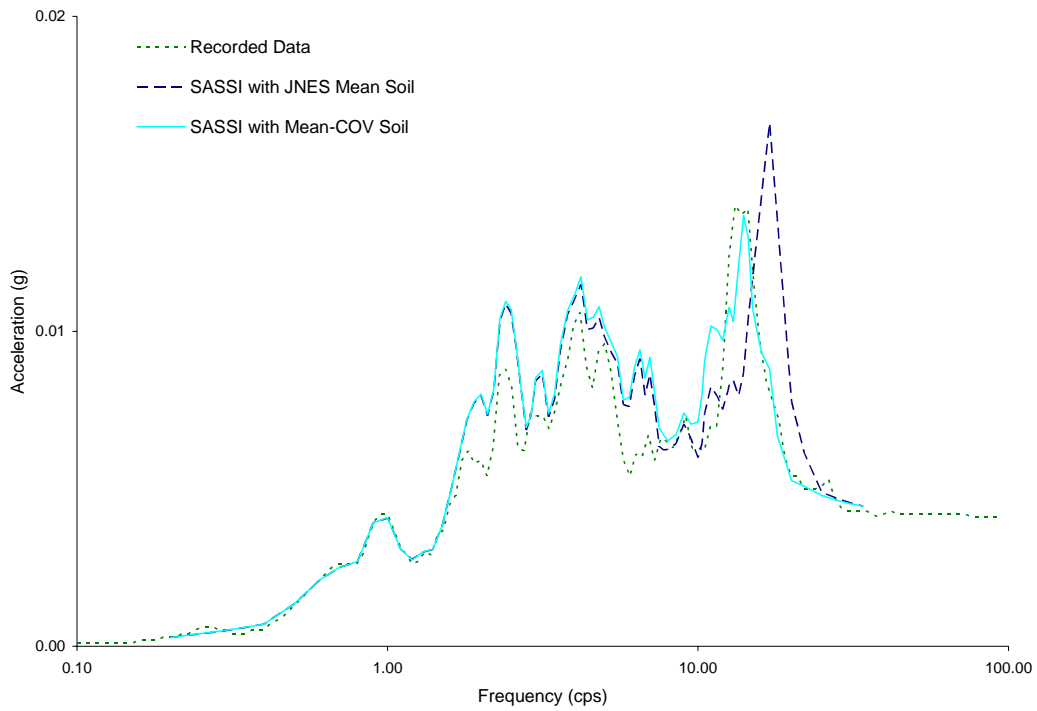


Figure 3.2-23 Comparison of Vertical Response Spectra at Basemat Center of Reactor for R-T Model

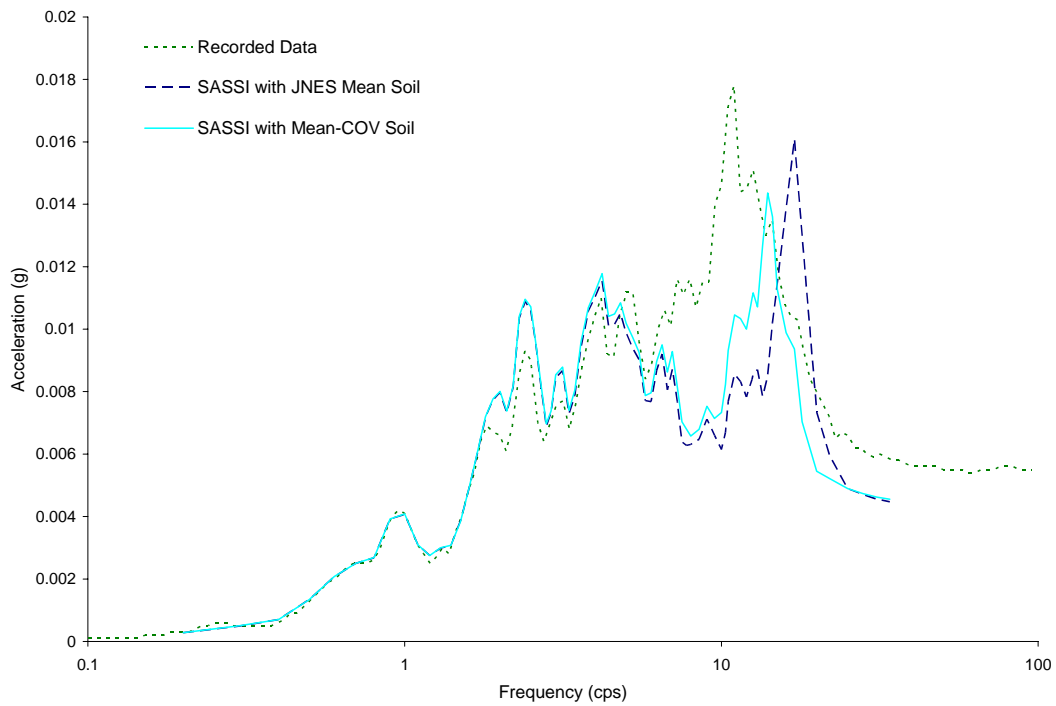


Figure 3.2-24 Comparison of Vertical Response Spectra at Roof Center of Reactor for R-T Model

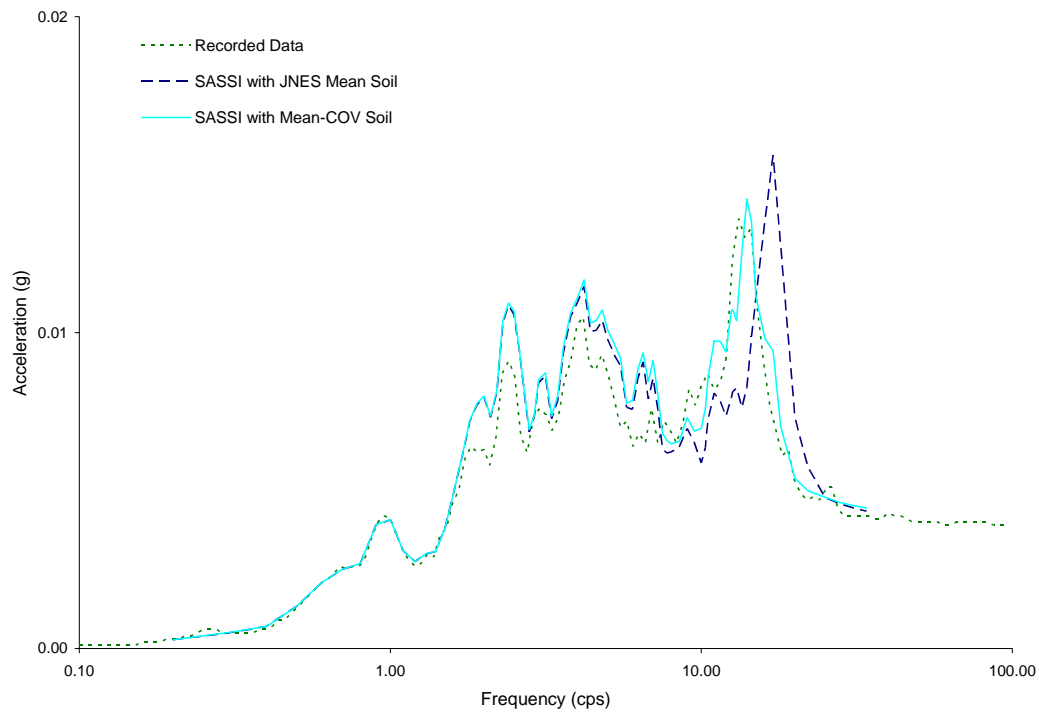


Figure 3.2-25 Comparison of Vertical Response Spectra at Basemat Center of Turbine for R-T Model

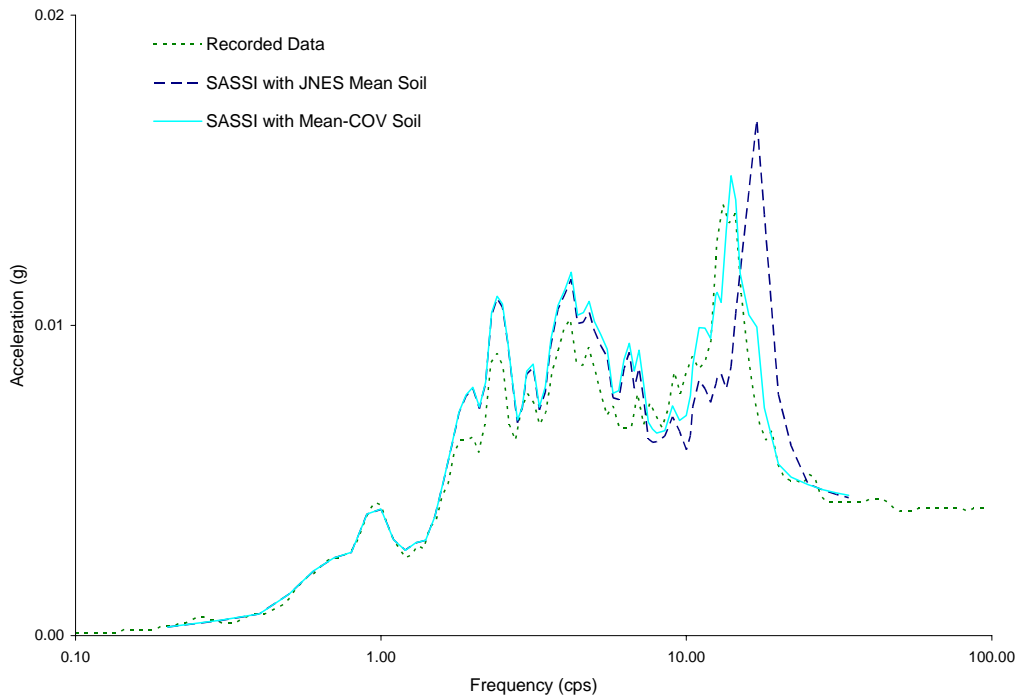


Figure 3.2-26 Comparison of Vertical Response Spectra at Roof Center of Turbine for R-T Model

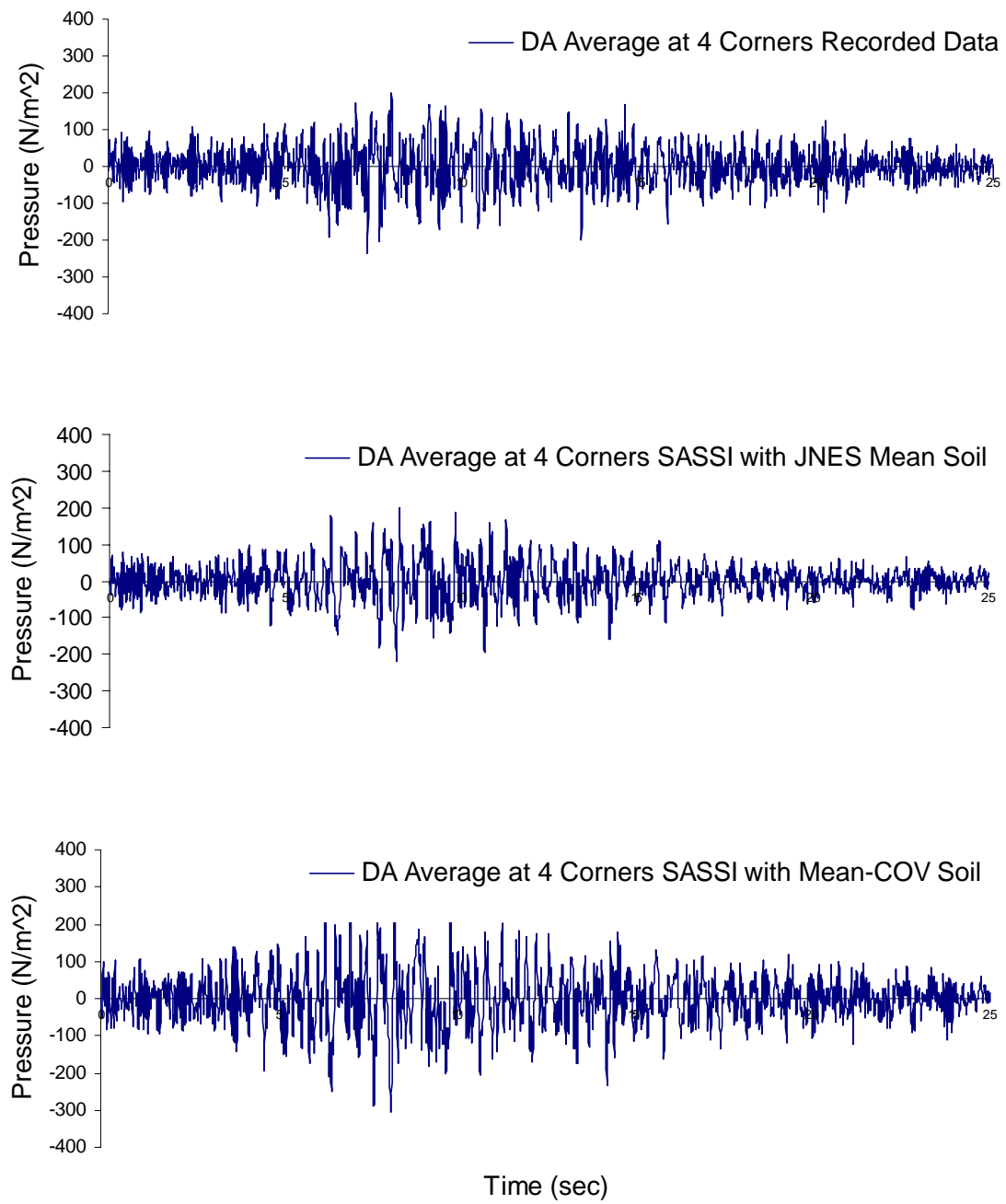


Figure 3.2-27 Comparison of Averaged Vertical Seismic Induced Soil Pressure for DA

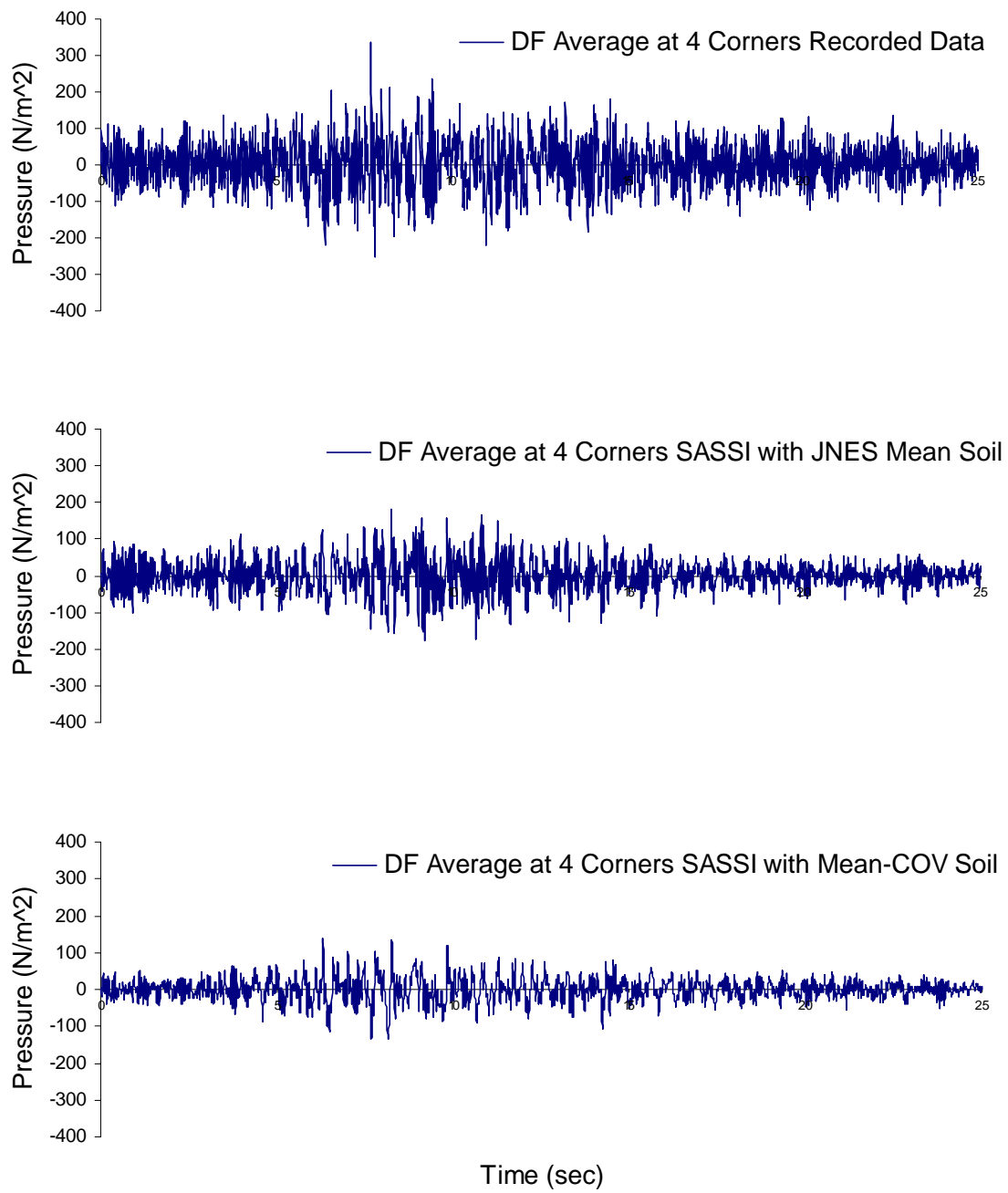


Figure 3.2-28 Comparison of Averaged Vertical Seismic Induced Soil Pressure for DF

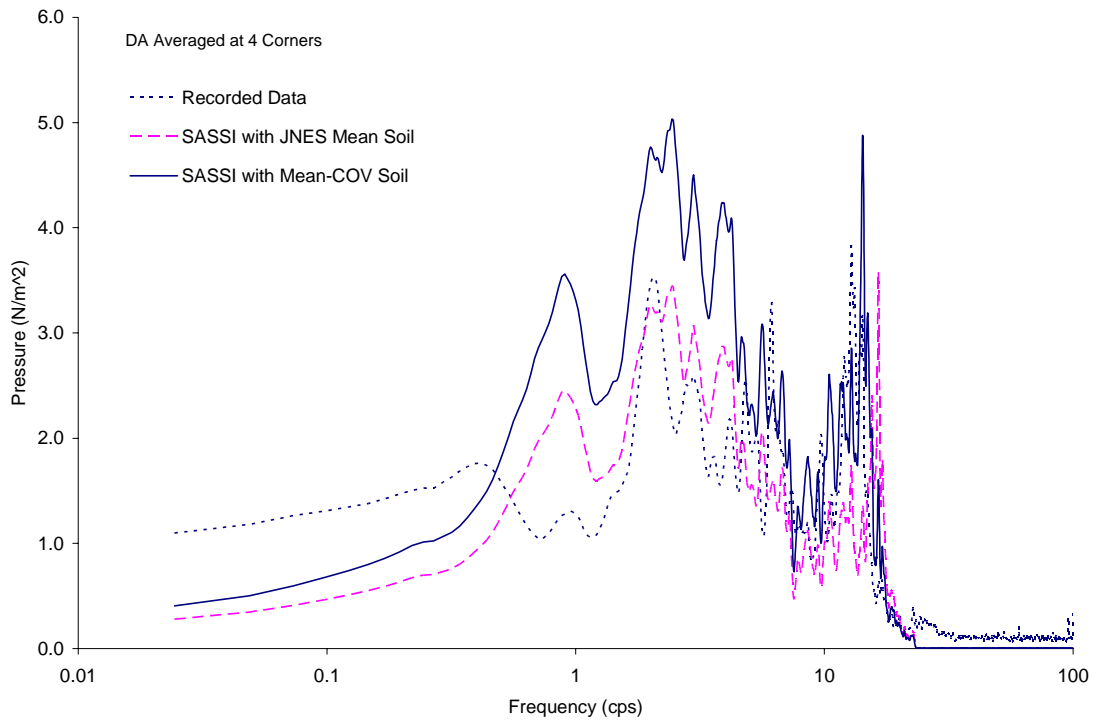


Figure 3.2-29 Comparison of Fourier Spectra of Vertical Soil Pressure at DA Basemat

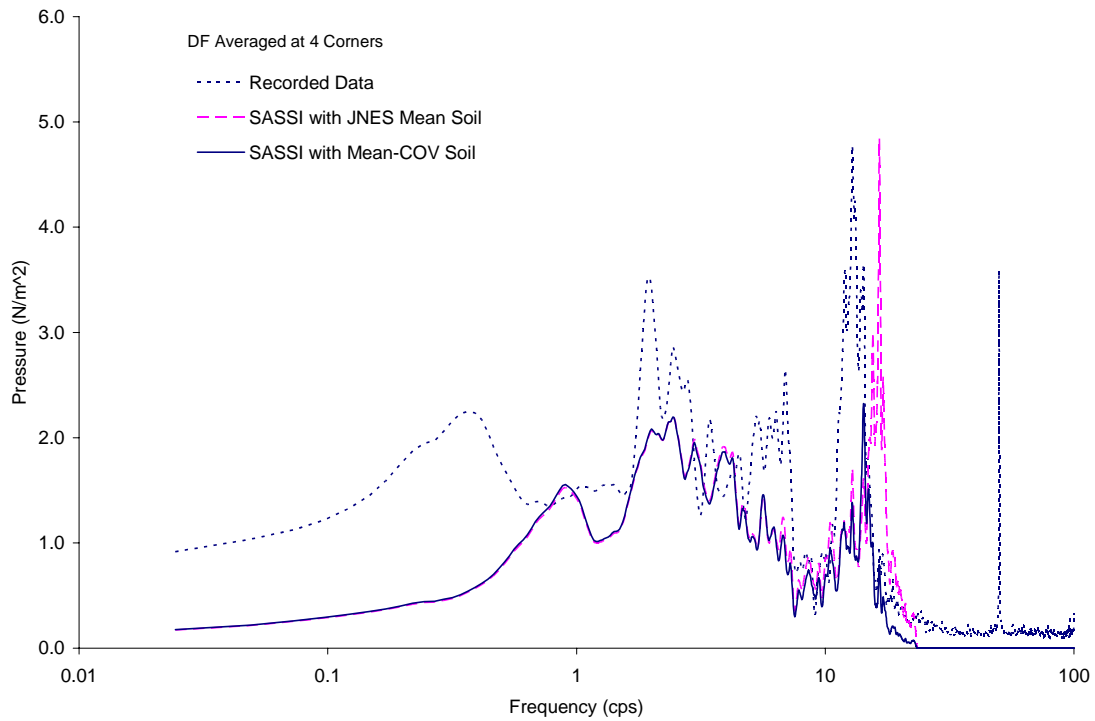


Figure 3.2-30 Comparison of Fourier Spectra of Vertical Soil Pressure at DF Basemat

3.3 Methodology Assessment

As discussed above, BNL performed SASSI analyses for the JNES test models of both the twin reactor and R-T configurations. Comparisons were made between the SASSI results and the JNES field recorded earthquake responses in terms of ISRS and the soil pressures for both horizontal and vertical directions. Insights learned in comparing the analysis with the test data are then used to assess the performance of the SASSI analysis.

For the ground motion analyzed, SASSI performed extremely well in predicting the test model's ISRS response, as exhibited by the comparisons. Although the soil uncertainty plays a critical role in the correlation, the level of the soil uncertainty is well within the range of the current understanding in geotechnical applications. Due to the nature of the narrow band frequency content of an actual earthquake motion, the correlation of the analysis with test data is sensitive to the uncertainty inherent in the soil property. In addition, SASSI did not capture well the spectral peak at the roof of the reactor building.

However, for seismic induced pressures, the correlation between the analysis and the test data indicates that 1) the analysis can generally capture the frequency content of the test data, and 2) better prediction is obtained for the vertical analysis than the horizontal analysis. The reason for less accurate horizontal pressure correlation, aside from the high noise/signal ratio inherent in the recorded data, is that the horizontal response is primarily induced by the SH-waves which generate the predominant shear stress in the soil, therefore, the soil pressure becomes a secondary stress component. While for the vertical response, the system is subjected to the P-wave which induces pressures as the primary stress in soils. Therefore, as shown by these pressure comparisons, the pressure correlations were much better for the vertical response than the horizontal response.

4 LS-DYNA ANALYSIS

This section describes the correlation analysis of the JNES test models using the LS-DYNA code. The LS-DYNA analysis is performed for the same two configurations as were analyzed using SASSI. One configuration has two identical reactor buildings located in close proximity to each other, and the second configuration consists of a reactor building and a turbine building in close proximity. The LS-DYNA analysis models are described first, followed by the discussion of the results of comparisons with the JNES recorded data, and the performance assessment of the LS-DYNA analysis.

4.1 Twin Reactors Test Model

4.1.1 LS-DYNA Modeling Description

The approach taken for the LS-DYNA analysis of the twin reactor configuration is to represent the structures and the near field soil in an explicit finite element model, and to connect the boundaries of the near field soil to a series of transmitting boundary elements to prevent the outgoing waves that approach the boundaries from reflecting back into the soil-structure system. This is often referred to as the direct method for treating the SSI solution.

Given the size of the model structures and the amount of soil which needs to be included in the finite element model, it is a monstrous task to develop the explicit finite element model using LS-DYNA. Based on an experience learned from a companion study [Xu, 2005] on developing the SSI models using LS-DYNA, a LS-DYNA explicit finite element model is carefully constructed considering the wave propagation issues balanced with the time needed to obtain the solution. Figure 4.1-1 shows the finite element mesh of the soil-structure model and Figure 4.1-2 provides a zoom-in view of the structures and the surrounding soil. To take advantage of the symmetry, only a half of the soil-structure system is included in the model. The near field soil is modeled with brick elements and is connected with a circular outer boundary to prevent outgoing waves from being trapped in possible corners of any discontinued boundary (so called “corner effect”). Since the ground motion input is specified at a depth of 13.2m below the ground surface, the mesh for the near field soil is then extended 1m below the location of the ground input motion definition to allow for simulating the bedrock in the transmitting boundary elements in LS-DYNA. The transmitting boundary used in the LS-DYNA analysis is of the Lysmer type [Lysmer, 1969] and is described in detail in Section 2.2.2 of this report.

As shown by the zoom-in view of the model in Figure 4.1-2, the twin structures are modeled with detailed finite elements, including bricks and shells. The structures are connected with the surrounding soil using the tied interfaces which are discussed in Section 2.2.2 of this report. Since the ground motion input is very small and is not believed to induce any non-linear behavior of the soil-structure system (such as interface separation or relative slipping, etc.), the gravity effect is not included in the analysis model. The damping is modeled using the frequency independent part damping option in LS-DYNA which is essentially a Rayleigh damping for different material parts as discussed in Section 2.2.2 of this report.

In order to comprehend the size of the LS-DYNA model for the twin reactor configuration, the model statistics are provided as below. The LS-DYNA model of the soil-structure system requires 212428 nodes, 189078 brick elements and 1500 shell elements. It is

believed that given the size of this model, it may not be practical and effective to apply the same approach in an actual design of a NPP facility in the context of the linear response analysis. However, in the context of this study, such detailed LS-DYNA modeling is an important and necessary exercise to validate the adequacy and accuracy of other relatively more effective and practical approaches to SSI analysis.

4.1.2 LS-DYNA Analysis Results and Comparisons with JNES Recorded Data

The following sub-sections discuss the results from the LS-DYNA analysis and their comparisons with the JNES measured response data. The horizontal responses are discussed first, followed by the comparisons of the vertical responses. The key results used for the comparison between the LS-DYNA analysis and the JNES recorded data include ISRS and the seismic induced soil pressures.

Horizontal Response Analysis

The horizontal response analysis is performed by applying the input motion in the north-south (NS) direction. The ISRS results are computed at the centers of the basemat and the roof, and the respective accelerometer recordings are designated in Figure 3.1-2 as B1A-NS0 and RFA-NS0, respectively. The comparisons between the LS-DYNA predicted ISRS and the accelerometer recordings are plotted in Figure 4.1-3 and Figure 4.1-4, for the basemat and the roof, respectively.

Two sets of the analysis results are presented in these figures, which consider the effect of the soil uncertainty on the response parameters in the LS-DYNA results. The first analysis is performed using the JNES soil geotechnical data, which is interpreted as the best estimate soil property referred to in the figures for this study as the mean soil V_s (V_s represents the material shear wave velocity of the soil). The second analysis is performed by adjusting the mean soil V_s to achieve the best fit of the computed ISRS to the recorded ISRS. The purpose is to assess the soil uncertainty effect on the response calculation.

Due to the nature of the narrow amplified frequency band inherent in the seismic input, the ISRS computation is sensitive to the property of the soil column. As depicted in Figure 4.1-3 and Figure 4.1-4 for the basemat and roof ISRS comparisons, the predicted spectral peak using the mean soil profile is much higher than the recorded spectral peak. The best fit of ISRS to the recordings is performed by reducing the shear wave velocity V_s of the soil column by 5%, which are shown as the solid lines in these figures. Although there is still some mismatch in the amplified high frequency range, the overall comparison between the analysis using modified soil column and the recorded ISRS is fairly good. For the roof response, the recording shows two salient peaks in the amplified frequency range, and the second peak appears to be associated with the adjacent structure-structure effect. Similar to SASSI analysis, the LS-DYNA analysis model does not appear to capture well the second spectral peak.

In addition, a 5 percent reduction in V_s of the mean soil profile is equivalent to about 10 percent in stiffness reduction of the corresponding soil column if the lognormal distribution is assumed for the soil stiffness. In an uncertainty analysis, this translates to a value of about 0.1 for the COV of the soil stiffness reduction (coefficient of variation which is defined as [standard deviation]/mean). The value of 0.1 for the soil COV is within the range of uncertainty typically understood in geotechnical engineering

applications, and even smaller than the analysis performed by SASSI as discussed earlier using a COV=0.2 for the same test configuration.

Figure 4.1-5 through Figure 4.1-10 present the JNES recorded time history data of the seismic induced soil pressure and the corresponding LS-DYNA analysis results using the aforementioned soil columns. The soil pressure sensors were installed on the test structure, the locations of which are indicated in Figures 2-18 and 2-19. As shown in the figures, the locations where the pressure sensors were installed are designated with circles. However, only the solid circles represent the sensors which have actually recorded the earthquake event. The sensors selected for the pressure comparisons are S1, S2 and S4 on the south side, and N3, N6 and N13 on the north side.

The seismic induced soil pressures from the LS-DYNA model are computed in the soil elements closest to the locations of the pressure sensors, using the stress component perpendicular to the wall. Unlike the SASSI program, which applies the material damping in computing soil pressures, the damping does not affect the soil pressure calculation in the LS-DYNA analysis.

The comparison between the recorded pressure time history and the LS-DYNA result for the sensor S1 is shown in Figure 4.1-5, which is located on the north side wall near the basemat. The LS-DYNA result appears to be slightly larger than the recorded pressure (about a factor of 2). The occurrences of the pressure peaks are consistent between the sensor and the computed results, which indicate that there are good phase correlation between the LS-DYNA model and the test data.

Figure 4.1-6 shows the comparison at the sensor S2, which is located near the mid height of the wall below grade. As indicated in the figure, the recorded sensor appears to be overwhelmed by the noise present in the record. In addition, the pressure amplitude is much smaller than other locations (e.g., S1). There does not seem to be a comparable comparison between the analysis and test data at this sensor location.

The pressure comparison at the sensor on the upper portion of the wall is presented in Figure 4.1-7, which shows comparable time history responses between the analysis and the recorded data. However, the pressure estimate appears less sensitive with changing the soil column stiffness by 10 percent as apposed to the ISRS calculation in which the spectral peaks are keyed to the prescribed soil stiffness.

Figure 4.1-8 through Figure 4.1-10 present the pressure time histories on the south side of the twin structures both for the sensor recordings and the LS-DYNA results. As shown by these figures, the observations made for the characteristics of the pressure comparisons on the north side of the structures are very similar to that of the south side. Since the ground input analyzed is a small earthquake event which virtually ensures the linear elastic response for the structures, the similarity in the pressure comparisons for both sides of the structures is therefore expected.

The comparisons of the SSI characteristics between the analysis and the recorded data are further examined in the frequency domain. To this end, the Fourier spectra of the pressure time histories from both the recorded data and the LS-DYNA analysis are computed and presented in Figure 4.1-11 through Figure 4.1-16. For the pressure sensors near the basemat (S1, N3) as indicated in Figure 4.1-11 and Figure 4.1-14, the comparison of the Fourier spectra show that the frequency content is closely matched

between the computed and recorded pressure responses, and the computed amplitudes also mostly envelope the recordings. The recorded amplitude is higher than the computed amplitude in the frequencies less than 0.7 Hz. In addition, the recorded Fourier spectrum has finite amplitude near zero frequency, which appears to be induced by the noise in the recording.

The irrational behavior of the low frequency response in the recordings is further corroborated with the earlier examination of the pressure time histories for the sensors located near mid height of the wall (S2, N6). As depicted in Figure 4.1-12 and Figure 4.1-15, a very high noise/signal ratio appears to be present in the recorded pressures at these locations. The frequency domain comparisons further substantiate the observation made earlier in the time domain comparisons.

Finally, the frequency domain comparisons for the sensors near the ground surface (S4, N13) are shown in Figure 4.1-13 and Figure 4.1-16. For these sensors, the LS-DYNA results generally envelope the recorded data. Especially for the sensor N13, a nearly perfect match was obtained between the LS-DYNA result using the modified soil column and the recording. Similar to other locations, the recorded pressure responses still show the upward drift in low frequencies.

Vertical Response Analysis

As explained in Section 3.1.2 of this report, the vertical seismic analysis is a rather complicated process in which the response quantities are influenced by both two orthogonal horizontal motions and one vertical motion. Therefore, the averaged sensor pressure response is computed to remove the horizontal influence and is then compared with the LS-DYNA analysis using the vertical seismic input only.

Following this analysis approach, the vertical response analysis is performed by applying the recorded free field motion in the vertical direction at the control point located 13.2m below grade. The vertical ISRS results are computed at the center of the basemat and the roof, which have accelerometer recordings designated in Figure 3.1-2 as B1A-V0 and RFA-V0, respectively. The comparisons between the predicted vertical ISRS and the vertical accelerometer recordings are shown in Figure 4.1-17 and Figure 4.1-18 for the basemat and the roof, respectively.

Similar to the horizontal response analysis, the effect of the soil uncertainty is considered by the LS-DYNA model. The first analysis is performed using the JNES soil geotechnical data, which is interpreted as the best estimate soil property which is designated in the figures for this study as the mean soil V_p (V_p represents the material compressional wave velocity of the soil). Since the vertical response is controlled by the compressional wave, the second analysis is therefore performed by adjusting the mean soil p-wave velocity V_p to achieve the best fit of the computed vertical ISRS to the recorded vertical ISRS.

As shown in these figures for the vertical ISRS comparison, the LS-DYNA results with both JNES soil data and the BNL best fit soil column compare very well with the recorded ISRS in both frequency content and spectral peaks. The uncertainty in the soil property is small, which is 2.5% of the mean soil p-wave velocity (equivalent to 0.05 for the COV of the soil stiffness reduction) in achieving the best fit of the response spectra.

In addition, the vertical response result appears to have a better comparison with the recordings than the horizontal response analysis.

The seismic induced pressures on the base of the test model are computed by LS-DYNA using both soil columns. As mentioned above, to remove the influence of the horizontal inputs from the recorded vertical pressure measurements on the basemat, the averaged sensor pressures are used to compare with the LS-DYNA calculated soil pressure on the basemat. Figure 4.1-19 and Figure 4.1-20 show the averaged vertical pressure time histories from the JNES data and the computed basemat pressures for both the north and south structures. The analysis appears to over-predict the vertical pressure for both structures, when comparing with the averaged value of the recorded pressures.

To examine these pressure comparisons in frequency domain, the pressure time histories are transformed into the frequency domain as Fourier spectra, as shown in Figure 4.1-21 and Figure 4.1-22. By comparing respective Fourier spectrum plots between the recording and the analysis results, it is shown that the analysis predicts similar frequency content of the pressure response, however, this is much higher amplitude than the recordings. This observation is consistent with the time history comparisons. Further, the recording for the south structure shows the upward drift in Fourier amplitude in low frequencies, which implies that the recorded pressures have a high noise/signal ratio.

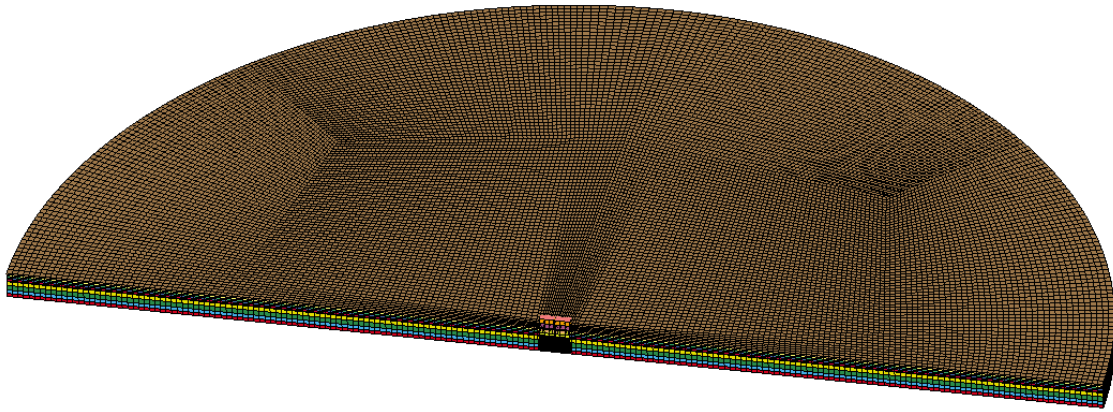


Figure 4.1-1 LS-DYNA Model for Twin Reactors Test Configuration

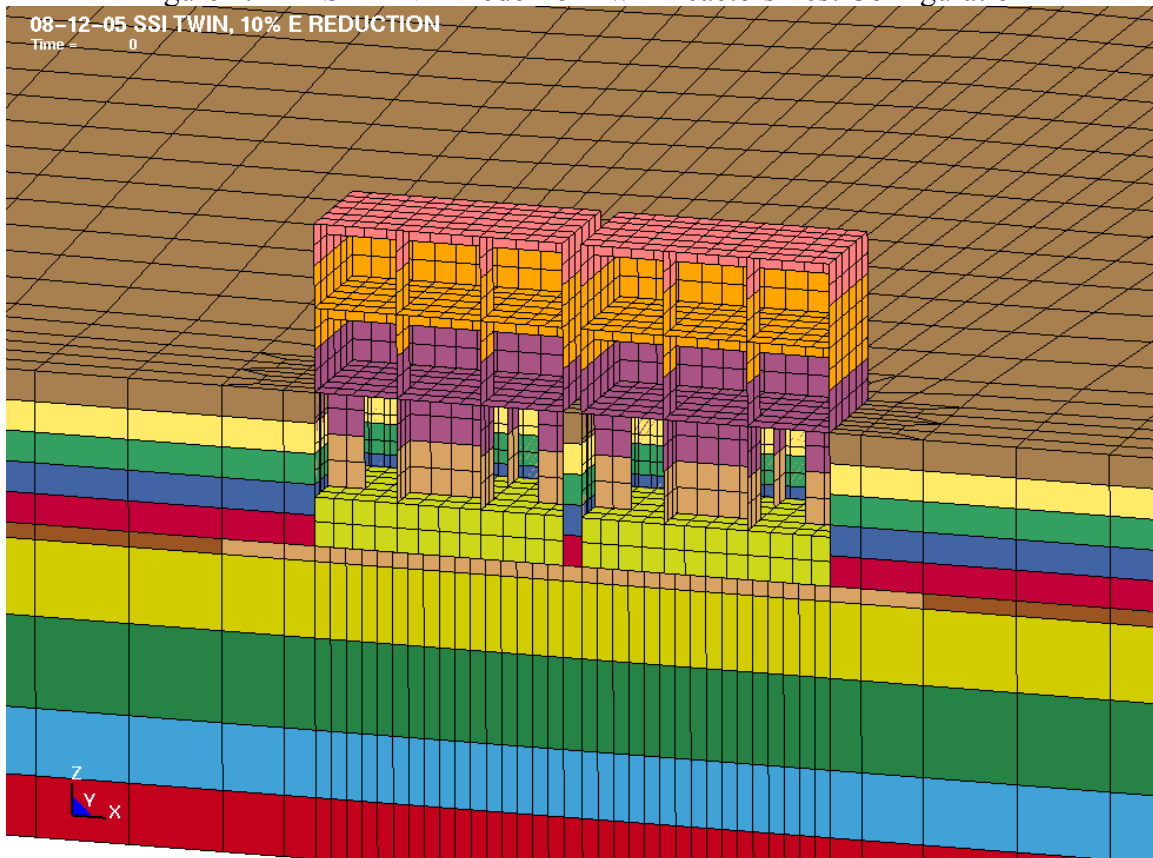


Figure 4.1-2 Zoom-in View of LS-DYNA Model of R-T Test Configuration

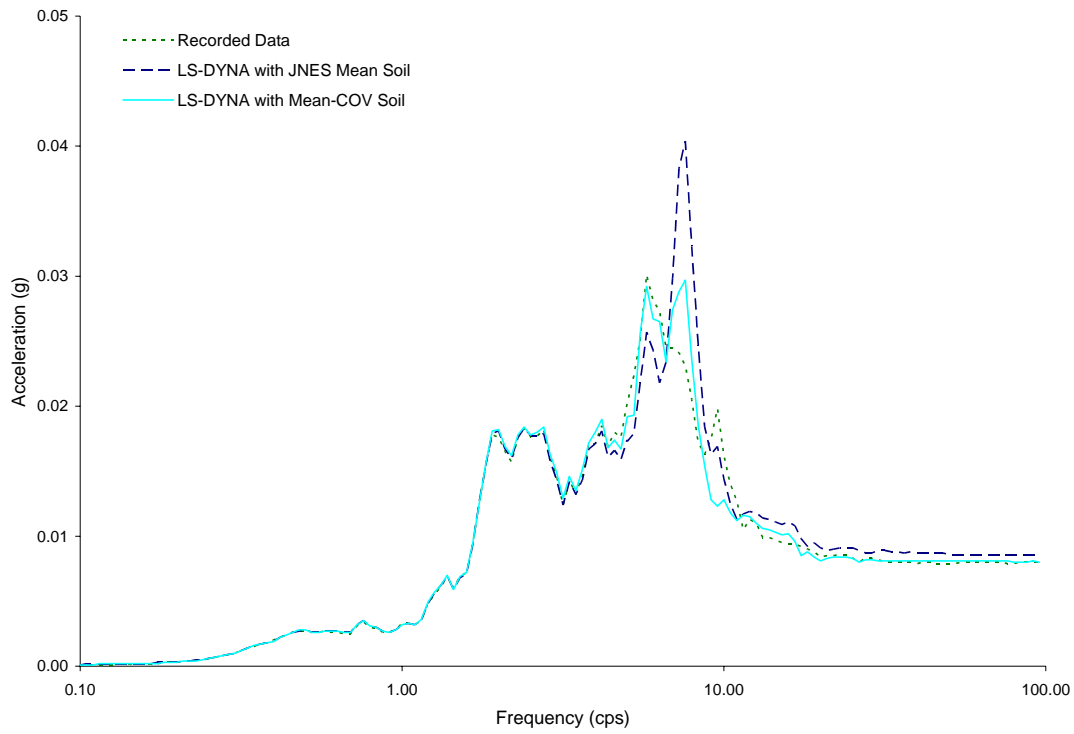


Figure 4.1-3 Comparison of Horizontal Response Spectra at Basemat Center of Twin Reactors Model

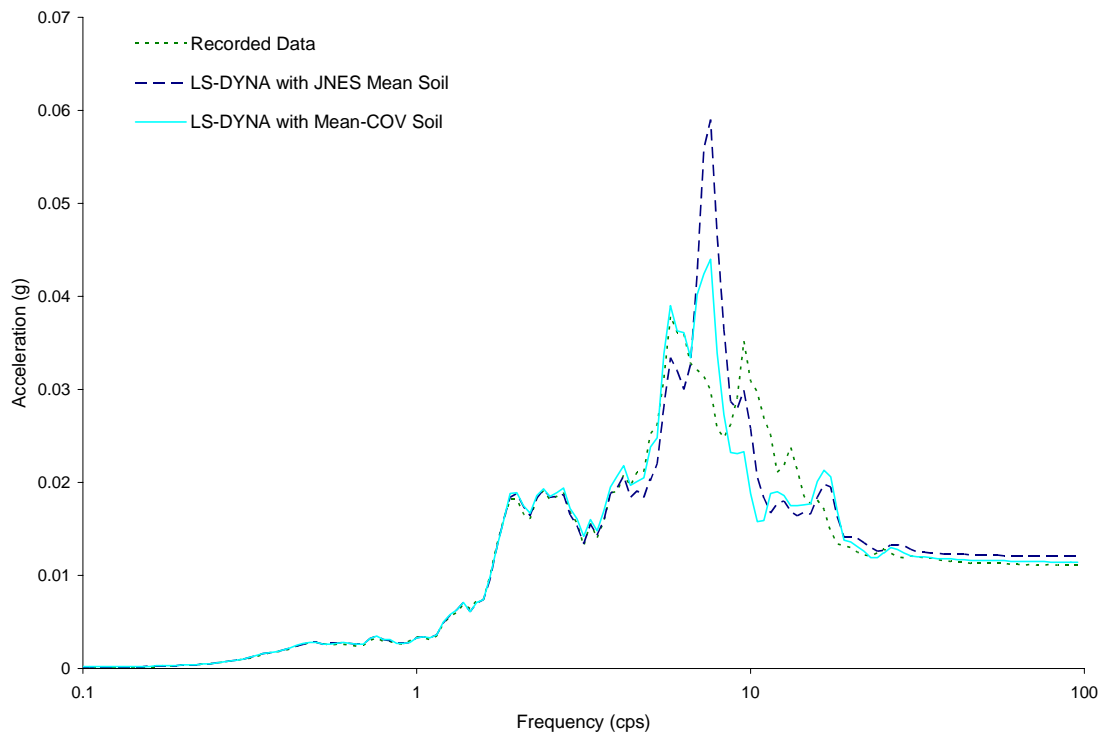


Figure 4.1-4 Comparison of Horizontal Response Spectra at Roof Center of Twin Reactors Model

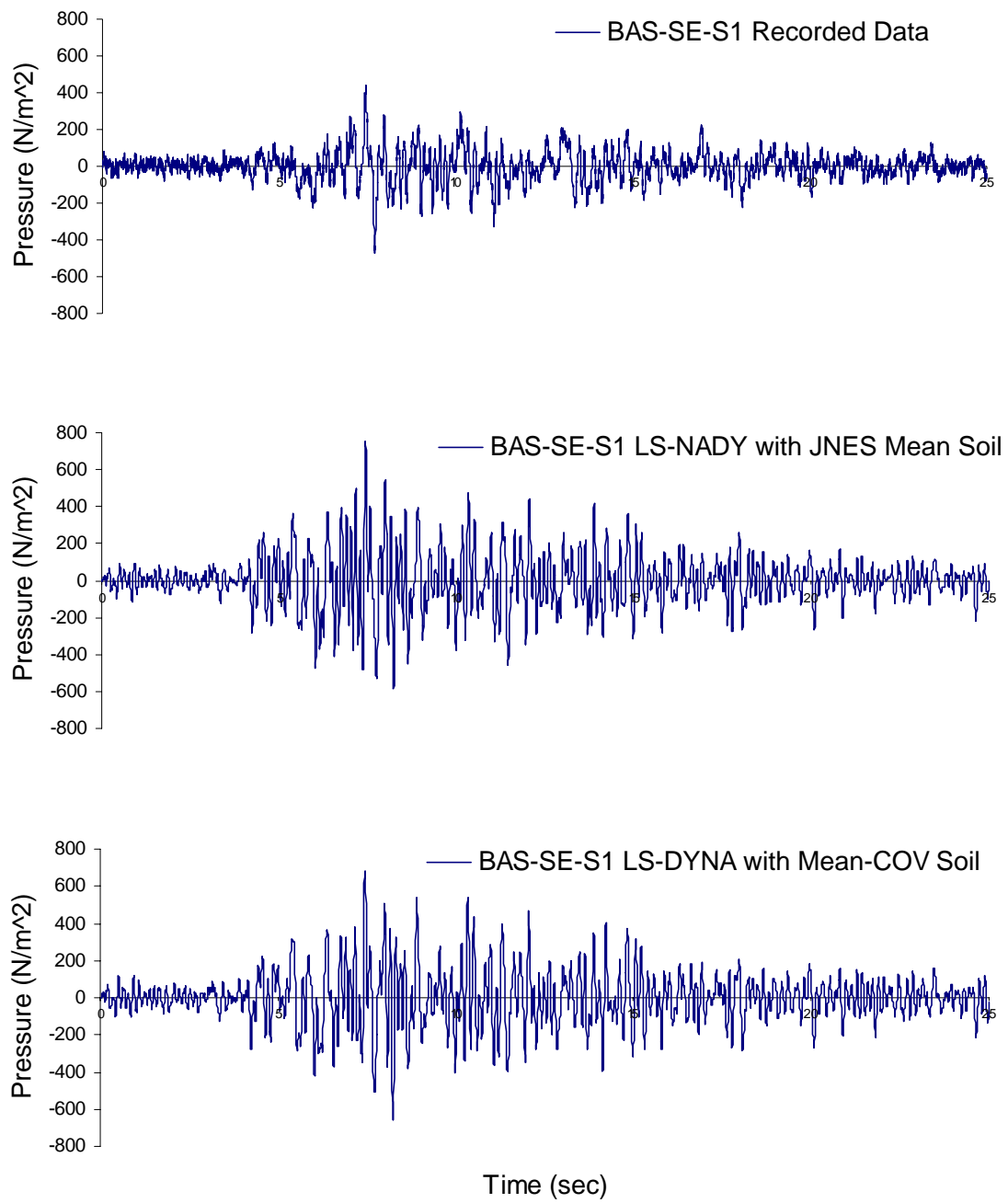


Figure 4.1-5 Comparison of Seismic Induced Soil Pressure at Sensor BAS-SE-S1

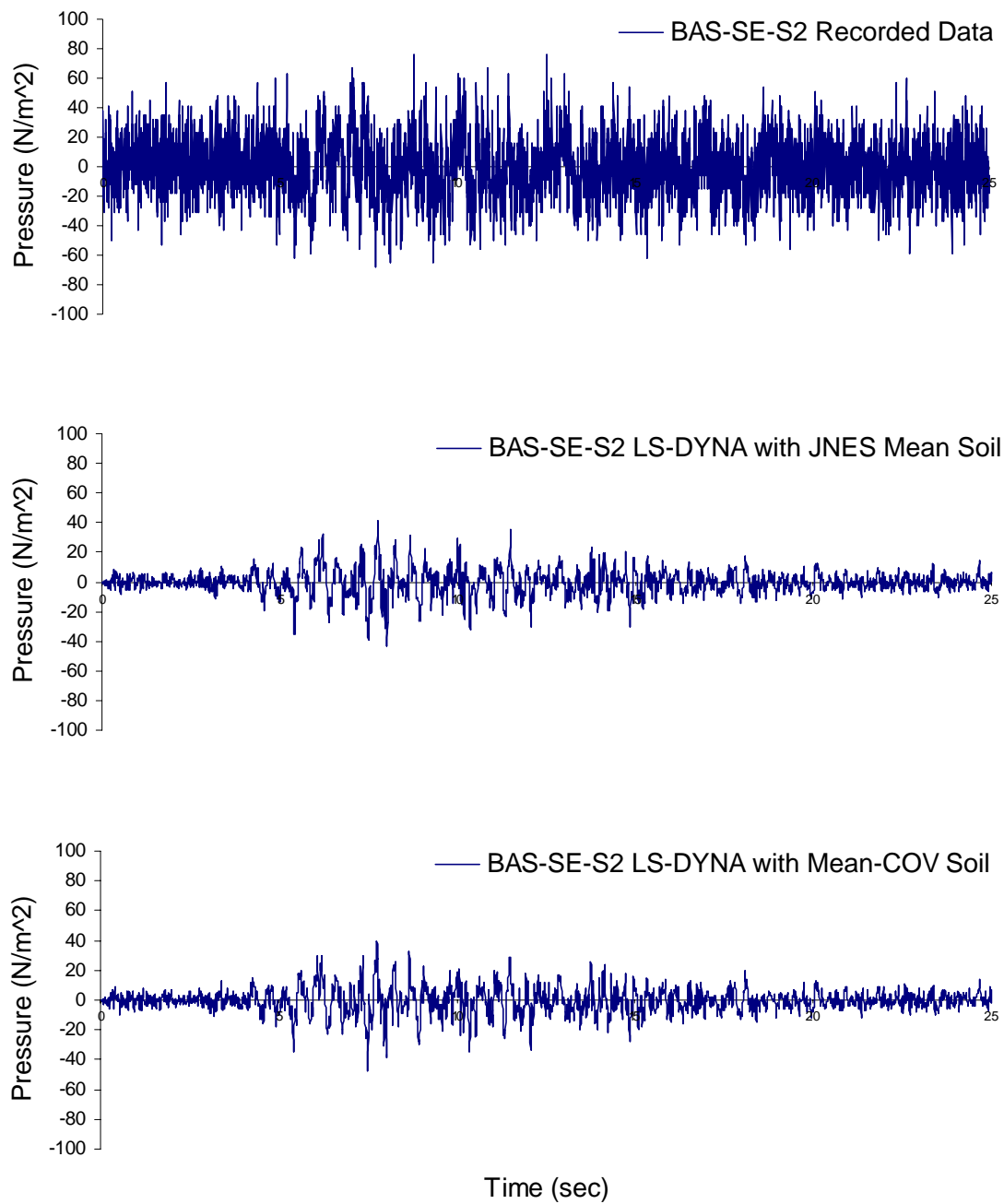


Figure 4.1-6 Comparison of Seismic Induced Soil Pressure at Sensor BAS-SE-S2

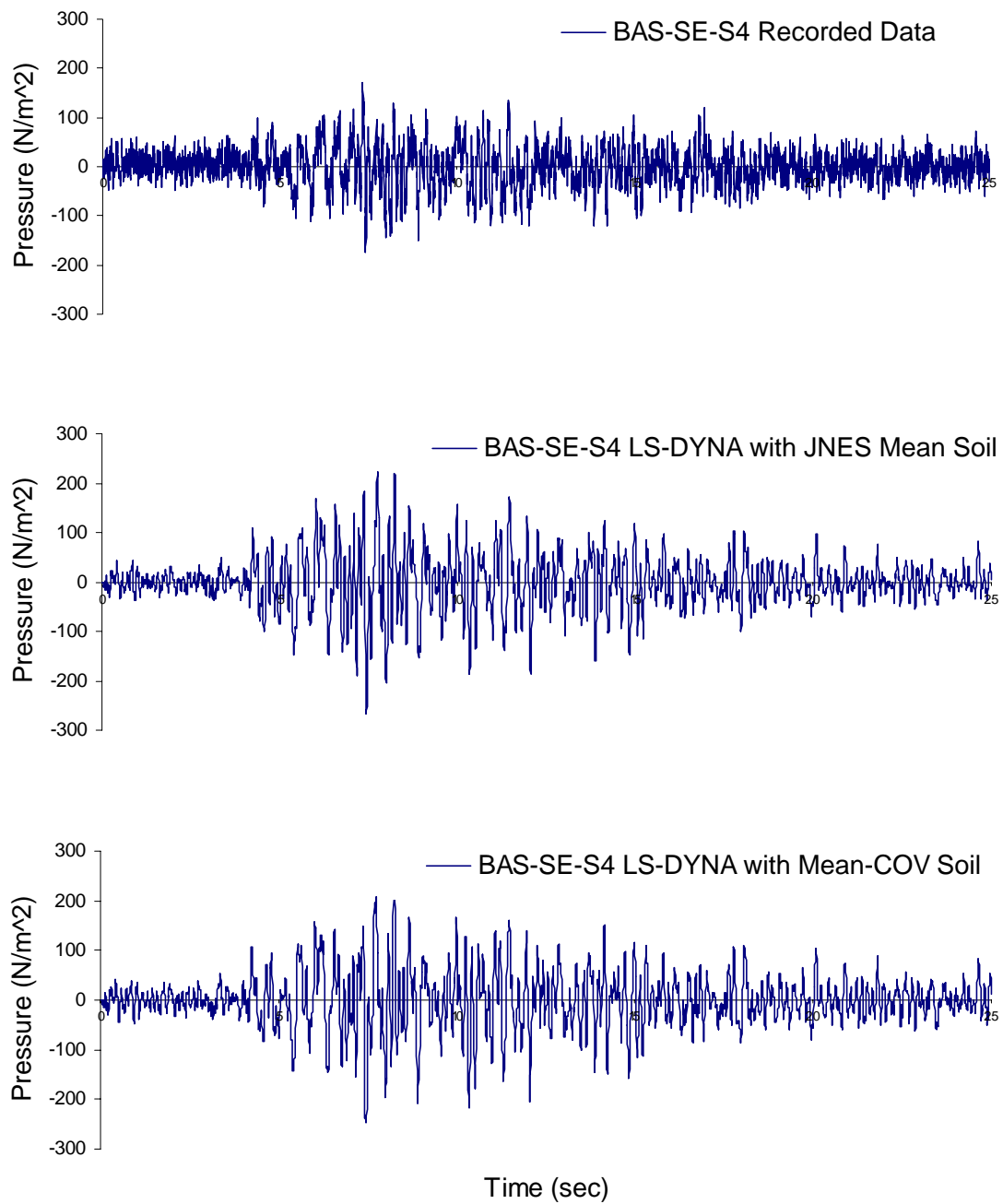


Figure 4.1-7 Comparison of Seismic Induced Soil Pressure at Sensor BAS-SE-S4

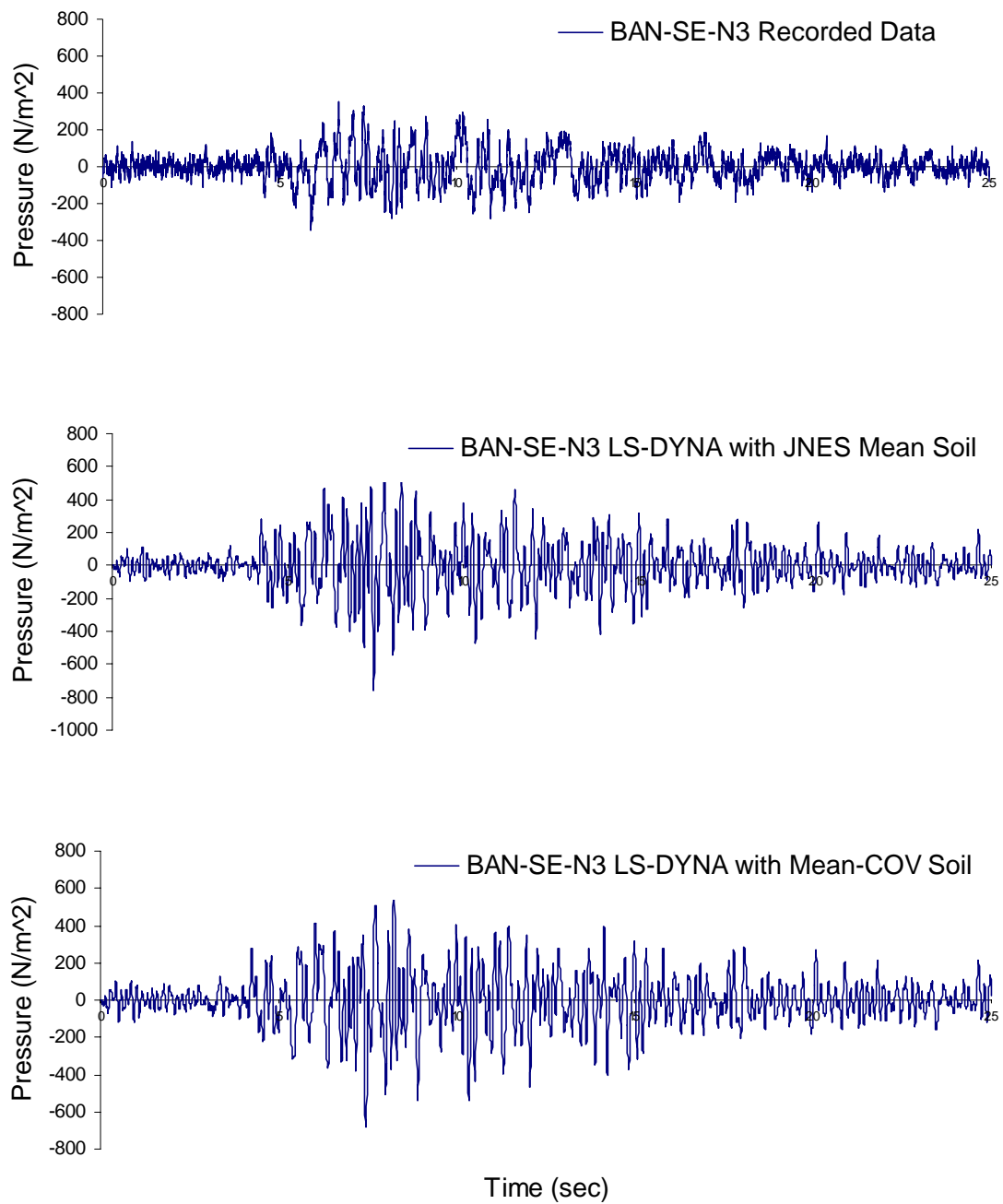


Figure 4.1-8 Comparison of Seismic Induced Soil Pressure at Sensor BAN-SE-N3

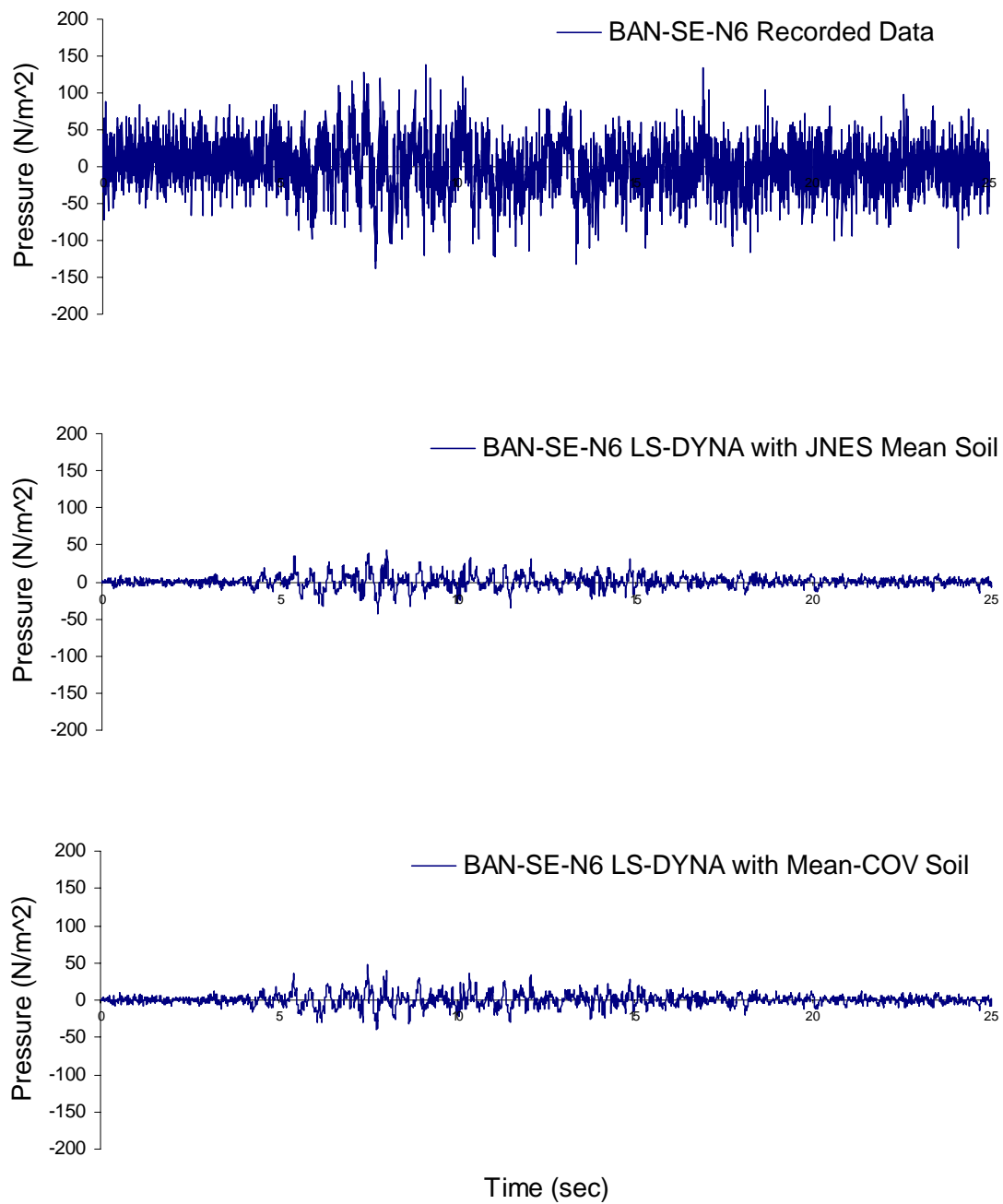


Figure 4.1-9 Comparison of Seismic Induced Soil Pressure at Sensor BAN-SE-N6

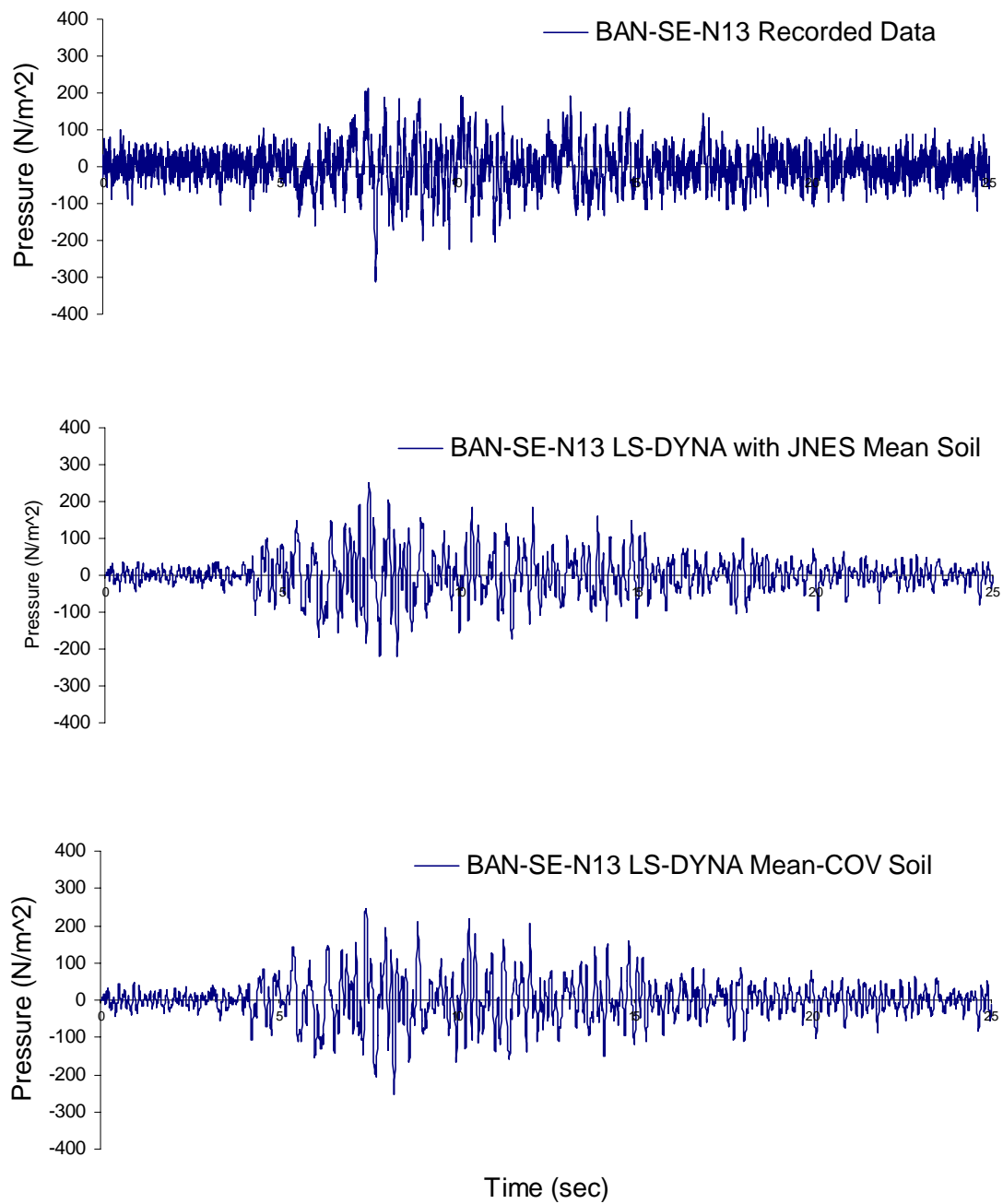


Figure 4.1-10 Comparison of Seismic Induced Soil Pressure at Sensor BAN-SE-13

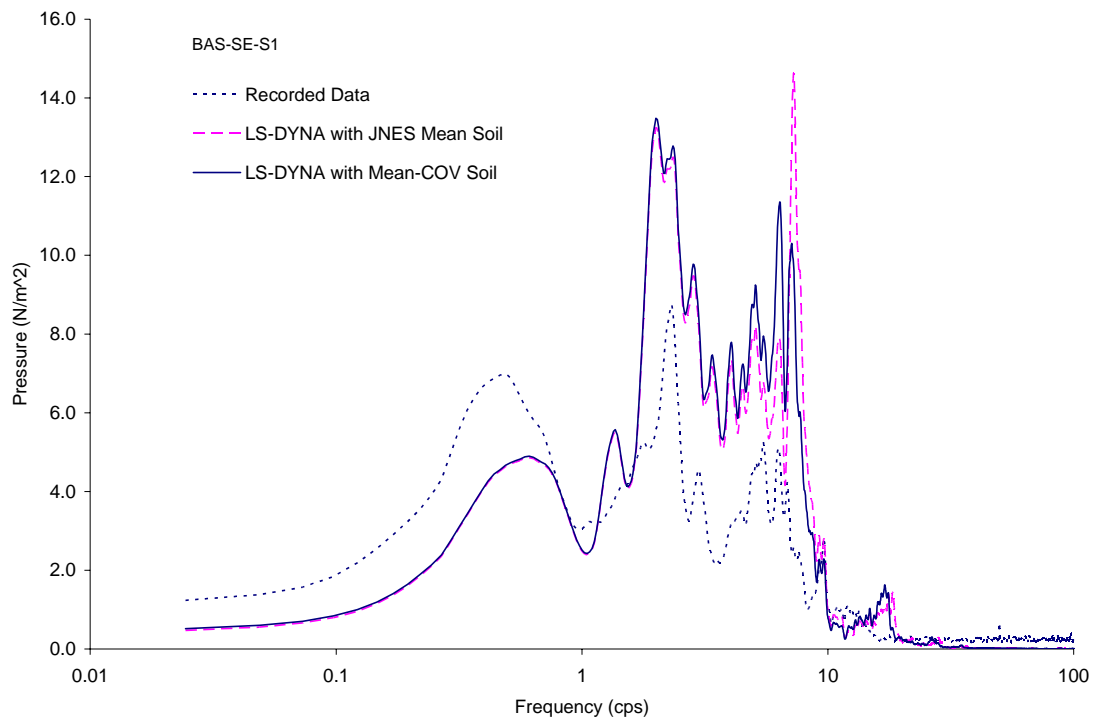


Figure 4.1-11 Comparison of Fourier Spectra of Soil Pressure at Sensor BAS-SE-S1

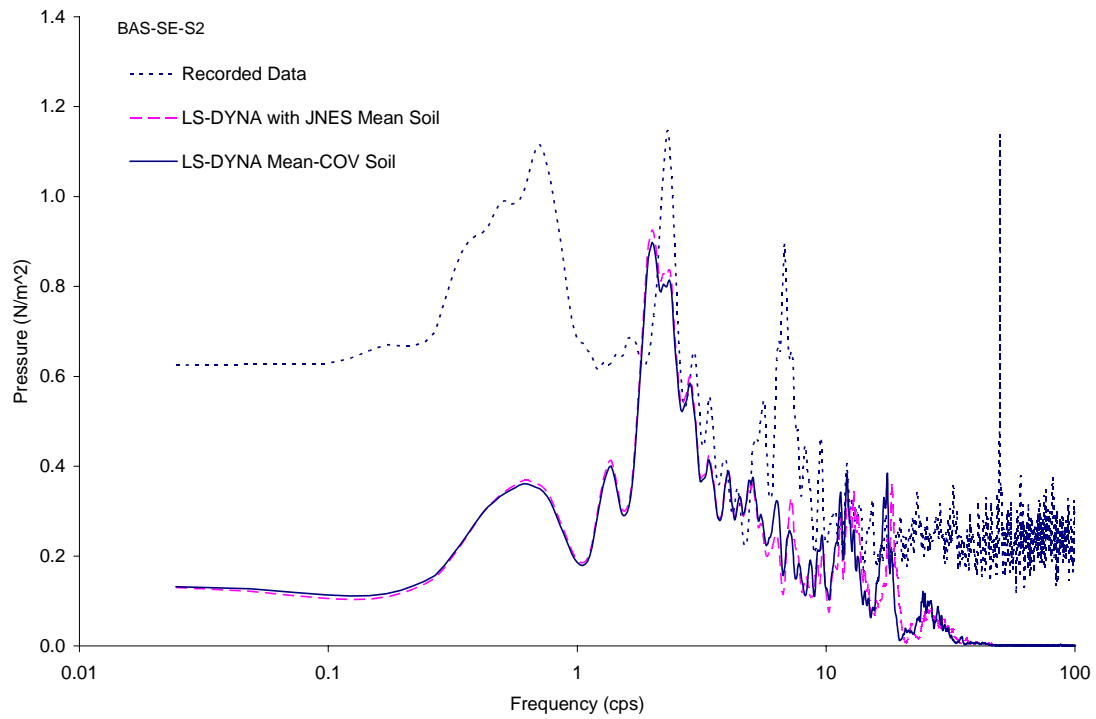


Figure 4.1-12 Comparison of Fourier Spectra of Soil Pressure at Sensor BAS-SE-S2

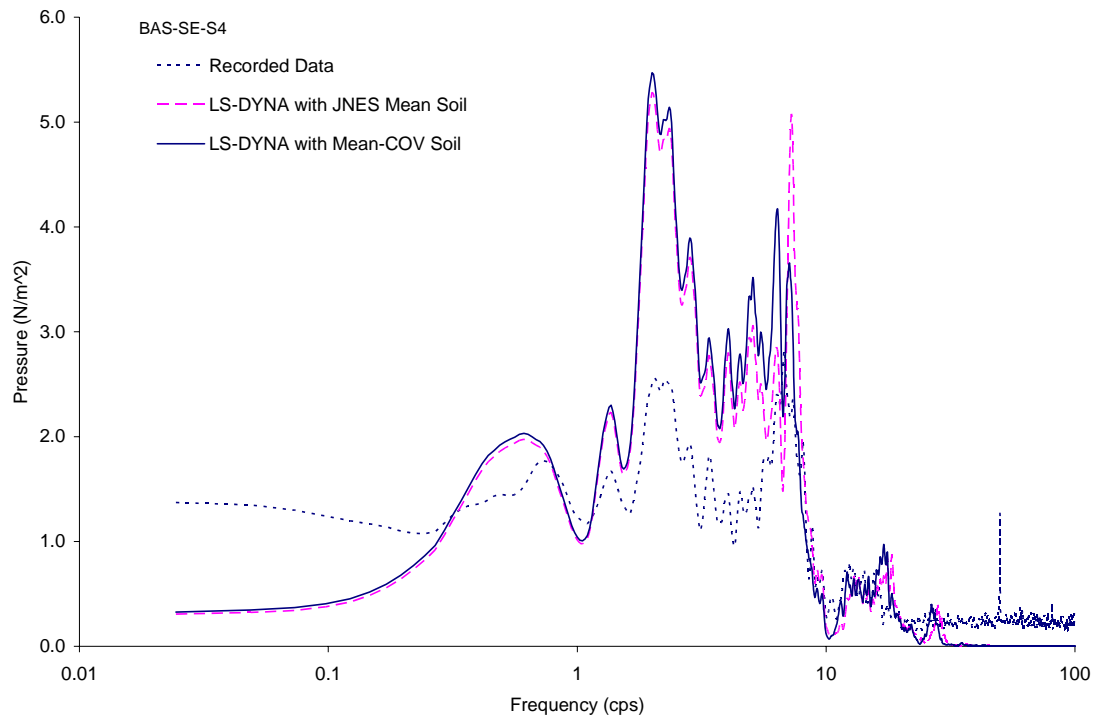


Figure 4.1-13 Comparison of Fourier Spectra of Soil Pressure at Sensor BAS-SE-S4

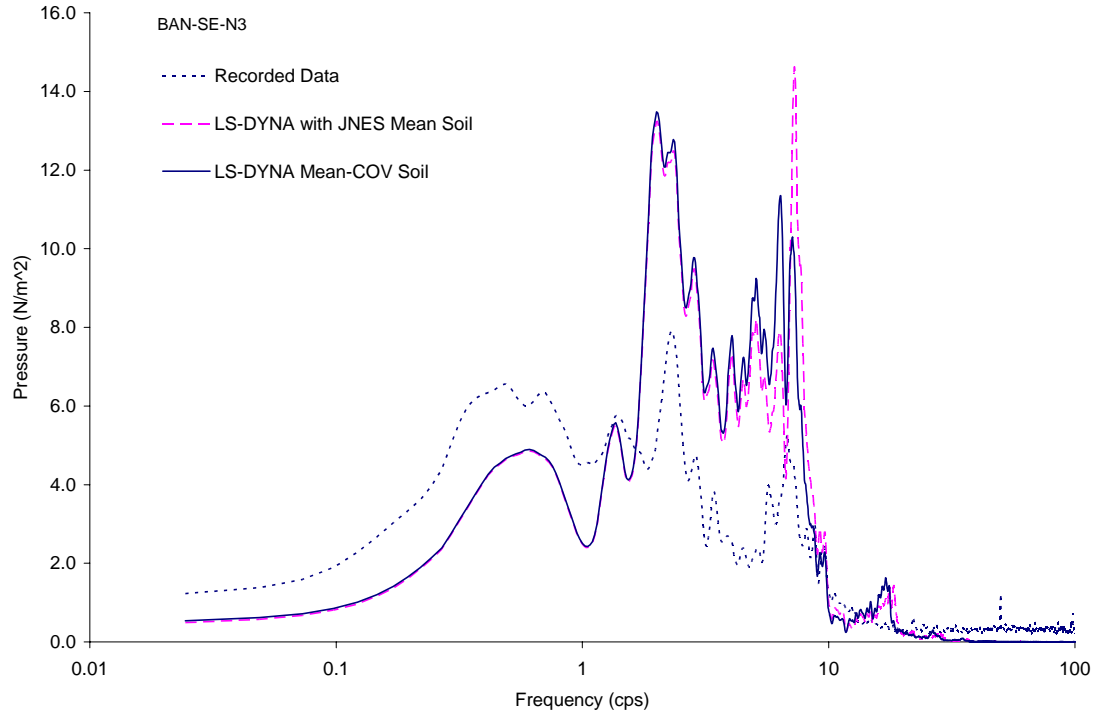


Figure 4.1-14 Comparison of Fourier Spectra of Soil Pressure at Sensor BAN-SE-N3

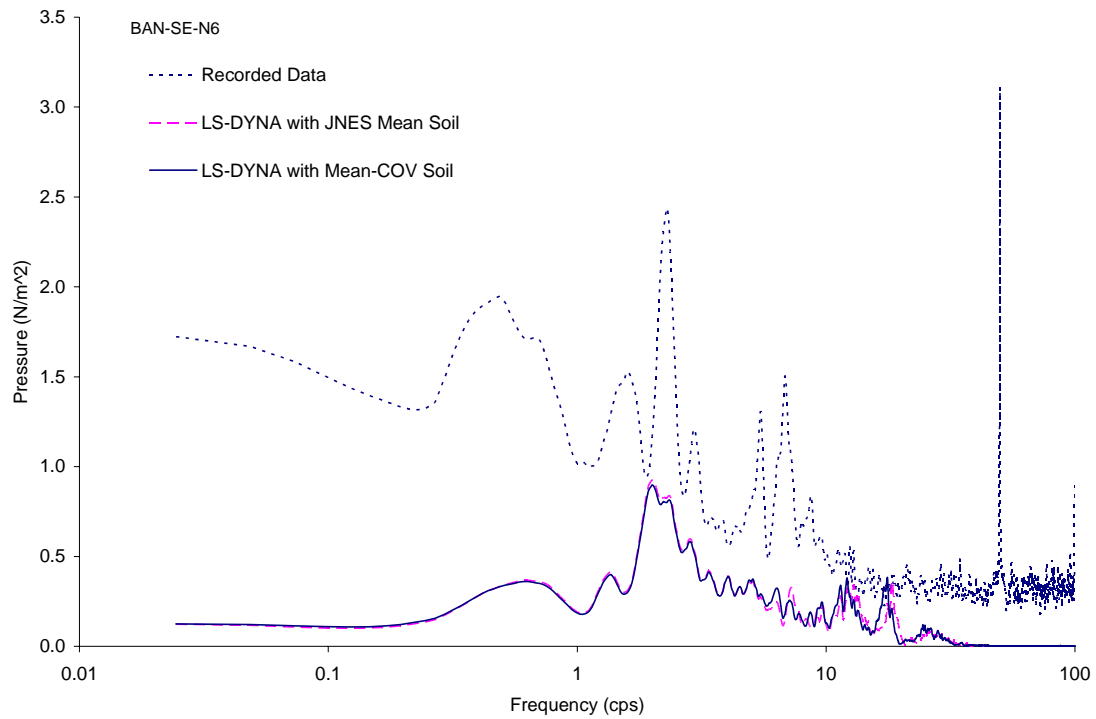


Figure 4.1-15 Comparison of Fourier Spectra of Soil Pressure at Sensor BAN-SE-N6

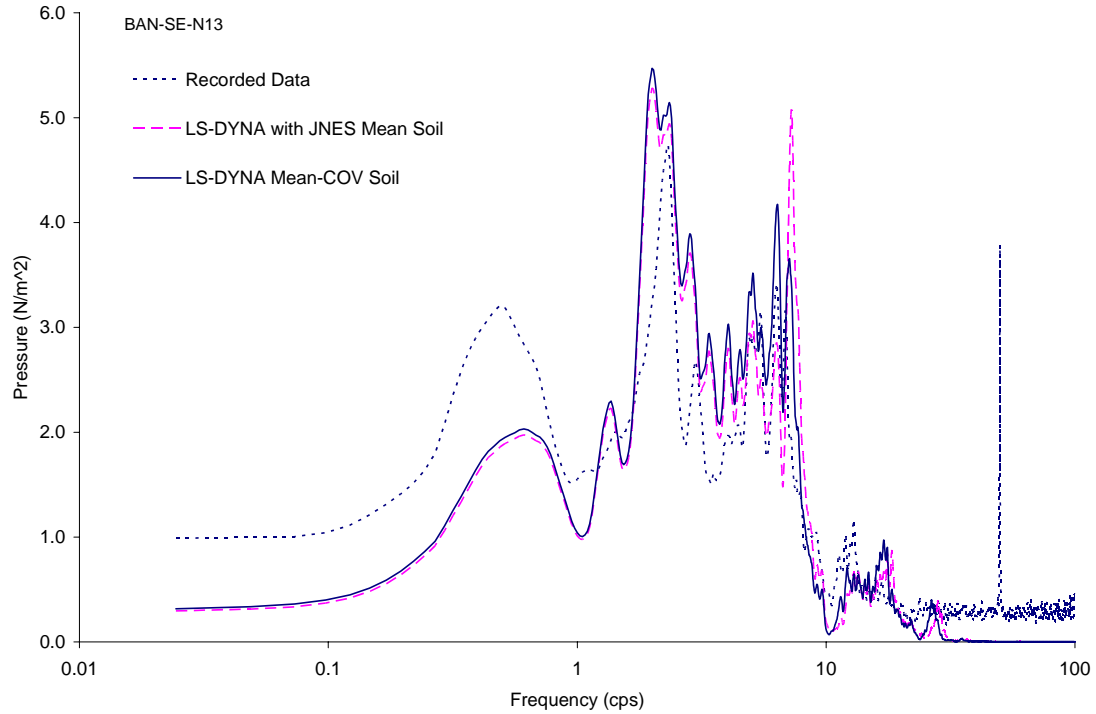


Figure 4.1-16 Comparison of Fourier Spectra of Soil Pressure at Sensor BAN-SE-N13

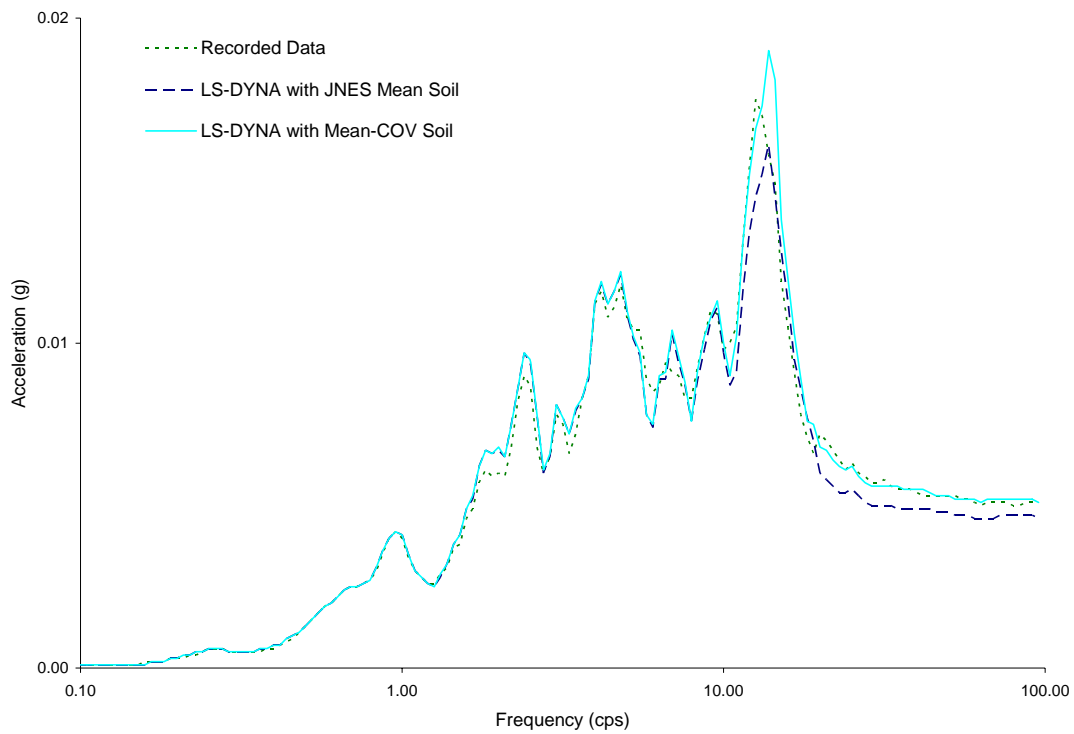


Figure 4.1-17 Comparison of Vertical Response spectra at Basemat Center of Twin Reactors Model

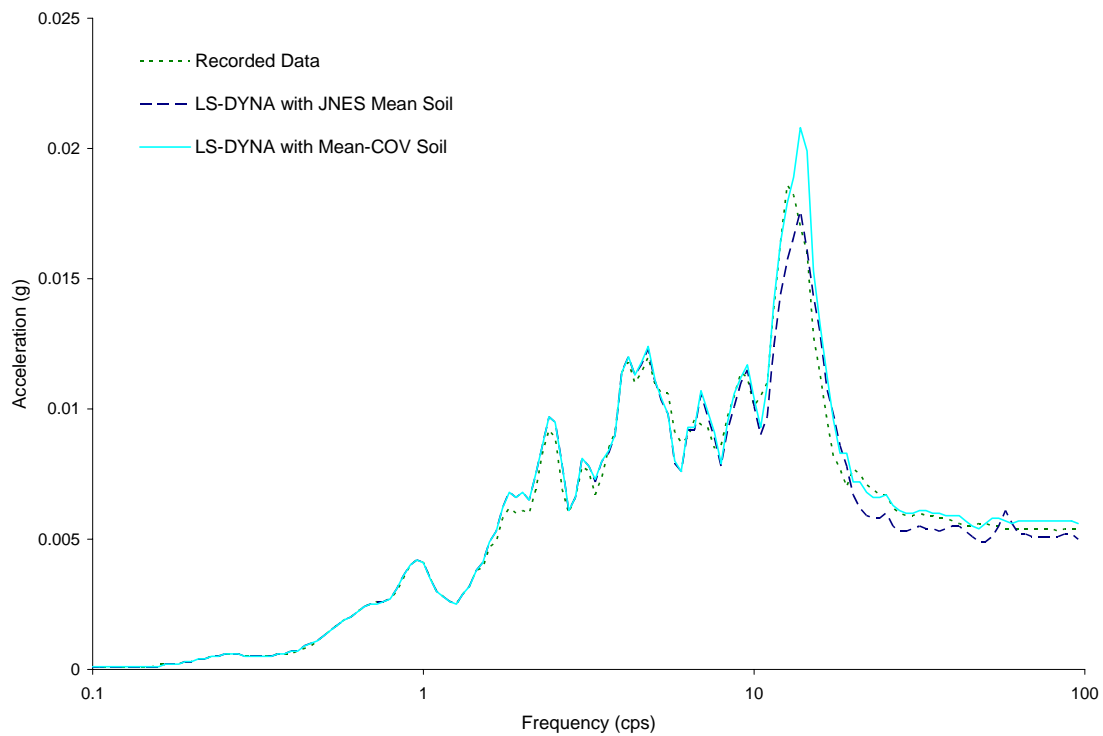


Figure 4.1-18 Comparison of Vertical Response spectra at Roof Center of Twin Reactors Model

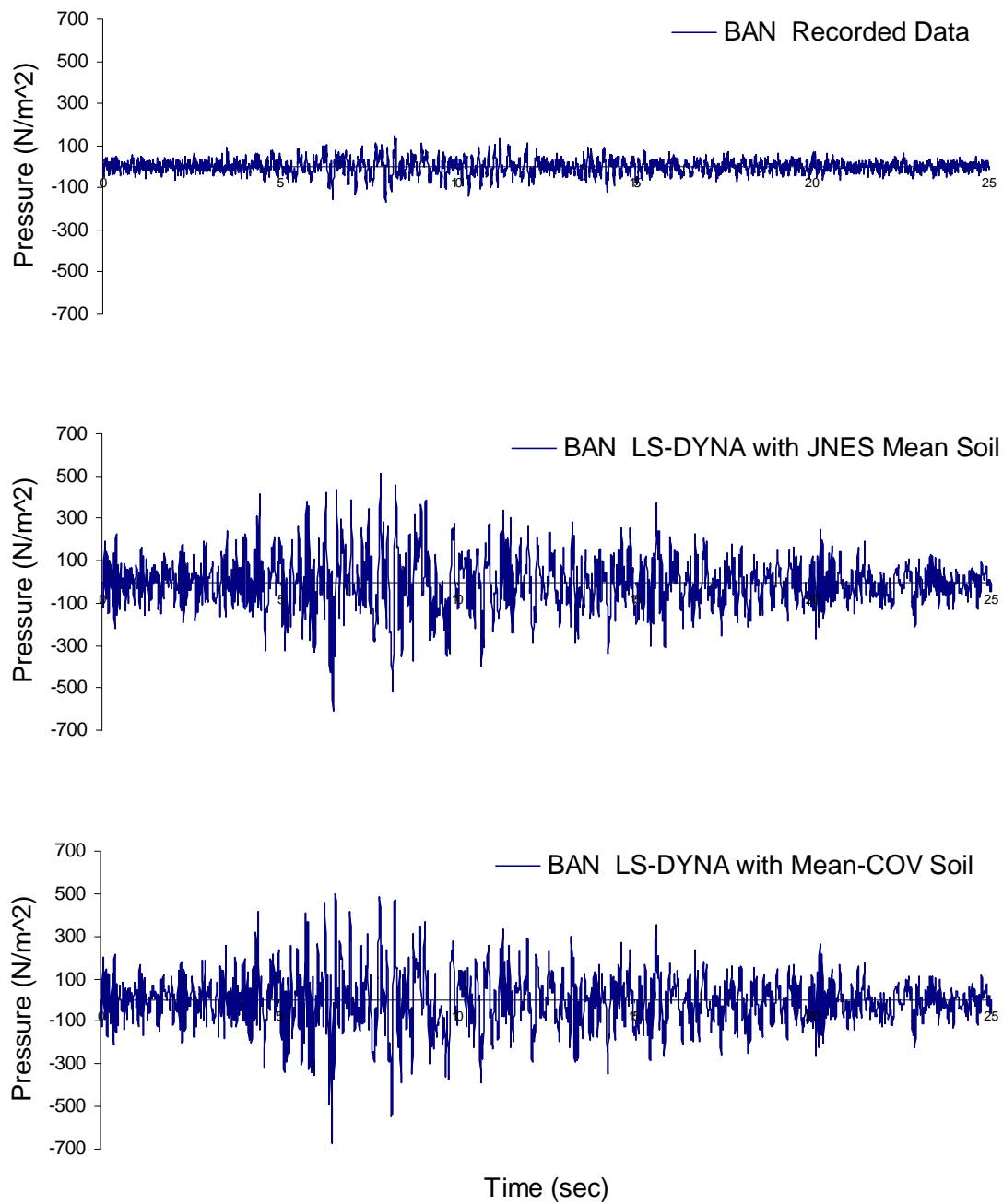


Figure 4.1-19 Comparison of Vertical Soil Pressure on BAN Basemat of Twin Reactors Model

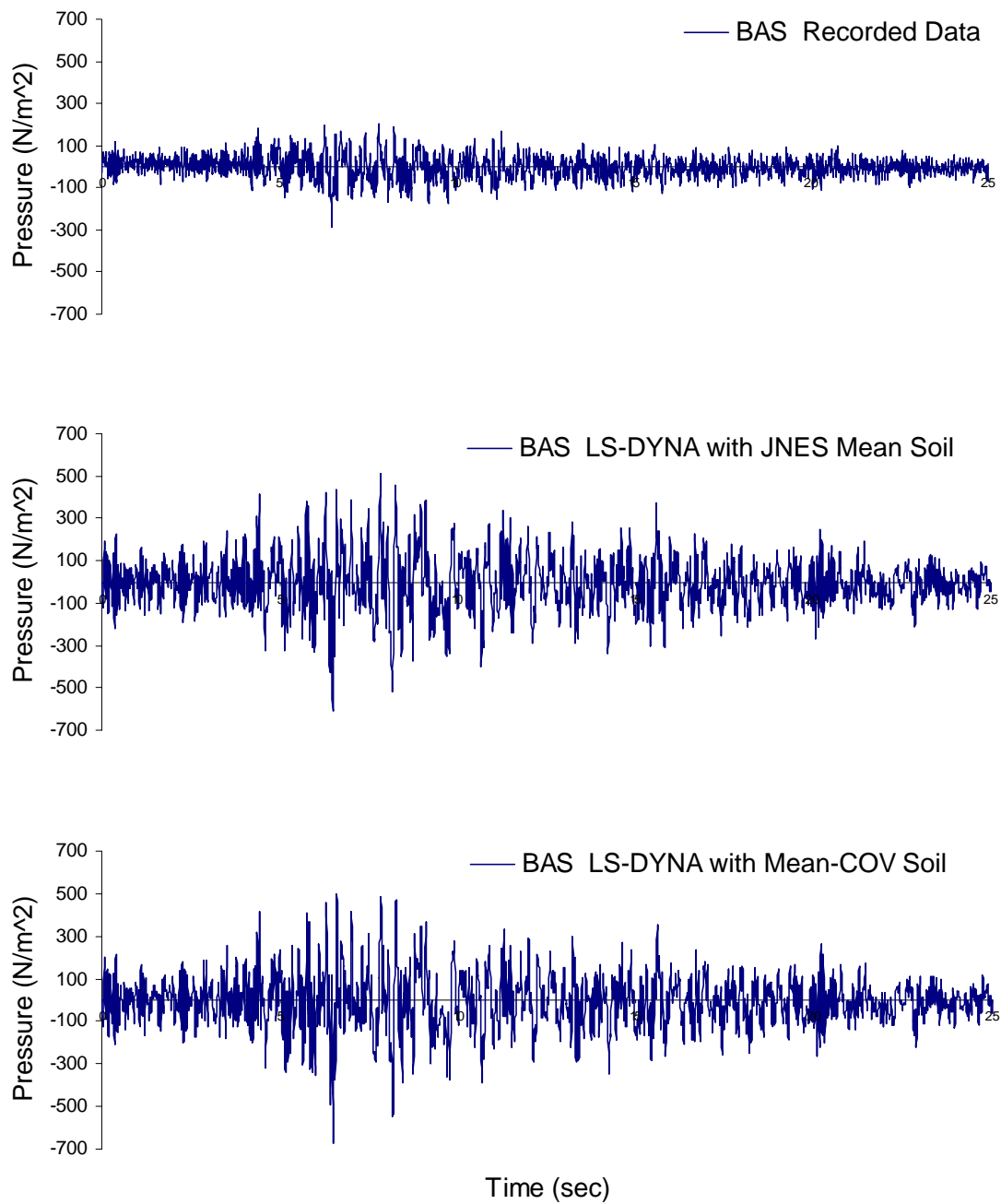


Figure 4.1-20 Comparison of Vertical Soil Pressure on BAS Basemat of Twin Reactors Model

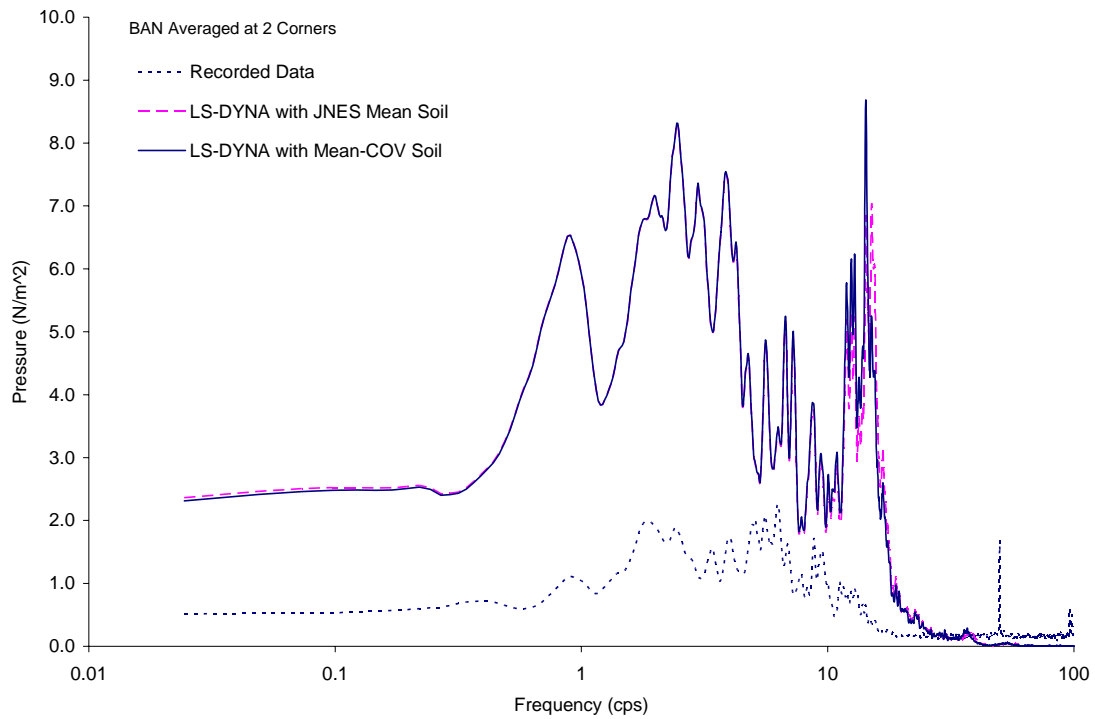


Figure 4.1-21 Comparison of Fourier Spectra of Vertical Soil Pressure on BAN Basemat of Twin Reactors Model

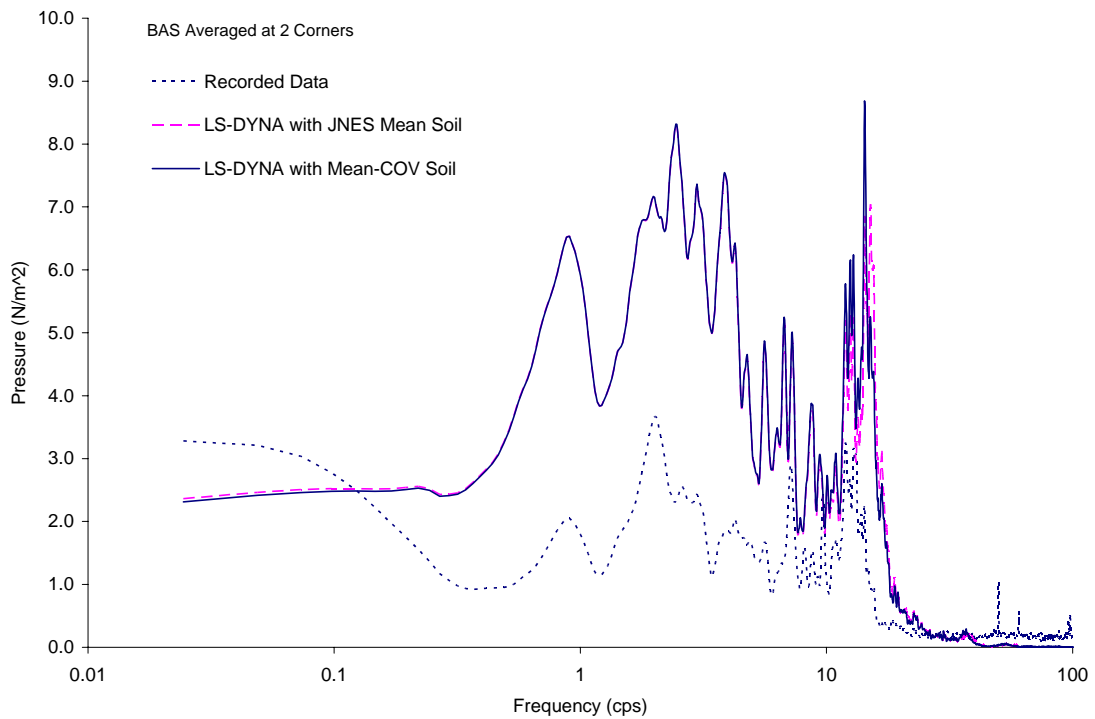


Figure 4.1-22 Comparison of Fourier Spectra of Vertical Soil Pressure on BAS Basemat of Twin Reactors Model

4.2 R-T Test Model

4.2.1 LS-DYNA Modeling Description

The configuration for the reactor-turbine (R-T) model consists of an scaled reactor structure (the same structure as the twin reactor configuration) and a turbine structure which is located about 0.1m from the reactor structure as shown in Figure 2-4. The turbine building has dimensions of 6.4m by 10m in plane and 6.75m in height, and weighs about 395 metric ton, and is embedded about 4m in the soil.

The LS-DYNA model developed for the R-T configuration uses the same approach as that for the twin reactor configuration. The finite element mesh of the model and the zoom-in view of the test model and the surrounding soil are shown in Figure 4.2-1 and Figure 4.2-2. Since the input motion for the R-T model is defined at about 35m below the ground surface, the LS-DYNA finite element mesh, therefore, extends in the vertical direction 1m below the depth for the input motion (36m below the ground surface). The reason is to allow for the transmitting boundary elements to assume the property of the half-space rock foundation.

In the horizontal direction, as depicted in Figure 4.2-1, the near field soil model extends out to about 300m from the center with a circular outer boundary. Both the base and side boundaries are attached to the transmitting boundary elements simulated with the Lysmer dampers to ensure non reflection of outgoing waves. The R-T structures are modeled with explicit 3-D brick and shell elements. Given the small ground input, only elastic response is expected for the R-T structures. Therefore, the LS-DYNA model ignores the gravity effect and applies the LS-DYNA tied-interface feature (see Section 2.2.2 for details) to connect the structures to the surrounding soil.

The LS-DYNA model for the R-T response analysis consists of a total of 303047 nodes, 279264 3-D brick elements, and 1140 3-D shell elements. The input motions are defined in the soil located at 35m below grade, which are provided by JNES as shown in Figure 3.2-4.

4.2.2 LS-DYNA Analysis Results and comparisons with JNES Recorded Data

The key results from the SASSI analysis and their comparisons with the JNES measured response data for the R-T configuration are discussed in this section. The horizontal responses are presented first, followed by the comparisons of the vertical responses. Similar to the twin configuration, the results of both the ISRS and the soil pressures are included for the comparison between the SASSI analysis and the JNES recorded data.

Horizontal Response Analysis

The horizontal response analysis is performed for the input motion applied in the north-south (NS) direction. The ISRS results are computed at the center of the basemat and the roof of the reactor and the turbine buildings, and the accelerometer recordings are depicted in Figure 3.2-3 as B1A-NS0 and RFA-NS0 for the reactor, and B1A-NS23 and RFA-NS0. The comparisons between the LS-DYNA computed ISRS and the JNES accelerometer recordings are shown in Figure 4.2-3 and Figure 4.2-4, for the basemat and the roof of the reactor building, and Figure 4.2-5 and Figure 4.2-6 for the basemat and the roof of the turbine building.

These comparisons show two sets of response results from the LS-DYNA analysis. These two responses are computed using the JNES best estimate soil data (referred to as the mean soil column) and the soil column which considers the soil uncertainty by best fitting to the recorded ISRS response, respectively. The soil uncertainty in terms of stiffness is determined by fitting the ISRS between the LS-DYNA analysis and the recorded data, and is estimated to be about $COV = 0.2$. The LS-DYNA computed ISRS using both soil columns are compared very well with the recorded spectra at the base. At the roof, the recorded spectra show two major peaks and the analysis is able to match the low frequency peak which is the primary peak. The second peak in the recorded spectra is located to the right of the primary peak, and is believed to be attributed to the structure-structure interaction. Although the LS-DYNA is able to predict this spectral peak, it could not match the frequency at which the spectral peak occurs. However, it may be explained by the fact that the soil property of the backfill between the two structures is not well characterized, and instead, the free field property is used in the LS-DYNA analysis.

The seismic induced soil pressure time histories on the R-T structural walls are then computed from the LS-DYNA results calculated using the two soil columns. These pressure time histories are compared with the recorded pressure time histories from the respective pressure sensors. Figure 4.2-7 through Figure 4.2-12 present both computed and the JNES recorded seismic induced pressure time histories for the pressure sensors located on the test structures as indicated in Figure 2-20 and Figure 2-21, which show the locations with circles where the pressure sensors were installed. However, only the solid circles represent the sensors which have actually recorded the earthquake event. The sensors selected for the pressure comparisons are N1, N2 and N4 on the north side wall of the reactor building, and S1, S3 and S4 on the south side wall of the turbine structure.

The seismic induced pressures from the LS-DYNA model are computed from soil elements closest to the locations of the pressure sensors, using the stress component perpendicular to the wall.

The comparison between the recorded pressure time history and the LS-DYNA computed pressure time histories shows a reasonable match for the sensors located on the reactor near the base (N1) and near the mid height of the embedded reactor wall (N2). For the pressure sensor near the ground surface (N4), Figure 4.2-9 shows a lower estimate of the peak pressure by LS-DYNA than the recorded pressure.

For the turbine building, the trend of higher computed pressures than the recordings appears to be evident for all the pressure sensors compared, as indicated in Figure 4.2-10 through Figure 4.2-12. Also observed in these figures is that the pressure comparison made at the sensor near the ground appears better than the other sensors.

To compare the LS-DYNA results with the sensor data in the frequency domain, the pressure time history responses of both computed and recorded data are transformed in the frequency domain in terms of Fourier spectra of the respective quantity. Figure 4.2-13 through Figure 4.2-15 present the Fourier spectra of the pressure responses on the north side wall of the reactor building. The Fourier spectra shown in these figures are smoothed using the algorithm described in Section 3.1.2 of this report. These comparisons show that a relatively good match of the frequency content is exhibited for all three locations. For all three sensor pressure data, there is a persistent upward drift in

the Fourier spectral amplitude in low frequency range. As discussed earlier in the SASSI comparisons, it is believed that the sensor data were affected by noise (due to the presence of finite amplitude near the zero frequency).

For the turbine building, the comparisons of the Fourier pressure spectra between the LS-DYNA estimate and the recordings are plotted in Figure 4.2-16 through Figure 4.2-18. As shown in these figures, the LS-DYNA analysis compares very well with the recordings for the sensors: DF-SE-S3 and DF-SE-S4. For the sensor DF-SE-S1, the estimate of the analysis is significantly higher than the recording. However, the overall frequency behavior of the recorded data for all sensors is captured by the analysis. The only problem area is the low frequency response where the recorded data show a persistent upward drift due to high noise/signal ratio in the recorded data.

Vertical Response Analysis

For the vertical pressure response, the layout of the pressure sensors on the basemat of the R-T model is shown in Figure 2-17, in which only the transducers located on the edges of the building basemat have actually recorded the pressure response; those sensors inside the basemat did not record any data. Therefore, in order to compare the vertical response analysis results with the recorded vertical pressure data, the horizontal effect on the vertical recorded pressure data need to be removed. This is done by taking an average over all vertical pressure data on the basemat. Therefore, the LS-DYNA vertical response result is compared with the averaged sensor pressure response.

The LS-DYNA vertical response analysis is performed by applying the recorded free field motion in the vertical direction at the control point located 35m below grade. The vertical ISRS results are computed at the center of the basemat and the roof, which are compared with the respective accelerometer recordings at these locations as designated in Figure 3.2-3 as B1A-V0 and RFA-V0 respectively. Note that the roof center of the reactor building is not instrumented with the accelerometer in the vertical direction; therefore, the accelerometer installed on a corner of the roof is used instead for the comparison. The comparisons between the predicted vertical ISRS and the vertical accelerometer recordings are shown in Figure 4.2-19 and Figure 4.2-22, for the basemat and the roof, respectively.

Similar to the soil uncertainty considered for the horizontal response analysis, the effect of the soil uncertainty is also considered for the vertical response analysis by varying P-wave velocity of the soil (V_p). One set of results is computed using the JNES soil geotechnical data, which is interpreted as the best estimate soil property which is designated in the figures for this study as the mean soil V_p . Since the vertical response is controlled by the compressional wave, the second analysis is therefore performed by adjusting the mean soil p-wave velocity V_p to achieve the best fit of the computed vertical ISRS with the recording.

As shown in these figures for the vertical ISRS comparison, the LS-DYNA estimates match both the frequency content and the spectral peaks across most of the frequency band, except for the high frequency peak at which the SASSI result with the JNES soil shifts to a lower frequency. However, when the uncertainty of about 10% the mean soil p-wave velocity (equivalent to 0.2 for the COV of the soil stiffness reduction) is incorporated, excellent comparisons are achieved between the LS-DYNA calculated spectra and recorded ISRS, with the exception for the reactor roof. As described above,

the accelerometer used for the roof comparison is located on a corner rather than in the center of the roof, therefore, the recorded ISRS at this location has both vertical and horizontal inputs, which is the reason why the LS-DYNA result did not agree with the recorded ISRS response for the reactor roof. Furthermore, the vertical LS-DYNA analysis achieves much better comparison between the computed vertical ISRS and the accelerometer recordings than the respective horizontal response analysis.

The seismic induced pressures on the basemat are then computed in the LS-DYNA analysis for both the mean and the mean minus 0.2 of COV soil columns. As mentioned above, to remove the influence of the horizontal inputs from the recorded vertical pressure measurements on the basemat, the sensor pressures at the corner locations as shown in Figure 2-17 are averaged. The averaged vertical sensor pressures are then compared with the predicted pressures computed at the center of the basemat. Figure 4.2-23 and Figure 4.2-24 plot the averaged vertical pressure time histories from the JNES recorded vertical pressures and the LS-DYNA computed basemat pressures for both the reactor and the turbine structures. As indicated by these figures, LS-DYNA computed pressures match well with the averaged recorded vertical pressure data.

Comparison of the computed and recorded pressure data is then made by transforming the time history data into the frequency domain where their respective Fourier spectra are computed and smoothed using the algorithm described in Section 3.1.2 of this report. These Fourier spectra are plotted and compared as shown in Figure 4.2-25 and Figure 4.2-26. Again, good comparisons are obtained between the analysis and recorded vertical pressure data.

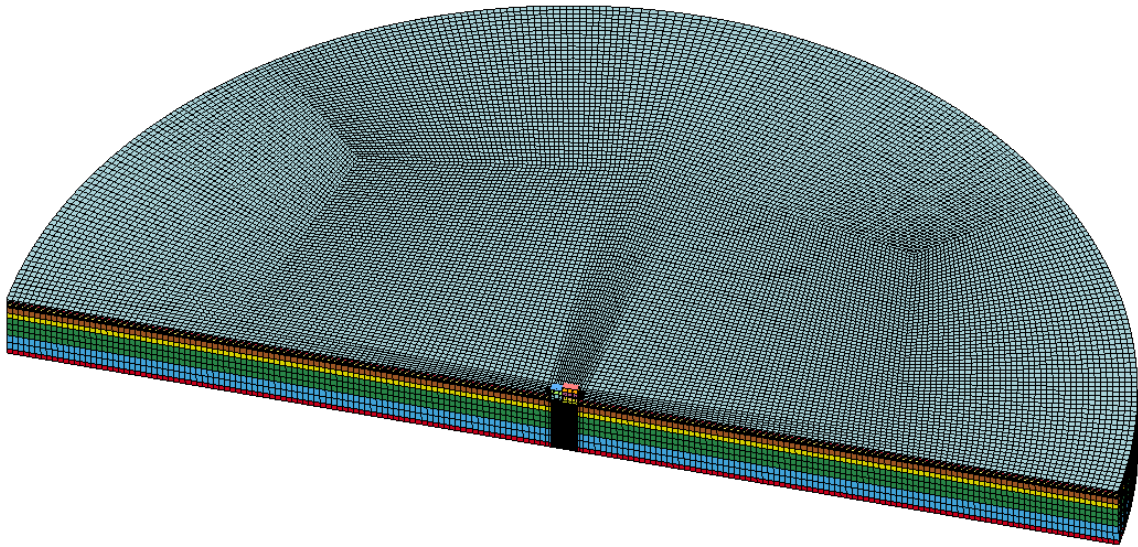


Figure 4.2-1 LS-DYNA Model of R-T Test Configuration

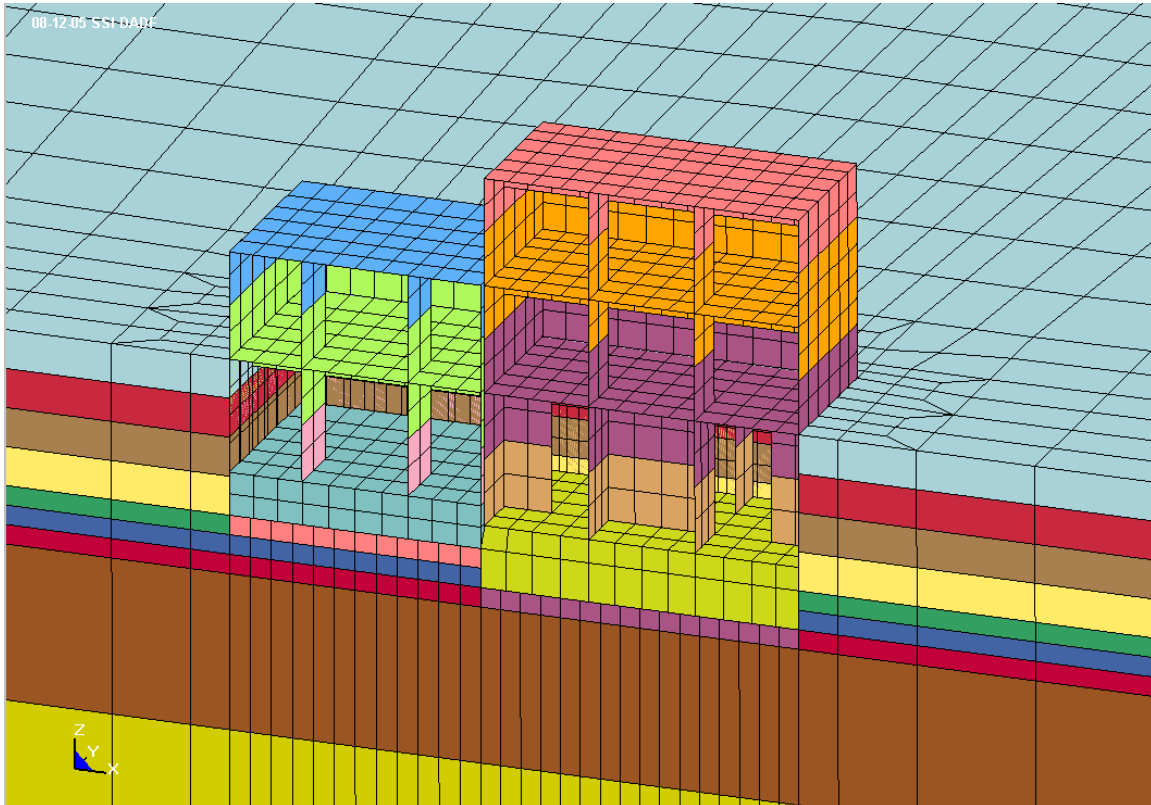


Figure 4.2-2 Zoom-in View of LS-DYNA Model of R-T Test Configuration

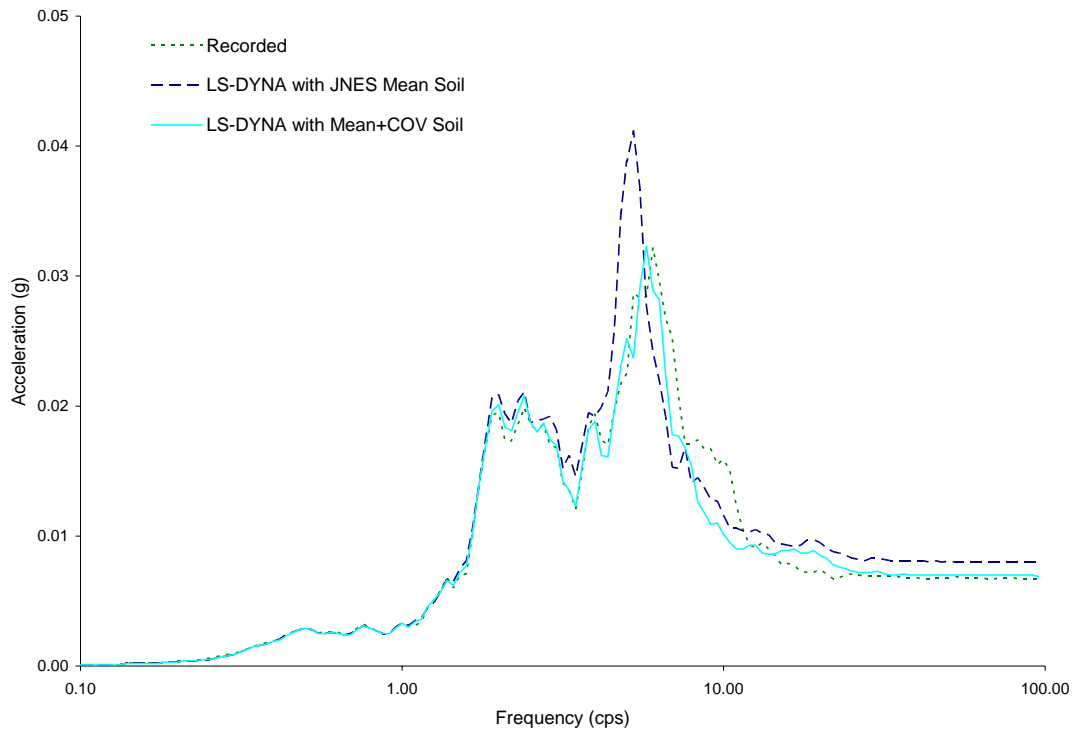


Figure 4.2-3 Comparison of Horizontal Response at Basemat Center of R-T Reactor

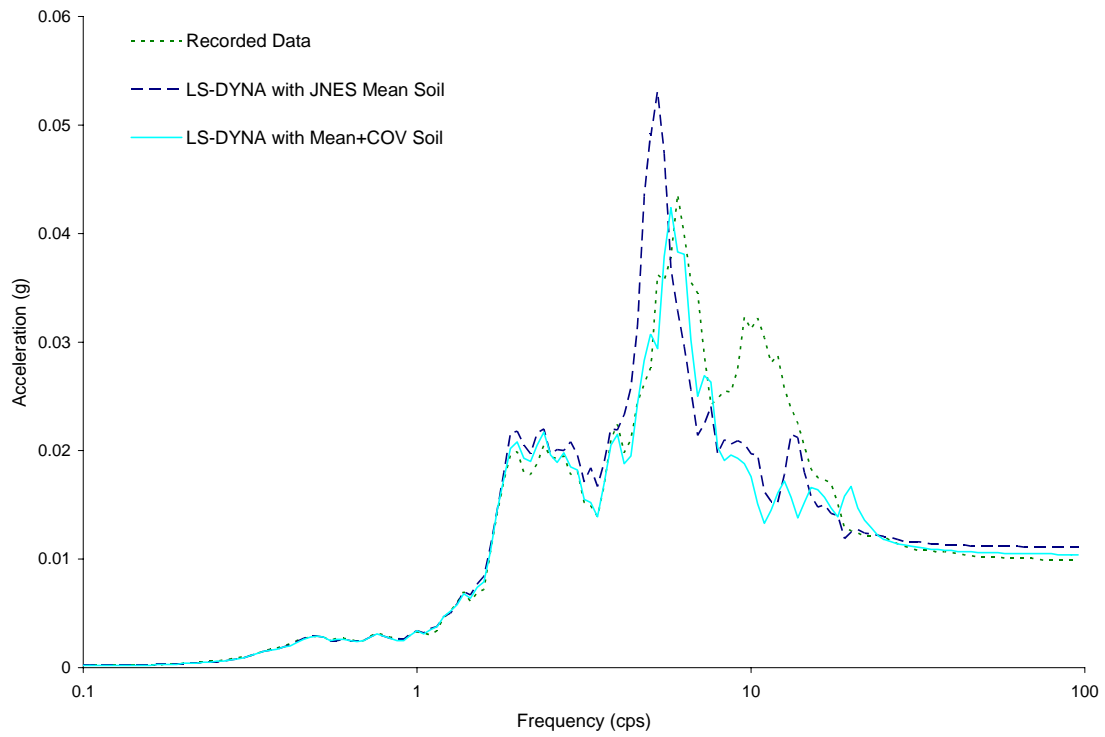


Figure 4.2-4 Comparison of Horizontal Response at Roof Center of R-T Reactor

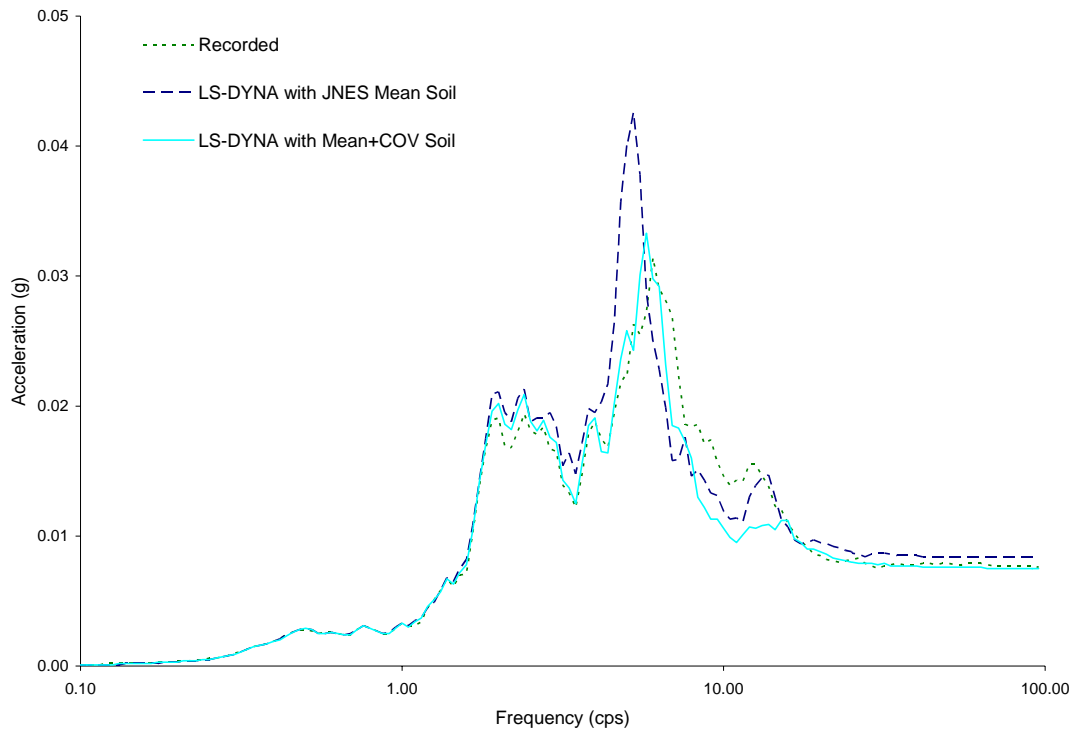


Figure 4.2-5 Comparison of Horizontal Response at Basemat Center of R-T Turbine

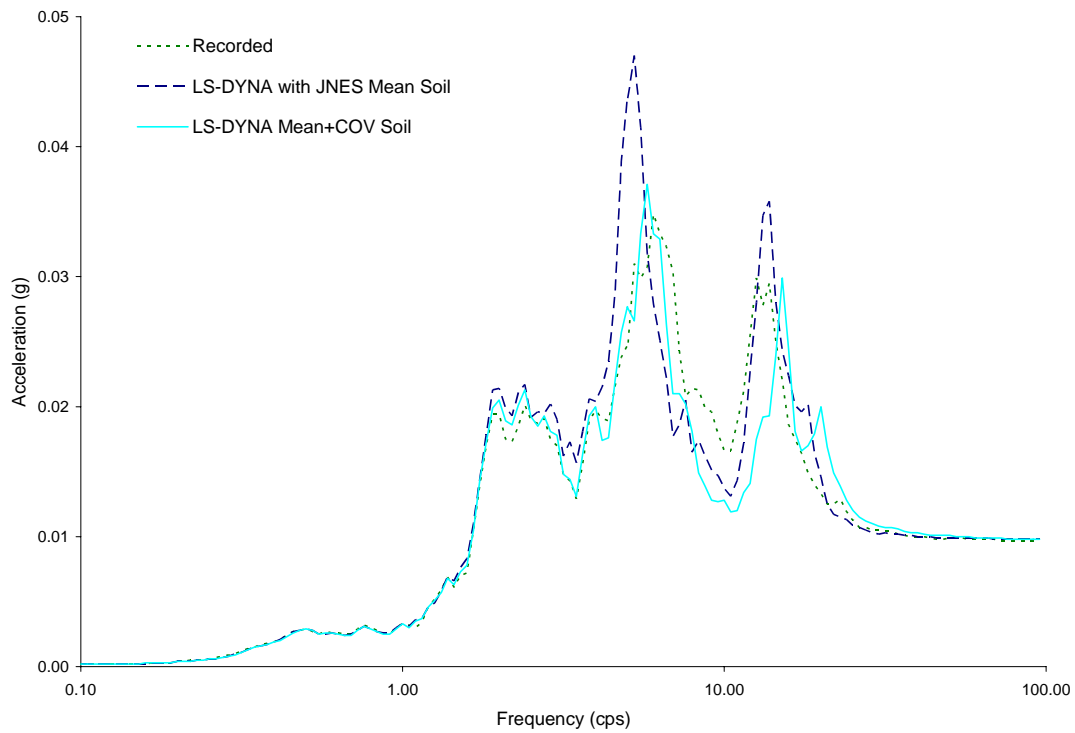


Figure 4.2-6 Comparison of Horizontal Response at Roof Center of R-T Turbine

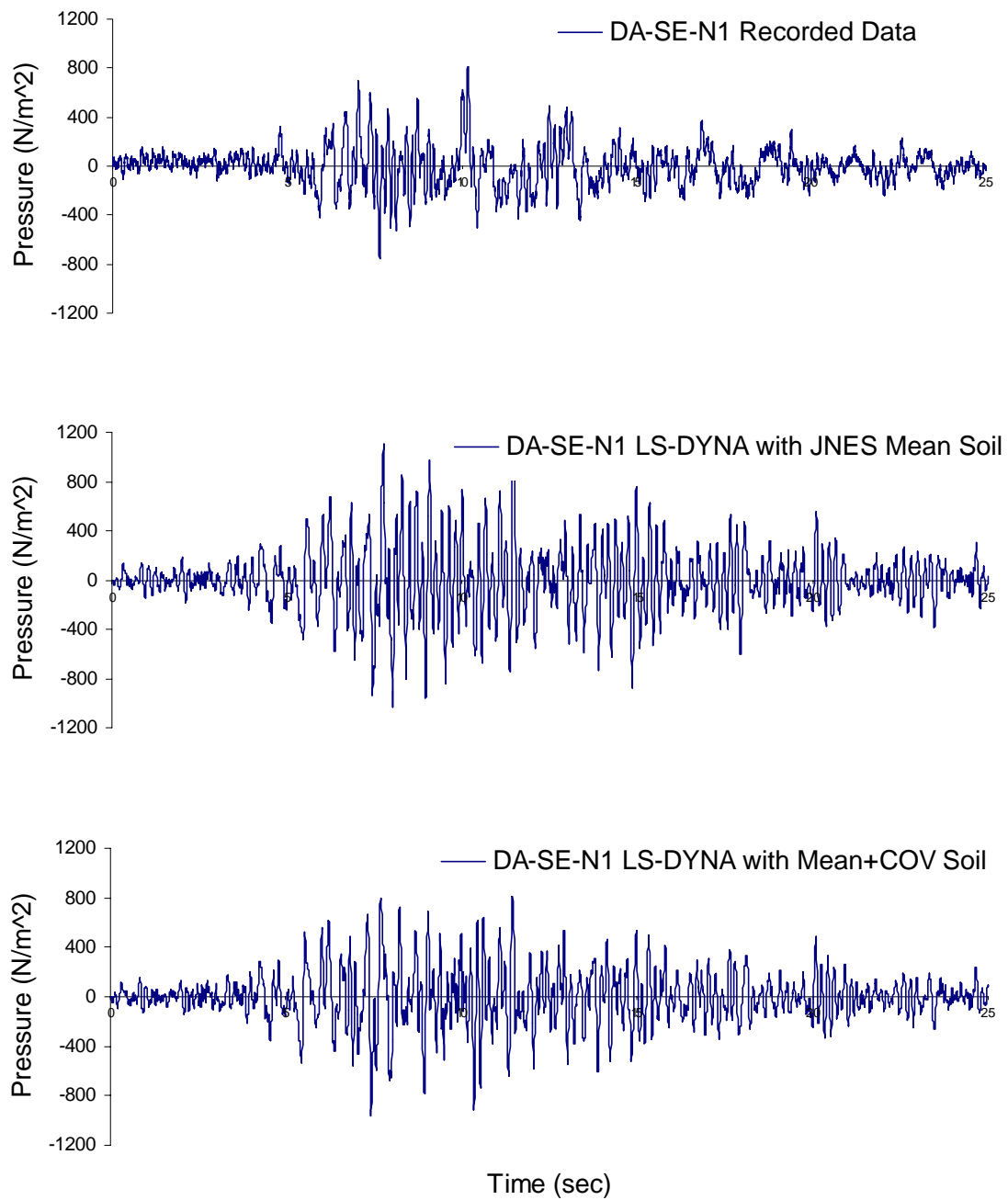


Figure 4.2-7 Comparison of Seismic Induced Soil Pressure at Sensor DA-SE-N1

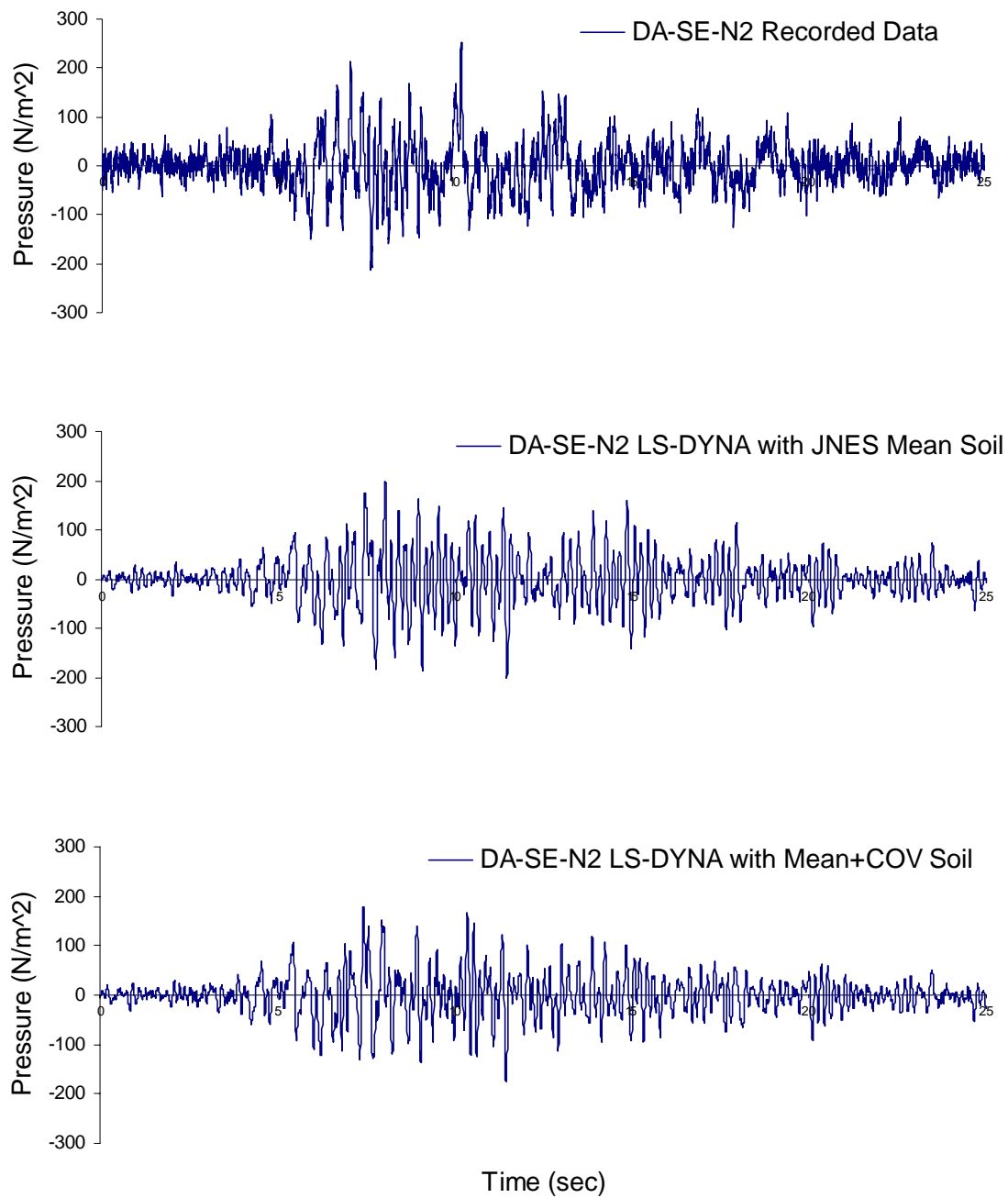


Figure 4.2-8 Comparison of Seismic Induced Soil Pressure at Sensor DA-SE-N2

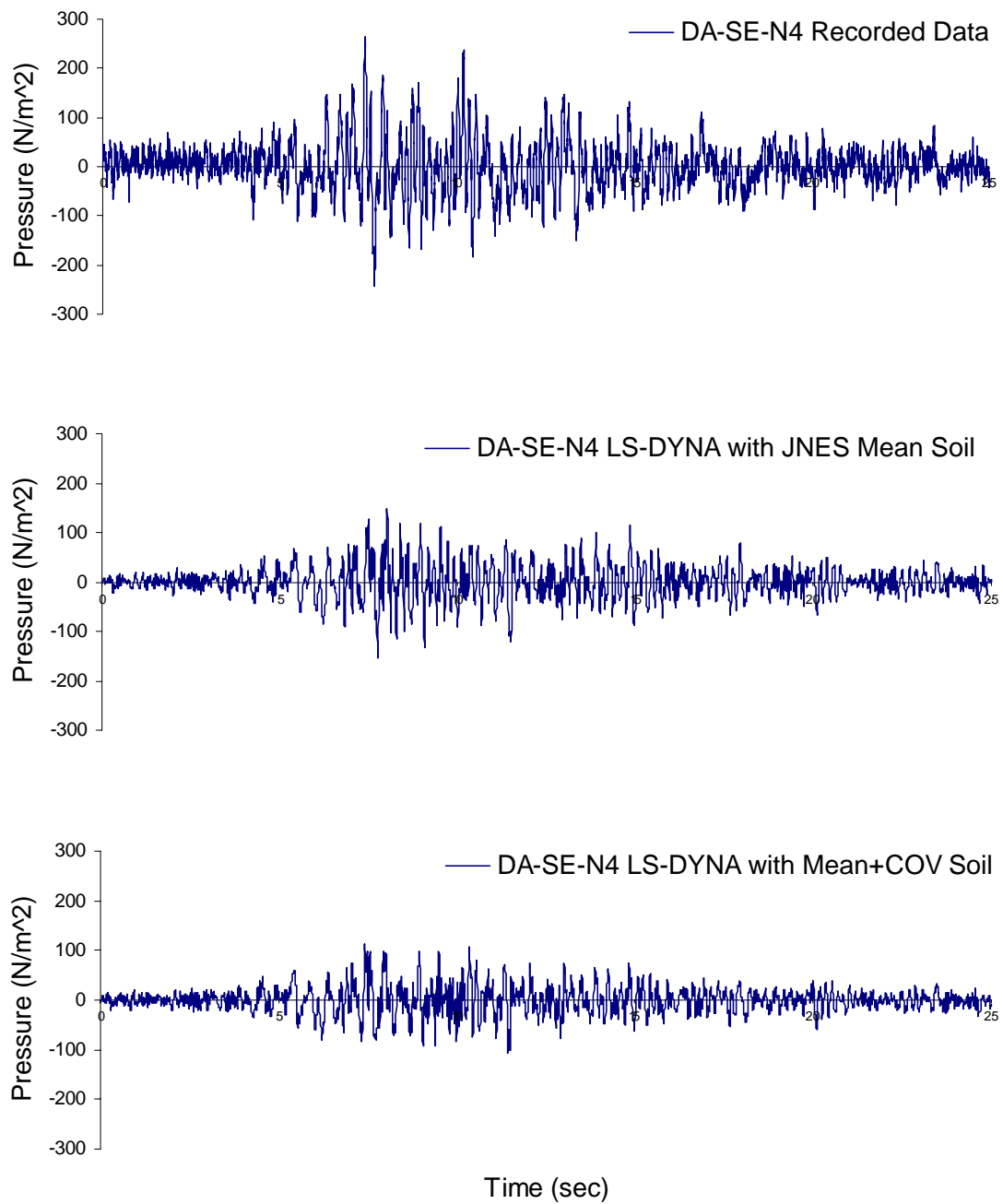


Figure 4.2-9 Comparison of Seismic Induced Soil Pressure at Sensor DA-SE-N4

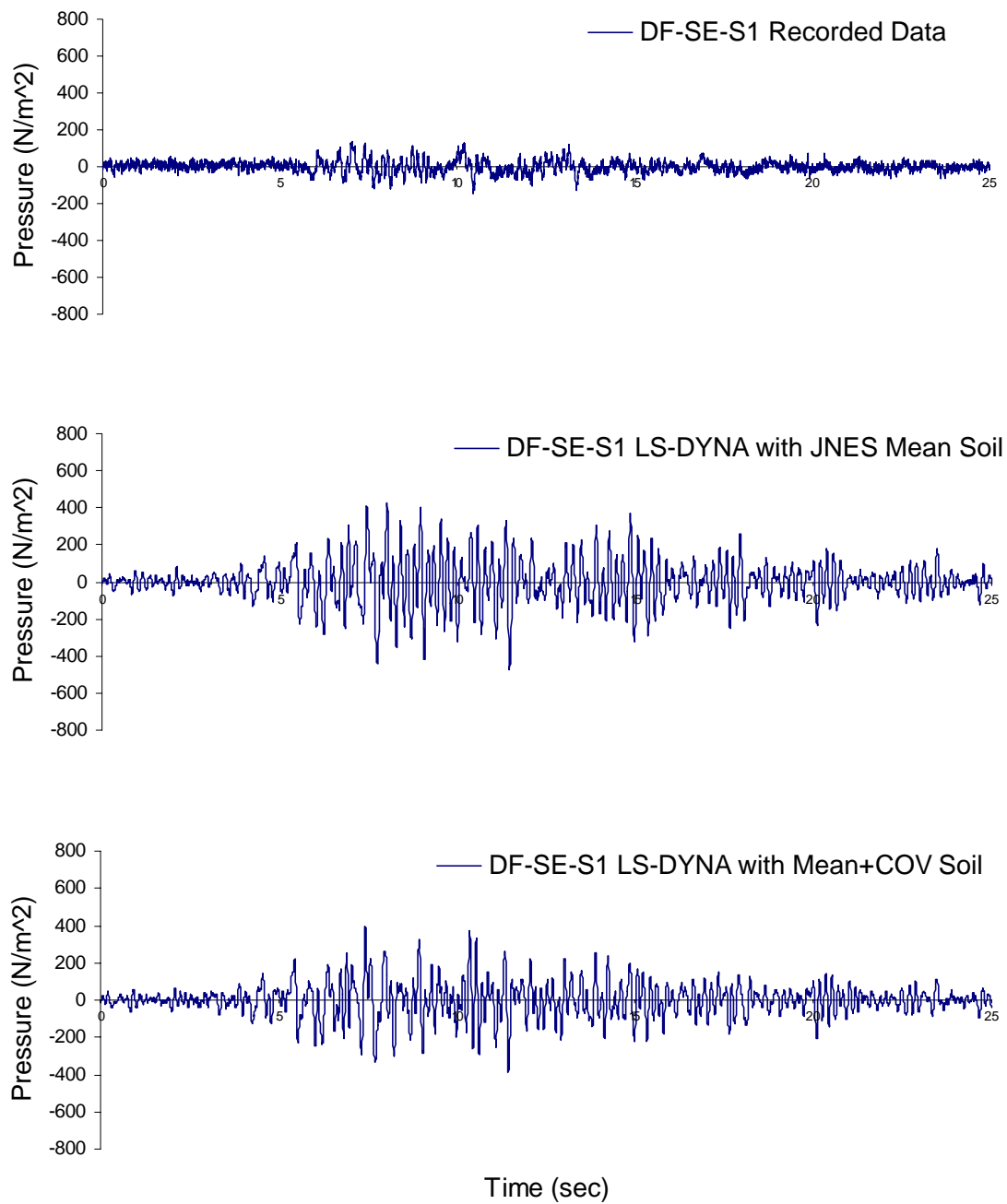


Figure 4.2-10 Comparison of Seismic Induced Soil Pressure at Sensor DF-SE-S1

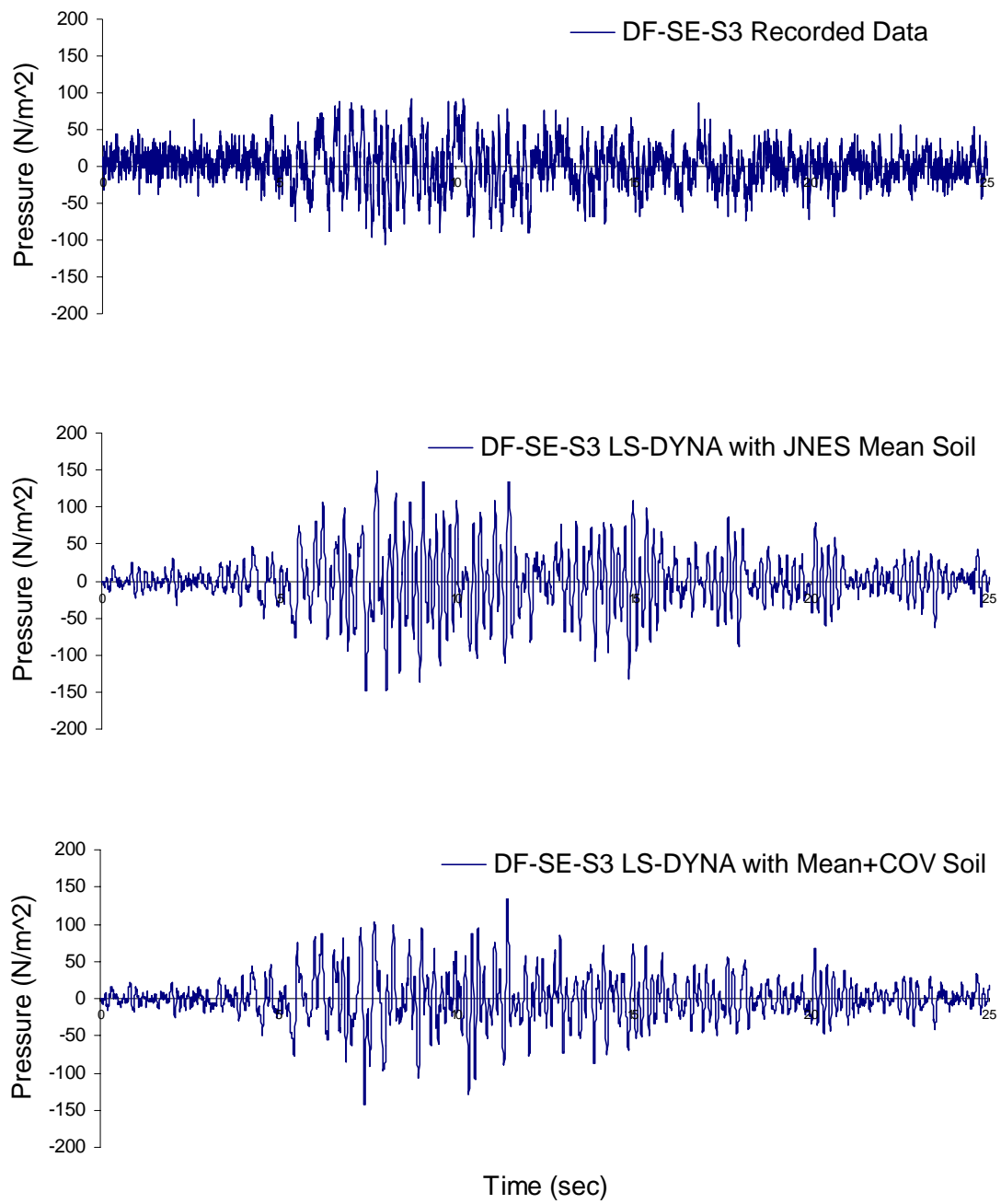


Figure 4.2-11 Comparison of Seismic Induced Soil Pressure at Sensor DF-SE-S3

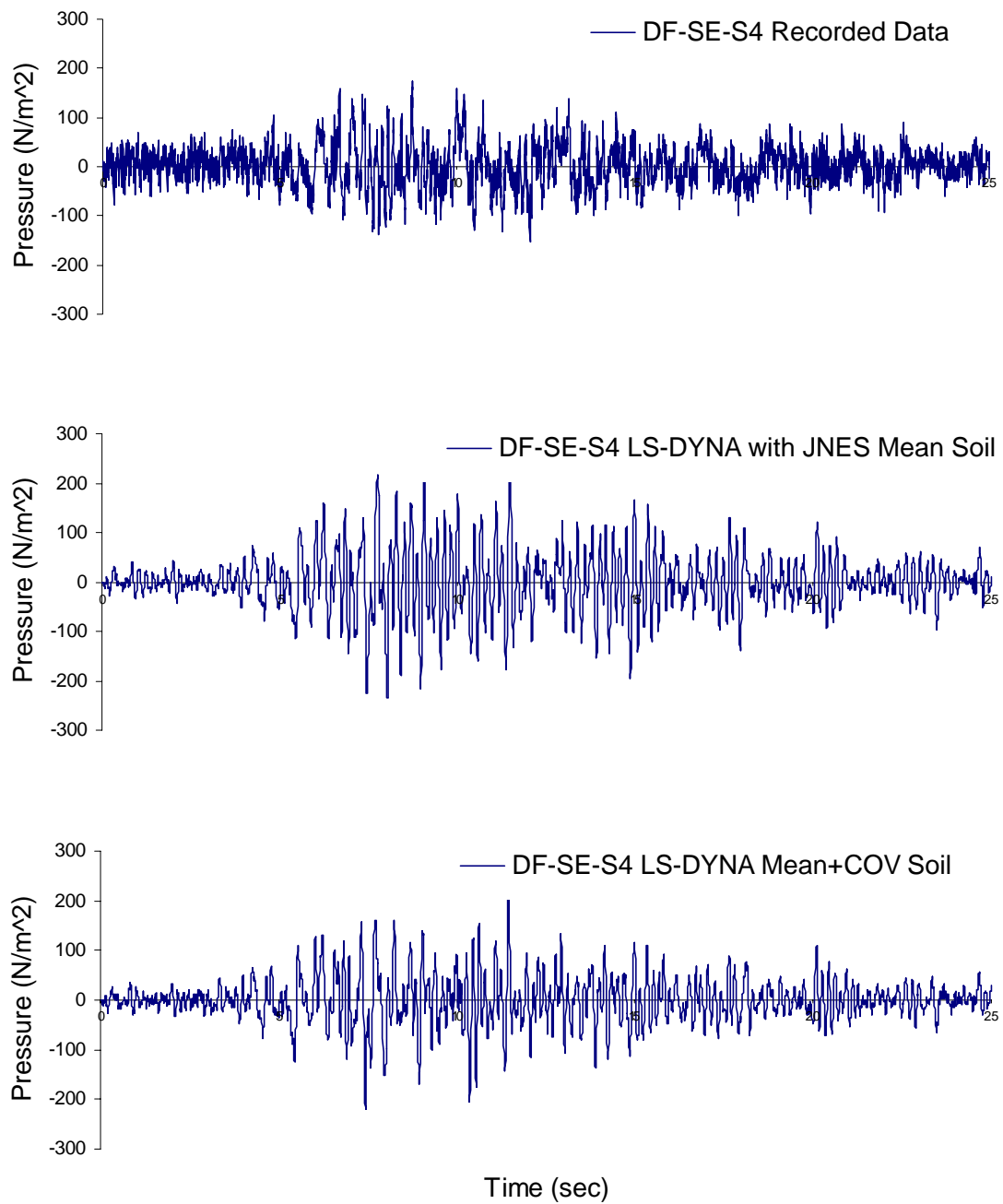


Figure 4.2-12 Comparison of Seismic Induced Soil Pressure at Sensor DF-SE-S4

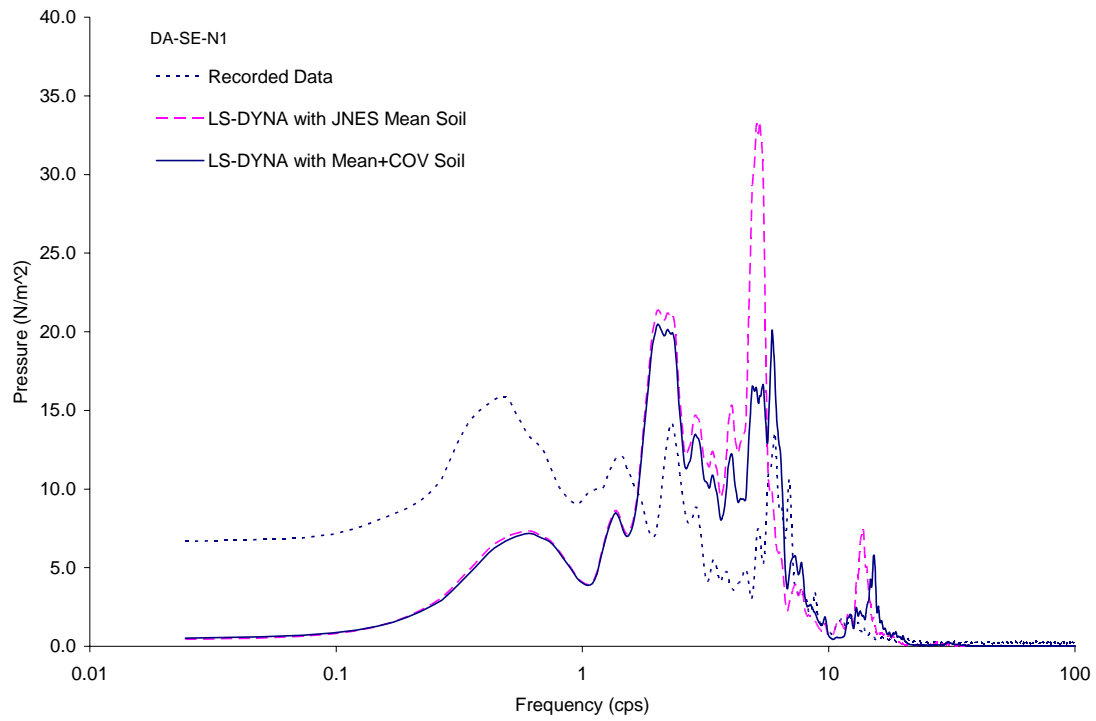


Figure 4.2-13 Comparison of Fourier Spectra of Soil Pressure at Sensor DA-SE-N1

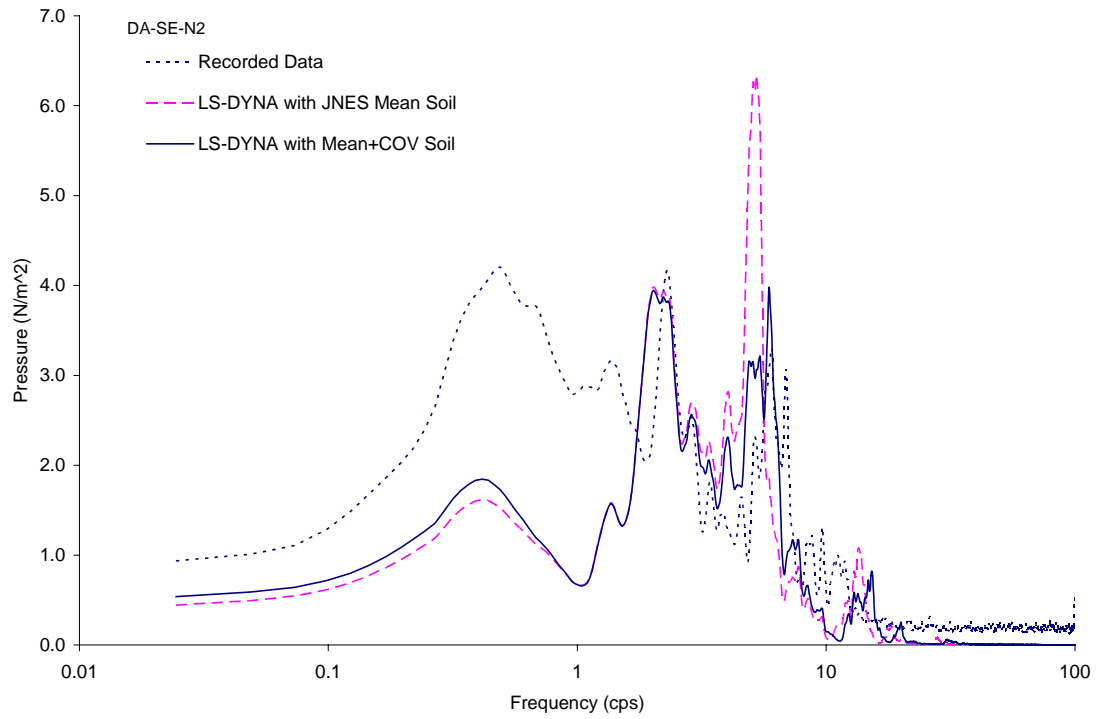


Figure 4.2-14 Comparison of Fourier Spectra of Soil Pressure at Sensor DA-SE-N2

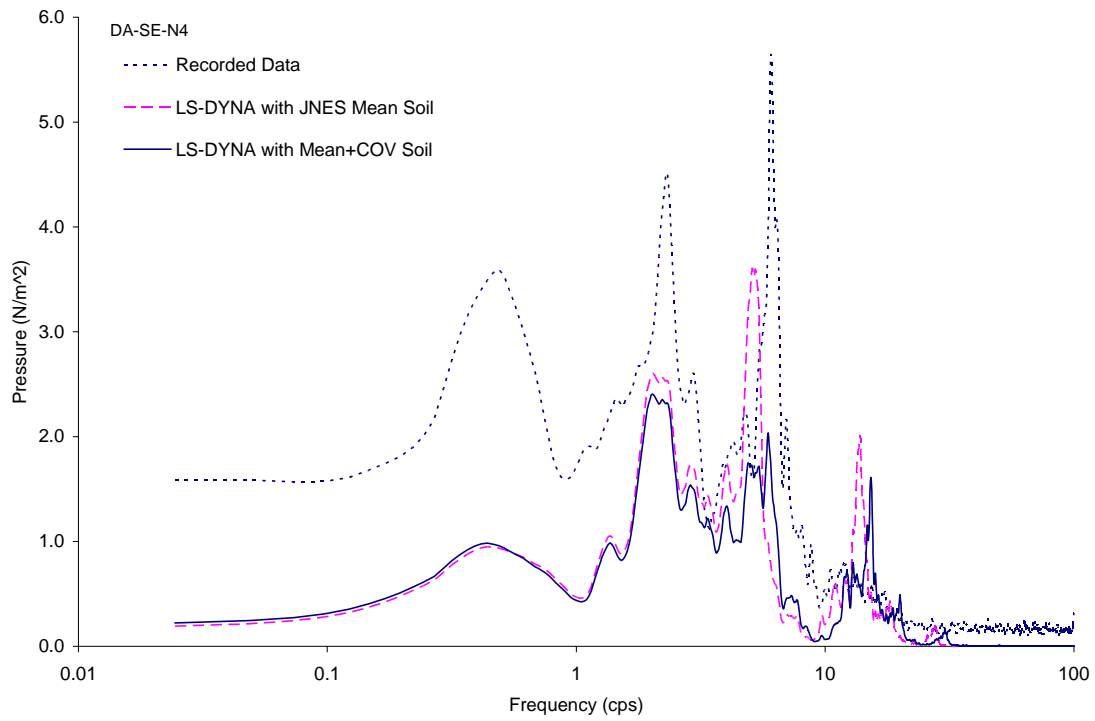


Figure 4.2-15 Comparison of Fourier Spectra of Soil Pressure at Sensor DA-SE-N4

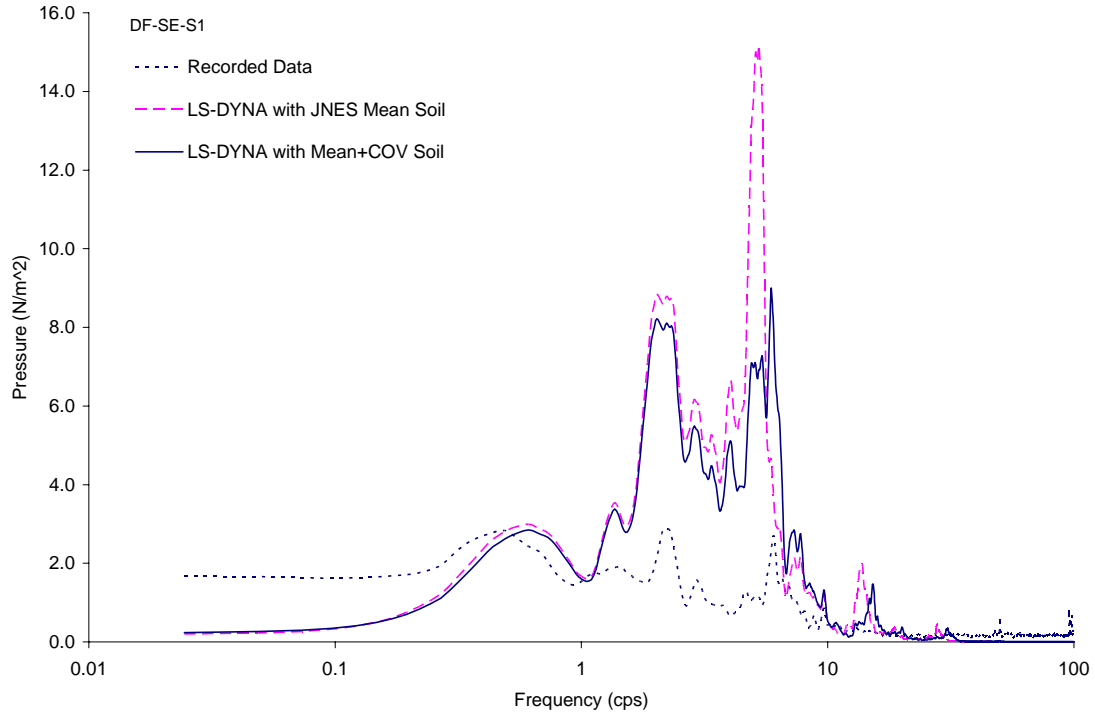


Figure 4.2-16 Comparison of Fourier Spectra of Soil Pressure at Sensor DF-SE-S1

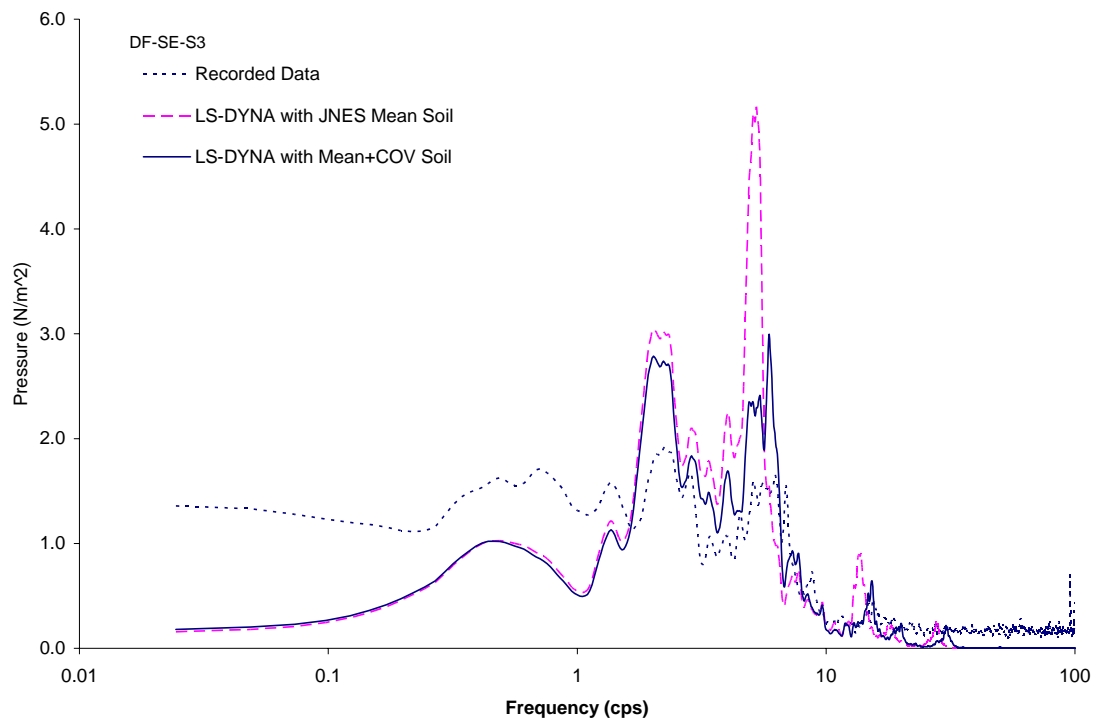


Figure 4.2-17 Comparison of Fourier Spectra of Soil Pressure at Sensor DF-SE-S3

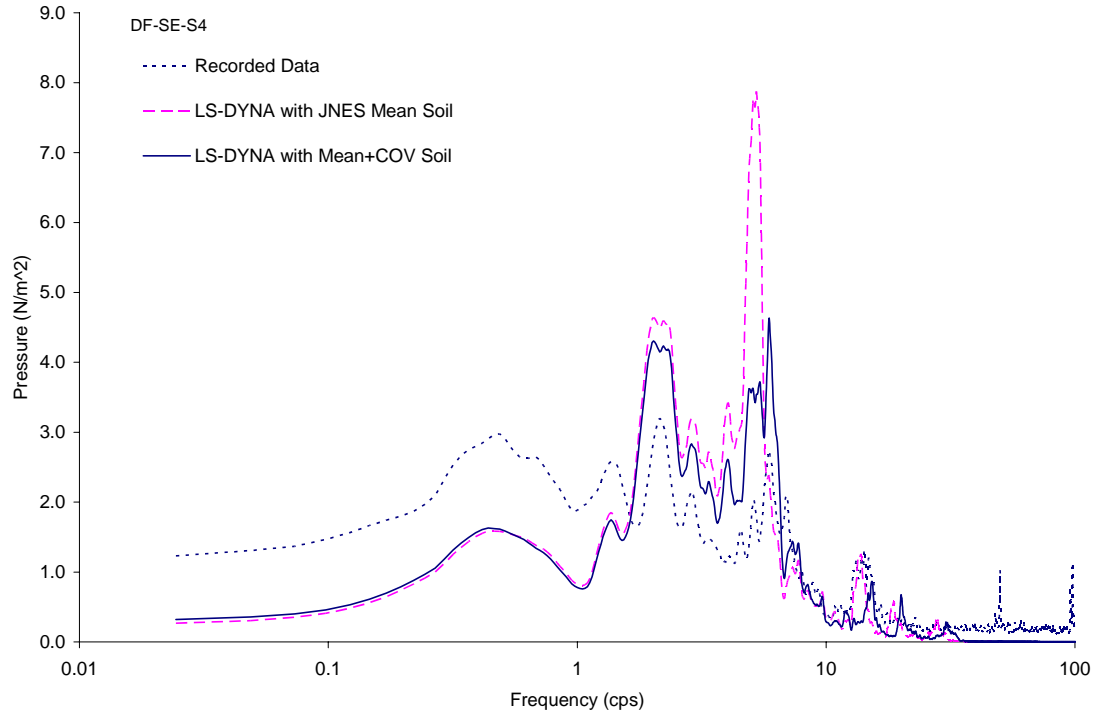


Figure 4.2-18 Comparison of Fourier Spectra of Soil Pressure at Sensor DF-SE-S4

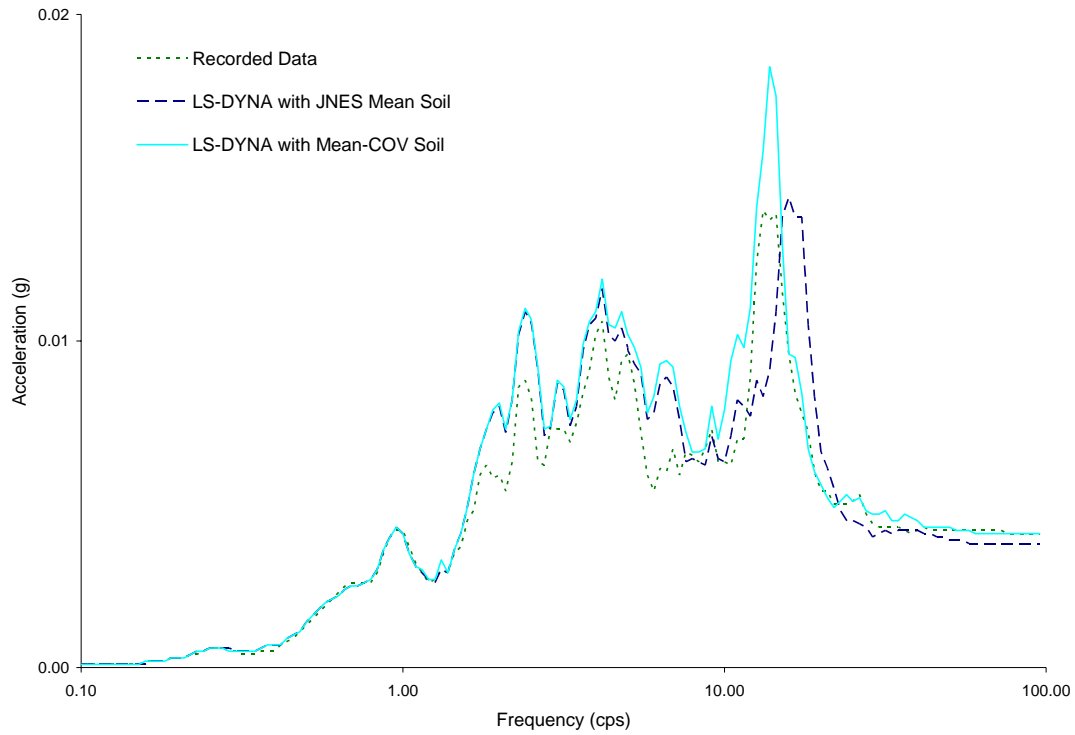


Figure 4.2-19 Comparison of Vertical Response Spectra at Basemat Center of R-T Reactor

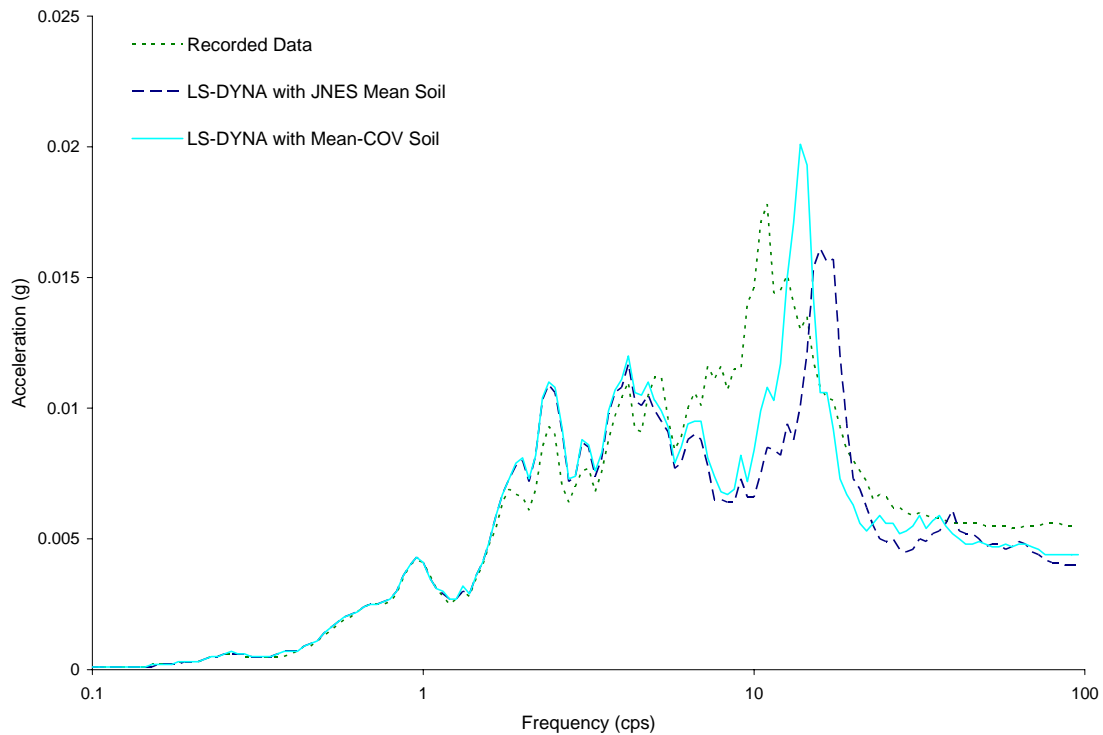


Figure 4.2-20 Comparison of Vertical Response Spectra at Roof Center of R-T Reactor

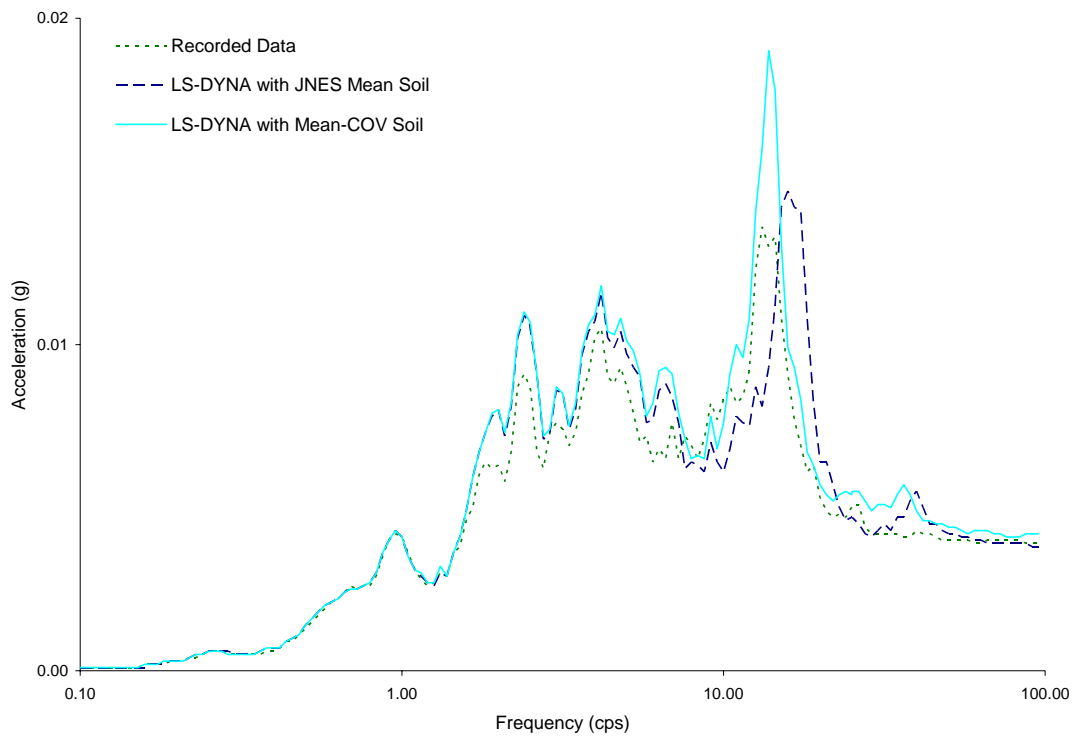


Figure 4.2-21 Comparison of Vertical Response Spectra at Basemat Center of R-T Turbine

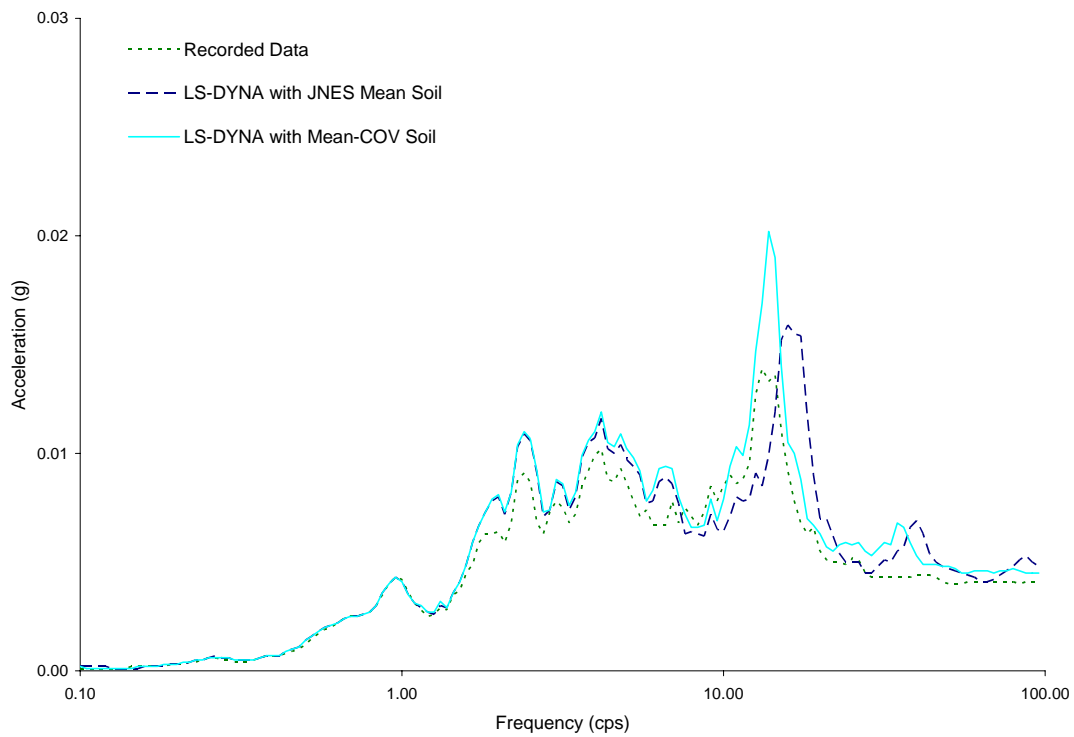


Figure 4.2-22 Comparison of Vertical Response Spectra at Roof Center of R-T Turbine

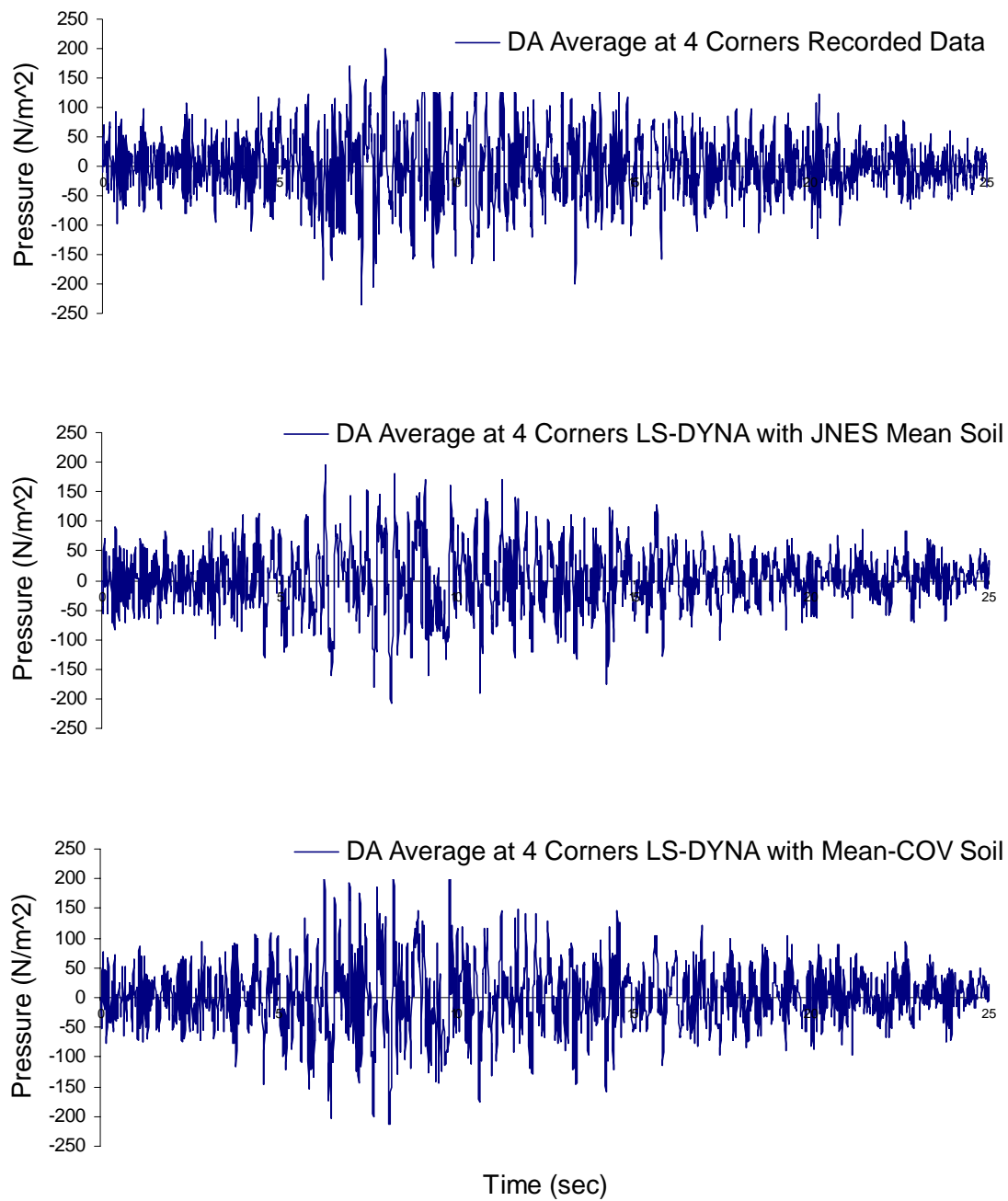


Figure 4.2-23 Comparison of Seismic Induced Vertical Soil Pressure on Basemat of R-T Reactor

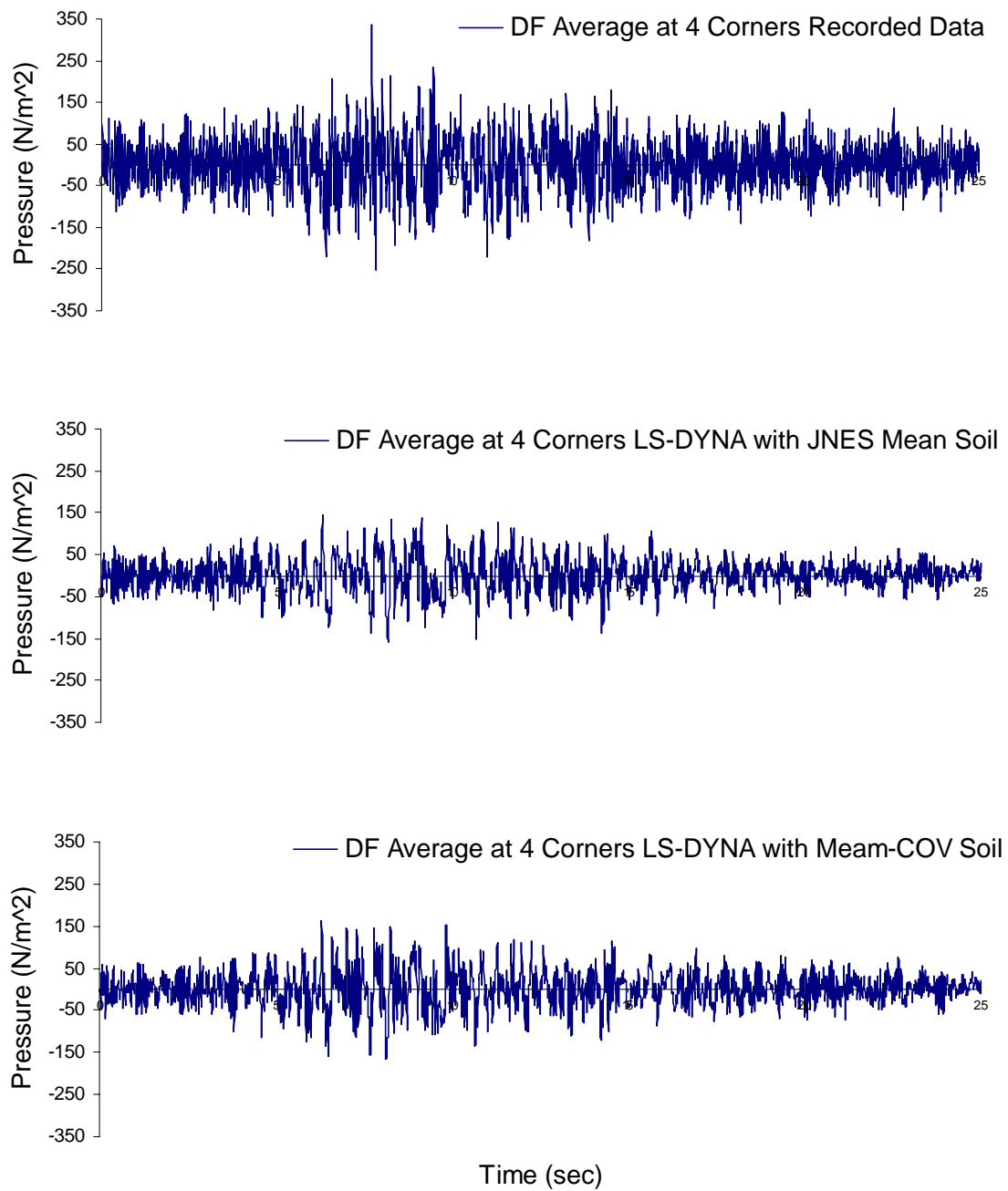


Figure 4.2-24 Comparison of Seismic Induced Vertical Soil Pressure on Basemat of R-T Turbine

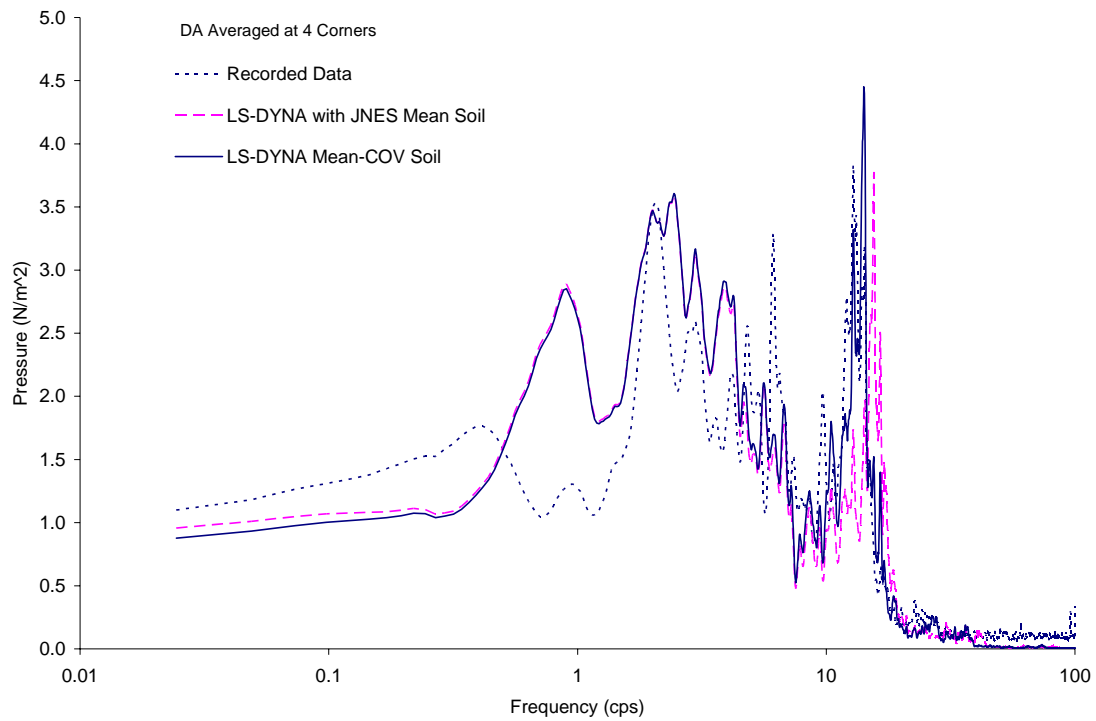


Figure 4.2-25 Comparison of Fourier Spectra for Vertical Soil Pressure on Basemat of R-T Reactor

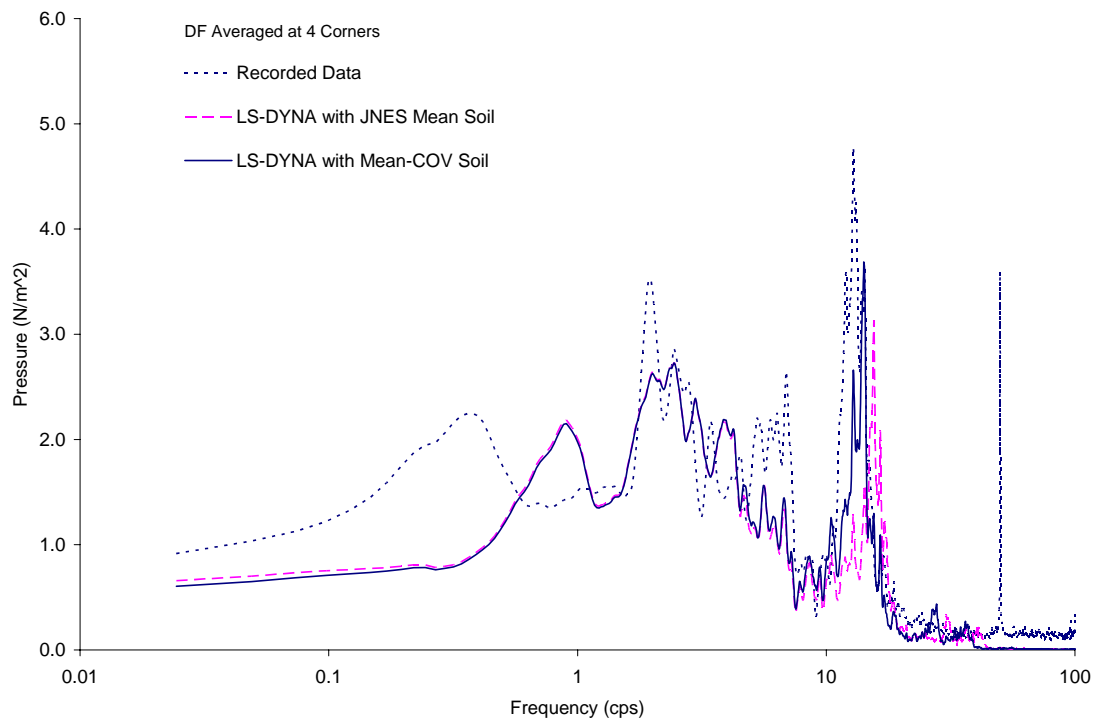


Figure 4.2-26 Comparison of Fourier Spectra for Vertical Soil Pressure on Basemat of R-T Turbine

4.3 Methodology Assessment

As discussed above, BNL performed LS-DYNA analyses for the JNES test models of both the twin reactor configuration and R-T configuration. Comparisons were made between the LS-DYNA results and the JNES field recorded earthquake responses in terms of ISRS and the soil pressures for both horizontal and vertical directions. Based on these comparisons, an assessment can be made regarding the performance of the LS-DYNA models.

For the small level ground motion analyzed, the linear analysis using LS-DYNA performed extremely well in predicting the test model's ISRS, as exhibited by the comparisons. Although the soil uncertainty estimated for the LS-DYNA analysis is different in some cases from the corresponding SASSI analysis, nonetheless, the range of the soil uncertainty is well within the range acceptable in geotechnical engineering applications. The only exception is that in the ISRS comparison for the DA roof location, the LS-DYNA analysis fails to capture the second spectral peak which is deemed to be due to the structure-structure interaction effect. The reason for it may be due to the lack of information on the soil property of the backfill between the reactor and the turbine structures (The analysis assumes the free field property for the backfill).

For seismic induced pressures, the correlation between the analysis and the test data indicates that 1) the analysis can generally capture the frequency content of the test data, and 2) better prediction is obtained for the vertical analysis than the horizontal analysis. The reason for less accurate horizontal pressure correlation, aside from the high noise/signal ratio inherent in the recorded data, is that the horizontal response is primarily induced by the SH-waves which generate shear stress predominant in the soil, therefore, the soil pressure is a secondary stress. While for the vertical response, the system is subjected to the P-wave which induces pressures as the primary stress in soils. Therefore, as shown by these pressure comparisons, the pressure correlations were much better for the vertical response than the horizontal response. The same conclusion was also reached for the SASSI analysis.

To place the assessment of the modeling performance in a broader perspective, the twin reactor configuration is selected to compare the response parameters computed from the LS-DYNA and SASSI analyses. For the ISRS, Figure 4.3-1 and Figure 4.3-2 present the comparison of the LS-DYNA and SASSI computed horizontal ISRS, together with the JNES recorded data. These figures show that using the JNES soil column, LS-DYNA and SASSI compute similar ISRS in both the shape and the amplitude, when incorporating the soil uncertainty, both codes also predict about the same ISRS which agree reasonably with the JNES recorded data, though slightly different ranges of the soil uncertainty are employed by the two codes.

Further, to examine the soil pressure predictions by the two codes, Fourier spectra of the computed horizontal soil pressures by the two codes, together with the recorded sensor pressures, are plotted in Figure 4.3-3 through Figure 4.3-8. As shown by these comparisons, the pressures computed using the two codes mostly envelop the recorded pressures, with the exception for the sensors BAS-SE-S2 and BAN-SE-N6, which are shown in Figures 4.3-4 and 4.3-7. As indicated in these figures the computed pressures are much lower than the respective recorded data, especially for low frequency range. As discussed in the previous sections of this report, these two sensors which are located

near the mid-height of embedded wall appear to be contaminated with noises (upward drift in low frequencies). For other pressure sensors, the results using modified soil columns correlate better with the recorded pressures. In addition, the LS-DYNA computed pressures appear closer to the recorded pressures than the SASSI results, although not to the extent that one would reach a different conclusion about the performance of the two codes.

With respect to the vertical response comparisons, Figure 4.3-9 and Figure 4.3-10 provide the vertical ISRS computed by the two codes, together with the JNES recorded ISRS. The two computer codes basically predict very similar ISRS that are close to the recorded ISRS. Similar to the horizontal analyses, the uncertainty range of the soil columns estimated by the two codes are slightly different with LD-DYNA having a smaller value. For the vertical soil pressures, Figure 4.3-11 and Figure 4.3-12 present the comparisons between the two codes and with the recorded pressures. From these comparisons, SASSI estimates the vertical soil pressures much closer to the recorded pressures than LS-DYNA. However, for some frequencies, the SASSI estimate of the soil pressures fall below the recorded pressures. On the other hand, LS-DYNA grossly over-predicts the pressure responses. It should be mentioned that the upward drift in the low frequencies of the recordings should be ignored for the reason as discussed earlier in this section.

Finally, the uncertainty in the soil properties was estimated by both SASSI and LS-DYNA by fitting the ISRS response. The uncertainty of the soil property is characterized by the COV of the soil stiffness. With a total of eight different cases analyzed, the two codes estimated the same COV for only one case. Nonetheless, for all cases, the estimated COVs never exceed 0.2, which is well with the range of the geotechnical engineering understanding. Figure 4.3-13 summarizes the various analysis cases performed for both JNES soil data and BNL estimated soil uncertainties using both SASSI and LS-DYNA.

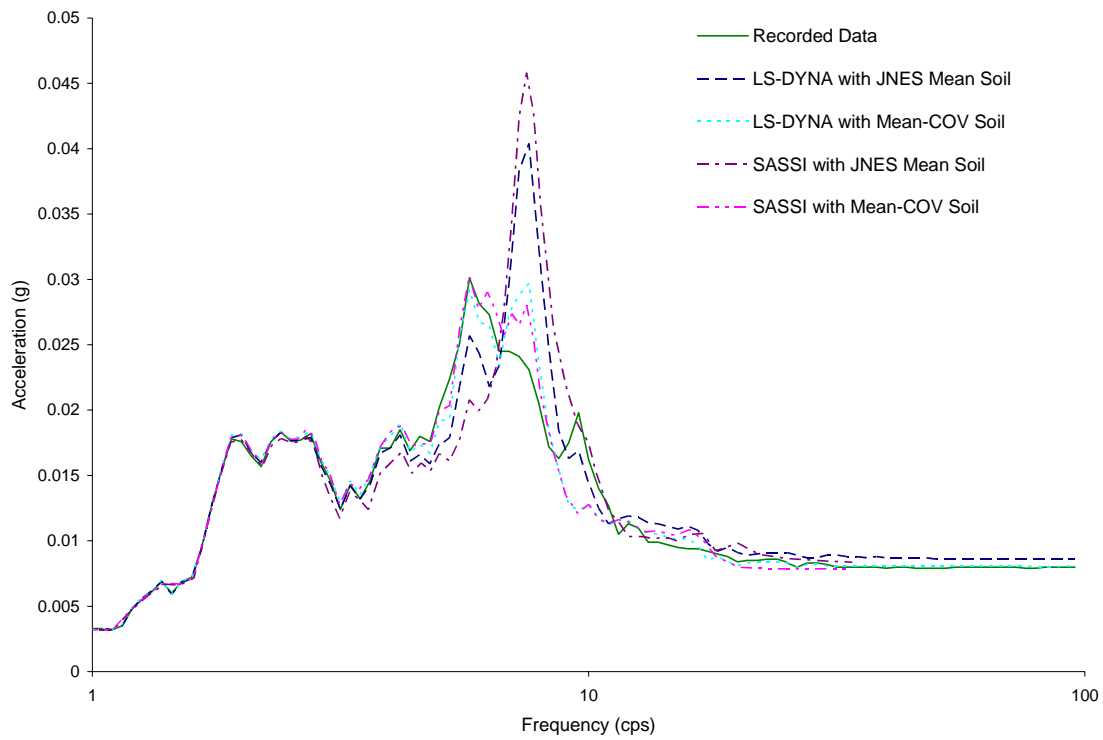


Figure 4.3-1 Comparison of Response Spectra at Basemat of Twin Reactors Model between LS-DYNA and SASSI

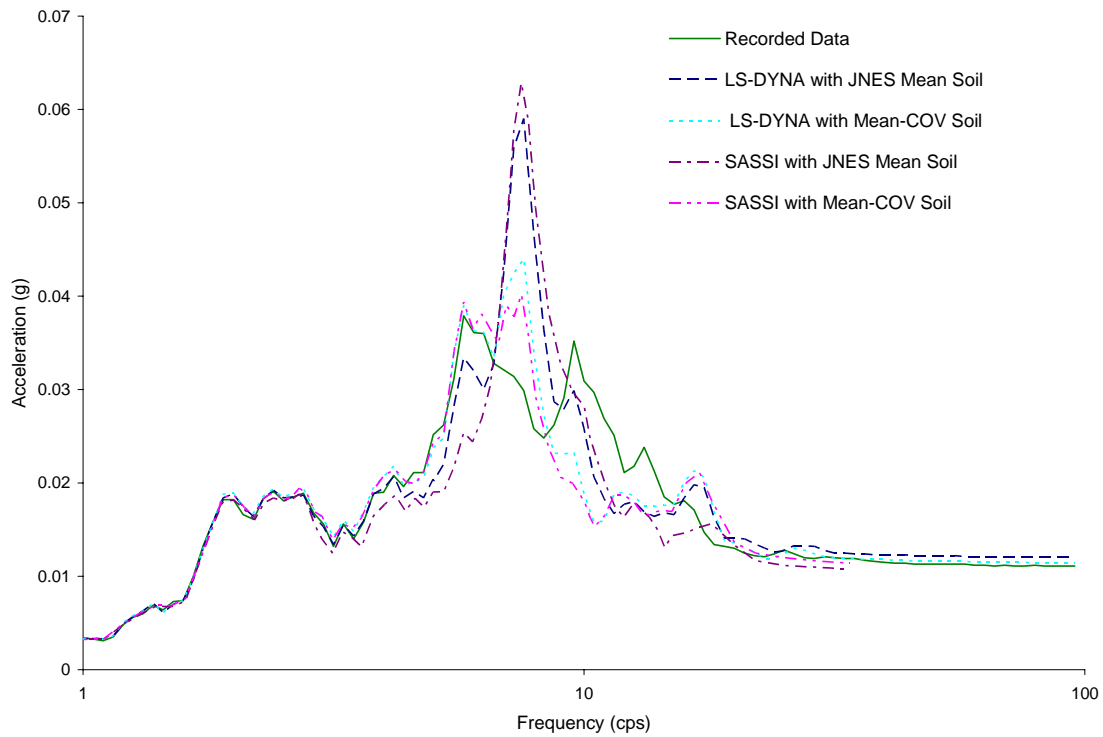


Figure 4.3-2 Comparison of Response Spectra at Roof of Twin Reactors Model between LS-DYNA and SASSI

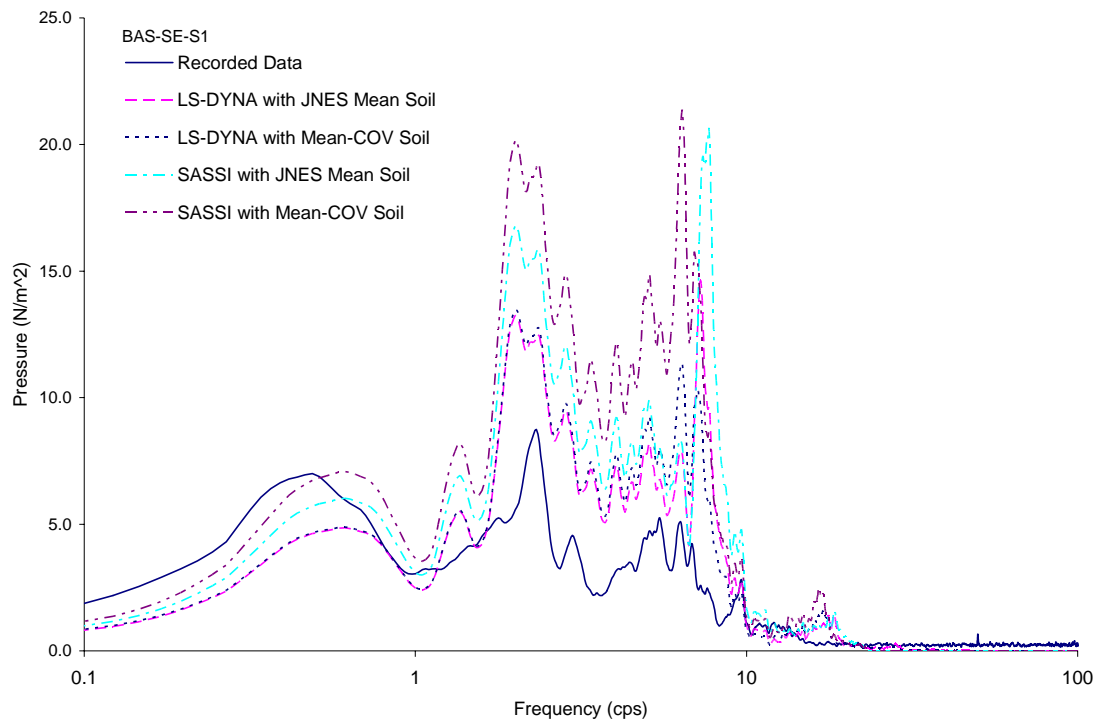


Figure 4.3-3 Comparison of Fourier Spectra of Soil Pressure at Sensor BAS-SE-S1 of Twin Reactors Model between LS-DYNA and SASSI

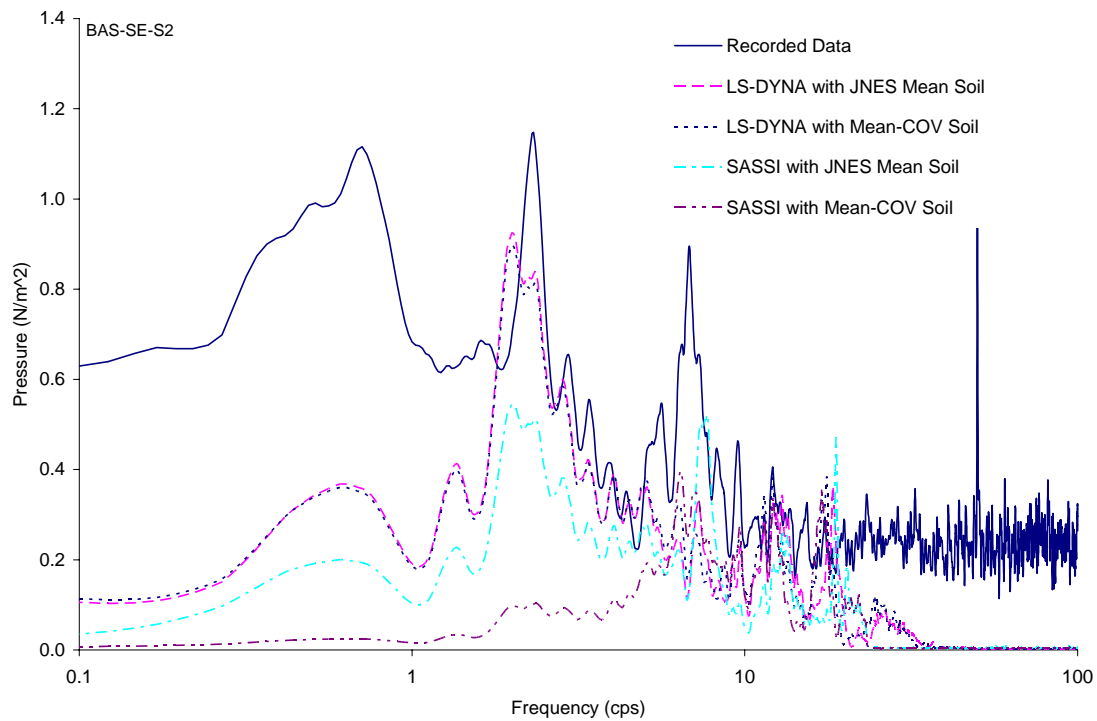


Figure 4.3-4 Comparison of Fourier Spectra of Soil Pressure at Sensor BAS-SE-S2 of Twin Reactors Model between LS-DYNA and SASSI

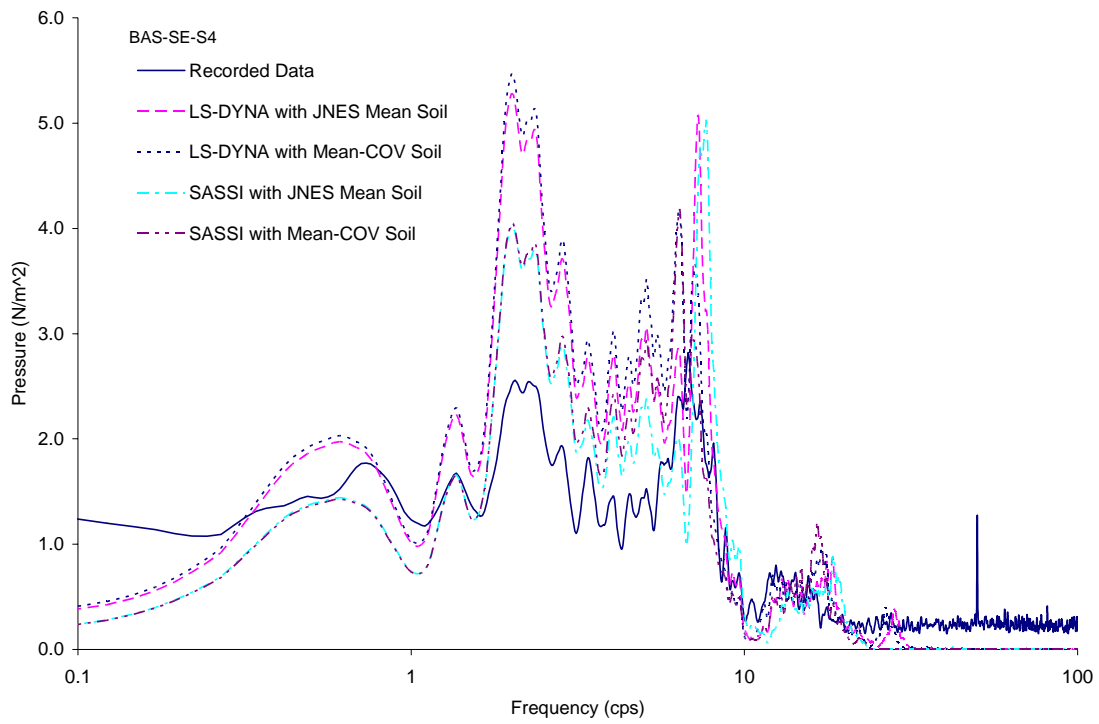


Figure 4.3-5 Comparison of Fourier Spectra of Soil Pressure at Sensor BAS-SE-S4 of Twin Reactors Model between LS-DYNA and SASSI

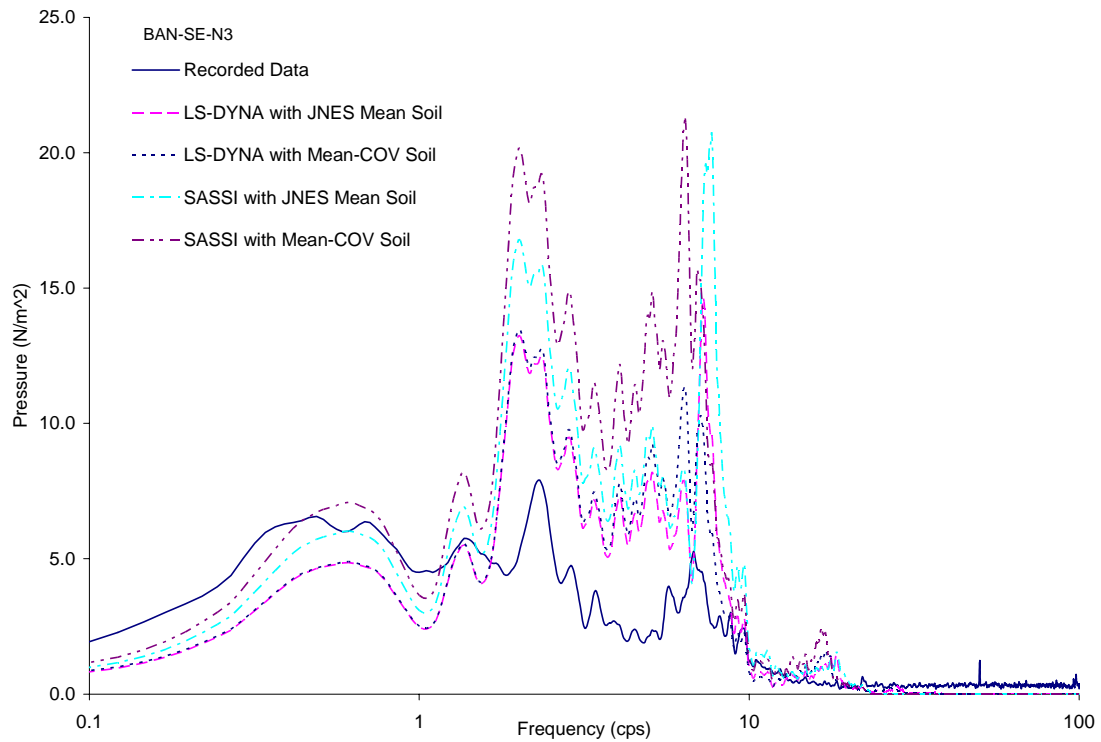


Figure 4.3-6 Comparison of Fourier Spectra of Soil Pressure at Sensor BAN-SE-N3 of Twin Reactors Model between LS-DYNA and SASSI

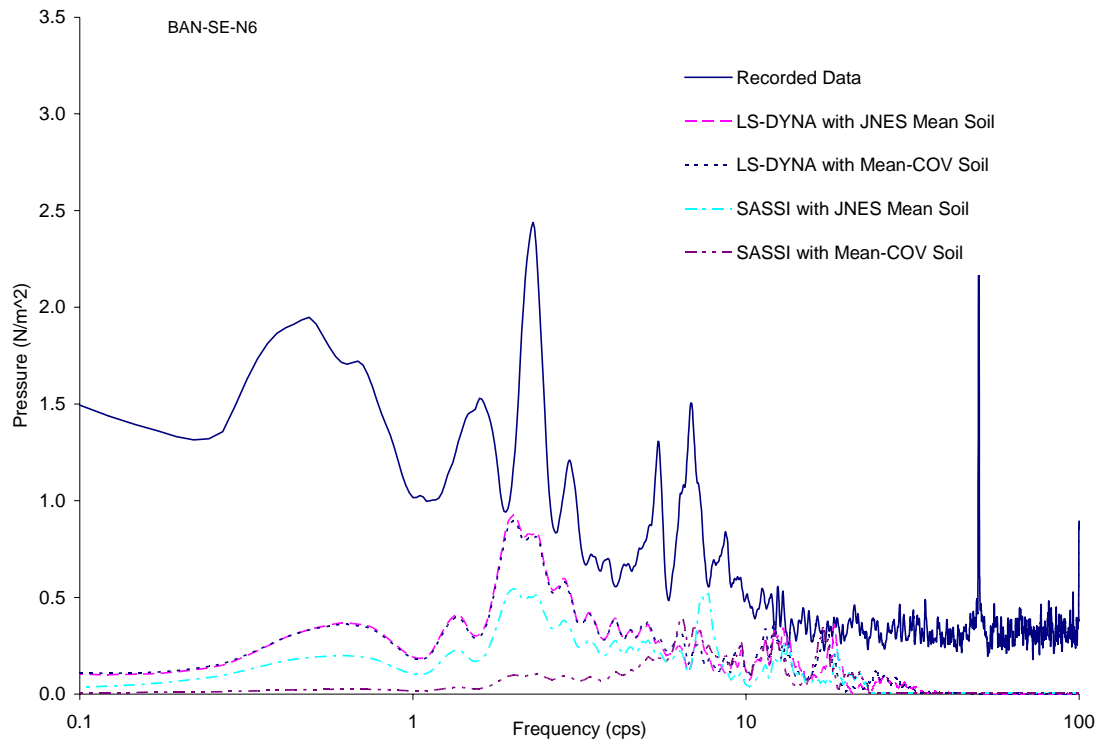


Figure 4.3-7 Comparison of Fourier Spectra of Soil Pressure at Sensor BAN-SE-N6 of Twin Reactors Model between LS-DYNA and SASSI

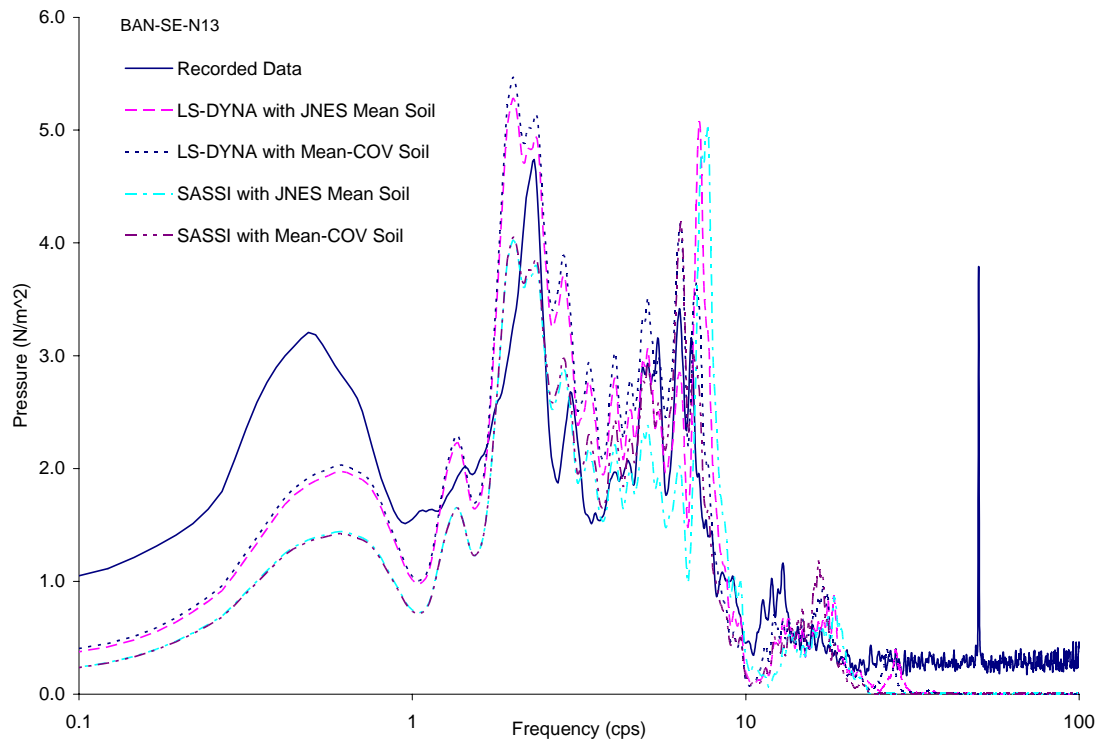


Figure 4.3-8 Comparison of Fourier Spectra of Soil Pressure at Sensor BAN-SE-N13 of Twin Reactors Model between LS-DYNA and SASSI

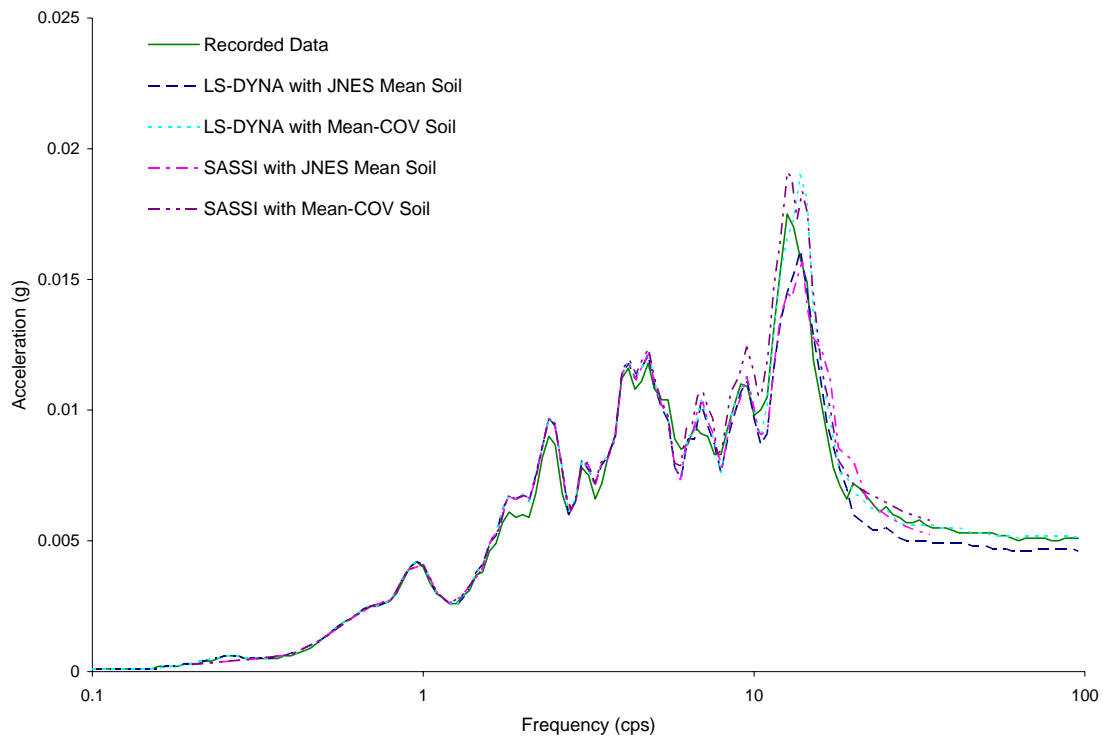


Figure 4.3-9 Comparison of Vertical Response Spectra at Basemat of Twin Reactors Model between LS-DYNA and SASSI

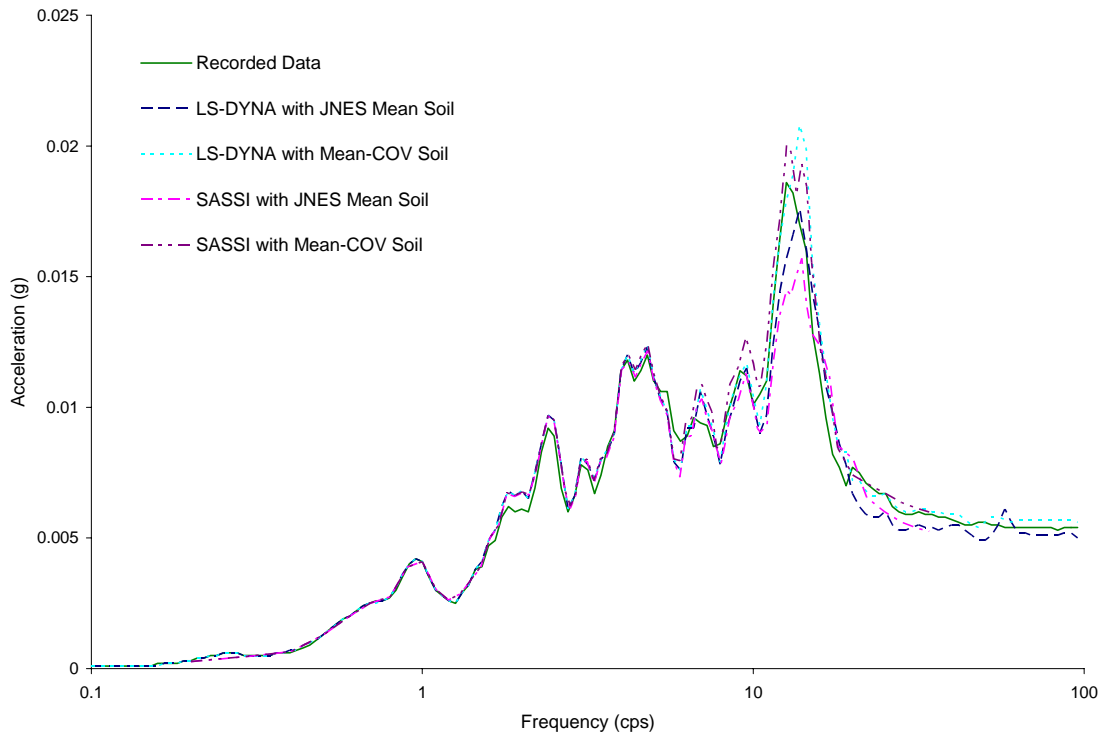


Figure 4.3-10 Comparison of Vertical Response Spectra at Roof of Twin Reactors Model between LS-DYNA and SASSI

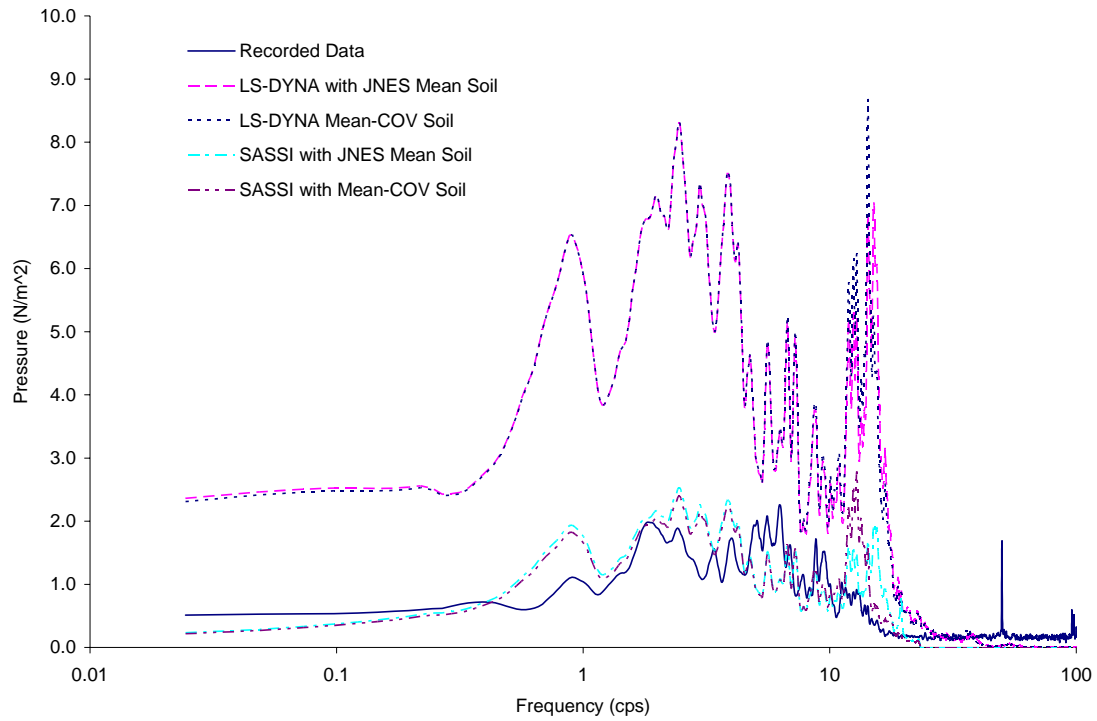


Figure 4.3-11 Comparison of Fourier Spectra of Vertical Soil Pressure on BAN Basemat of Twin Reactors Model

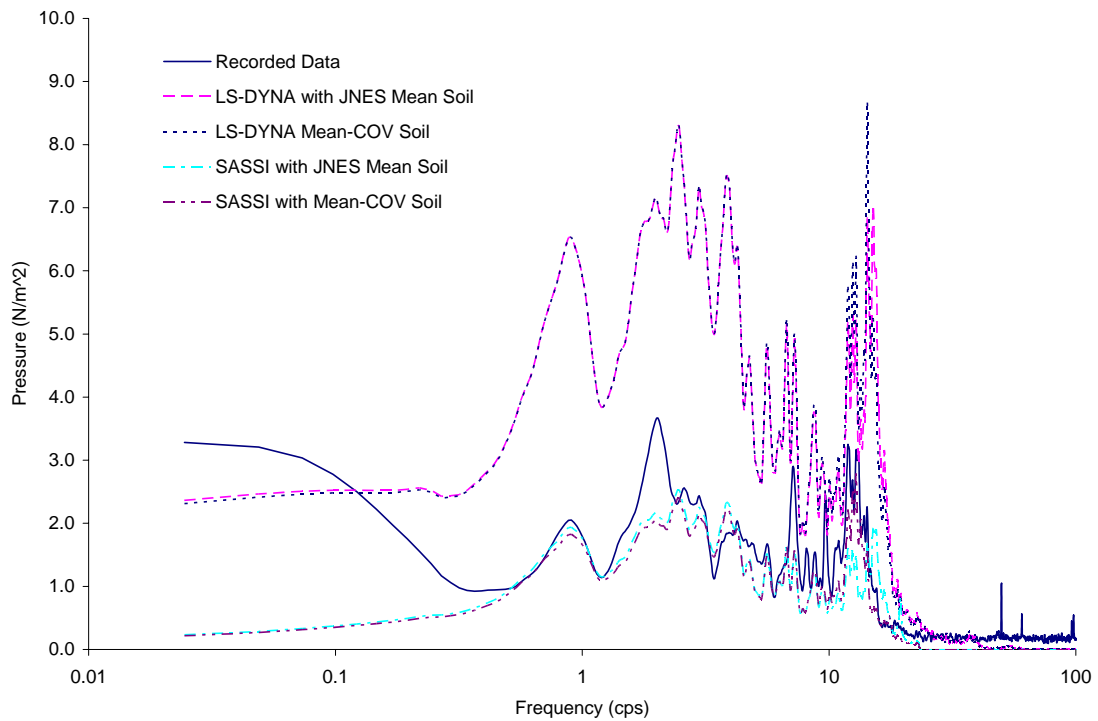


Figure 4.3-12 Comparison of Fourier Spectra of Vertical Soil Pressure on BAS Basemat of Twin Reactors Model

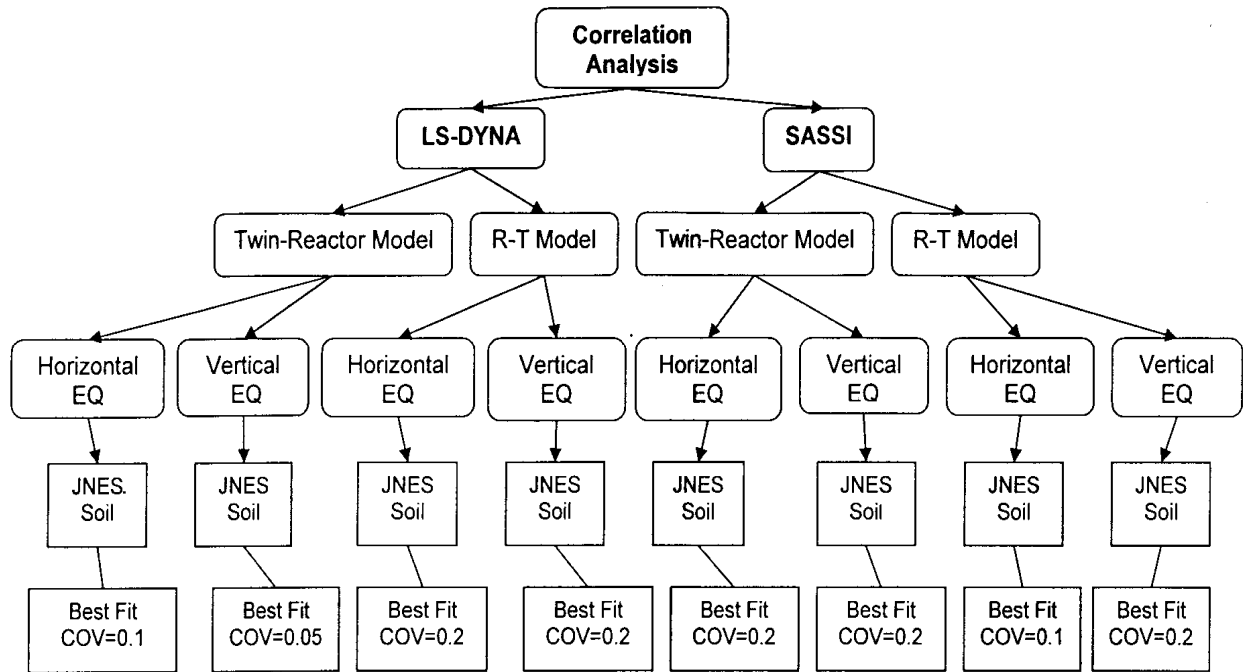


Figure 4.3-13 Summary of Analytical Cases and Associated Soil Uncertainties Performed for this Report

5 CONCLUSIONS AND RECOMMENDATIONS

This report presented a correlation analysis in which two computer codes, namely SASSI and LS-DYNA, were employed to perform SSI analyses for the JNES field test model structures. The analysis results in terms of in-structure response spectra (ISRS) and the seismic induced soil pressures were compared with the JNES recorded data at different sensor locations. The correlation analysis was performed for an earthquake event which is believed to induce only elastic response in the soil-structure systems studied, and no soil degradation is deemed to occur.

In the process of performing the SSI analyses, the JNES geotechnical soil data were treated as the best estimate or mean soil properties, and the uncertainty of the soil properties was estimated by the SASSI and LS-DYNA computer codes using the best fit to the recorded ISRS. By incorporating the soil uncertainty in the SSI analyses, an assessment can be made of the analytical capability of the two codes, which employed vastly different approaches to treating the SSI effect. The insights into the modeling performance by both computer codes are also obtained from the comparisons between the analysis results and the JNES recorded response data.

Based on the study performed, the following observations and conclusions are reached.

1. For the low level ground motion analyzed, both SASSI and LS-DYNA performed extremely well in predicting ISRS for the test models, as exhibited by the comparisons.
2. The level of uncertainty in the soil properties for the site was estimated by the SASSI and LS-DYNA programs through best fit to the ISRS computed from the JNES recorded response data. Although the soil uncertainty level is computed different for the two computer codes, the uncertainty estimates are well within the range of acceptable practice in geotechnical engineering applications.
3. The computation models by both codes appear to have difficulties in capturing the ISRS peaks induced by the structure-structure interactions. This may be due to the lack of information on the soil property of the backfill between the structures (The analysis assumes the free field property for the backfill).
4. For seismic induced side soil pressures, both codes can generally capture the frequency content of the test data and the analyses using modified soil columns correlate well with the recorded pressures. In addition, the LS-DYNA computed pressures appear closer to the recorded pressures than the SASSI results, although not to the extent that one would reach a different conclusion about the performance of the two computer codes.
5. As discussed in Section 4.3, a number of pressure gauges were identified having been contaminated with noises, thus resulting in differences in the comparison of the recorded data with the computed response.
6. With respect to the vertical response analyses, both codes computed very similar ISRS that are close to the recorded data. Similar to the horizontal analyses, the uncertainty estimates of the soil columns for the site by the two computer codes are slightly different with LS-DYNA having a smaller range.

7. For the vertical soil pressures, SASSI estimates the vertical soil pressures much closer to the recorded pressures than LS-DYNA. However, for some frequencies, the SASSI estimate of the soil pressures fall below the recorded pressures. On the other hand, LS-DYNA grossly over-predicts the pressures with respect to the recordings. It should be mentioned that the upward drift in the low frequencies of the recordings should be ignored due to the noise contained in the recorded data.
8. With respect to the effort required to develop the SSI models and to compute the SSI responses, the level of effort required for running the SASSI program amounts to only a small fraction of what is required for executing the corresponding LS-DYNA analysis. Although LS-DYNA has an advantage of many built-in non-linear features, it would not be a practical and effective choice when linear SSI responses are sought. For such cases, SASSI is the better choice.

In summary, the SASSI and LS-DYNA computer codes have reasonably captured the seismic response parameters in terms of ISRS and the seismic induced side and base pressures when the response parameter is in the linear regime. The level of soil uncertainty for the site estimated by both computer codes through best fitting the recorded ISRS is well within the range currently employed in the geotechnical engineering practice.

However, this study only validated the methods for linear SSI response analyses, which can not be extended to addressing SSI effects due to strong ground motions. In the later cases, many non-linear phenomena are expected to occur in the response of the soil-structure systems, such as the soil-structure interface separation and large degradation in the soil properties, which affect the SSI response calculations by various codes. The adequacy and accuracy of the SSI analyses performed using the SASSI and LS-DYNA computer codes remain to be validated for documented strong ground motion data. Therefore, one goal of future research is to collect strong ground motion data to extend the correlation analysis as described in this report to the non-linear SSI regime and to develop insights into the performance of these analysis programs (LS-DYNA and SASSI) for computing structural wall pressure induced by large earthquake events.

REFERENCES

Cohen, K., et al., 1983, "Silent Boundary Methods for Transient Analysis," in Computational Methods for Transient Analysis, Belytschko, T. and Hoghes, T. J. R. editors, North-Holland, New York, pp. 301-360.

Hirotsu, T., et al., 2001, "Model Test on Dynamic Cross Interaction of Adjacent Buildings in Nuclear Power Plants – Laboratory Test." Trans. 16th SMiRT, Washington DC.

Iguchi, M., et al., 1987, "Model Tests on Interaction of Reactor Building and Soil," Trans. 9th SMiRT, Vol. K1, pp. 317-322, Lausanne, Switzerland.

Kitada, Y., et al., 2001, "Model Test on Dynamic Cross Interaction of Adjacent Buildings in Nuclear Power Plants – Overview and Outline of Earthquake Observation in the Field Test," Trans. 16th SMiRT, Session K10/5, Washington DC.

LSTC, 2001, "LS-DYNA User's Manual," vols. 1 & 2, Version 960.

Luco, J. E., "Approximate External Boundaries for Truncated Models of Unbounded Media," Proceedings, 3rd UJNR Workshop of Soil-Structure Interaction, Menlo Park, CA, March 2004.

Lysmer, J., et al., 1969, "Finite Dynamic Model for Infinite Media," J. Eng. Mech., Div. ASCE, pp. 859-877.

Lysmer, J., et al., 1981, "SASSI – A System for Analysis of Soil-Structure Interaction," Report No. UCB/GT/81-02, Geotechnical Engineering, University of California, Berkeley.

Lysmer, J., et al., 1999, "SASSI2000 – Theoretical Manual," Revision 1, Geotechnical Engineering, University of California, Berkeley.

Nasuda, T., et al., 1991, "Embedment Effect on Soil-Structure Interaction," Trans. 11th SMiRT, Vol. K1, K06/1, pp. 111-116, Tokyo, Japan.

NRC RES Advanced Reactor Research Plan, 2002, Rev. 1 Draft report, ML021760135.

Wolf, J.P. and Song, C., 2000, Finite-Element Modeling of Unbounded Media, John Wiley & Sons, West Sussex, England.

Xu, J., et al., 2005, "Assessment of Seismic Analysis Methodologies for Deeply Embedded NPP Structures," Draft NUREG/CR.

Xu, J., et al., 2003, "Collaborative Study of NUPEC Seismic Field Test Data for NPP Structures," NUREG/CR-6822.

Xu, J., et al., 2003, "Current Practice for Deeply Embedded/Buried NPP Structures Subject to Seismic Loadings," BNL Report Y-6718-091603.